MOLECULAR MOBILITY AND INTERACTIONS IN BIOPOLYMER-SUGAR-WATER SYSTEMS

by

Imad Akil Farhat, BSc, MSc

Thesis submitted to the University of Nottingham for the degree of

Doctor of Philosophy

November 1996

Department of Applied Biochemistry and Food Science
University of Nottingham
Sutton Bonington
Loughborough LE12 5RD - UK

Abstract

Since a significant range of food products may be regarded as biopolymer-sugar-water systems, questions relating to their production, structure and storage characteristics are of importance to the food industry. Information on molecular mobility and organization should provide genuine insight into such issues.

The molecular properties of various biopolymer-sugar-water systems have therefore been studied using nuclear magnetic resonance (NMR) and Fourier transform infrared (FTIR) spectroscopies, and wide angle x-ray diffraction (WAXS).

In general, the hydration of biopolymers in the water content range 0 to 1 g of water per g of dry matter, yielded an increase in the degree of order. ^{13}C solid state NMR studies of xanthan powders showed an increasingly ordered structure at water contents exceeding 20% (dry weight basis) and a maximum degree of molecular organization above 75% water. This was supported by the results derived from FTIR and WAXS studies on the same material. Similar results were found in gelatin systems. The amide 1 band (~1660 cm^{-1}) of the FTIR spectrum of the protein was deconvoluted into its individual components and the intensity of the components arising from ordered segments of the protein increased with hydration indicating a progressive ordering of the protein.
The hydration of biopolymer-sugar mixtures was also investigated. Maize-sucrose (90:10 and 95:5) extrudates were studied using ^{1}H NMR relaxation as a function of moisture content; the results showed a 'quantum' increase in the mobility of the sugar at water contents between 15 and 20%. This was explained in terms of 'dissolution' of the sugar in the aqueous phase as a result of its increased preferential hydration.
Further proofs of unequal partitioning of water during the hydration of biopolymer-sugar mixtures were obtained from an FTIR study of gelatin-sugar films. The intensity changes of the amide 1 band suggested a preferential hydration of the protein in the early stages of hydration, followed by a phase where the hydration of the sugar was favoured. On the

basis of these experimental results, a model describing the process of hydration of biopolymer-sugar systems was proposed.

In addition to the investigation of the rotational mobility of water in biopolymer and biopolymer-sugar systems, the translational mobility of water in such systems was also studied using pulsed field gradient NMR techniques. The self-diffusion coefficient of water in biopolymer gels showed a strong dependence on the diffusion time indicating the obstructive role of the polymer network. The diffusion coefficient of water was also reduced by increasing the concentration of the gel and the presence of sugar. Preliminary results obtained by comparing gels prepared by heating with those obtained by extrusion, suggested that the translational mobility of water was affected through modifications of the gel matrix.

The retrogradation of amylopectin-sugar (70:30 and 90:10) extrudates was studied adopting a molecular dynamics approach derived from glass-transition theory. While water enhanced exponentially the rate of retrogradation, the effect of other plasticizers such as sugars was more complex. The rate results were regarded as a function of the offset of the storage temperature from the glass-transition temperature ($T-T_g$).

While fructose enhanced greatly the rate of amylopectin recrystallization, 30% xylose inhibited this reordering process. In contrast, sucrose increased the rate of retrogradation at low ($T-T_g$) (<60°C). The results suggested that sucrose could depress the rate constant at high ($T-T_g$). The impact of added sugar depended, therefore, on the sugar type and concentration in the system.

The presence of the sugar in the system was found to affect the polymorphic form of the recrystallized amylopectin possibly implicating the sugar in the cell unit of the crystal.

The retrogradation kinetics were modelled using the Lauritzen-Hoffman theory employing the ten-Brinke equation to calculate T_g and the Flory equation to calculate the melting temperature (T_m). These calculations permitted the simulation of the joint effects of water content and storage temperature on the kinetics of the retrogradation of amylopectin.

ACKNOWLEDGEMENTS

I would like to express my gratitude to the ACTIF II consortium for the financial support throughout my PhD, and to the *'Centre Culturel HARIRI'* for the financial assistance during my BSc. and MSc. in France.

My very special thanks go to Professor J.M.V Blanshard for his support, supervision and valuable guidance, and also to Professors J.R Mitchell and W Derbyshire for their support and advice.

I also want to thank Jenny Melvin, Dr W MacNaughtan, Mike Chapman, Val Street and Phil Glover for their assistance throughout this project and their valuable friendship. Many thanks to the European Erasmus/Comett students Patrick Moreau, Edouard Loisel, Antje Becker, Sandra Orset and Pedro Saez Rojo who helped in some of the practical work.

I would like to thank my parents and especially my mother for their love, guidance and patience, and Kurshid for her support every single day of these last three years (and hopefully for the rest of my life !)

And finally, my thanks go to my friends Keith and Kath Brasnett who made me feel at home in England.

This thesis and all my future achievements are dedicated to

the memory of my father

May his memory be my guide
as long as I live

Table of Contents

List of figures

Chapter 2

Chapter 3

Chapter 4

Chapter 5

Chapter 6

List of tables

Chapter 2

Chapter 3

Chapter 4

Chapter 5

Chapter 6

List of abbreviations

XRD	x-ray diffraction
WAXS	wide angle x-ray scattering
NMR	nuclear magnetic resonance
FTIR	Fourier transform infrared
DSC	differential scanning calorimetry
DMTA	dynamic mechanical thermal analysis
CP	cross polarization
MAS	magic angle spinning
SSD	spinning side band
FT	Fourier transform
T_1	spin-lattice relaxation time (s)
T_2	spin-spin relaxation time (s)
T_2^+	spin-spin relaxation time shortened by magnetic field inhomogeneity (s)
T_2^*	spin-spin relaxation time decreased by field inhomogeneity,diffusion,exchange, etc.
T_g	glass-rubber transition temperature (K)
T_m	melting temperature (K)
D	self-diffusion coefficient of water in the sample ($m^2\ s^{-1}$)
D_0	free self-diffusion coefficient of water ($m^2\ s^{-1}$)
ci	crystallinity index
w/w	weight for weight
d.s.b	dry solid basis
a_w	water activity
RH	relative humidity
$90°_x$	90 degree pulse around the x-direction
ν	frequency (Hz)
ν	wavenumber (cm^{-1})
γ	magnetogyric ratio (rad $T^{-1}\ s^{-1}$)

μ	magnetic dipole moment (A m^2)
B_0	permanent magnetic field (T)
B_1	rf magnetic field (T)

Introduction

1. Project background

This thesis is the outcome of a project which was carried out as part of the ACTIF 2 (Amorphous Crystalline Transition In Food) LINK programme involving MAFF (Ministry of Agriculture, Fisheries and Food), the DTI (Department of Trade and Industry) and 14 multinationals companies (Allied-Lyons, BAT, Bruker, Cadbury, Clextral, Danone, Firminich, Grand Metropolitan, Kraft, Nabisco, Nestlé, Unilever, Weetabix and Zeneca).

The aim of ACTIF 2 can be summarized by its focus statement: '*to study and exploit the significance of* ***molecular mobility*** *for processing and storage of principally food materials under conditions contingent to the* ***glass-rubber transition***'.

ACTIF 2 came as the logical follow up of the ACTIF 1 programme in which the glass-rubber transition in food systems was thoroughly investigated and HYDRA (the hydration of hydrophilic materials in food and drug delivery applications) which concentrated on studying the hydration of biopolymer systems of importance in the food and pharmaceutical industries. ACTIF 1 established the occurrence of the glass-transition in food systems, investigated the effect of system composition i.e the presence of plasticizers and applied the physical approach employed in polymer science to develop a systematic understanding of the glass-rubber behaviour of food biopolymers in the water content range between 0-20%.

ACTIF 2 used the concepts established in ACTIF-1 to study and predict the behaviour

of a ternary system consisting of a biopolymer, an intermediate sized molecule and a small molecule which can be viewed as a simple model of food and pharmaceutical systems, but now under conditions contingent to the glass-rubber transition.

Six interdependent application areas were developed, with molecular mobility as a central and common theme. The six areas were :

- ***Texture:*** the impact of sugars and water upon the mechanical properties of biopolymer systems.
- ***Processing:*** the effects of different processing protocols, and especially the exploitation of shearing forces, upon the functional properties of biopolymers.
- ***Diffusion:*** a phenomenon which is fundamental to storage stability, chemical reactions, flavour release, drug delivery and the metabolism of microbiological organisms.
- ***Enzyme activity and chemical reaction at low water contents:*** a study of lysozyme activity and the Maillard reaction at reduced water content.
- ***Flavour:*** the dynamics of flavour retention/release in the glassy and the rubbery states.
- ***Microbiology:*** The significance of the *rpoS* gene in maintaining the microbial viability and the possible exploitation of signalling molecules.

A variety of physical techniques were used to study the molecular mobility and order. While a collection of NMR methods (high resolution solution and solid state NMR, time domain low resolution pulsed NMR, microscopy, etc.) were employed in addition to other techniques such as x-ray diffraction, FTIR, head space flavour analysis as well as several rheological (texture analysis, DMTA) and calorimetric procedures (DSC).
In addition to the scientific interaction between academic and industrial partners, effective technology transfer was a major objective of such a Link Scheme. In fact, several methodologies and experimental protocols developed by one partner, have been utilized by other members of the programme.

2. Scientific and industrial relevance of mixed systems

A system containing one or more biopolymers, one or more intermediate sized molecules in addition to one or more small molecules constitutes the generic model of typical food and pharmaceutical systems.
Biopolymers such as botanical or microbial polysaccharides (starch, cellulose, xanthan, etc.) and plant and animal proteins (gluten, gelatin, ovalbumin, etc.) are used in both food and pharmaceutical systems for their nutritional, drug delivery or physical (viscosity, thermal and chemical stability, etc.) properties. While intermediate sized molecules in pharmaceutical systems are usually medically active substances, in food systems a large variety of intermediate sized molecules are present naturally or added during processing such as sugars and maltodextrins, lipids, peptides, flavours and vitamins. Small molecules such as water, CO_2, O_2, etc. are present as part of the composition of these systems or incorporated subsequently during preparation or consumption.

A simple, ternary, biopolymer-sugar-water system was selected as a model for typical food systems of interest to the companies sponsoring the project.
In addition to starch and gelatin as representatives of natural polysaccharides and proteins respectively in the ternary system, the hydration properties of the microbial xanthan gum were investigated. The behaviour of four different sugars (sucrose, fructose, xylose, glucose) in these mixed systems was investigated.

While chapter 2 reviews the structure and properties of the various components used, chapter 3 describes the materials and method used, in addition to a brief reminder of the basis of the methodologies employed. Chapter 4 reports a series of studies of the hydration of biopolymers and biopolymer-sugar systems, whilst chapter 5 describes the translational mobility of water in these systems. Chapter 6 outlines in some detail the role of water and sugars on the reordering of gelatinized waxy maize starch extrudates. A general discussion and conclusion constitute the final chapter.

Structure and functional properties of starch, gelatin and xanthan

1. Starch

Starch constitutes a large proportion of the world's food energy intake. It is found mainly in the storage organs of plants in the form of granules.

Table 2.1 Starch content of typical raw foods (g per 100 g of dried edible portion). Recalculated from Linnecar (1995)

	Wheat flour	White rice	Old potatoes	Cowpea
Starch content (% in dry matter)	89%	89%	79%	53%

1.1 Structure of the starch granule

1.1.1 Chemical composition and morphology

Regardless of their botanical source, starch granules are primarily composed of two glucose polymers, the largely linear poly (1→4)-α-D-glucan (amylose) and the highly branched amylopectin where the linear poly (1→4)-α-D-glucan chains are connected through (1→6)-α- linkages.

The relative amylose / amylopectin content in the starch granule depends on its botanical

source. (Morrison *et al.*, 1984 and Guilbot *et al.*, 1985). Likewise, the shape and size of the granules depends on the origin of the starch as shown in the review by Jane *et al.* (1994). These workers used scanning electron microscopy (SEM) to study the morphology of 54 different starches. The results relevant to this work are summarized in Table 2.2.

Table 2.2 Shape, size and composition of some typical starch granules

Botanical source	Shape (a)	Diameter (μm) (a)	Amylose % (b)
Wheat	lenticular, polyhedral	2-38	26 - 31
Maize	polyhedral, irregular	5-20	28
Waxy maize	polyhedral, polygonal	5-15	0 - 1
Rice	polyhedral, irregular	3-8	14 - 32
Potato	ellipsoid	12-60 x 15-75	23

(a) Jane et al. (1994)
(b) Amylose content (% of amylose + amylopectin) based on data from Guilbot and Mercier, 1985

1.1.2 The constituent polysaccharides of the starch granule

1.1.2.1 Amylose

Amylose is essentially a linear glucose polymer, the degree of polymerisation (DP) depending on the source of the starch granule. Takeda *et al.* (1987a) reported small DP values for wheat amylose (DP=570) and relatively large ones for potato amylose (DP=4920) and the possibility of some α(1→6) branching, between 3 and 20 per amylose molecule.

An important property of amylose molecules is the ability to complex iodine by forming

a single helix around the polyiodide ion. The resulting characteristic blue colour (maximum absorption at 620-680 nm) is employed for chemical characterization of the granule.

Amylose-lipid complexes are formed in a similar manner, which yield a characteristic V-type x-ray diffraction pattern (Mercier *et al.*, 1979 and 1980). Amylose in the granule can be found as a 'free' amylose or complexed with lipids.

1.1.2.2 Amylopectin

Amylopectin is a large molecule with a degree of polymerization between 3.10^5 and 3.10^6 (Zobel, 1988). Up to 5% of the total linkages are $\alpha(1\rightarrow6)$ leading to a ramified structure with an average constituent chain length of between 20-27 glucan units (Guilbot *et al.*, 1985; Takeda *et al.*, 1987).

French (1972) proposed a 'cluster' model to describe the branched amylopectin structure. The amylopectin chains were classified into A chains with an average DP between 15-20 linked by their reducing end group through an $\alpha(1\rightarrow6)$ linkage to the longer B chains having an average DP≈45. The B chains are linked in a similar manner to other B chains or to the C chain. There is a single C chain per amylopectin molecule. The A chains are organized as double helices and these form clusters at regular intervals through the molecule (Robin *et al.*, 1974 and 1975) (Fig 2.1).

Although this model is generally accepted to describe the structure of amylopectin, Hizukuri (1986) suggested a polymodal model where the B chains are further subdivided into 4 different types: the B1 chains which carry one cluster (DP 20-24), the B2 chain (DP 42-48) linking two clusters, the B3 chain (DP 69-75) carrying three clusters and finally B4 chains linking 4 clusters.

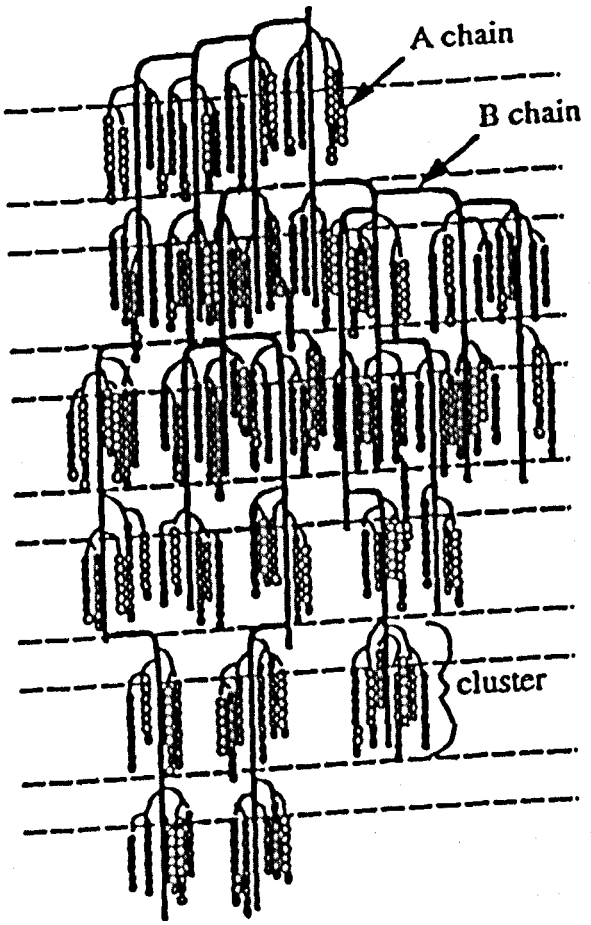

Figure 2.1 The 'cluster' structure for amylopectin proposed by Robin *et al.* (1974, 1975) based on the model described by French (1974).

1.1.3 The organization of the various components in the granule

1.1.3.1 Growth rings

The birefringence patterns of starch granules viewed from different angles led French (1972) to the conclusion that the molecules in the starch granule are arranged radially. This was supported by small-angle light scattering studies (Borch *et al.*, 1972). Furthermore, Nordin *et al.* (1970) suggested, using ^{3}H labelling, that the non-reducing end groups of the molecules were concentrated at the surface of the starch granules.

The examination of starch granules by optical and electron microscopies reveals concentric rings (French, 1984). These growth rings had different susceptibilities to digestion by α-amylase and therefore Hollinger *et al.* (1975) suggested a model where the rings were alternately amorphous and semi-crystalline.

The thickness of these layers has been the subject of several studies. Transmission electron microscopy (TEM) results suggested a thickness between 120 and 400 nm for waxy maize starch (Yamaguchi *et al*, 1979) and between 100 and 200 nm for barley starch (Buttrose, 1960). The thickness of the semi-crystalline rings is believed to be 2 to 4 times larger than the amorphous rings (Mussulmann et *al.*, 1968).

1.1.3.2 The semi-crystalline growth ring

The semi-crystalline rings are composed of alternating crystalline and amorphous lamellae. The periodicity of these lamellae was measured using TEM and values of 7±1 nm were reported by several workers (Kassenbeck, 1975 and 1978; Yamaguchi *et al.*, 1979). However, values between 9 and 10 nm have been found by small-angle x-ray scattering, SAXS (Sterling, 1962) and small-angle neutron scattering, SANS (Blanshard *et al.*, 1984). Blanshard suggested that the value of 9 nm describes more accurately the situation in native hydrated starch granules and attributed the smaller value recorded by microscopy to water loss during sample preparation. More recently, Oostergetel and Van Bruggen (1989) found good agreement between their TEM and SAXS results and reported values between 9.2 nm for potato starch and 10.5 nm for barley starch confirming the hypothesis proposed by Blanshard *et al.*(1984).

Several lines of evidence suggest that the crystallinity of the granule is mainly associated with the amylopectin component. Indeed, the crystallinity, measured by wide angle x-ray diffraction, on waxy maize starch which contains virtually no amylose is comparable to the crystallinity of normal maize starch containing around 28% amylose (dry

polysaccharide basis). Furthermore, amylose may be leached out of the starch granule without disrupting the crystalline structure (Zobel, 1988).

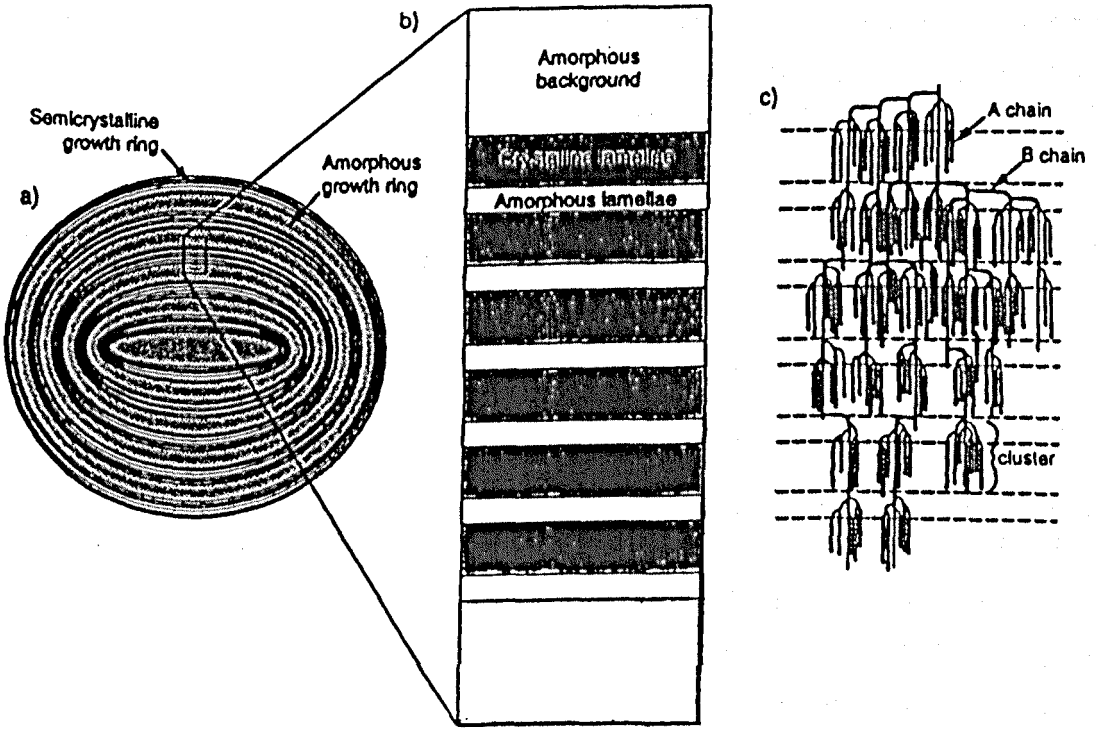

Figure 2.2 A model of the starch granule structure according to Jenkins *et al.* (1994):
a: the concentric amorphous and semi-crystalline growth rings
b: the semi-crystalline lamellar stack embedded in the amorphous background region
c: the cluster structure of amylopectin

Consequently, Robin *et al.* (1974 and 1975) suggested a model where the semi-crystalline growth ring consists of a radial arrangement of amylopectin clusters. The double helical structure of the A chains forms the crystalline lamellae whereas the region with many branching points yields the amorphous lamellae (Fig 2.1). SANS studies by Blanshard *et al.* (1986, 1987) led to a model (Fig 2.3) of the starch crystallites which has been endorsed and refined by recent SAXS investigations (Cameron *et al.*, 1992 and 1993; Jenkins *et*

al., 1993 and 1994). In a detailed study of wheat starch, it has proved possible to determine the length of a cluster (the crystalline lamella) and the adjacent branch-point section (the amorphous lamella) as 6.65 nm and 2.2 nm respectively (Fig 2.2). The precision possible with these more refined experimental and analytical procedures offers exciting opportunities for relating molecular structure to granular architecture.

1.1.3.3 Distribution of lipids and amylose in the growth ring

a. Lipids :

Blanshard *et al.* (1984) succeeded in 'masking'. the polysaccharide components of the SANS spectrum recorded with wheat starch granules by immersion in a H_2O / D_2O mixture of a particular composition (48:52 v/v). This enabled them to observe the residual lipid pattern. By comparing normal and defatted wheat starch, they concluded that the lipids had a periodicity of 15-16 nm. This, combined with WAXS results where a tangential crystallite size of 14-15 nm was reported (French *et al.*, 1984), led Blanshard (1986) to propose a model where the amylopectin crystallites are imbedded in a radial arrangement of the hydrophobic lipids (Fig 2.3).

b. Amylose

In the model described earlier, Blanshard suggested 3 different radially arranged (Kassenbeck, 1978) states of amylose: (i) free amylose, (ii) amylose-lipid V-type helical complex and (iii) the hybrid amylose / amylopectin helix where amylose could have co-crystallized with the amylopectin A chains (Fig 2.3). The relative proportion of these 3 states of amylose could explain the difference of behaviour between starches in terms of capability of amylose to form a complex with iodine and the subsequent infrared

dichroism properties (Blanshard, 1987).

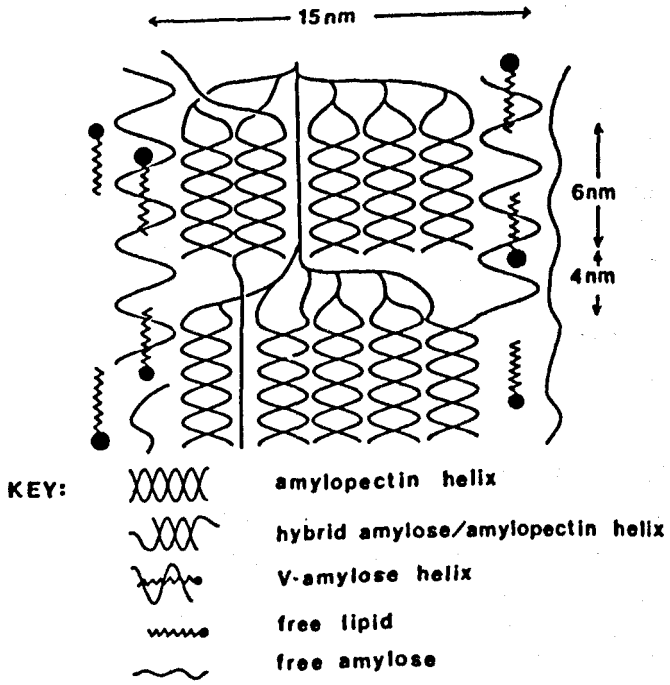

Figure 2.3 The distribution of the main starch components in the crystallites according to Blanshard (1987)

1.1.4 The crystalline structure

As described earlier, amylopectin is believed to be the main contributor to the crystalline component of the starch granule. The A-chains and the external B-chains of the amylopectin readily form double helices which associate in pairs. The types of arrangements of these pairs of double helices giving rise to the 2 main starch polymorphs have been described by several workers and refined by Imberty *et al.* (1988 and 1991). In the case of the A-type crystal, the left handed, parallel stranded double helices are arranged in a monoclinic crystal unit cell (a = 2.12, b = 1.17 and c = 1.07 nm) which contains 12 glucose units, the repeating unit being maltotriose.

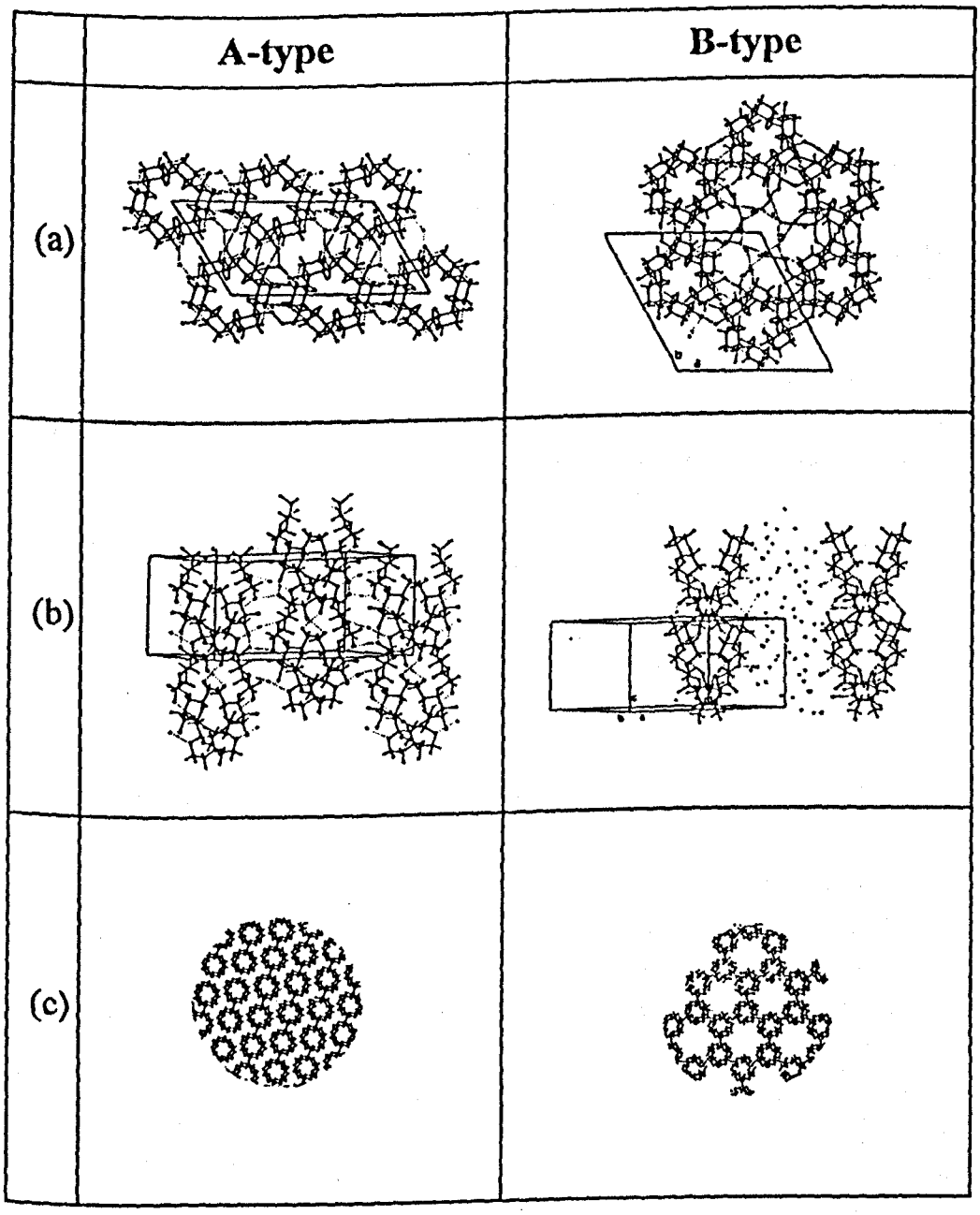

Figure 2.4 The structure of the A and B type starch polymorphs

a: the projection onto the (a,b) plane. The hydrogen bonds are indicated in broken lines and the water molecules in dark circles (Imberty *et al.*, 1991)

b: as viewed along the fibre axis (c direction) (Imberty *et al.*, 1991)

c: a wider view of the projection onto the (a,b) plane (Gernat *et al.*, 1993)

This arrangement is stabilised by hydrogen bonding between the helices and with the 4 water molecules present in the cell unit (Fig 2.4). These water molecules are essential to the crystalline structure and their removal disrupts the crystal integrity.

The B-type crystal resembles the A-type except that the packing of the six left-handed double helices is hexagonal (a = b = 1.85 and c = 1.04 nm). There are 36 molecules of water in the the cavity at the centre of the 6 double helices (Fig 2.4). Imberty *et al.* (1991) reported that conversion from the B to the A polymorphs was possible in low humidity and high temperature environment. Similar polymorph changes have been reported by Marsh (1986) for wheat starch (Fig 2.7). The results of further studies on waxy maize starch are reported in chapter 6.

1.2 Properties of starch

1.2.1 Gelatinization

12.1.1 Swelling and gelatinization

Gelatinization is the most important starch characteristic in terms of industrial applications. In practice, gelatinization refers to the loss of order as measured by birefringence or x-ray diffraction, and the associated swelling of the granule. The process of gelatinization has been described by Blanshard (1987) as the result of the breaking of hydrogen bonds between the poly α-1,4-glucan chains in the crystallites. This rupture of hydrogen bonds is usually achieved by heating in excess water, but can also be obtained, without heating, by the use of solvents such as liquid ammonia or DMSO (Banks *et al.*, 1967) or mechanically by milling (Lelièvre, 1974).

Starch granules are insoluble in cold water. When aqueous suspensions of starch are heated, the granules swell. The swelling is reversible until a certain temperature known

as the gelatinization temperature where material, principally the linear amylose, leaches from the granule and the structure of the granule is disrupted.

The typical amylograph shown in Figure 2.5 illustrates a real time monitoring of gelatinization. As the starch suspensions are heated, the viscosity increases sharply as a result of the swelling of the granules to reach a maximum at the gelatinization temperature. Beyond this temperature, continuous heating and stirring of the gel causes the disruption of the granules leading to a drop in viscosity. It is clear from Figure 2.5 that the amount of the high molecular weight, branched amylopectin in the starch is the main factor in the gelatinization process and the rigidity of the resulting gel.

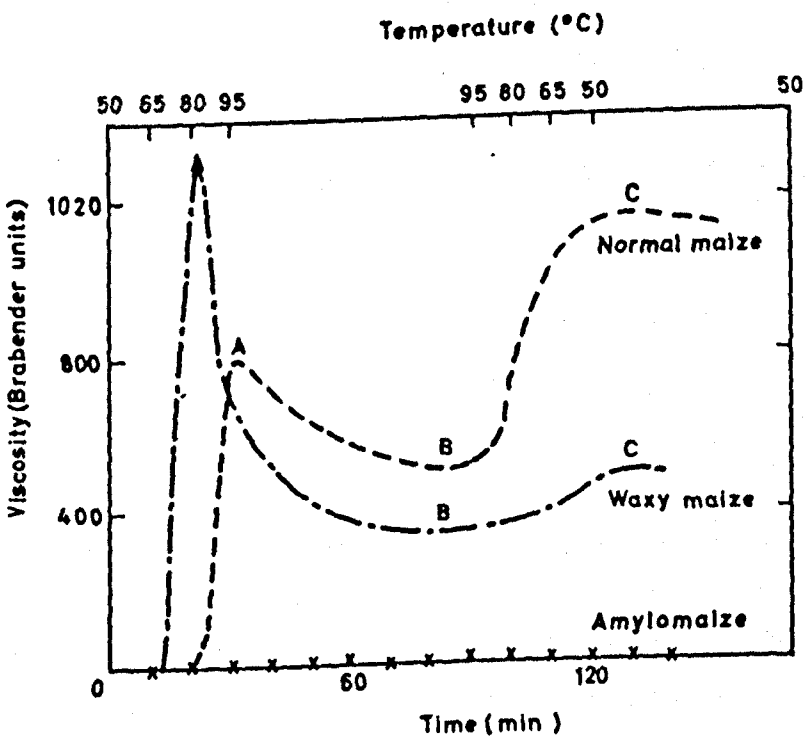

Figure 2.5 The paste viscosity as a function of heating time / temperature (adapted from Greenwood, 1979) for 3 starches with different amylopectin contents: waxy maize (99-100%), normal maize (72%) and amylomaize (20-48%); the amylopectin content data were adapted from Guilbot *et al.* (1985) and Morrison *et al.* (1984) and are quoted as % of the total amylose and amylopectin.

1.2.1.2 Effect of water and sugars on the gelatinization

Lelièvre (1973) examined the effect of water content on the gelatinization temperature by regarding the gelatinization as a melting phase transition and employing the approach developed in the field of synthetic polymers by Flory (1953). The melting temperature (T_m) decreased with the starch concentration. Details of the effect of water content on T_m are reported more extensively in chapter 6.

This approach was extended by the same author (Lelièvre, 1976) to model the role of sugars in increasing the melting temperature of starch. The prediction of the experimental results was satisfactory and therefore is potentially extremely valuable for the baking industry, especially in cake type systems where several types of sugar are employed and where the sugar content is relatively high.

The effects of water and sugars on the gelatinization of starch have been comprehensively reviewed by Blanshard (1986 and 1987).

1.2.2 Retrogradation

1.2.2.1 Scientific and commercial relevance

The recrystallization of gelatinized starch, frequently referred to as retrogradation, has received intensive attention since the beginning of the century (review by Katz,1928 of his work published between 1912 and 1916) due to its commercial importance. Indeed, since the degree of order in a system is an important parameter affecting both the molecular mobility in the system, and its mechanical properties, it will inevitably have an impact on the texture and the consumer perception of starch based food products. Other aspects such as flavour release can be affected by the retrogradation of the starch polysaccharides.

Consequently, there is a need for a systematic understanding of the retrogradation process

and the effects of various parameters (storage temperature, concentration, additives) on its kinetics and structural properties (the type of crystalline structure).

1.2.2.2 The nature of starch retrogradation

The basis for an understanding of starch retrogradation was made by the observations of Boussingault some 140 years ago (1852). Indeed, Boussingault showed that the deterioration of bread crumb on storage by the process now known as staling or retrogradation, was not due to moisture loss. He also showed that the changes are thermally reversible as he reported that deteriorated bread could be 'refreshened' by heating to 60°. Much later, x-ray diffraction studies by Katz (1928) demonstrated that bread staling was primarily due to the recrystallization of starch on storage.

The effects of moisture content, storage temperature and presence of additives on the retrogradation of starch based systems have been studied by many workers, the main results are reviewed in the following sections.

1.2.2.3 Effect of moisture content and storage temperature

a. The retrogradation rate

The retrogradation of starch can be described using the approach developed for synthetic polymers (Wunderlich, 1976; Tiller, 1991) which has been applied to some semi-crystalline biopolymers such as starch (Marsh *et al.*, 1988). An extensive review of the role of water in food systems in general, and in retrogradation in particular, was reported by Slade *et al.* (1991). Three important stages in the crystallization process have been described, namely nucleation, crystal growth and maturation. Temperature has a major

and different impact on each of these stages, the consequences of which decide the shape of the overall crystallization rate - storage temperature relationship.

The rate of crystallization is negligible at temperatures below the glass transition point (T_g). On heating above T_g, the rate increases and reaches a maximum value but then decreases to zero at temperatures approaching the melting point (T_m). This typical 'bell' shaped diagram (Fig 2.6) is thought to be the result of the combined effects of temperature on the nucleation and the propagation stages of the crystal formation. The reduced rate as the biopolymer approaches its T_g was attributed to the very limited molecular mobility which would be necessary for crystal growth through the diffusion of polysaccharide chains and side chains (Levine *et al.*, 1987; Slade *et al.*, 1991).
The reduction in the crystallization rate as the system approaches T_m was explained by a melting of the nucleation centres (Wunderlich, 1976).

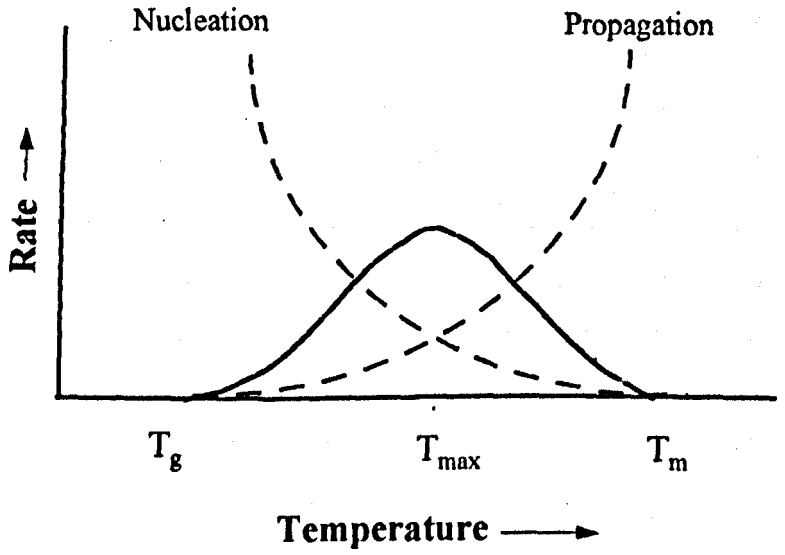

Figure 2.6 Diagram representing of the effect of temperature on the crystallization kinetics of partially-crystalline polymers

The biopolymer molecular mobility can be enhanced by the presence of plasticizers as described in the last section of this chapter. Consequently, increased water content leads to an increase in the rate of retrogradation as demonstrated clearly in chapter 6. Furthermore, the values of T_g and T_m are highly dependent on moisture content. Increased water contents shift both T_g and T_m to lower temperature as described in more detail in chapter 6 leading to a displacement of the rate versus temperature diagram.

The shape of the rate - temperature diagram, and the effect of water content on T_g and T_m is thought to explain the origins of the negative temperature coefficient for the staling bread (relatively high water content) and the positive coefficient for cakes (low water content system) (Cornforth *et al.*, 1964).

b. The resulting crystalline structure

Katz (1928) observed in his early work that the retrogradation of bread yielded a B-type crystalline structure although the raw material had an A-type structure. Shortly after, Katz *et al.* (1930) reported success in recrystallizing starch solutions into A crystals under controlled conditions. This was later confirmed by Bear and French (1941) who prepared A- type material by the recrystallization of a 50% corn starch solution at relatively high temperatures (50°C).
B-type crystals were obtained from the same solutions by storage at lower temperature. These observation were later confirmed by several workers (Doi *et al.*, 1969 and Wu *et al.* 1978) which led Marsh (1986) to construct a 'state' diagram (Fig 2.7) describing the A/B crystal type resulting from the recrystallization of gelatinized starch as a function of water content and storage temperature.

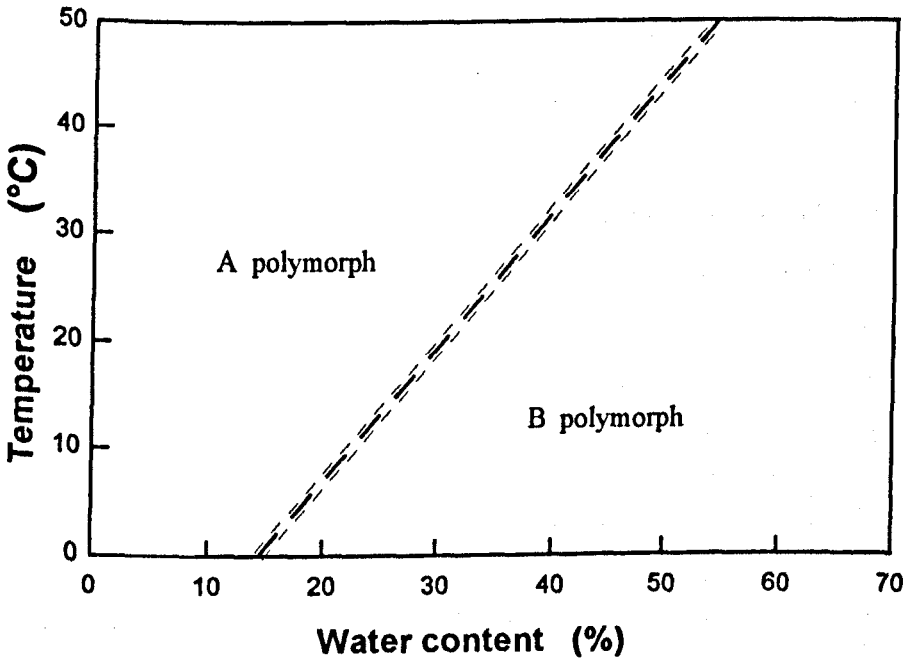

Figure 2.7 Schematic representation of the dependence of the crystal type of retrograded starch on temperature and water content (adapted from Marsh, 1986)

1.2.2.4 Effect of added intermediate sized molecules - emphasis on the role of added sugars

The impact of sugars and other small and intermediate sized molecules on retrogradation is of considerable importance in baked products and breakfast cereals, where intermediate sized molecules are naturally present (lipids, sugars, etc.), or added to improve the properties and the perception (sugars, maltodextrins, flavours, etc.) of the final product but sometimes to control the retrogradation of the starch component. Despite the amount of work in this field, the control of the retrogradation process is still largely empirical and only partially effective (Ring *et al.*, 1987).

In 1978 Maxwell and Zobel were the first to report the effect of sugars on the staling of

starch gels. This was followed in 1981 by a US patent (Maxwell and Zobel, 1981). Miura *et al.* (1992) studied the effects of various polyols and emulsifiers on the retrogradation rate of non-glutinous rice starch. Their results suggested that such additives retarded the retrogradation process, and proposed that this effect resulted from the formation of a "water-structure" in the presence of polyols and of specific interactions between the starch chains and the emulsifier molecules.

The effect of added sugars on the retrogradation of starch have been investigated by several workers (Marsh 1986; Cairns *et al.*, 1991; I'Anson *et al.*, 1990). Marsh (1986) found that sucrose, maltose and xylose delayed the retrogradation of wheat starch gels, fructose to enhance this recrystallization and xylose to inhibit the process. I'Anson *et al.* reported that glucose slowed retrogradation while sucrose and ribose entirely inhibited the retrogradation of wheat starch - sugar - water 1:1:1 gels. In contradiction, Wang *et al.* (1994) demonstrated the enhancing effect of sugars and maltodextrins on the retrogradation of starch, and correlated the results with the glass transition temperature of the system.

1.2.2.5 Effect of processing

Although the method of formation of the starch gel is thought to affect the retrogradation rate, there has been no systematic study and understanding of this aspect. Several workers have reported the role of the time/temperature protocol on the staling properties of bread. Faridi *et al.* (1984) reported that egyptian balady bread baked at 260°C for 6-7 minutes staled more rapidly than the bread baked at a higher temperature for a shorter baking time (540°C for 1 min).

Likewise, Inaba *et al.* (1988) demonstrated that rice cakes produced conventionally retrograded faster than those obtained by extrusion cooking.

1.2.2.6 Modelling the retrogradation kinetics

Several models for the retrogradation kinetics have been reported in the literature, many of which depend upon the technique used (Roulet *et al.*, 1988). However, the Avrami model (1941), which is described in more detail in chapter 6, seems to be the most widely used in polymer crystallization studies.

2. Gelatin

Veis (1964) described 'the gelatins' as being a class of proteinaceous substances that do not exist naturally but are derived from the largely insoluble collagenous tissues found in most animals by one of several procedures which generally result in the destruction of the ternary, secondary and, to some extent, the primary structure of collagen.
Although this section focuses on the structure and properties of gelatin, a brief review of the structure of the 'parent' protein, collagen, is given as it is of primary importance for the understanding of some of the major characteristics which prompt the industrial and scientific interests in gelatin, in particular, the gel formation on cooling of gelatin solutions

2.1 Industrial production and applications

2.1.1 Applications

Gelatin is the most widely used hydrocolloid in the food industry due its various advantageous properties such as the range of textures that can be produced, the ease of solution and the thermal reversibility of the changes on gelation, etc. in addition to its relatively low production cost.

The use of gelatin is not limited to foodstuffs. It is considered to be one of the most versatile natural product and, because of its wide range of physical properties such as the formation of gels and films of interesting flexibility, elasticity and surface active properties (Ward *et al.*, 1977), gelatin has found several industrial applications which are noted below.

(i) Photographic films: gelatin is often used as binding agent for light-sensitive photographic layers which are essentially silver halide microcrystals embedded in a binding medium.

(ii) Pharmaceutical applications: gelatin is widely used in medicated pastilles, capsules and suppositories. It is also used as a bacteriological medium.

(iii) Emulsion technology: gelatin is used as an emulsifying agent in many cosmetic, pharmaceutical, water paints and disinfectant products.

Due to its viscosity, gelatin is also used in electroplating to control crystal growth. This is in addition to numerous other technological applications such as printers rollers, gummed paper, packaging, abrasive cloths and paper and many woodworking applications.

The range of properties required in this variety of applications is often the result of the reversible gel-forming characteristic of gelatin. Various amounts of plasticizers such as glycerol and sorbitol are added to obtain the optimum flexibility of gelatin films.

2.1.2 Conversion of collagen to gelatin

The manufacture of gelatin which consists of the conversion of collagen of different degrees of solubility into soluble gelatin by acid or alkaline treatments of collagen has been reviewed by several authors (Veis, 1964) and therefore will not be discussed in detail. In the acid conversion process, the collagenous raw materials (usually pig and rabbit skins) are soaked in inorganic acid solutions (up to 5%) for 10-30 hours. Several extractions are

carried out under different temperature conditions resulting in gelatin batches of different grades (depending on gel strength and viscosity).
Alkaline processing is the most widely used process for the manufacture of gelatins and glues. The collagen stock is hydrated in cold water, and the stock is soaked in excess lime for periods between 3-10 months (depending on the quality required for gelatin). After completion of the liming process, the stock is extracted in a series of successively higher temperature as described for the acid process.

The rigidity of the gel formed under standard conditions is the main factor defining its commercial value.
The routine method for rigidity testing was developed in 1925 by Bloom and consists of the determination of the weight required to make a 0.5 inch diameter, flat bottomed plunger depress the surface of a a gel composed of 7.5 g gelatin in 105 ml water by 4 mm. The weight to the nearest gram is quoted as the 'Bloom' of the sample. Commercial gelatins have Bloom values in the range 80-320 g (Ward *et al.*, 1977).

2.2 Collagen

The structure and properties of collagen have been extensively studied for more than half a century. The physical and chemical properties of collagen have been the subject of several comprehensive reviews such as those by Ward *et al.*(1977), Bornstein *et al.*(1979), Parry *et al.*(1979) and many others. Electron microscope studies carried out in the 1950s (Schmitt *et al.*, 1955) suggested that the basic unit of collagen was a rod-like triple-helix of about 260 nm long and 1.5 mm diameter. The three component helices are left-handed with 3 residues per turn (Balian *et al.*, 1977) and are arranged parallel to each other. When viewed down their axis, these 3 helices are set at the intersections of an equilateral triangle of 0.5 nm side. The 3 constituent helices (α-chains) with a molecular weight of about 95 000 are then further twisted about a common axis to give a slight right-handed

helix forming the collagen monomer with an average molecular weight of approximately 300 000. In some collagens, two of the α-chains are identical (α_1) while the third is slightly different (α_2) in terms of amino acid composition.

Ledward (1986) attributed the maintenance of the secondary structure of collagen principally to the amino acid composition of the individual α-chains. The high content of pyrrolidine residues i.e proline and hydroxyproline (more than 22% of the total residues for pig skin collagen - Table 1) imposes a great steric hindrance to rotation around the peptide bonds leading to a *trans* poly-L-proline II type helical conformation (Fig 2.8). Additionally, the occurrence of glycine as every third residue (glycine content ~33 % - Table 2.3) enables the individual helices to approach closely and establish interchain hydrogen bonds. The number of hydrogen bonds between the chains per tripeptide and the involvement of water in any of these bonds is still a matter of discussion (Bornstein *et al.*, 1979). Such triple helices were found to be sensitive to heating and ionic strength (Ramachandran, 1958 and 1967).

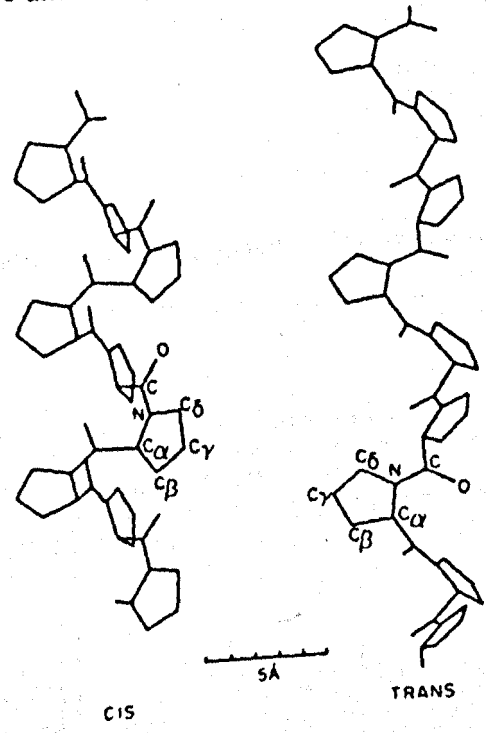

Figure 2.8 The poly-L-proline II *cis* and *trans* helices (Ledward, 1986). This type of structure is further stablized by interchain hydrogen bonds associating the 3 chains

The wide angle x-ray diffraction pattern of collagen has been characterized since the early 1940s (Astbury, 1940; Ramachandran, 1967). Three spacings were reported for collagen powders and fibres: (i) 2.86 Å , (ii) 11 to 15 Å in addition to the diffuse half-halo at (iii) 4.6 Å corresponding to 2θ angles of about 31.2°, 5.9° to 8° and 19.3° respectively (the 2θ values are calculated for the x-ray wavelength λ=0.154 nm, the wavelength used in this project, which facilitates the comparison with the experimental results reported in chapter 4).

2.3 Structure of gelatin

2.3.1 Chemical composition and physicochemical properties

The amino-acid composition of pig skin gelatin (used in this project) reported by Eastoe (1961 and 1977) showed that glycine, proline, alanine and hydroxyproline accounted for nearly two thirds of the total amino acid composition, and virtually no tryptophan or cystine.

Table 2.3 Composition of pig skin gelatin (Eastoe *et al.*, 1961 and 1977). The values are given as number of residues per 1000 total residues.

Glycine	330	Glutamic acid	72.1	Lysine	26.6	Phenylalanine	13.9
Proline	131.9	Arginine	49	Valine	25.9	Isoleucine	9.5
Alanine	111.7	Aspartic acid	45.8	Leucine	24	Hydroxylysine	6.4
Hydroxyproline	90.7	Serine	34.7	Threonine	17.9	Histidine	4
Cumulative percentage	***66.4 %***		***86.6 %***		***96 %***		***99.4 %***

Isoelectric points of pH≈8.9 (Ames, 1944) and pH≈5 (Ames, 1952) were reported for gelatins produced by acid and alkaline treatments respectively. The molecular weight of α-gelatin (Fig 2.9) is believed to be close to 90,000 (Piez, 1967). The existence of high molecular weight multichain gelatin structures has been demonstrated by Courts *et al.* (1958).

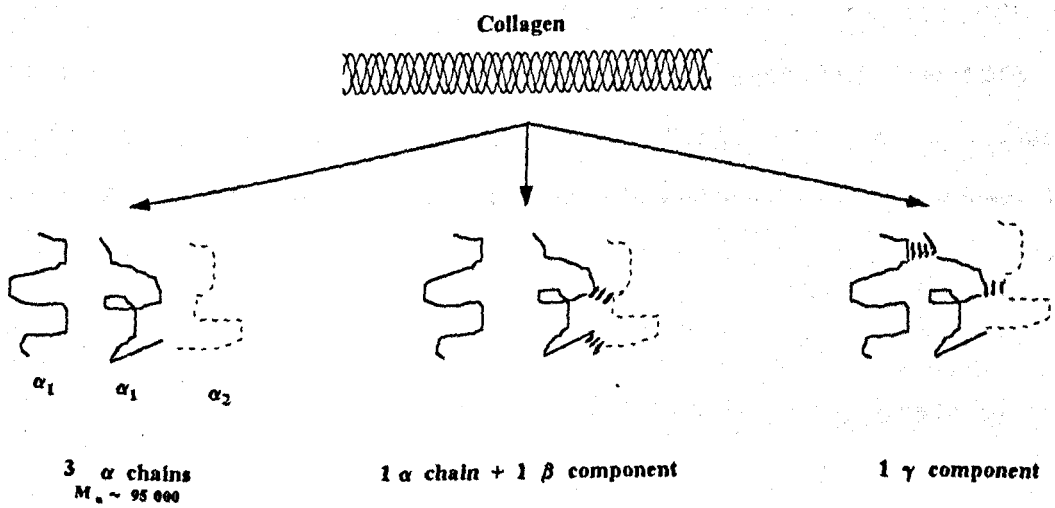

Figure 2.9 Schematic diagram of the collagen-gelatin conversion (Veis, 1964)

2.3.2 Gelation

The cooling of an aqueous solution of gelatin to temperatures below 40°C under the optimum conditions of concentration, pH and ionic strength, results in the gelation of gelatin. The results obtained by electron microscopy, wide angle x-ray diffraction, etc. suggest that the pyrrolidine-rich regions of the gelatin chains act as nucleation sites for the formation of network junction sites (Flory *et al.*, 1960; Harrington *et al.*, 1961; Ledward *et al.*, 1968). Indeed, as a consequence of the undercooling, these regions tend to adopt the poly-L-proline helical form described earlier (Fig 2.8) which then aggregate in a collagen-like triple helix forming a junction site which is necessary for the establishment

of the gel network (Ledward, 1986). Recent NMR studies by Naryshkina *et al.* (1982) have shown that some water molecules are reorientated and bound within the structure as the gelation takes place. Electron microscope evidence suggested that the junction points could contain aggregates of more than one triple helix (Lewis, 1981; Tohyama *et al.*, 1981).

Harrington and Rao (1970) suggested a model for the formation of gelatin gels based on the renaturation of gelatin chains to form collagen-like structures (Fig 2.10). They showed that the degree of renaturation depended on the gel concentration. In dilute gels (<0.1 g l^{-1}), all α-chains renature according to first order kinetics. In contrast, the renaturation process in more concentrated systems (>2 g l^{-1}) was more likely to be a third order process.

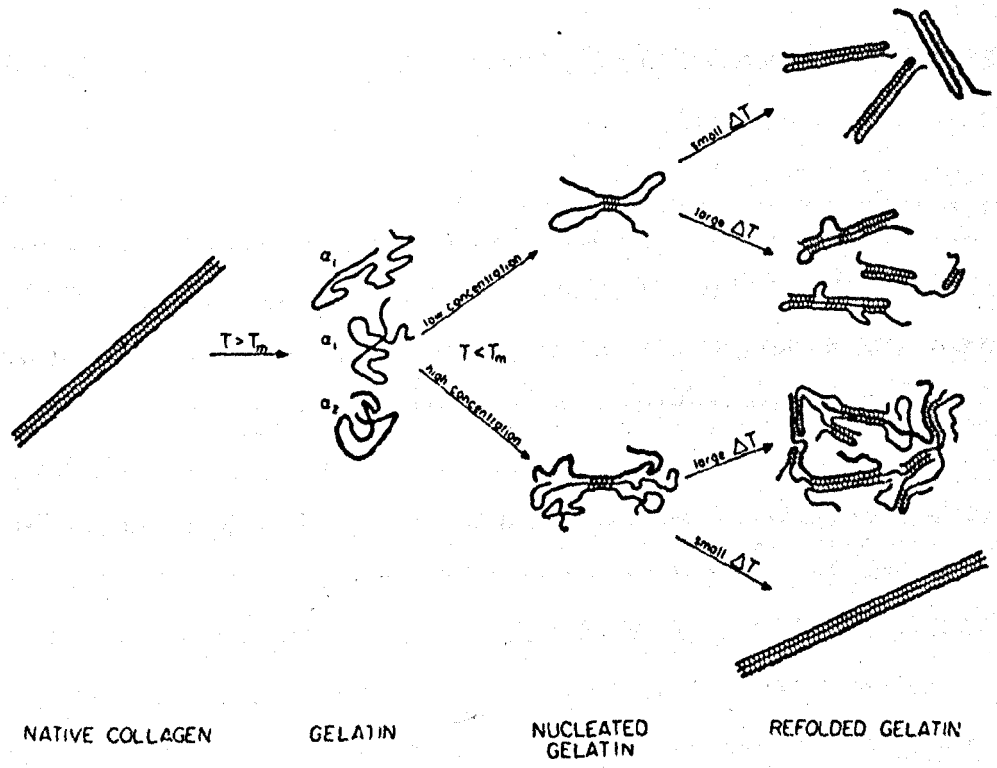

Figure 2.10 The model suggested by Harrington *et al.* (1970) for the mechanism of gelatin gelation by mean of renaturation of the collagen-like refolded gelatin structure as a function of the concentration and the undercooling (ΔT)

The relatively slow and incomplete renaturation in concentrated α-gelatin systems is thought to be due to the reduced probability of 3 chains becoming aligned in the manner required for the formation of the triple helix. This could prove to be the reason why the renaturation of γ-gelatins is much faster than with α and β gelatins (Fig 2.9).

3. Xanthan gum

3.1 Properties and applications

Xanthan is a high molecular weight (2.10^6 - 50.10^6 g mol^{-1}) extracellular polysaccharide produced by *Xanthomonas campestris* through the aerobic fermentation of carbohydrates such as starch, corn syrup, cane or beet glucose or sucrose. The nitrogen source may be one of several proteinaceous products (soy bean meal, cottonseed flour, casein). Ions (Na^+, K^+, Mg^{2+}) and trace elements (Fe, Mn, etc.) are important for the growth of the microorganisms (Sutherland, 1990). Before polymer recovery the fermentation broths are pasteurised. The cells are removed by filtration or centrifugation. Xanthan broth may be treated with dialdehyde (polyglyoxal) to improve the dispensability of the product on re-solution after drying. The polymer is precipitated by the addition of propan-2-ol.

As a result of its various interesting chemical and rheological properties such as shear thinning, stability over a wide range of pH and temperature, sweet perception, etc., xanthan has found numerous applications in the food (salad dressings, yoghurts, etc.), pharmaceutical (lotions, gels, toothpastes, etc.) and oil (drilling mud formulation, oil recovery, etc.) industries.

3.2 Structure

The primary structure of xanthan is a cellulosic backbone with a charged trisaccharide side chain attached to the carbon C3 of every second glucose unit (Fig 2.11). Various substrains of *Xanthomonas campestris* give different pyruvation and acetylation levels of xanthan.

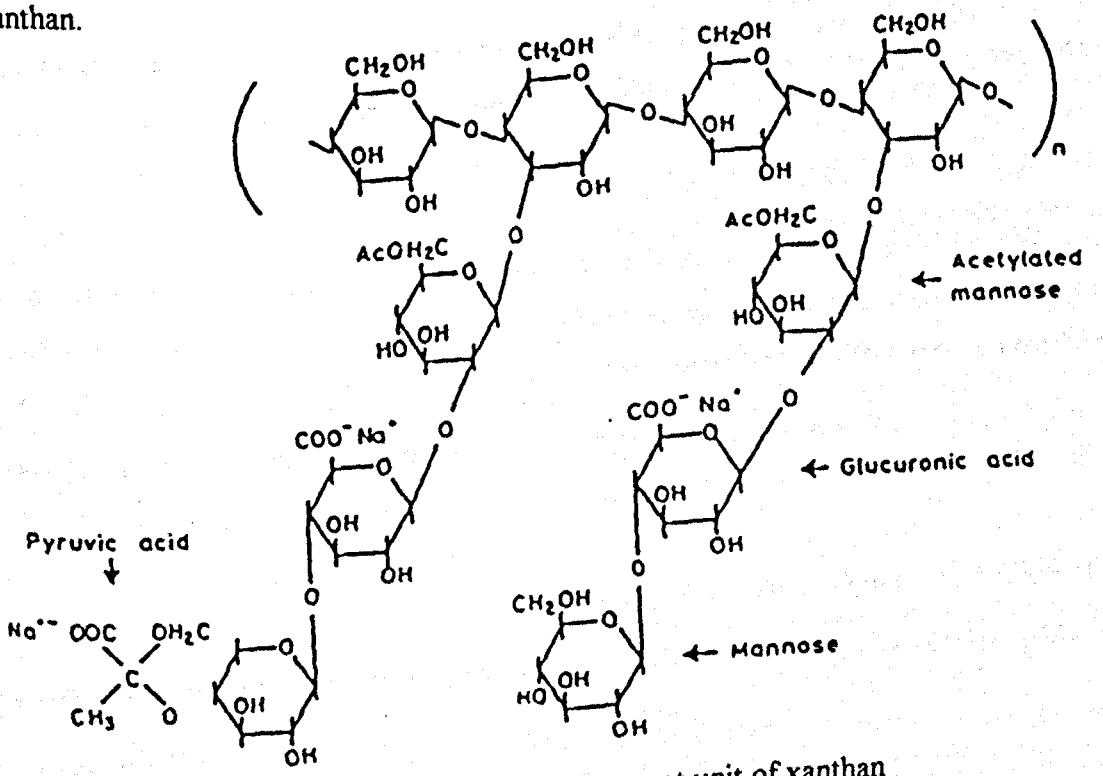

Figure 2.11 The molecular structure of the repeat unit of xanthan

The ordered conformation, stabilised in salt solution has been described by Moorhouse *et al.*(1977) as a 5/1 helix (pitch 4.7 nm) (Fig 2.12). A compact double helix has been described by Xie and Lecourtier (1992) but many contradictions concerning the double/single helical structure persist. In solution, xanthan undergoes an order/disorder transition with change in temperature and ionic strength. Conformational changes occur in the sidechains which move away from close association with the ordered backbone allowing the backbone to undergo a conformational transition (Morris *et al.*, 1977).

Evidence for a conformational transition of the molecule come from qualitative studies using ^{1}H and ^{13}C NMR (Callet *et al.*, 1987), differential scanning calorimetry (Kitamura *et al.*, 1989), optical rotation and circular dichroism. The order/disorder transitions have been described by many workers in different conditions of temperature (Muller *et al.*, 1988) and salt concentration (Lecourtier *et al.*, 1986). The ordered rod conformation (single or double helix) is stabilised in high ionic strength or at low temperature.

The effect of the sidechain substitution on the geometry of the backbone has been studied by Millane *et al.* (1989) by x-ray fibre diffraction. They demonstrated that the side chain terminal sugar units are not critical determinants of an ordered molecular structure of xanthan.

The transition from the random coil to a higher local order (rod conformation) and further to a long-range ordered network is obtained by decreasing the temperature or increasing the ionic strength or decreasing the shear rate. The last factor could explain the shear thinning property of xanthan.

The two properties of xanthan gum that affect greatly its industrial utilisation are solubility and viscosity in water and salt solution. The order of addition of salt and xanthan is found to be crucial for these two properties and resulted in the definition of a parameter widely used in industry, the 'brine tolerance' of a particular xanthan material which is the ratio between the viscosity of a solution of xanthan in distilled water where salt has been added and the viscosity of a solution of xanthan in a salt solution.

Although xanthan has been investigated more extensively than any other linear polysaccharide, many contradictions over which various parameters are crucial in the ordering process persist in the literature. Furthermore, little is known concerning the behaviour of the material at low water contents, although it is believed that the early stages of the hydration of a biopolymer often have significant effects on the solubility of the material. In addition to 2 other biopolymers, the hydration of xanthan in low water content conditions (up to 1g of water per g of dry solid) and its impact on the degree of order have been investigated in chapter 4.

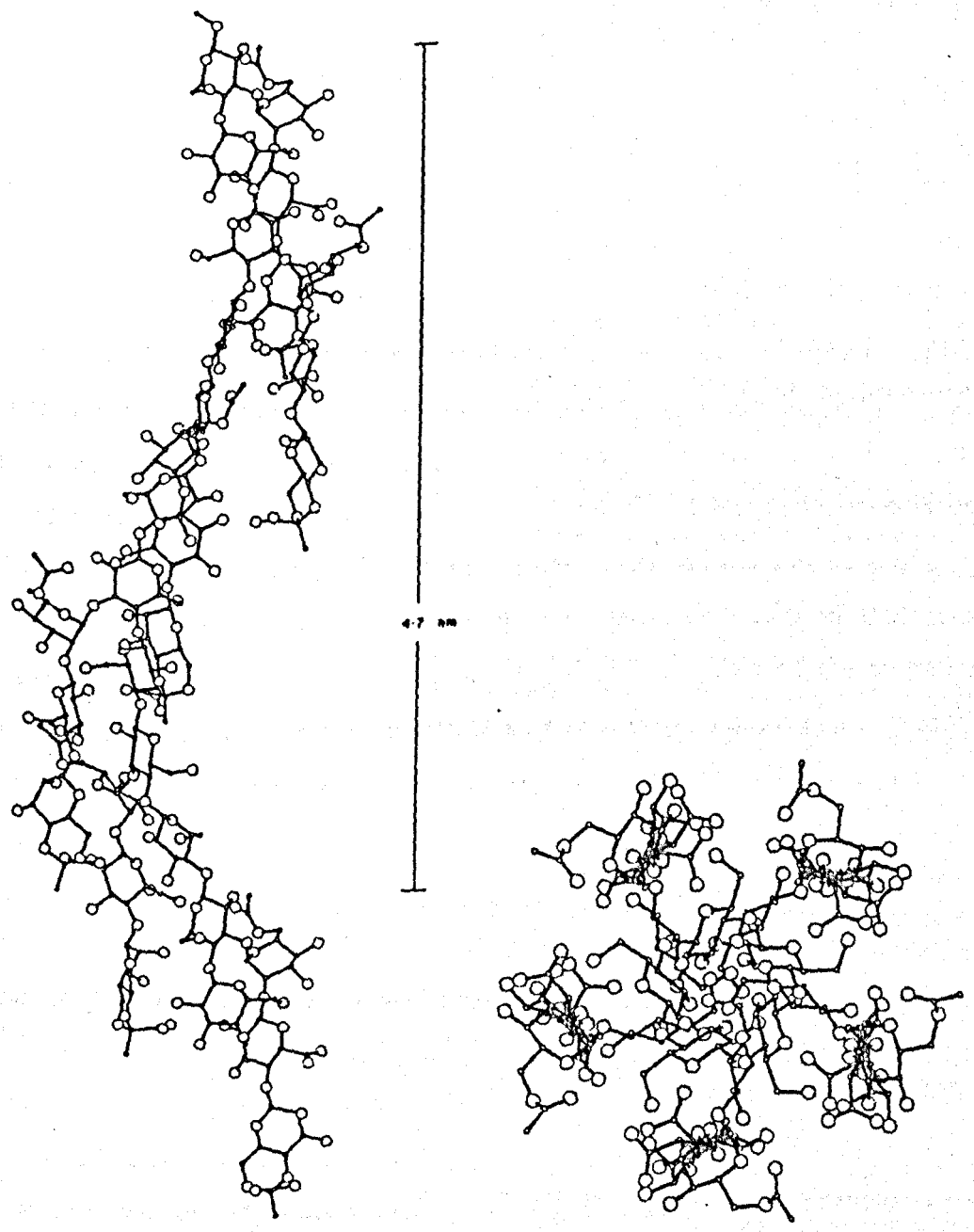

Figure 2.12 Molecular conformation of the ordered (5/1 helix) structure of xanthan (Moorhouse *et al.*, 1977)

a: viewed perpendicular to the helix axis

b: viewed down the helix axis

4. The hydration of biopolymers

4.1 Industrial and scientific relevance

The interaction between water and biomolecules and biomolecule mixtures is of considerable scientific and commercial interest due to the role of water in the stability and functional properties of the main constituents of the majority of food and pharmaceutical systems. Clearly, the hydration behaviour of biopolymers is of great relevance to various important processes such as protein structure, chemical and enzymatic reactivities. Additionally, water is a principal factor in the stabilization and the efficiency of drug delivery systems where biopolymers constitute the matrix or carrier of the active molecules. Consequently, the need for a rational understanding of the hydration properties of biomolecules is increasingly necessary since dried and low moisture foods which are rehydrated subsequently during the cooking or directly through mastication are widely used.

4.2 Effect of hydration on the molecular dynamics

The enhanced mobility of biopolymers with increased hydration levels has been acknowledged unanimously by all the workers active in this field. Several reviews (Gregory, 1995; Rupley and Careri, 1991; Mitchell and Hartley, 1996) have described the effect of water on the dynamics of biopolymers and the implications of this effect on the chemical and biological properties of these biopolymers. Indeed, it is now accepted that molecular mobility is a major factor determining the chemical and biological reactivities which yield in desirable processes such as enzyme activity, Maillard browning and less desirable ones such as microbial growth, bread staling and many other processes leading to the deterioration of food products (Slade *et al.*, 1991).

A schematic representation of the effect of water activity on the relative rate of these

processes is shown by the diagram reported by Labuza (1970) (Fig 2.13).

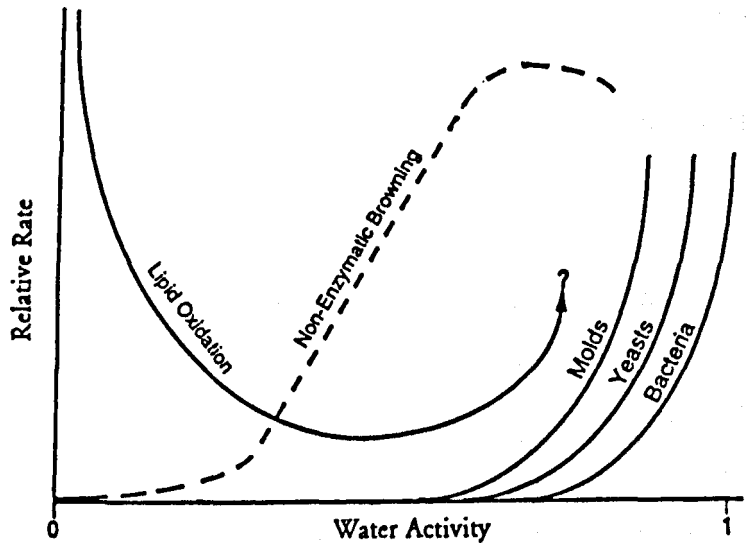

Figure 2.13 Effect of water activity on typical food biopolymer reactions (Labuza, 1970)

Although several workers have warned of the dangers of the uncritical use of a_w (Slade and Levine, 1991; Mustapha *et al.*, 1996 and 1997), they recognized that in practical situations, this diagram provides a reasonably good measure of stability and safety. Indeed, Mustapha used water/glycerol mixtures to adjust the amount of liquid phase and the a_w and thereby demonstrated that molecular mobility is the decisive parameter in defining the rate of Maillard browning and not the water activity.

A better understanding of the role of water on the dynamics of biopolymers is achieved by employing the plasticization theory widely used in synthetic polymer science. Such an approach is developed in detail in the last section of this chapter.

4.3 Effect of hydration on the ordering of biopolymers

There is much evidence to suggest that conformational changes occur in many

biopolymers during the early stages of hydration (Gregory, 1995; Mitchell *et al.*, 1996; Hartley, 1996). One important aspect of the hydration-dehydration process of biopolymers is the hysteresis phenomenon in which sorption and desorption paths are not equivalent in terms of the amount of water incorporated in the sample at a particular relative humidity. Several workers have related hysteresis to the structural modifications occurring during the hydration-dehydration process (Bryan, 1987; Labaki *et al.*, 1991). Bryan (1987) has suggested several models relating these conformational changes to the water sorption. These models were based on the effect of rate of the change of biopolymer conformation relative to the duration of the sorption process.

The increase in the degree of three-dimensional order throughout hydration observed in the majority of cases has been extensively investigated using different spectroscopic techniques. Solid state ^{13}C-NMR studies of lysozyme and BSA have shown that the distribution of conformational states observed in the dry protein becomes much narrower on hydration (Gregory *et al.*, 1993; Kennedy *et al.*, 1990; Hartley, 1996). Belton (1994) has recently reviewed the use of NMR to study protein hydration.

Several workers (Kumosinski *et al.*, 1991 and 1993; Harris *et al.*, 1995) have described the use of FTIR to elucidate the secondary structure of proteins. The frequencies of the amide bands were assigned to individual conformations of the protein, and were subsequently used to probe conformational transitions during the hydration-dehydration of proteins (Prestrelski *et al.*, 1993; Farhat *et al.*, 1996a). The frequency assignment was based upon theoretical calculations performed on synthetic polypeptides (Krimm *et al.*, 1986). Kumosinski *et al.* (1991 and 1993) found a satisfactory correlation between the conformational results obtained by FTIR and those obtained by NMR and x-ray diffraction.

The majority of reported studies considered the mobilization of the biopolymer and its ordering separately. Consequently, an investigation combining the dependent processes of molecular dynamics and molecular order is believed to be of particular interest and is, therefore, attempted in chapter 4.

4.4 Hydration of mixed systems

While, as described in the previous section, a considerable knowledge on the hydration of individual biomolecules has accumulated, little is known about the hydration of biomolecule mixtures and especially about the distribution of water between the individual components in such systems and the resulting effects on the molecular and macroscopic properties of mixed systems. All food and pharmaceutical systems are composed of several components with different molecular and physical properties. Very often the ability to take up water is different for each of the components of the mixture (Fig 2.14). Consequently, it is not unreasonable to believe that different amounts of water are associated with the various components and, therefore, a systematic understanding of the hydration of mixed systems and the differential partitioning of water is increasingly necessary.

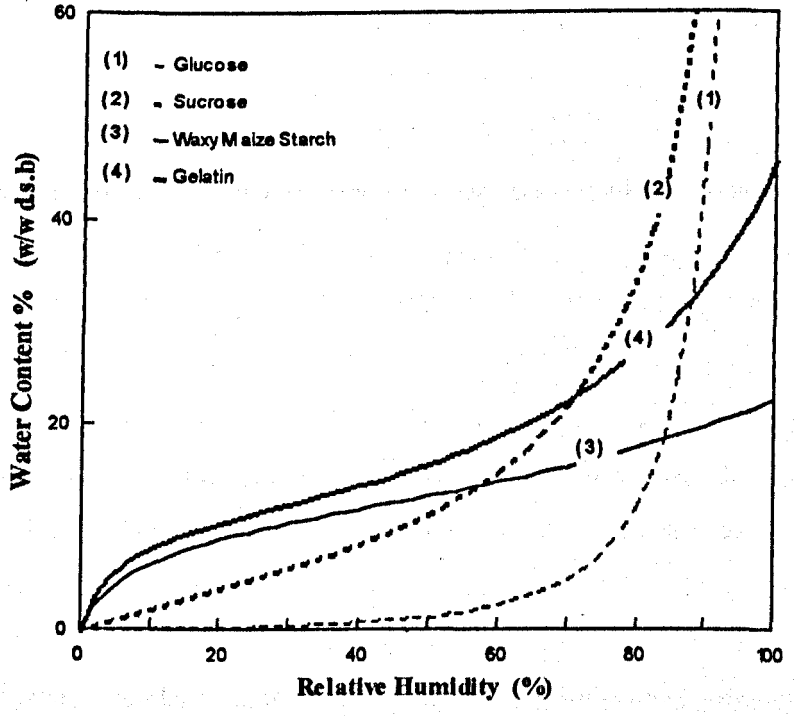

Figure 2.14 Water vapour sorption isotherms (25°C) of amorphous glucose, sucrose (Iglesias *et al.*, 1982), native waxy maize starch amylopectin and pig skin gelatin

The range of spectroscopic techniques commonly used to study the hydration of biomolecules such as NMR, FTIR, x-ray diffraction, etc. could provide valuable information on the hydration of biomolecule mixtures such as biopolymers, biopolymer-sugar, etc. . Useful information concerning the molecular interactions between the various components in biopolymer mixtures using x-ray diffraction has been reported by Hartley *et al.* (1995). Indeed they have optimized the use of the linear relationship between the amount of water associated with starch and its degree of crystallinity as measured by x-ray powder diffraction in order to estimate the unequal partitioning of water in biopolymer mixtures in a semi-quantitative manner. Chinachoti *et al.* (1984 and 1991) employed the sorption isotherms of starch, sugars and salts (molecular and ionic solutes) in order to assess the interaction between the individual components of the biopolymer-solute-water ternary systems and suggested that interactions between the biopolymer and the solute would lead to a smaller water uptake due to the unavailability of some hydration sites on each species. They understandably reported a dependence of such interactions on the a_w which was wrongly ignored by other workers (Kaminski *et al*, 1994; Hartley *et al.*, 1996). The preferential hydration of proteins has been investigated by Kuntz *et al.* (1974). However, the confirmation of the interpretation of their results in terms of preferential partitioning of water needed other sources of information such as NMR, FTIR, etc. as they could not determine the amount of water bound to the protein. Leiras *et al.* (1991) indirectly suggested the preferential hydration of sucrose at high a_w in a starch-sugar mixture when they reported the possible solubilization of sucrose at high a_w values. Such observations were confirmed more systematically in a study describing the hydration of maize-sucrose systems (Farhat *et al.*, 1996b and chapter 4 of this thesis). While NMR can offer a valuable insight to the water distribution between different molecular species assuming identifiable individual chemical shifts, FTIR can also prove to be very useful for the study of systems where proteins are one component since the amide bands can often be readily identified in the mid-infrared spectra.

5. The glass-rubber transition

The glass-rubber transition is of great scientific and industrial significance. Eisenberg (1984), stated that 'the glass transition is perhaps the most important single parameter which one needs to know before one can decide on the application of many non-crystalline polymers'. Slade and Levine (1991) defined a glass as an amorphous supercooled liquid of extremely high viscosity (between 10^{10} and 10^{13} Pa s). A material can form a glass if the crystallization is inhibited by steric hindrance, kinetics, etc.

Although the glass-transition concept has been widely used in the field of synthetic polymers for several decades, it is comparatively recently that the glass-rubber transition theories have been applied to food systems (White and Cakebread, 1966). The development of the polymer science approach for the understanding of the glass-rubber behaviour of food biomolecules was pioneered by Levine and Slade and elaborated in particular, by the series of papers and reviews reported by Levine and Slade (1986, 1988, 1991), Orford *et al.* (1989, 1990), Roos and Karel (1990, 1991), Kalichevsky *et al.* (1992, 1993), Blanshard (1993, 1995), Noel *et al.* (1990).
The realisation that many food systems are not at thermodynamic equilibrium provided a favourable milieu for the development of the approach based on the glass-rubber transition theories to describe the behaviour of food systems (Slade and Levine, 1991). Such an approach places, implicitly, much more emphasis on the dynamics of the various components of the system.

5.1 Molecular mobility in the glassy and rubbery states

Usually the characterisation of the glass-rubber transition has been obtained by studying the discontinuity in the changes in the thermal and rheological properties of a system as a function of sample temperature or composition. However, several workers have

reported similar discontinuities in the various measurable parameters describing the molecular mobility such as NMR spin-relaxation (Kalishevsky *et al.*, 1992a; Ablett *et al.*, 1993), rotational correlation times (Sandrecski *et al.*, 1988; Roozen *et al.*, 1990 and 1991; Le Meste *et al.*, 1991), translational diffusion (Karel *et al.*, 1988, 1991; Ablett *et al.*, 1993), etc. Despite this slight 'discontinuity' in the diffusion behaviour around the glass transition, Ablett *et al.* (1993) reported a considerable diffusion rate for water in pullulan samples even after the system had undergone the rubber to glass transition, i.e was in the glassy amorphous state. Hills *et al.* (1995) demonstrated important translational and rotational mobilities of water in maltose-water glasses. Furthermore, the results reported by Ehrlich *et al.* (1990) showed no abrupt change in the diffusion behaviour of an ESR probe at T_g.

The situation in terms of molecular mobility in the glassy and rubbery states can be summarised as follows: (i) the molecular mobility of the matrix molecules in a system is very reduced in the glassy state, but considerably enhanced in the rubbery state, (ii) the mobility of small, interstitial molecules can be observed in glassy biomolecular systems.

The enhanced stability of food systems in the glassy state is attributed by the majority of the workers active in the field to the reduced mobility below T_g.

5.2 Review of main glass-transition theories

Various theories have been developed to explain the discontinuities in heat capacity, thermal expansion coefficient, compressibility, viscosity, molecular mobility observed during the glass-rubber transition (Fig 2.15). In this section, the basic concepts behind the principal theories are reported. For more details, the reader is advised to consult the reviews by Slade and Levine (1991), Mansfield (1993) and Kalishevsky (1993c).

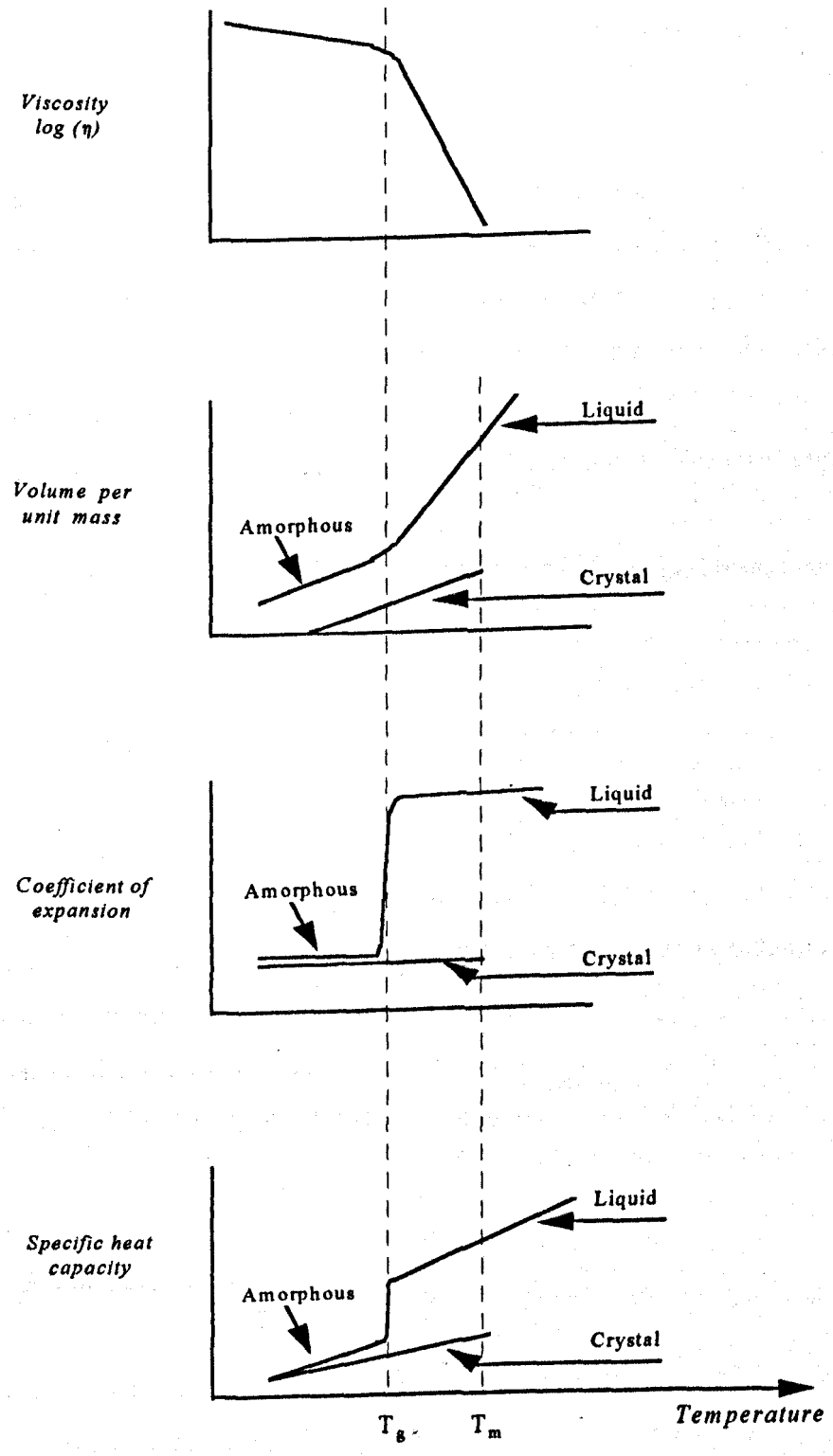

Figure 2.15 Schematic plots of the changes around the T_g of (a) the viscosity, (b) the volume per unit mass, (c) the expansion coefficient and (d) the specific heat in both amorphous and crystalline states (adapted from Allen, 1993 and Blanshard, 1995).

5.2.1 Thermodynamic or entropy theories

The glass transition behaves like a second order transition with discontinuities in the thermal and calorific properties. These theories were developed by Gibbs *et al.* (1956 and 1958) based on Flory's (1953) work. They suggested that the glass transition occurs when the relaxation time of the system, which is controlled by the configurational entropy, exceeds the measurement time scale.

However, this approach has been criticized for various reasons. The most important being that thermodynamic theories assume that the system is at equilibrium although it has now been accepted that the glass transition is a kinetically determined transition.

5.2.2 Free volume theory

If the individual molecules were considered, as a first order approximation, to be spheres, in the glassy state the unoccupied volume or free volume is very reduced. For molecules to change their conformation or their motional state, they must be able to move into the free volume. An increase in the temperature to values above T_g (the rubbery state), yields an increase in the free volume resulting in an enhanced molecular mobility (rotational and translational). This theory can be visualised by the simplified diagrams in Figure 2.16.

5.2.3 Kinetic theories

It is now widely accepted that the experimental determination of T_g depends on the frequency, the heating rate and the sample history. Even the determination of the free volume is performed by kinetically dependent processes such as viscosity or volume expansion.

Instead of attempting a molecular understanding of the glass transition phenomenon, this

approach is based on describing the observed rate dependent behaviour in terms of several relaxation times. For example, Choy *et al.* (1978) used two relaxation time constants, one depending on temperature while the other depended on the structure.

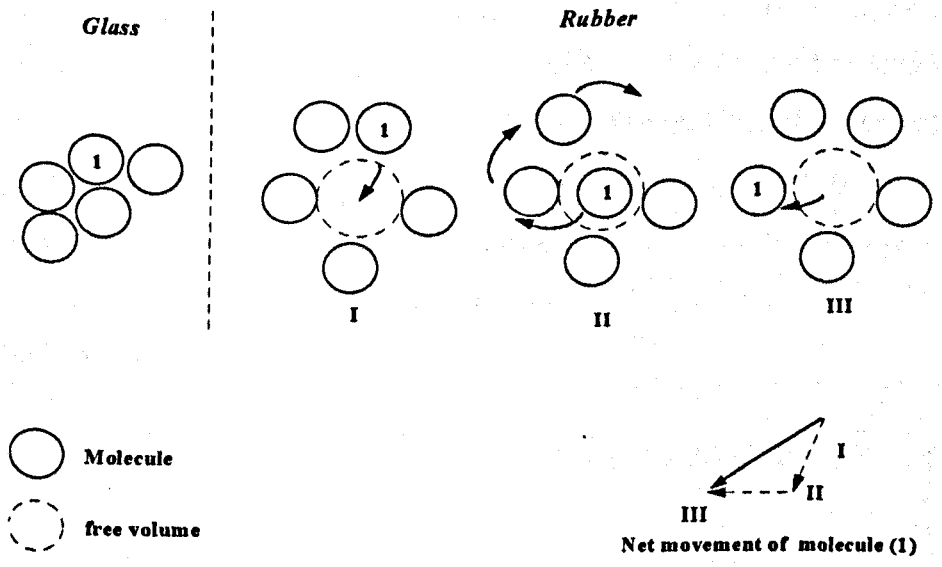

Figure 2.16 Schematic representation of the free volume theory to explain the glass-rubber transition

5.3 The state diagram

A typical state diagram of a small carbohydrate - water system as a function of the concentration (Levine *et al.*, 1986) is shown in Figure 2.17 where increased water contents lead to a decrease in the T_g.

T_g' corresponds to the intersection of the kinetically determined glass curve for homogeneous solute-water mixtures and the non-equilibrium liquidus curve for T_m of ice (Slade and Levine, 1991). The location of the (W_g',T_g') point depends on the solute, and W_g' indicates the maximum amount of moisture in the glass. Slade and Levine suggested

that this amount of water is "rendered unfreezable in a practical time frame" as the water molecules are held in the glass by the extremely high local viscosity (~10^{12} Pa.s) and not by specific binding on the solute. However, as reported earlier, Ablett *et al.* (1993) reported that water diffusion extends into the glassy state despite the overall high viscosity of the system, and therefore, if an amount of water molecules (W_g') is unfreezable, it must be, at least partially, a consequence of specific interactions with the solute. Furthermore, Hyde *et al.* (1991) found that probe molecules must exceed a certain size to be fully coupled into the T_g of the polymer. The mobility of water and other small molecules when the system is in its glassy state can be explained by the use of the free volume theory as the free volume required by a small molecule such as water is negligible compared to the unoccupied space needed by larger solute molecules (especially biopolymers).

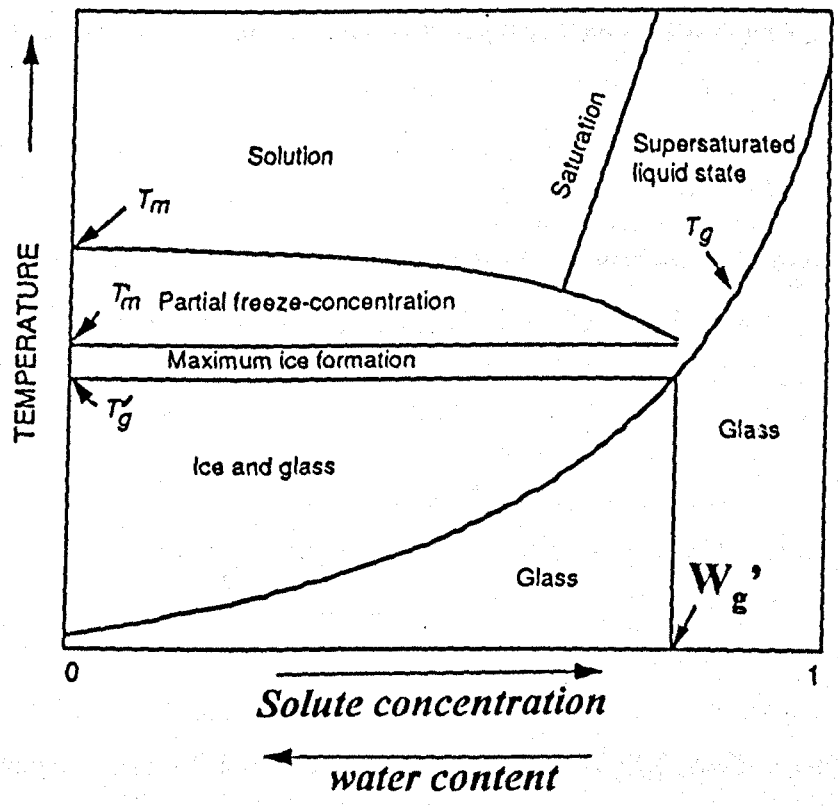

Figure 2.17 Schematic state diagram for an aqueous solution of a hypothetical glass-forming small carbohydrate. (Adapted from Roos *et al.*, 1993)

5.4 Plasticization in multicomponent systems

5.4.1 Definition

In general (with the exception of some antiplasticization cases), the presence of low molecular weight additives reduce the T_g of the system for two reasons: (i) the increase in the free volume and (ii) the reduction of the average molecular weight. The plasticization is only effective where the polymer and plasticizer are compatible.

5.4.2 Plasticization of biopolymers by water and other small molecules

Water is by far the most effective plasticizer of biopolymers due to its small molecular weight and therefore low T_g and its relatively large change in heat capacity (ΔC_p).
Many workers have reported the plasticizing effect of water on small carbohydrates (Orford *et al.*,1990) and several biopolymers (e.g studies by Orford *et al.*,1990; Kalichevsky *et al.*, 1992b and 1993).
Kalichevsky and Blanshard (1992 and 1993) have also studied the combined plasticizing role of water and sugars on several biopolymers including amylopectin, gluten and casein (Fig 2.18).

5.4.3 Prediction of the T_g of multicomponent systems

Since 'real' systems such as food, pharmaceutical and synthetic polymer products usually consist of several components, the prediction of the T_g of a mixed system from the glass-transition temperatures of the individual components is of particular industrial and scientific interest. The T_g of a compatible mixture generally falls between the T_gs of the individual components, except where very strong interactions occur. Examples of

such exceptions were first reported by Lesikar (1975 and 1977).

Although the early work concentrated on predicting the T_gs of polymer mixtures, several models describing the T_g of polymer-diluent systems have been derived. These models were reviewed in some more detail by Kalichevsky *et al.* (1993a)

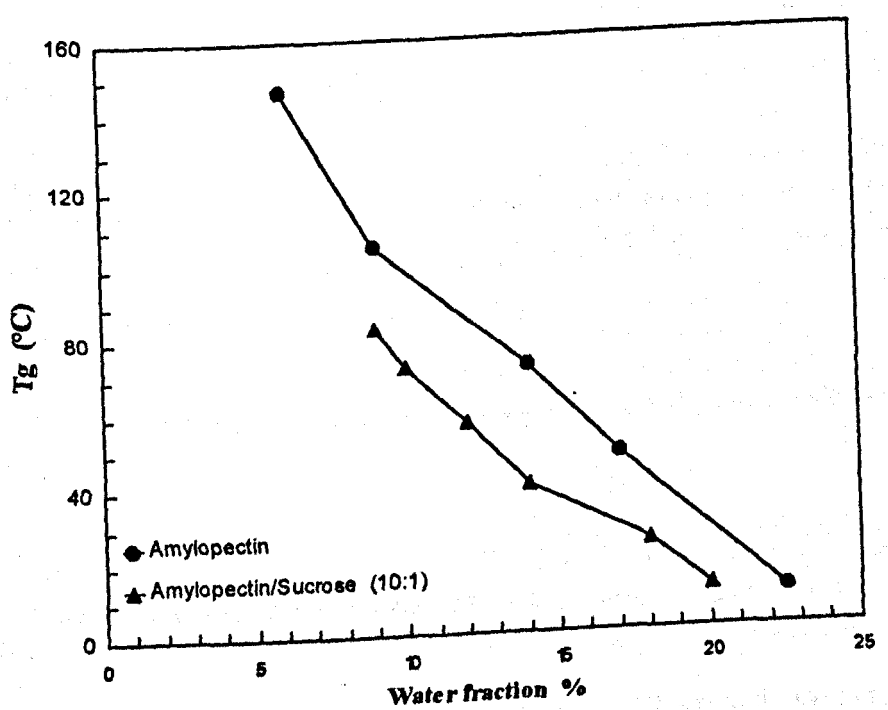

Figure 2.18 Role of water and sucrose as plasticizers of amylopectin. Glass transition results measured by DSC (adapted from Kalishevsky, 1993)

5.4.3.1 Free volume approach

The glass-transition temperature of a polymer-diluent mixture was calculated using the free volume theory (Bueche, 1962) with the general equation

$$Tg = \frac{\sum \Delta\alpha_i V_i Tg_i}{\sum \Delta\alpha_i V_i} \qquad (2.1)$$

where $\Delta\alpha$ is the difference in the volume expansion coefficients above and below T_g, and V is the volume fraction of the component *i*.

5.4.3.2 Thermodynamic approach

Couchman and Karasz (1978) derived an equation to describe the composition dependence of T_g assuming continuity of configurational entropy at T_g, intimate miscibility and no crystallinity or crosslinking.

$$\ln(Tg) = \frac{\sum W_i \Delta Cp_i \ln(Tg_i)}{\sum W_i \Delta Cp_i} \qquad (2.2)$$

Where W_i is the weight fraction of component *i*, and ΔCp is the difference in specific heat capacity between the liquid and the glassy states at T_g.

However, equation 2.2 assumes that ΔCp is independent of temperature. This assumption was found to be not valid by ten Brinke *et al.* (1983) who suggested, to the first order, that ΔCp is inversely proportional to the temperature and therefore derived the following equation:

$$Tg = \frac{\sum W_i \Delta Cp_i Tg_i}{\sum W_i \Delta Cp_i} \qquad (2.3)$$

Kalichevsky *et al.* (1993a) demonstrated clearly that the T_g of biopolymer-water and biopolymer-sugar-water mixtures was best modelled using equation 2.3 .

Materials and Methods

Introduction

This chapter describes the basic concepts of the methodologies used to prepare the various biopolymer-sugar-water systems and of the techniques employed to study the degree of order and mobility in these ternary systems. The format is standard, each section commences with an introduction to the particular method followed by the details of the experimental procedure and parameters adopted.

The two main methodologies of sample preparation described were (i) the isopiestic hydration of dry powders and thin films and (ii) the extrusion cooking of starch and protein sugar water systems.

Nuclear magnetic resonance, Fourier transform infrared and wide angle x-ray diffraction have been used to investigate the physico-chemical behaviour of the mixed systems and also of the individual components in these mixtures. NMR and FTIR provided information on a short distance scale order, while x-ray diffraction was used to assess the degree of long range order (>10nm). NMR techniques were used to provide information on molecular mobility in the system in terms of molecular tumbling and chemical exchange and also on translational motion. The latter was investigated using pulsed field gradient techniques.

Materials

Amylopectin as waxy maize starch was obtained from National Starch and Chemical Co.

Commercial grade, limed pig skin gelatin, 260 Bloom (Batch No : DE1685) and xanthan gum were supplied from Sanofi Bio-Industrie.

Maize grits were donated by Maizecor Foods Ltd. The specifications from the supplier indicated that these samples contained 8-9.5 % protein, a maximum 1% of lipid, and that the starch was composed of approximately 25% amylose and 75% amylopectin.

Fructose, glucose, sucrose and xylose were purchased from Sigma Chemical Co. and were used in the crystalline state. Commercial grade sucrose (British Sugar) was used in the preparation of samples by extrusion as large quantities of raw materials were needed.

Potato starch and other chemicals were purchased from Sigma Chemical Co. (Poole,UK) unless stated otherwise.

In general, the biopolymers contained approximately 10% water (w/w d.s.b) whilst the moisture content of the sugars was less than 0.5%.

Methods

1. Sample preparation

1.1 Hydration

1.1.1 Static hydration

The native or pre-processed materials were dried prior to hydration in a vacuum oven at 70°C for 16 hours. Other investigators have utilised higher temperatures e.g 105°C. This was avoided as there was a concern that samples should not suffer thermal degradation (sugar caramelization, Maillard reaction in protein-sugar sustems, etc.).

A range of moisture contents was then obtained by storing the dried samples in air tight containers over saturated salt solutions for an average of 10 days at 25±1°C as described by Nyquist (1983). The salts used were those reported by Nyquist to give a stable RH

value in the temperature range between 20 and 30°C.

1.1.2 Dynamic hydration

Dynamic, isopiestic hydration was used to hydrate biopolymer films for the FTIR studies, and was achieved by the circulation of air at different relative humidities (RH) obtained by humidifying by passing through saturated salt solutions (Table 3.1).

Table 3.1 Relative humidities (RH) of the saturated salt solutions used in the isopiestic hydration process (at 25°C)

Salt	RH (%)	Salt	RH (%)	Salt	RH (%)
LiCl	11	K_2CO_3	44	NaCl	75
CH_3COOK	22	$NaCr_2O_7$	54	KCl	85
$MgCl_2$	30	$CuCl_2$	67	KNO_3	95

1.1.3 Moisture content

The water contents were defined by drying using a vacuum oven at 70°C until the difference in successive values (2 hours time gap) of the sample weight was less than 1% of the total weight loss. This drying time was typically 16 hours . All moisture contents values are reported on a percentage dry weight basis i.e **g of water per 100 g of total dry solid** (w/w d.s.b). The error on the defined water contents was estimated to be less than ±0.5 %.

The water contents of the gelatin and gelatin-sugar films, used in the FTIR investigation, were difficult to determine accurately in the absence of a microbalance and the Karl-Fischer determination of moisture contents was not reliable. Hence, the amount of water

in a film hydrated to a certain water activity value (estimated by the RH of the hydrating air-water vapour) was assumed to be equal to the water uptake by a freeze-dried gelatin-sugar of the same composition (sugar type and concentration) placed in the same hydrating conditions (RH and temperature).

1.1.4 Sorption isotherm of biopolymers and sugars

The measurement of the water uptake as a function of the water activity or the relative vapour pressure (or relative humidity RH) at a particular temperature yielded the water vapour sorption isotherm.

The sigmoidal isotherms exhibited by most biomolecules can be described using the multilayer sorption BET theory (Brunauer *et al.*, 1938) or the more general GAB (Guggenheim-Anderson-de Boer) model:

$$\frac{W}{W_m} = \frac{c\,k\,x}{(1-k\,x)\,(1-k\,x+c\,k\,x)} \qquad (3.1)$$

Where W_m is the monolayer water coverage, k and c are two constants and $x = P/P_0$ is the relative vapour pressure (P being the experimental water vapour pressure and P_0 the water vapour pressure of pure water at the same temperature).

Although some workers (D'Arcy *et al.*, 1970; Kuntz *et al.*, 1974; Cerofolini *et al.*, 1980) have been critical of the application of the BET theory for the interpretation of sorption isotherms, others (van den Berg, 1985) showed clearly that the GAB equation describes accurately the sorption isotherms of food systems up to values of $x = 0.9$. Furthermore, the models proposed as an alternative to the BET, although based upon different theoretical backgrounds, yield a very similar expression describing the $W = f(x)$ profiles. A point of caution should be made; such models tend to over-parameterize the $W = f(x)$ function with parameters which are difficult to associate with any physical significance.

Figure 3.1 shows the typical sorption isotherms (25°C) obtained by static, isopiestic hydration. The satisfactory correlation between the measured results and the GAB fits is

clear on the plot. The value found for W_m of 0.108 for amylopectin is consistent with that of 0.11 found for starch by van den Berg (1981).

Although the sorption isotherms were used in the interpretation of some results (chapter 4), the full discussion of the significance and suitability of various models is outside the scope of this work.

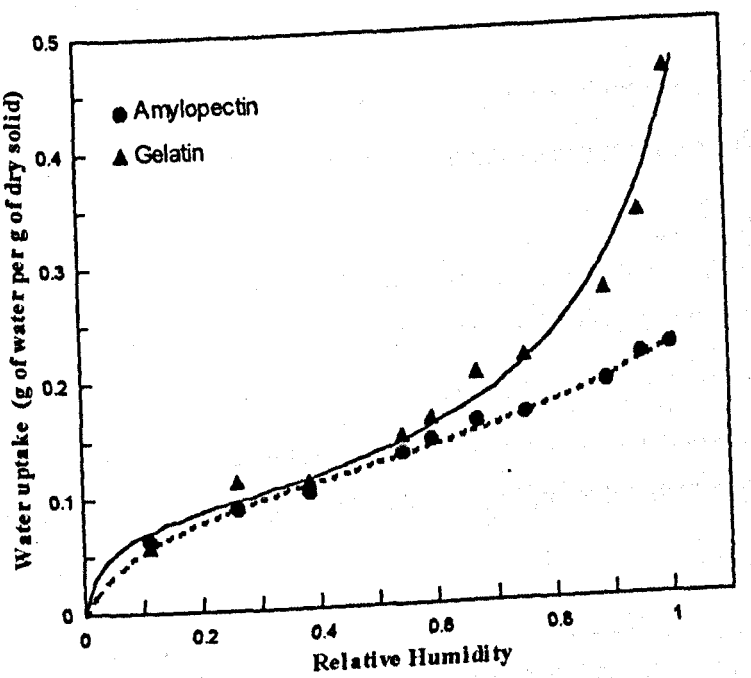

Figure 3.1 Water sorption isotherms of gelatin and amylopectin (25°C). The solid lines represent the GAB fit for the experimental results.

1.2 Extrusion

1.2.1 The extrusion process (Harper, 1981)

Extrusion cooking is now a widely used processing technique in the food as well as other industries for several practical reasons: (i) extruders provide mechanical energy for melting, cooking and texturizing food products, (ii) the final product can be shaped by selecting the appropriate exit dies and, (iii) thorough mixing of the ingredients can be

achieved. Extrusion has been extensively used in the production of pasta, puffed snack foods, and many breakfast cereals, etc.

Different types of extruders can be found. These vary in size, shape and, most importantly, the method of operation. While hydraulic extruders use a piston to force the dough through the die, and roller extruders use two rotating rollers for this purpose, a screw type extruder is based on the rotation of the screw (one or two screws) to drive the melt through the die.

Screw extruders rely on drag flow to move material down the barrel and to develop pressure at the die. The friction of the material against the barrel wall generates heat and the forward motion of the melt.

Twin screw extruders are more efficient than single screw extruders as they offer a narrower residence time distributions and, can be counter or co-rotating. Co-rotating, intermeshing, twin screw extruders offer several advantages relative to other screw configurations, the most important ones being: (i) good mixing properties, (ii) the capability to handle sticky materials such as food ingredients and (iii) the possibility of using high screw speeds.

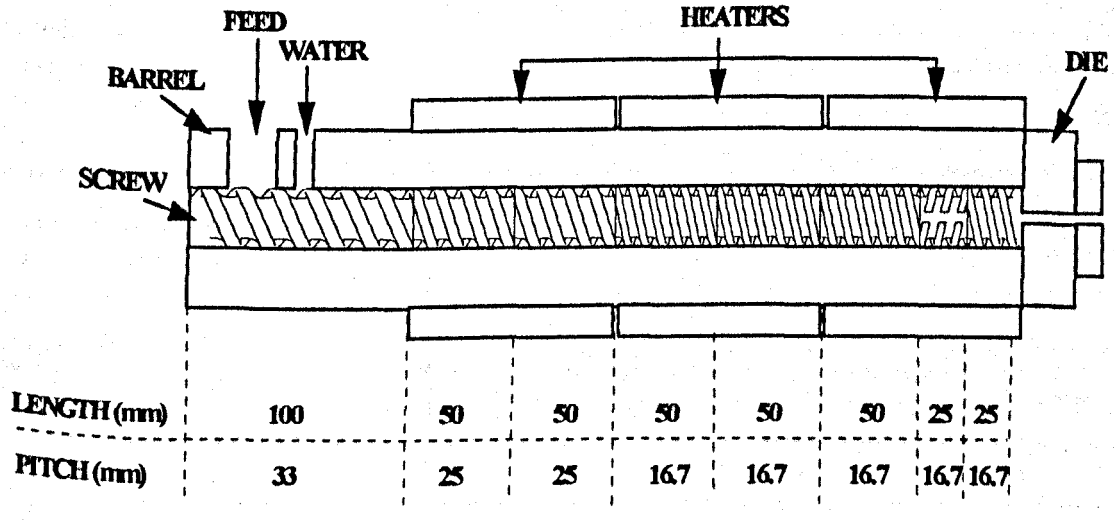

Figure 3.2 Diagram of the main components of a screw extruder (adapted from Melvin, 1996)

1.2.2 Operational conditions

Biopolymer-sugar samples were pre-mixed using a Kenwood Peerless planetary mixer for 1 hour and then extruded using a Clextral BC-21 co-rotating, intermeshing, twin screw extruder. The barrel had four temperature zones (t_1, t_2, t_3 and t_4), a useful length of 40 cm and a 16:1 length to diameter ratio (Fig 3.2).

Different extrusion conditions were used for amylopectin-sugar and gelatin-sugar systems. As the two biopolymers had different structures and hydrophilicity and thus different physical properties (T_g, solubility in water, gelation condition, viscosity, etc.) the optimal extrusion conditions for each biopolymer were different and were as listed Table 3.2 . However, the difference in the operational conditions between amylopectin and gelatin were not significant as no comparison of the effects of the two extruder configurations and parameters was attempted.

Table 3.2 The extrusion conditions used for amylopectin-sugar and gelatin-sugar extrudates

	amylopectin *and* amylopectin-sugar	**gelatin *and* gelatin-sugar**
Temperature profile (°C)		
t_1	40	40
t_2	110	90
t_3	120	110
t_4	80	80
Screw speed (rpm)	300	200
Feed rate of the solid (kg/h)	6	5

A 1 mm x 30 mm slit die was used to produce non-expanded gels. Distilled water was

pumped into the second zone of the barrel to give the desired amount of moisture in the final sample taking into account the moisture content of the raw materials (~10% for the biopolymers and less than 0.5% for the sugars w/w d.s.b). The samples were collected in the form of strips (80 mm length, 25 ± 5 mm width and 1.5 ± 0.5 mm thickness), wrapped in polyethylene films and then sealed in air-tight bags to prevent loss of water. The moisture loss after more than 4 weeks of storage was found to be less than 2%.

The experimental conditions listed above were used for all but one of the systems investigated. Maize grits - sucrose extrudates used in chapter 4 were supplied by Dr J. Fan (Fan, 1994) and were prepared as follows : known amounts of maize and sucrose (0%, 5% and 10% - based on maize grits, % dry basis) were mixed as described above and fed into the extruder at a rate of 11 kg/h. The temperature profile was 40/160/110/170 °C and a single 3.0 mm diameter circular die was used in the die plate. The expanded extrudates had approximately an 18% water content (% wet basis) i.e ~22% water d.s.b. After the extrudates had been cooled to room temperature, they and the raw maize grits were ground to fine powders using a laboratory mill with a 0.5 mm sieve. The powders were dried and rehydrated isopiestically for the NMR and x-ray diffraction studies. This gave a range of moisture contents between 0 and 35 g of water per 100 g of dry solid.

During the extrusion process the barrel temperature, screw speed, back pressure, screw torque and feed rate were monitored by a computer and their values were used for the calculation of the specific mechanical energy as follows :

$$SME \ (J\ kg^{-1}) = \frac{screw\ torque\ (N\ m) \ x \ screw\ speed\ (s^{-1})}{mass\ flow\ rate\ (kg\ s^{-1})} \qquad (3.2)$$

1.3 Film preparation for FTIR

1.3.1 Film casting

Thin films were needed in order to obtain transmission infrared spectra. These films were obtained by drying a known volume of a solution of the components under investigation in controlled conditions. A 1% solution (wet basis) of biopolymer or biopolymer/sugar mixture was prepared in distilled, deionized water. The solution was then stirred very gently for 5-10 minutes in order to eliminate air bubbles. An aliquot 1 ml of this solution was transferred onto a ZnSe window. The window was then dried over P_2O_5 for 2 days. The thickness of the films was estimated to be approximately 25 µm as described below. The volume of the film is given by :

$$V = \frac{m}{d} = l\,S = l\,\pi\,\frac{D^2}{4} \qquad (3.3)$$

Where d is the density (~ 1.5 10^3 kg.m^{-3}), m is the weight of the film estimated from the volume of the solution used: m = 0.01 g, S is the film surface, D the diameter (D=1.85 10^{-2} m) and l the film thickness.

1.3.2 Hydration

The film and the apparatus were dried by the circulation of dry nitrogen for 30 minutes prior to hydration. The film was considered dry when changes in the amplitudes of the water bands (at approximately 3300-3500 and 1630 cm^{-1}) in the FTIR spectrum were of the same order as the experimental spectral noise.

Progressive rehydration of the film was achieved by a flow of air of controlled relative humidity. A range of relative humidities was obtained by bubbling air through different saturated salt solutions. The 'humidified' air was passed subsequently over the sample film which was on a ZnSe window within a controlled atmosphere chamber specifically built for this study.

A hydration time of 60 minutes was found to be optimum for the maximum hydration effect as seen in Figure 3.3. After data acquisition, the air was redirected through the next salt solution (giving rise to a higher RH value).

(a)

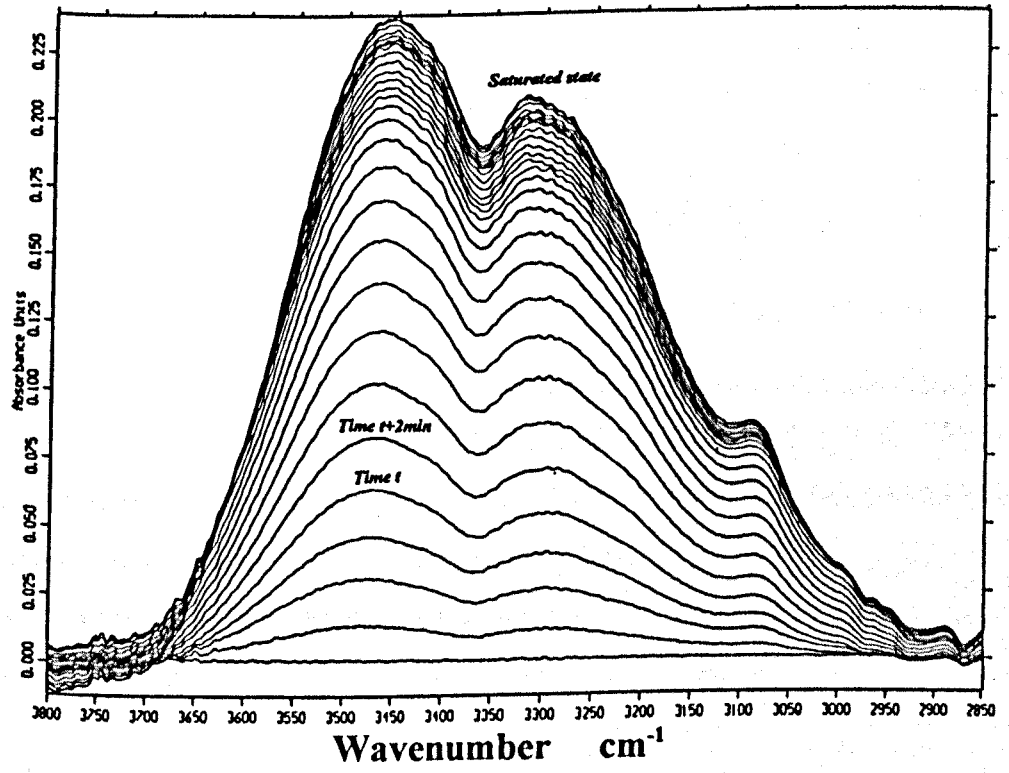

(b)

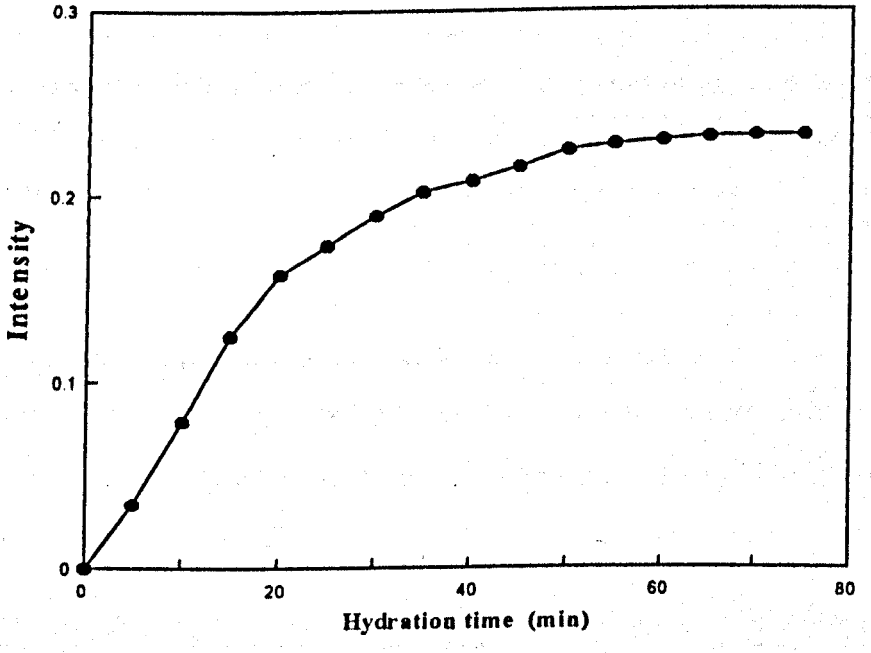

Figure 3.3 Effect of hydration time (RH=100%) on the direct difference FTIR spectrum of a gelatin film. Spectra were recorded at 2 minutes time intervals.

2. Analytical techniques

2.1 Fourier transform infrared spectroscopy

2.1.1 Vibrational spectroscopy

The chemical bonds and the angles between the atoms composing a molecule are not rigid. The molecule thus consists of a set of coupled harmonic oscillators and, if disturbed from its equilibrium state, it will vibrate in such a way that the motion can be considered to be a superposition of a number of simple harmonic vibrations.

A vibrating molecule may interact with electromagnetic radiation of an appropriate frequency. If the radiation has the same frequency as one of the normal modes of vibration, it may be possible for the molecule to absorb the radiation. The energy absorbed will later be lost from the molecule, either by re-radiation or, more usually, by transfer to other molecules in the form of heat energy. An infrared absorption spectrum of a material is obtained simply by allowing an infrared beam to pass through the sample and determining the fraction absorbed at each frequency within some particular range. The frequency at which a band in the absorption spectrum appears is equal to the frequency of one of the normal modes of vibration of the molecules of the sample (Bower *et al.*, 1989).

2.1.1.1 Calculation of vibrational frequencies

The vibrational frequency of an A-B bond can be calculated by Hooke's law, which correlates the frequency with the bond strength and the atomic masses.

$$\nu = \frac{1}{2\pi}\sqrt{\frac{F}{\mu}} \qquad \frac{1}{\mu} = \left(\frac{1}{m_A}+\frac{1}{m_B}\right) \qquad \bar{\nu} = \frac{\nu}{(c/n)} \qquad (3.4)$$

where ν is the frequency (Hz) and $\bar{\nu}$ is the wavenumber (cm^{-1}), F the force constant of the bond, μ the reduced mass of the vibrator, m_A and m_B the atomic masses, c the velocity of light (~3 10^{10} cm s^{-1}) and n is the refractive index of the medium ($n_{air} \approx 1$) (Colthup *et al.*, 1990).

Molecules with large assemblages of atoms possess many vibrational frequencies. Indeed, for a non-linear molecule with N atoms, the number of vibrational modes is (3N-6). The six degrees of freedom subtracted from the total of 3N translational degrees of freedom of N atoms are the degrees of freedom of the undistorted molecule, i.e. the translations and rotations of the whole molecule parallel to or about three mutually perpendicular axes. Each of the different vibration modes may give rise to a different absorption band, often causing bands to overlap. In principle, the system is coupled but, to the first order, many of the observed bands may be associated with the vibration of atoms in identifiable bands.

Quantum theory applies and therefore vibrational energy can only increase by quantum jumps, so that the energy difference between successive vibrational levels is $\Delta E = h\nu$.

2.1.1.2 Infrared absorption

In order to 'observe' an absorption band the particular vibration should produce a fluctuating electric dipole. In the simplest picture, each atom carries an effective fractional charge which depends on the nature of the atoms to which it is bonded. An electric field acting on these charges causes a distortion of the molecule and, in so doing, causes a change in the net electric dipole momentum of the molecule. The electric field (E) of the incident radiation varies sinusoidally with frequency. If the frequency of E coincides with the frequency of a suitable mode, this mode can be set into resonant vibration and the radiation will then be absorbed (Fig 3.4).

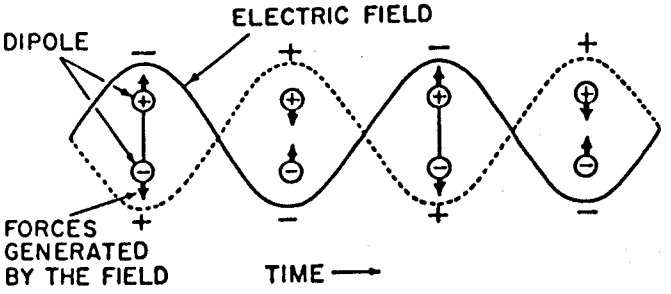

Figure 3.4 Forces generated on a dipole by an oscillating electric field (Colthup *et al.*, 1990)

2.1.1.3 Factors influencing vibrational frequency and intensity

a. Frequency

The vibrational frequency of a bond is expected to increase when the bond strength increases, and also when the reduced mass of the vibrator decreases. Many factors influence the precise frequency of a molecular vibration but it is often impossible to isolate one effect from another. These can be mesomeric, inductive, mass, angle, conformational effects or effects due to the solvent, to intra-molecular hydrogen bonding, vibrational coupling or Fermi resonance.

b. Intensity

The intensity of a vibrational absorption band depends principally on the dipolar moment of the bond. Thus, highly dipolar bonds such as O-H, C-O, C=O, N-H, C-N in biopolymers generate large absorbance values. For example, the carbonyl and amine bands are dominant in the infrared spectra of proteins.

Any modification of the dipolar moment of a bond by means of perturbation of the charge distribution would affect frequency and have a great effect on the band intensity.

c. *Example : Effect of hydrogen bonding on the infrared absorbance by amide bands*

The amide bond responsible for the linkage of successive amino acids to form peptides and proteins illustrates well the effects of intramolecular (in the secondary structure) or intermolecular (with H_2O through hydration) hydrogen bonding.
The amide bands, and more importantly the amide 1 and 2 bands, of the infrared spectrum of peptides and proteins provide a valuable source of information about the 3-dimensional structure of such molecules and the effects of hydration as reported by Krimm *et al.* (1986), Kumosinski *et al.* (1993), Tanfani *et al.* (1995) and many others.

- The amide 1 and 2 bands:

The amide 1 band occurs at frequencies between 1690 cm^{-1} and 1630 cm^{-1}, the exact figure depending on the secondary structure of the polypeptide (Krimm *et al.*, 1986; Kumosinski *el al.*, 1993). The absorption is generated primarily from the stretching vibration of the C=O bond (~80%). The so-called amide 2 band, appearing in the 1570-1540 cm^{-1} region, is due to a combination of the bending of the N-H band (~40%) with the C-N stretching vibration (~60%) (Fig 3.5-a).

- Effect of hydrogen bonding:

The C=O and N-H groups constitute hydrogen bonding sites as illustrated by Figure 3.5-b. The consequence of hydrogen bonding is a perturbation of the electronic distribution i.e the dipolar moments and the force constants of the various bonds and angles, leading to measurable effects on the frequencies (equation 3.4) and intensities of the amide 1 and 2 bands. While an increase of the intensities of both bands is anticipated as a result of the enhanced electric dipolar moments, the frequency shifts are a little more complex to predict.
For the amide 1 band, a shift to lower wavenumbers is anticipated as a result of the combined effects of the decrease of the force constant of the C=O bond (bond strength),

plus an increase in the reduced mass of the C-O vibrator as it is coupled with H-O. In contrast, the amide 2 is expected to shift to higher wavenumbers as the force constant of the C-N bond is enhanced both by an increased 'stiffness' of the H-N-CO angle due to the 'immobilisation' of H through hydrogen bonding and the increased strength of the C-N bond.

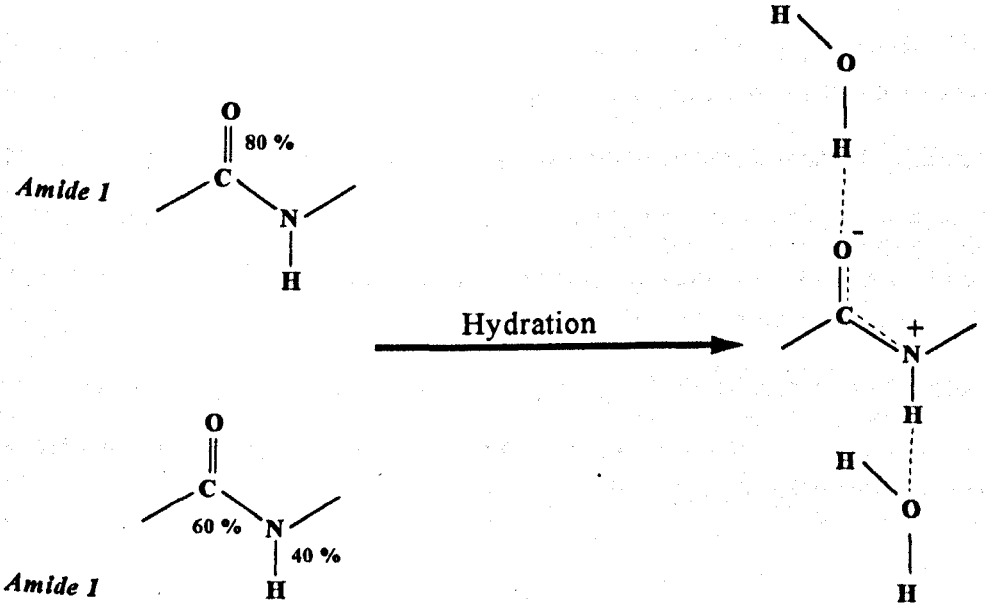

Figure 3.5 The amide 1 and 2 bands (a) before and (b) after association with water by means of hydrogen bond.

2.1.2 The FT spectrometers in infrared spectroscopy

There are two main types of infrared spectrometers depending on the manner in which the infrared frequencies are handled. In contrast to the dispersive instruments in which the infrared light is separated into its individual frequencies using a grating monochromator, in the interferometric instruments all the frequencies are allowed to interact with the sample to produce an interference pattern, and this pattern is then analysed mathematically using a Fourier transform (FT) to determine the individual frequencies and their intensities.

Dispersive infrared spectrometers suffer from several disadvantages such as (i) low sensitivity as most of the light is lost in the narrow focussing slits, (ii) speed, since the acquisition of a spectrum takes several minutes and, (iii) wavelength accuracy.

2.1.2.1 Interferometric infrared spectrometer

The principle of the Fourier transform infrared spectrometer is based on the interferometer first perfected in 1887 by Albert Michelson which can be described by reference to Figure 3.6. Monochromatic light *F* from the source strikes the beam splitter, which is designed to split the incident beam *F* exactly into two halves. One is transmitted as beam *F2* to a plane mirror *M2* and reflected back to the beam splitter; the other half is reflected as beam *F1* to another plane mirror *M1*, where it is reflected back to the beam splitter. Both beams are then recombined as beam *R* which passes through the sample compartment and is finally focussed on the detector.

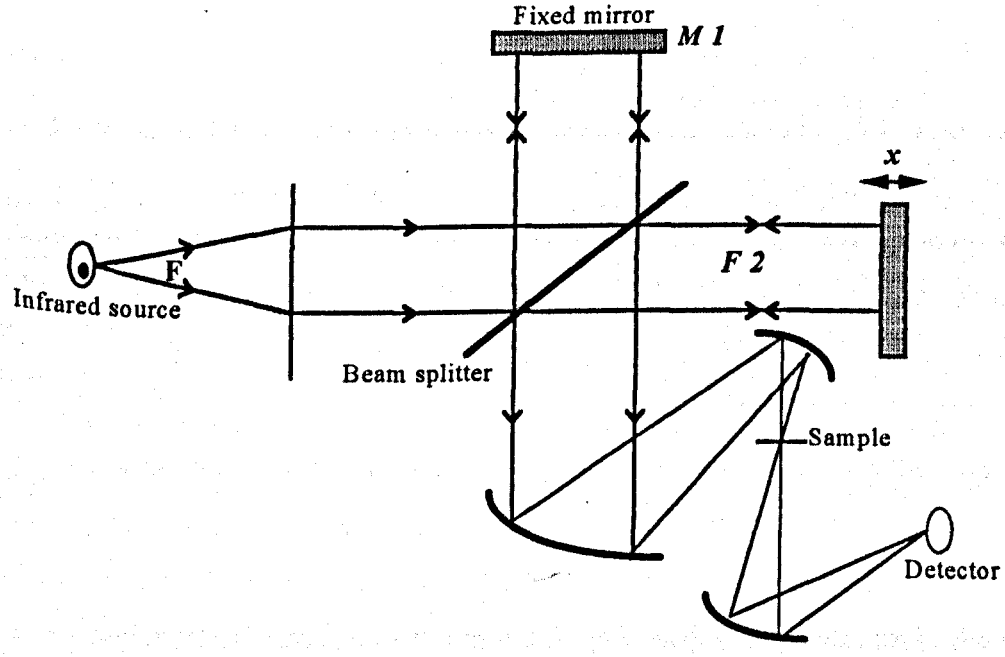

Figure 3.6 The Michelson interferometer at the centre of the FTIR spectrometer.

Whilst the mirror (*M2*) is fixed at a distance *L* from the beam splitter, *M1* is not fixed at the same position *L* but can be moved very precisely back and forward around *L* by a distance *x*. Thus when *F1* and *F2* recombine again on the beam splitter they exhibit a path length difference or optical retardation of $2x$, i.e the partial beams are spatially coherent and will interfere when they recombine. The quantity actually measured by the detector is thus the intensity $I(x)$ of the combined infrared beams. This will be a function of the moving mirror displacement *x*, and represents the so-called interferogram.

The interferometer produces and recombines the two wave trains with a relative phase difference, depending on the mirror displacement. These partial waves interfere constructively, yielding maximum detector signal, if their optical retardation is an exact multiple of the wavelength, i.e. $2x = n\lambda$ ($n = 0, 1, 2,...$). In contrast, minimum detector signal and destructive interference occur if $2x$ is an odd multiple of $\lambda/2$.

The resultant intensity, seen by the detector at a frequency ν, is given by the equation 3.5 where δ is the difference in the optical path between *F2* and *F1* i.e $2x$

$$I(\nu , \delta) = \frac{I_0(\nu)}{2} [1 + \cos(2 \pi \nu \delta)] \qquad (3.5)$$

This relationship is useful for practical measurements, because it allows precise tracking of the movable mirror. In fact, all modern FT-IR spectrometers use the interference pattern of the monochromatic light of a He-Ne laser to control the change in optical path difference. The wavelength of the red light of the He-Ne laser used for continuous spectrum calibration is 632.8 nm and corresponds to 15804 cm^{-1}.

When polychromatic radiation passes through the interferometer, as is the case during the recording of infrared spectra, the intensity measured for any value of path difference is the integral of the above expression (equation 3.5).

The Fourier transformation of the integral $I(\delta)$ yields the spectrum in the frequency domain $I(\nu)$. In addition to the high wavenumber accuracy and the high sensitivity, FT-IR offers other advantages such as high speed. The measuring time in FT-IR is the time needed to move the mirror over a distance proportional to the desired resolution. As the

mirror can be moved rapidly, complete spectra can be measured in fractions of a second enabling the acquisition of a considerable number of scans in order to improve the signal/noise ratios in highly absorbing samples.

2.1.1.2 Source and detector

The source of the infrared radiation is a heated rod of ceramic material (~1300 °C).

Thermal detectors based on pyroelectric materials or on solid state semiconductor devices based on photovoltaic or photoconductive principles are the most widely used detectors. Pyroelectric detectors are less sensitive than thermocouples but have a considerably faster response and this makes them particularly suitable for the use in FTIR spectrometers. Pyroelectric substances, such as deuterated triglycerine sulfate (DTGS) or lithium tantalate (LiTaO3), are used at room temperature. Crystals of these highly polar materials exhibit an electric polarization along certain axes, and if, for example, they are heated in one area by an incident infrared radiation, the changes in the crystal lattice in this area will lead to an imbalance of polarization with respect to the rest of the crystal. This imbalance which is proportional to the infrared intensity is measured by connecting electrodes to the different faces of the crystal.

2.1.2.3 Sampling techniques

FTIR offers a variety of sampling procedures depending on the physical state (solid, liquid or gas) and form (solution, thin film, powder, etc.) of the sample under investigation. The most commonly used sampling methods in polymer science are:

- *Transmission mode :* the beam travels through the sample which is often in the liquid/solution state. Thin films can be also used. The sample is located inside a specific

cell made of a material transparent in the mid-infrared region (ZnSe, CaF_2, KBr, etc.)

- *Attenuated total reflectance* (ATR) : suitable for liquids and some gels. A small volume of sample is placed onto the surface of a ZnSe cell. Infrared light entering the crystal at a particular incidence angle (typically 45° or 60°) is reflected along the interior of the crystal. However, each time the infrared radiation impinges on the crystal-sample interface, the beam partially penetrates the sample which coats the surface where it is partially absorbed, and carries spectral information as it is reflected back.

- *Diffuse reflectance infrared Fourier transform* (DRIFT) : often used to study powders. A particular arrangement of mirrors eliminates much of the specular radiation reflected on the surface of the particles. The diffuse reflectance radiation, which is transmitted through at least one sample grain, contains all the structural information.

- *Infrared microspectroscopy:* the coupling of a microscope to an FTIR spectrometer permits an infrared microanalysis in transmission and reflection modes. FTIR micro-spectroscopy has found several applications in mapping sample compositions, for example, to study phase separated systems.

2.1.3 Experimental conditions

FTIR spectra of gelatin-sugar films were obtained using a Bruker IFS 48 infrared spectrometer controlled by a PC running the OPUS 2.0 software and equipped with a DTGS detector operating at room temperature. The spectra were obtained between 4000 and 650 cm^{-1} with a spectral resolution of 4 cm^{-1} from the FT of 100 scans (with the exception of the results monitoring the hydration kinetics (Fig 3.3) where only 16 scans were acquired). The spectrometer was operated in a temperature controlled laboratory at 22°C±2. Water vapour and CO_2 were minimized by means of continuous purging of the sample compartment with a dry air flow.

Spectra were acquired using both the **standard direct** mode where the background spectrum was recorded with no sample in the spectrometer, and the **direct difference** mode described by Poole *et al.* (1982) where the background spectrum was measured on the dry sample. The direct difference method allows the subtraction of the spectrum of the dry sample prior to the Fourier transform.

At each relative humidity step during the dynamic hydration of the gelatin-sugar films, after waiting for hydration to equilibrate (~ 60 minutes), both the standard and the direct difference mode spectra were recorded by loading the specific background spectrum acquired with and without sample respectively, prior to hydration, and these were saved on the PC storage disk as shown in Figure 3.7. This procedure possesses the advantage that the identical sample is used and the identical position of the sample examined.

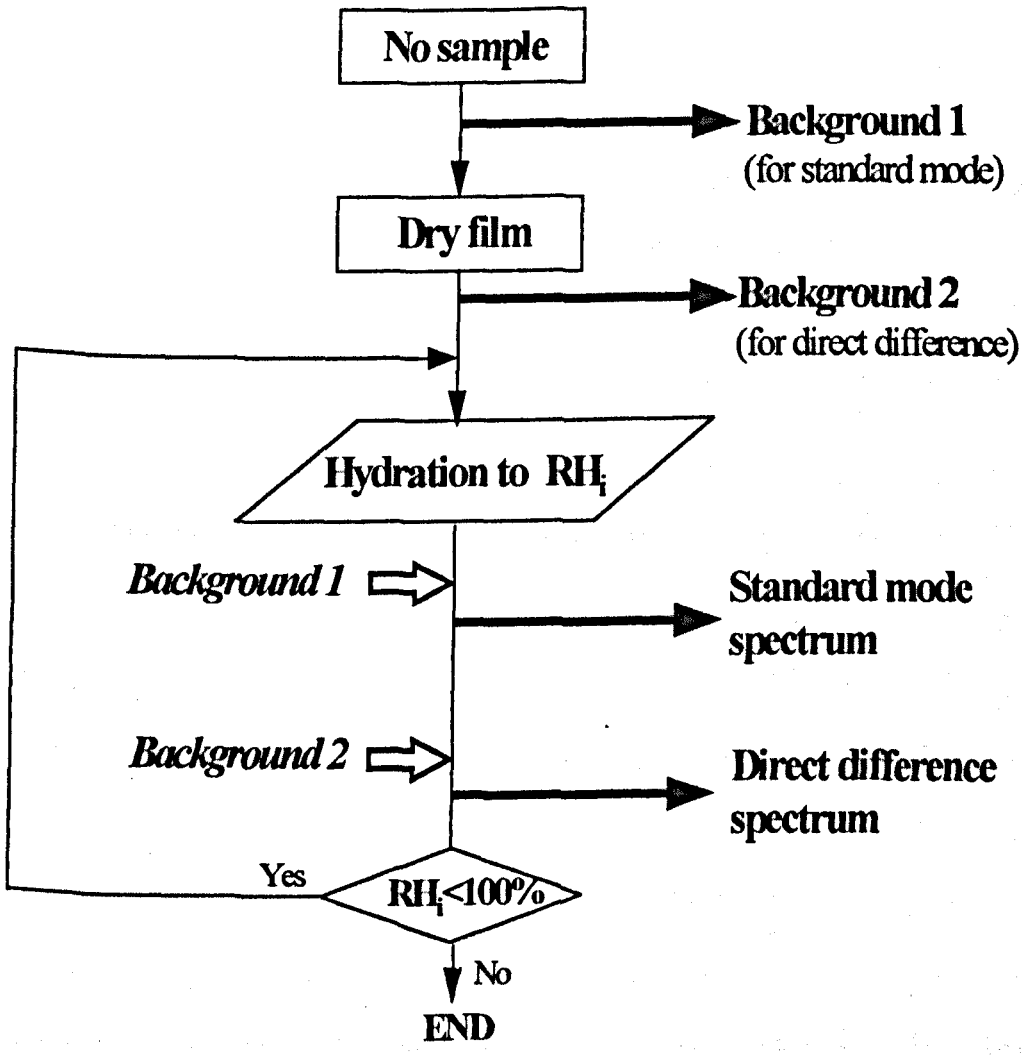

Figure 3.7 Flow chart illustrating the experimental procedure for the acquisition of both standard mode and direct difference FTIR spectra during the hydration of gelatin-sugar films. The full arrows pointing to the outside of the chart indicate acquired data whilst the shallow arrows pointing to the inside indicate data loaded from the storage disk.

2.2 *Nuclear Magnetic Resonance*

Since the first published work on nuclear magnetic resonance by Bloch *et al.* (1946) and Purcell *et al.* (1946), NMR has become the single most widely used spectroscopy as a consequence of the wealth in information that the technique provides on various systems at the molecular level. Although the elucidation of molecular structures constitutes the largest share of the use of NMR, important dynamic information about molecular mobility can be obtained directly or indirectly (spin-relaxation, MRI, diffusion and flow, etc.).

2.2.1 *Theoretical background* (Harris, 1983; McBrierty *et al.*, 1993)

The nuclear spin (I) of atoms with an odd mass number is a half-integer. The nuclear magnetic momentum μ is given by :

$$\mu = \gamma p = \gamma \hbar \sqrt{I(I+1)} \qquad (3.6)$$

where γ is the magnetogyric ratio of the specific nuclei, p is the spin angular momentum and $\hbar$ Planck's constant ($\hbar$=1.055 x 10^{-34} J.s).
In the absence of a magnetic field the energy of a nucleus is independent of the quantum number m_I, but when a magnetic field of a strength B_0 is applied, the energy of the magnetic moment μ is given by $E = \mu B_0$.
There are then $(2I+1)$ non-degenerate energy levels, each of them corresponding to a value of m_I separated by $|\gamma \hbar B_0|$. Transitions between these levels are determined by the Bohr frequency condition :

$$\Delta E = h \nu = |\gamma \hbar B_0 \Delta m_I| \qquad (3.7)$$

These transitions are governed by the selection rule $\Delta m_I = \pm 1$ and $\hbar = h/2\pi$. Thus the frequency is given by :

$$\nu = \frac{\gamma}{2\pi} B_0 \qquad (3.8)$$

2.2.1.1 The Larmor precession

An alternative approach is to consider the classical theory describing the motion of a magnetic moment in a uniform magnetic field B_0. In the magnetic field B_0, the magnetic moments μ tend to align themselves in the same direction as B_0. However, due to the quantum restrictions described previously, in the case of a spin ½ (^1H, ^{13}C, ^{19}F, etc.) they will be distributed on 2 cones as shown in Figure 3.8. As B_0 exerts a torque on the component of μ perpendicular to its direction (z), μ will precess around B_0 on these two cones.

The angular velocity of the precession is given by $\omega = -\gamma B_0$ and thus the frequency also called the Larmor frequency is given by the same expression as equation 3.8 .

2.2.1.2 The magnetization

The total magnetic moment of a molecular species is also called magnetization M ($M = \sum \mu_i$).

In the absence of any magnetic field, $M = 0$, since the individual magnetic moments (μ_i) are randomly oriented. When B_0 is applied, these individual magnetic moments adopt the 'parallel' (lower energy) and the 'anti-parallel' positions on the cones described earlier. The difference between the populations (Fig 3.8) of these two states is given by the Boltzmann distribution :

$$\frac{n_L}{n_U} = \exp[-\frac{\Delta E}{k\ T}] \qquad (3.9)$$

As $\Delta E << k\,T$ and $n_L + n_U = N$

$$\Delta n = n_L - n_U = N \frac{\Delta E}{2\,k\,T} \qquad (3.10)$$

where N is the total number of nuclei, n_L and n_U are the numbers of spins in the lower (+½) and upper (-½) energy states respectively, T is the temperature and k the Boltzmann constant (k=1.38 10^{-23} $J.K^{-1}$).

$$M_0 = \Delta n\ \mu = \frac{1}{4} N (\gamma\ \hbar)^2 \frac{B_0}{k\,T} \qquad (3.11)$$

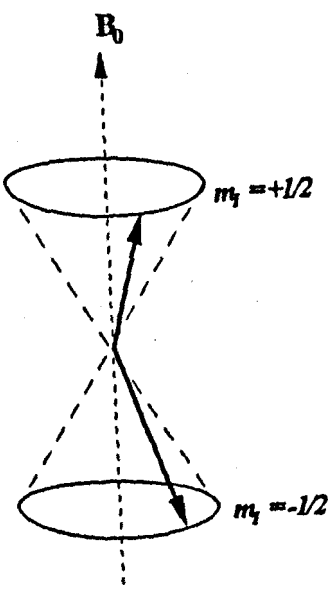

Figure 3.8 The precessional cones of a spin ½ in a magnetic field B_0

2.2.1.3 Spin relaxation - the Bloch equations

The Bloch equations describe, in a macroscopic classical manner, the lineshape e.g the molecular dynamics in a simple spectrum (The description of complex spectra requires the use of spin Hamiltonian). Equation 3.12 describes the motion of a magnetic moment in a magnetic field B:

$$\frac{dp}{dt} = \mu\ B \qquad (3.12)$$

Multiplying both sides of the equation by γ

$$\frac{d\mu}{dt} = \gamma \frac{dp}{dt} = \gamma \mu B \qquad (3.13)$$

Which is equivalent to equation 3.14 describing the macroscopic magnetization

$$\frac{dM}{dt} = \gamma M B \qquad (3.14)$$

Bloch assumed that the perpendicular and parallel components of M decay to M_0 exponentially with different time constants:

$$\frac{d}{dt}M_z = -\frac{M_z - M_0}{T_1} \qquad \frac{d}{dt}M_x = -\frac{M_x}{T_2} \qquad \frac{d}{dt}M_y = -\frac{M_y}{T_2} \qquad (3.15)$$

where M_x, M_y and M_z are the components of the magnetization M, T_1 and T_2 the longitudinal and the transverse relaxation times respectively.

In the NMR experiment, on the application of a small rf field B_1, the magnetic field experienced by the sample is $B = B_1 cos(\omega t) - B_1 sin(\omega t) + B_0$ and equation 3.15 becomes :

$$\frac{d}{dt}M_x = +\gamma(B_1 \sin \omega t\, M_z + B_0 M_y) - \frac{M_x}{T_2}$$

$$\frac{d}{dt}M_y = -\gamma(B_0 M_x + B_1 \cos \omega t\, M_z) - \frac{M_y}{T_2}$$

$$\frac{d}{dt}M_z = -\gamma(B_1 \cos \omega t\, M_y + B_1 \sin \omega t\, M_x) - \frac{M_z - M_0}{T_1} \qquad (3.16)$$

These equations can be simplified if they are re-expressed in a frame rotating at the frequency of B_1 (Fig 3.9).

The NMR signal recorded in a particular direction (often in the *x-y* plane) after the perturbation (B_1 rf pulse), called also free induction decay (FID), is studied directly (time

domain) or after Fourier transform (frequency) giving the classical NMR spectrum.

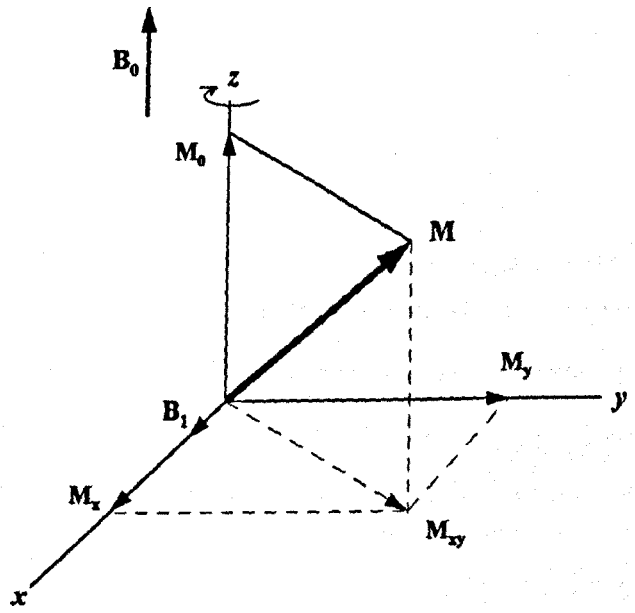

Figure 3.9 The magnetization M as described in the rotating frame

2.2.2 The spin-relaxation

2.2.2.1 Relaxation times

The use of short rf pulses enables the net magnetization M to be placed in any chosen direction. After this perturbation, the equilibrium is restored through relaxation mechanisms.

While the relaxation following a 180° pulse takes place purely by a spin-lattice mechanism (equation 3.17), transverse relaxation is responsible for the relaxation following a 90° pulse (assuming a homogeneous B_0) usually in an exponential manner (equation 3.18)

$$M_z(t) - M_0 = [M_z(0) - M_0] \exp(-\frac{t}{T_1}) \qquad (3.17)$$

$$M_y(t) = M_0 \exp(-\frac{t}{T_2}) \qquad (3.18)$$

2.2.2.2 Spin-relaxation and molecular dynamics

Spin-spin and spin-lattice relaxation are influenced by the mobility of the molecules containing the resonant nuclei. This is summarized in Figure 3.10 describing the behaviour of T_1 and T_2 in the case of isotropic motion characterized by a time constant τ_c; τ_c is the so-called correlation time which is the average time for a molecule to progress through 1 radian (Harris, 1983). When τ_c is much less than the reciprocal of the resonance frequency

$$\frac{1}{T_1} = \gamma^2 B_{0[x]}^2 J(\omega_0) \quad \textit{and} \quad \frac{1}{T_2} = \frac{1}{2 T_1} + \frac{1}{2} \gamma^2 B_{0[z]}^2 J(0) \qquad (3.19)$$

where $B_{0[x]}$ and $B_{0[z]}$ are the root mean square average components of an isotropic random local field B_0 in the x and z directions respectively. J is the spectral density given by:

$$J(\omega) = \frac{2 \tau_c}{1 + \omega^2 \tau_c^2} \qquad (3.20)$$

The presence of anisotropy or distributions of rates of motion complicates the NMR responses. The inhomogeneity of the field and the variability of the magnetic susceptibility introduce additional effects. Another source of complication is the occurrence of exchange between chemically shifted sites. Diffusion through different fields over the period of the NMR experiment also exerts an influence.

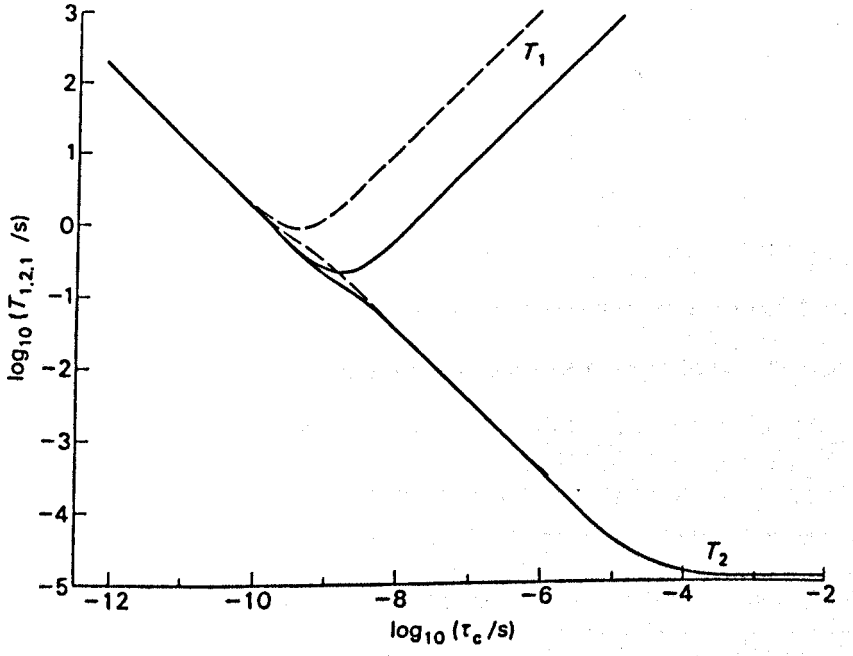

Figure 3.10 The dependence of T_1 and T_2 on the correlation time τ_c as calculated by Harris (1983) for $\nu_0 \approx 100$ MHz (solid line) and 400 MHz using a value of 0.2 mT for the root mean square random field.

2.2.3 *Pulsed Field gradient*

Stejskal and Tanner (1965) recognized that magnetic field inhomogeneity could be utilized to investigate the translational mobility of nuclear spins. Indeed, they devised a technique based on the use of a time-dependent field gradient and, later, Tanner *et al.* (1968) applied pulsed field gradient technique to study restricted self-diffusion in colloidal systems.

Nuclei are magnetically 'labelled' by applying a field gradient which phase codes the spins. The phase is then 'decoded' by a second field gradient pulse equivalent to the first one in width and amplitude. The motional history between the coding and the decoding gradients is probed by the study of the magnetization echo.

The details of the measurements of self-diffusion coefficients using pulsed field gradient NMR techniques are discussed subsequently in this chapter.

2.2.4 *Solid state NMR*

In liquids, rapid molecular tumbling and diffusion average out the direct dipolar coupling between nuclear magnetic moments; this phenomenon is often referred to as motional narrowing. In solids however, these interactions are not averaged to zero as a consequence of the reduced molecular motion. In crystalline solids, the observed NMR spectrum depends upon the orientation of the crystal and the study of the spectrum for different orientations yields information on the anisotropy. Powder samples can be considered as comprising a collection of crystallites at all orientations and yield a powder pattern spectrum. Although solid spectra are of interest, they do obscure some of the NMR parameters of great interest in both solid and solution state NMR, such as chemical shifts. The most commonly used method to obtain solid state spectra with enhanced chemical shift resolution is the 'magic angle spinning' technique (MAS).

2.2.4.1 The Magic Angle

The dipolar interaction between two nuclei i and j has the form :

$$\frac{\mu_i \mu_j}{r_{ij}^3} [3\cos^2\beta_{ij} - 1] \qquad (3.21)$$

where β is the angle between the r_{ij} vector and the magnetic field B_0. The broadening resulting from the dipolar interaction can be reduced if the factor $(3\cos^2\beta - 1)$ is nil e.g when $\beta=54.74°$ (the 'magic angle').

2.1.4.2 Sample spinning (MAS)

However, in solids, a particular nuclear magnetic dipole is coupled to a number of neighbours and, if the vector r_{ij} of one particular pair is at the magic angle relative to B_0 the other pairs usually are not. This problem can be overcome by spinning the sample rapidly (e.g few kHz).

If the sample rotation occurs about an axis situated at the angle θ from B_0, the angle β will exhibit a time dependence and so will the dipolar interaction (Fukushima *et al.*, 1981; McBrierty *et al.*, 1993). The resulting time dependence of β between the two extrema $\beta=(\theta-\alpha)$ and $\beta=(\theta+\alpha)$ is complex for any arbitrary values of θ and β. However, it can be readily demonstrated that the following relationship holds between the average value of $(3\cos^2\beta - 1)$ and the equivalent expressions for the angles α and θ (Harris, 1983):

$$< 3 \cos^2 \beta - 1 > = \frac{1}{2} (3 \cos^2 \theta - 1) (3 \cos^2 \alpha - 1) \qquad (3.22)$$

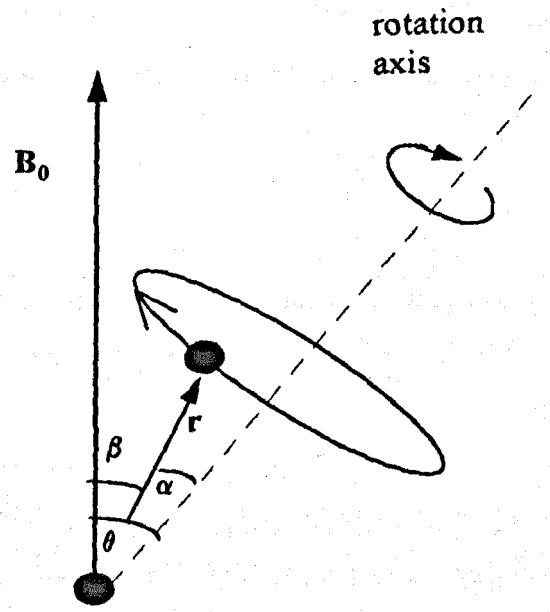

Figure 3.11 Spinning the sample about the magic angle (MAS).

The value of α is fixed for a rigid solid though, if the material is a powder, α and β can take all possible values. The value of θ can be selected by the operator. If a value of $\theta = 54.7°$ is chosen, equation 3.22 yields a nil value for $\langle 3\cos^2 \beta - 1 \rangle$ for all orientations. Consequently, the dipolar interaction is averaged to zero, eliminating the dipolar line broadening and therefore, increasing the spectral resolution (Fig 3.11).

2.1.4.3 Cross-polarization (CP)

The line broadening described above is only one of many difficulties faced during studies of dilute spins such as ^{13}C and ^{15}N. ^{13}C presents sensitivity related difficulties due to its isotopic natural abundance (1%) and its relatively small magnetogyric ratio (γ_{13C}=6.7283 10^7; γ_{1H}=26.7519 10^7 rad T^{-1} s^{-1}). Moreover, multiple pulse techniques are not always efficient as the spin-lattice relaxation times are often very long. These difficulties have been largely overcome by the optimization of magnetization transfer from the abundant ^1H to the^{13} C spins. This process known as cross polarisation is achieved by double irradiation. A 90° pulse is applied in the ^1H channel and the magnetization is spin-locked in the *y* direction of the rotating frame. The rf pulse is then applied in the ^{13}C channel (Pines *et al.*, 1973) and the amplitude of the B_1 (^{13}C) is adjusted to meet the Hartmann-Hahn (Hartmann *et al.*, 1962) matching condition :

$$\gamma_{(1_H)} B_{1_{(1_H)}} = \gamma_{(13_C)} B_{1_{(13_C)}} \qquad (3.23)$$

This energy transfer provides an additional relaxation pathway for ^{13}C. As protons usually have a T_1 shorter than ^{13}C, this leads to a shorter ^{13}C T_1, allowing the use of multipulse sequences and more scans to be acquired and therefore better signal/noise ratios.

In the CP experiment, it is important to optimize the contact time, particularly for polymers which have a relatively short $T_{1\rho}(^1H)$.

Better cross-polarization is achieved in rigid systems. Consequently in biopolymer systems where a range of molecular mobilities exist (for example in partially crystalline

materials), the spectra recorded using the CP-MAS methods usually illustrate the rigid solid components in these heterogeneous (in terms of mobility) systems.

2.2.5 *Experimental procedures*

2.2.5.1 ^{1}H spin-relaxation measurements

Proton relaxation experiments were performed using a Bruker bench top Minispec PC120 (Bruker Spectrospin Ltd.) operating at a resonance frequency of 20 MHz and a temperature of 40±0.1°C. The spectrometer was equipped with phase-sensitive and diode (magnitude) detectors and an 8 mm diameter probe. The Minispec was operated by a PC which ran pulse programmes especially developed for each application with automated phase cycling procedures and captured the recorded experimental results for subsequent calculation.

The real and imaginary components of the magnetization along the x and y axis were recorded and the component M in the x-y plane was then calculated:

$$M_{xy} = (M_x^2 + M_y^2)^{1/2}$$

The low resolution spectrometer used had several technical limitations such as a long dead time between the rf pulse excitation and data acquisition (10 μs), only a limited number of data points can be recorded (169 points) and a slow digitizer (minimum dwell time of 30 μs) and thus, when used directly, provided little information about the fast decaying component (T_2<40μs) of the FID.

This last limitation was partially overcome by the use of a special pulse programme, the 'interleaved-FID'. The free induction decays of 10 consecutive experiments with data points recorded at complementary times were merged enabling a 'virtual' dwell time of 2 μs for the time range between 10 and 20 μs, 4 μs between 20 and 40 μs, 10 μs for times up to 240 μs and finally a dwell time of 30μs for the remaining data points.

2.2.5.1.1 *Spin-spin relaxation* (T_2)

a. Free Induction Decay

The FID recorded after a 90° rf pulse on a sample is usually described by one or more exponential decay processes :

$$M_{xy}(t) = \sum M_{0\,i} \exp[-(\frac{t}{T_{2\,i}})] \qquad (3.24)$$

However, the results were found to be better described as a Gaussian decay. This was attributed to the Gaussian random distribution of the spins in solids where the dipolar interactions dominate the spin-spin relaxation process. The more mobile component of the FID was also believed to be Gaussian shaped as the field inhomogeneity was thought to be Gaussian. Thus equation 3.25 was used to model the free induction decay results.

$$M_{xy}(t) = \sum M_{0\,i} \exp[-(\frac{t}{T_{2\,i}})^2] \qquad (3.25)$$

The FID was conveniently described by two components: a rapidly decaying component with decay times (T_2 solid) of a few tens of μs and a slowly decaying component with decay times (T_2 liquid) of a few hundreds of μs. However, the protons in the complex biopolymer-water and biopolymer-sugar-water systems are anticipated to belong to a 'continuous' distribution in terms of mobility and consequently T_2.

The decay rate of the 'liquid' FID component may contain information on the dynamics of the molecules generating the signal. In a pure liquid, the decay rate may well be determined by the inhomogeneity of the magnetic field over the sample volume. However, for the samples studied in this project, the decay rate of the 'liquid' FID component was generally greater than that expected from the field inhomogeneity. There was also a dependence upon temperature and composition suggesting a relationship to

molecular mobility.

b. Spin-echoes

In addition to the transverse relaxation process, the loss of magnetization in the *x*-y plane as described by the FID is due to field inhomogeneities yielding a distribution of Larmor frequencies ν_0. This would lead to a dephasing of the magnetization vectors of that fraction of the nuclei described in a frame rotating at the mean Larmor frequency. Consequently the T_2 value calculated directly from the FID (T_2^*) is an underestimate of the 'real' T_2.

The problem of field inhomogeneities is often overcome using the spin-echoe pulse sequence where a train of refocusing 180° pulses is employed to rephase the magnetization vectors as shown in Figure 3.12-a . The recorded signal and the pulse program are shown in Figure 3.12-b . The top of the echoes is then treated with equation 3.24 where $t = 2n\tau$ (τ is the spacing between the $90°_x$ and the $180°_y$ pulses).

2.2.5.1.2 *Spin-lattice relaxation* (T_1)

The measurement of T_1 is very often performed using the 'inversion-recovery' pulse sequence since the 180° pulse is followed purely by spin-lattice relaxation, as stated earlier (Harris, 1983). The signal can then be monitored at any point in time by 'flipping' magnetization into the *x-y* plane by a 90° pulse where the FID can be recorded as previously described (Fig 2.13).

The pulse sequence is typically 180° - τ - 90°- acquisition of FID, where the FID is recorded for several spacing times τ (typically 20 values). The amplitudes of the FID recorded at 11 and 71 μs were used to describe the T_1 of the rigid (y_{11} - y_{71}) and the mobile (y_{71}) components respectively. These amplitudes recorded for different τ values were modelled using the equation:

$$M_{xy}(\tau) = \sum M_{0\,i}\,[1 - 2\,\exp(-\frac{\tau}{T_{1\,i}})] \qquad (3.26)$$

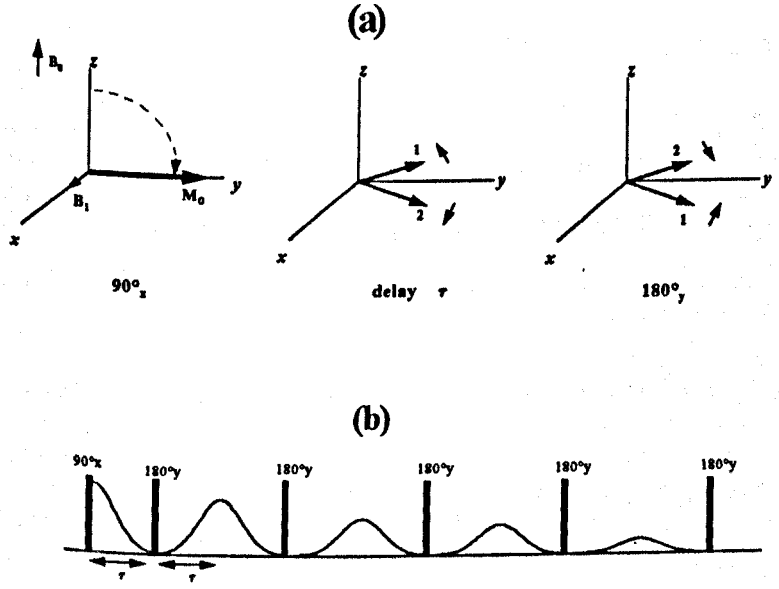

Figure 3.12 The spin-echo pulse sequence :
(a) the magnetization in the rotating frame
(b) the pulse sequence and the recorded NMR signal

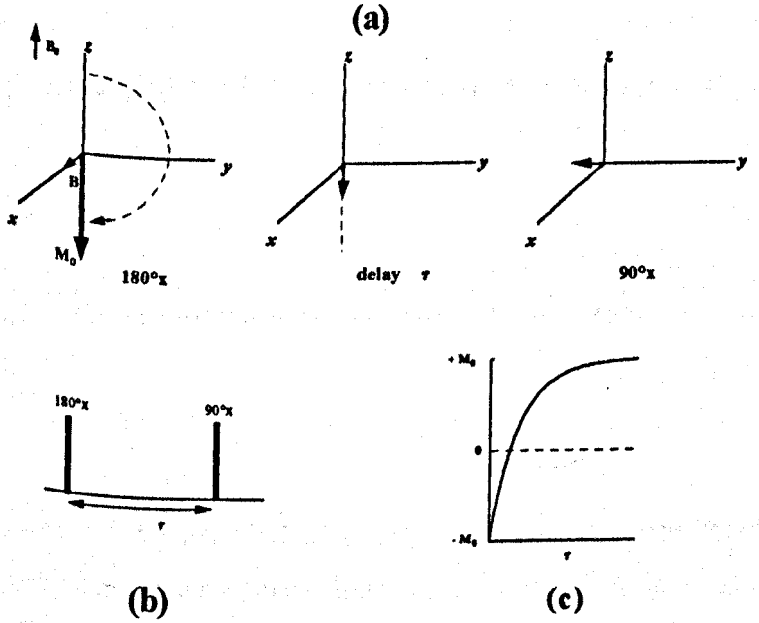

Figure 3.13 Measurement of T_1 by inversion recovery :
(a) The magnetization in the rotating frame (for a particular pulse spacing τ value)
(b) The inversion recovery pulse sequence
(c) The recorded results (1 point per experiment)

2.2.5.2 Pulsed Field gradient ^{1}H NMR

2.2.5.2.1 *Spin-echo technique (PFG-SE)*

The pulse sequence is the typical spin-echo $90°_x - \tau - 180°_y$ sequence described in the previous sections with two pulsed gradients applied in the *z* direction after the 90° and after the 180° pulses. The pulse sequence is therefore $90°_x - t_1 - G_z - t_2 - 180°_y - t_1 - G_z$ where $t_2 = \tau - (t_1 + \delta)$ and δ is the width of the field gradient pulse (Fig 3.14).
The intensity of the signal (top of the echo) recorded at 2τ is given by the following equation (Stejskal *et al.*,1965; Peshier *et al.*, 1993; Packer, 1996)

$$A(2\tau) = A(0)\exp(-\frac{2\tau}{T_2}) \exp[-\gamma^2 G^2 \delta^2 D(\Delta - \frac{\delta}{3}) - \frac{2}{3}\gamma^2 G_0^2 D\tau^3]$$

$$x \quad \exp[-\gamma^2 G G_0 \delta D(t_1^2 + t_2^2 + \delta(t_1 + t_2) + \frac{2}{3}\delta^2 - 2\tau^2)] \qquad (3.27)$$

This can be used in the following simplified form by replacing T_2 by T_2^*, the spin-spin relaxation time reduced by the field inhomogeneities G_0

$$A(2\tau) = A(0)\exp(-\frac{2\tau}{T_2^*}) \exp[-\gamma^2 G^2 \delta^2 D(\Delta - \frac{\delta}{3})] \qquad (3.28)$$

2.2.5.1.2 *Stimulated-echo technique (PFG-StE)*

While the spin-echo technique relies on spin-spin relaxation processes (T_2), the stimulated echo pulse sequence depends more on the T_1. The use of the PFG-StE method is particularly appropriate for systems with $T_2 << T_1$, e.g for samples with relatively low moisture contents.
In PFG-StE pulse sequence, after the first 90°, a second 90° pulse stores the

magnetization along the z axis for a time $(\tau_2 - \tau_1)$ during which relaxation takes place through a spin-lattice (T_1) process. A third 90° pulse brings the magnetization back into the x-y plane where it is recorded.

The simplified equation for the amplitude of the echo is similar to equation 3.28 (Stejskal *et al.*,1965; Peshier *et al.*, 1993)

$$A(2\tau) = A(0)\exp[-(\frac{2\tau_1}{T_2^+} + \frac{\tau_2-\tau_1}{T_1})] \exp[-\gamma^2 G^2 \delta^2 D(\Delta - \frac{\delta}{3})] \qquad (3.29)$$

In practice, for both techniques, the amplitude of the echo is measured for different gradient amplitudes (G) or different gradient width values (δ) and the diffusion coefficient D is then obtained from the slope of a plot of the echo attenuation (relative to the amplitude where no gradient is applied) versus G^2 or versus $\delta^2(\Delta-\delta/3)$ as shown for a sucrose solution in Figure 5.1 in chapter 5.

$$Ln(R) = Ln\frac{A(2\tau)_G}{A(2\tau)_{G=0}} = -\gamma^2 G^2 \delta^2(\Delta - \frac{\delta}{3}) D \qquad (3.30)$$

2.2.5.2.1 *Operating conditions*

A 20 MHz (^{1}H) Bruker bench top Minispec NMS120 (Bruker Spectrospin Ltd.) operating at a temperature of 40 ± 0.1°C was used. The samples were sealed in 8 mm diameter NMR tubes and held at constant temperature for 20 minutes in the spectrometer probe-head. Typically 8 scans were accumulated with optimum recycle delays ranging from of 1 to 10 seconds depending on the T_1 of the particular system investigated. The standard deviations on the measured D/D_0 values were found to be smaller than 0.04 in the spin echo technique and smaller than 0.09 in the case of the stimulated echo technique.

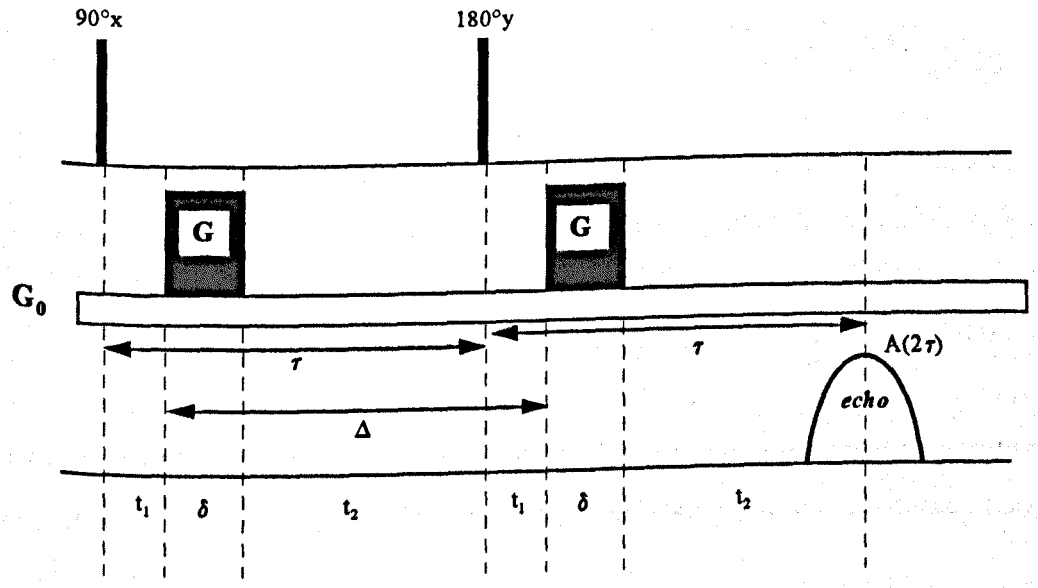

Figure 3.14 Pulsed field gradient spin-echo (PFG-SE) pulse sequence (adapted from Packer K.J, 1996)

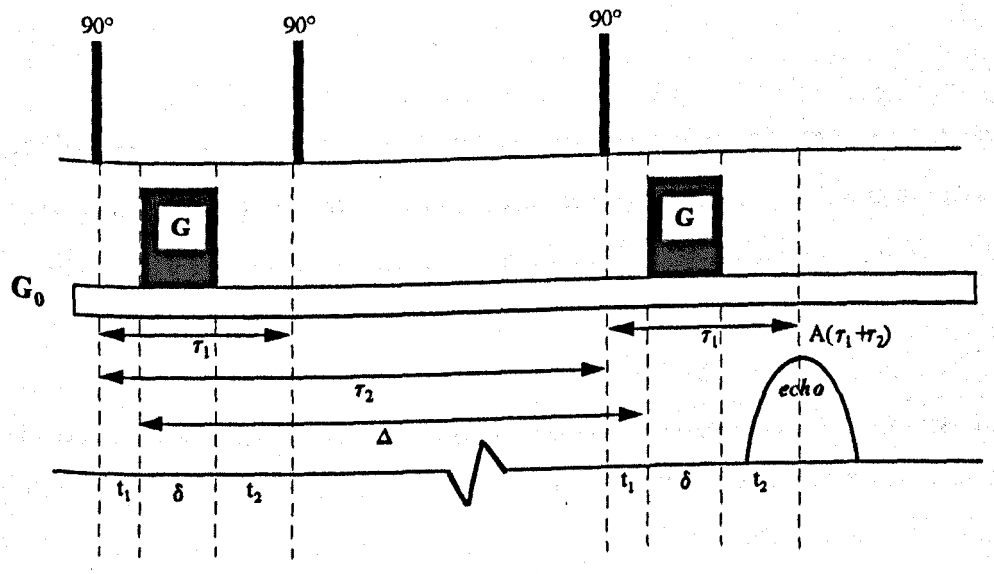

Figure 3.15 The stimulated echo sequence (PFG-StE) for measuring the self-diffusion coefficient (adapted from Peschier *et al.*, 1993)

2.2.5.2.1 *Experimental procedure* $\ln(R)$ vs G^2 or $\ln(R)$ vs $\delta^2(\Delta-\delta/3)$

The NMS120 spectrometer, although a new model had several technical limitations such as: (i) long field gradient switching times, limiting to a minimum value of 4 ms for τ in the PFG-SE or τ_1 for the PFG-StE, (ii) manual dialling of the field gradient amplitude leading to difficulties in obtaining reproducible values of G, and limiting the possibility of automated procedure and, (iii) due to software reasons, the measurements on water (standard) and the sample had to be done with the same operational conditions (gain setting, number of scans, recycle time, etc.) which were found often to be inadequate simultaneously for both systems.

While the limitation of long switching times could only be overcome by the use of an appropriate biphasic power supply accompanied by shielded field gradients which were not available on the spectrometer employed for these study, the other limitations were fully or partially resolved as described below.

A pulse program where the gradient width (δ) was changed and D was obtained from the slope of the plot $\ln(R)$ versus $\delta^2(\Delta-\delta/3)$ was used. This enabled full automation of data acquisition and the use of a fixed value of G, thereby avoiding errors due to the G manual manipulation of the gradient amplitude. Furthermore, relative self-diffusion coefficients were used rather than absolute values. Measurements were carried out for distilled water (D_0) and for the sample under investigation in the optimal conditions (optimum gain setting but with the same pulse separations, gradient separation, width and amplitude) and D/D_0 was obtained from the ratio of the gradients of the lines representing $\ln(R)$ as a function of $\delta^2(\Delta-\delta/3)$ (chapter 5 - Fig 5.1).

Moreover, rather than measuring only the signal amplitude at 2τ (or $\tau_1 + \tau_2$ in the case of PFG-StE), the pulse program enabled the recording of the entire echo. Subsequently, the maximum of the echo was found regardless of its position in time, and used to calculate D. This last procedure was used to avoid errors in the echo amplitude due to slight missetting of the balance of the two gradient pulses which cause shift of the echo. The pulse programs were written using Bruker's EXSPEL compiler while all analysis programs (including those used for the relaxation time analysis) were developed in Pascal.

2.2.4.3 ^{13}C solid state experiments

^{13}C cross-polarization and Fourier transform magic angle spinning (CP and FT-MAS) experiments were carried out at a temperature of 300 K using a Bruker CXP 300 operating at at ^{13}C frequency of 75 MHz with spinning speeds of 3 kHz. Proton and carbon 90° pulses of 5 μs were used. The optimum contact time for the CP-MAS was found to be 1 ms. Chemical shift values are quoted relative to adamantane (tricyclodecane) which was used as an external standard. An average of 4000 scans was accumulated; Gaussian line broadening (0 to 20 Hz) was applied. No attempt was made to eliminate the spinning side bands.

2.3 Wide angle x-ray diffraction

X-ray diffraction has become an important tool in the study of polymers as a result of the ability of the techniques to distinguish between ordered and disordered states. While amorphous systems produce x-ray patterns of a diffuse nature, crystalline systems on the contrary yield well defined, sharp x-ray diffraction features.

The scattering of x-rays of a given wavelength by matter takes place when the x-ray impinges on the electrons in the atom which then become secondary emitters of x-rays. The major part of the energy of scattering goes into coherent scattering having the same wavelength and phase as the incident x-ray. Because the electrons are not concentrated at a single point, the x-rays scattered coherently by the various electrons within an atom are out of phase with each other to an extent that depends on the scattering angle 2θ (Alexander, 1969).

The study of x-ray diffraction for scattering angles 2θ smaller than 3° is referred to as small angle x-ray scattering while wide angle scattering deals with 2θ angles up to 180° (often less than 90° for the study of polymers). In the next section, the basic principles and typical examples of wide angle x-ray are developed as the technique based on small angle scattering is outside the scope of this work.

2.3.1 *Bragg's law*

The relationship between the interplanar spacing d between scattering centres (atoms), the angle of deviation of the diffracted rays from the incident x-rays 2θ and the x-ray wavelength λ is given by Bragg law (1913) which is best demonstrated on the assumption that x-rays are 'reflected' by a set of crystallographic planes (Fig 3.16):

$$n\lambda = 2d\sin(\theta) \qquad (3.31)$$

where n a positive integer is the reflection order.

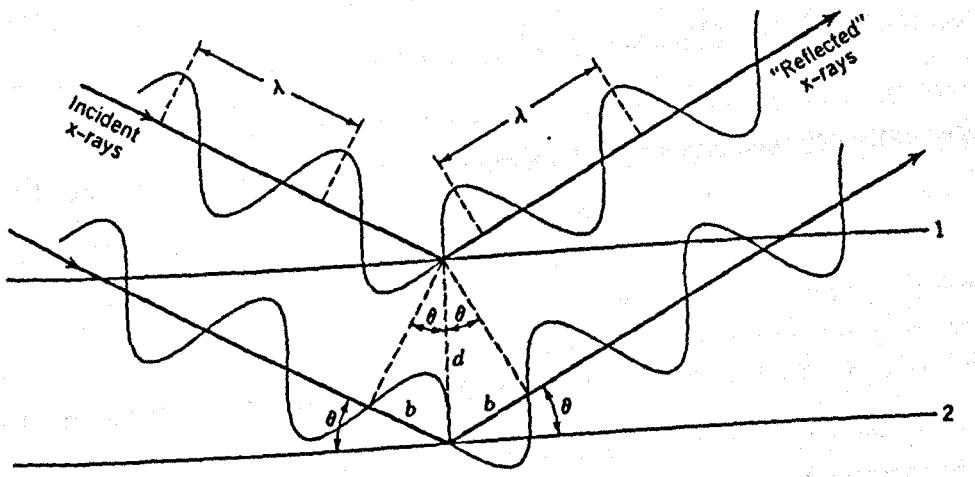

Figure 3.16 Geometry of the Bragg reflection analogy

2.3.2 *The intensity of diffraction*

The most important factor governing the intensity of x-ray scattered by a set of planes (h,k,l) at any point in space is the structure factor *F(hkl)*.

If x, y, z are fractional coordinates of the unit-cell edges a, b, c, respectively, a unit cell containing N atoms in which the nth atom is located at x_n, y_n, z_n. The structure factor can then be defined by :

$$F(hkl) = \sum f_n \exp[\, 2\pi\, i\, (h\, x_n + k\, y_n + l\, z_n)] \qquad (3.32)$$

where f_n is the atomic scattering factor for the nth atom.

A number of experimental factors modify the ideal intensity $|F|^2$ to yield the intensity that is actually observed, $I(hkl)$ (Alexander, 1969)

$$I(hkl) = P\, L\, j\, A\, |F|^2 \qquad (3.33)$$

P: the degree of polarization of the scattered x-rays by the electron of an atom $P=[1+\cos^2(2\theta)]/2$

L: the Lorentz factor which depends on the time during which a family of planes reflects x-rays $L = [\, \sin(\theta) \cos(\theta)\,]^{-1}$

j: the multiplicity factor is the number of different sets of planes that contribute to a single reflection (j =1 for single crystal diffractometry)

A: the absorption factor for x-rays, depends on the sample elemental composition, size, shape and the wavelength of the x-rays

2.3.3 *X-rays scattering by amorphous materials*

Although amorphous systems have no short or long range order of a truly crystalline nature, a minimal kind of short range order is thought to exist, an order consisting of most probable distances between neighbouring atoms and yielding the diffuse, non-crystalline patterns described above.

2.3.4 *Degree of crystallinity in polymers*

2.3.4.1 The x-ray crystallinity

The majority of polymers are semi-crystalline i.e two phases coexist in the same system: a crystalline phase (crystallites) interspersed with amorphous region. This agrees with the widely accepted 'fringed micelle' model used to describe semi-crystalline synthetic polymers (Wunderlich, 1976).

The physical and mechanical properties of polymers depend greatly on their degree of crystallinity (chapter 6). Different values of crystallinity are obtained from a range of techniques (x-ray, NMR, FTIR, density, etc.). The reasons for these differences lie often in the definition of crystallinity as, for example, the scale of order to which the technique is sensitive. While NMR, FTIR, etc. are sensitive to short range order (few chemical bonds), x-ray is more concerned with long range order (tens of nanometres).

The x-ray spectrum of semi-crystalline materials such as synthetic polymers and biopolymers is the result of the superposition of sharp features from the crystalline and the diffuse amorphous phases.

Furthermore, it is believed that the fraction of x-rays scattered by defectuous crystals contributes to the amorphous part of the spectrum. This makes the classical methods of calculating the crystallinity in semi-crystalline materials (which are based on the distinction between the amorphous and crystalline components of the spectrum) inaccurate as they lead to an under estimation of the degree of crystallinity. Consequently, the notion of the degree of crystallinity is being replaced by a relative crystallinity index as an indication of the three-dimensional order.

In the next 3 paragraphs, widely used methods of evaluating the x-ray degree of crystallinity in polymers (and specially starch) are reviewed.

2.3.4.2 Method of Hermans and Weidinger

The method described by Hermans *et al.* (1948) consists of measuring the integrated intensities of the crystalline peaks and that of the diffuse background after correction for the air and the incoherent scattering. A demarcation line between the crystalline and amorphous scattering is drawn over an angular interval that encompasses the principal

amorphous halo. An example of this method applied to the x-ray pattern of starch is illustrated in Figure 3.17. Some of the difficulties in using this method lie (i) in the availability of a fully amorphous sample and therefore the accuracy of the demarcation between amorphous and crystalline scattering and also (ii) in the choice of the angular range over which the calculation is to be carried out. The significance of this second problem is somehow diminished by the fact that the crystallinity value obtained should only be regarded as a relative index although some workers have wrongly reported absolute crystallinity values using this methods.

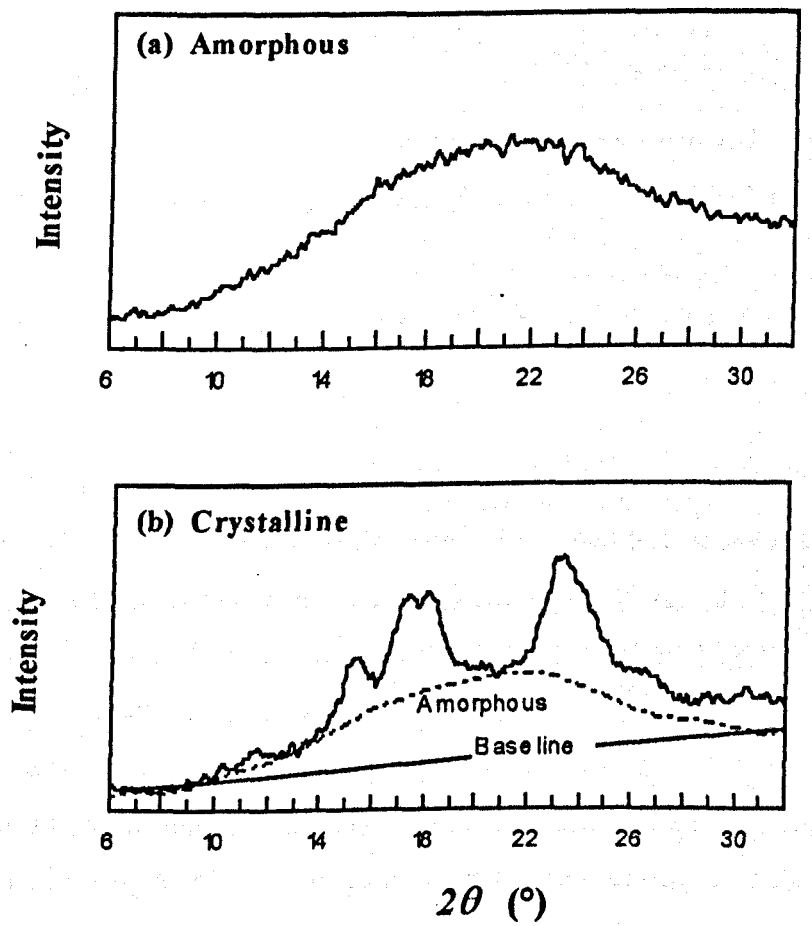

Figure 3.17 X-ray spectra of (a) amorphous gelatinized and (b) partially crystalline waxy maize starch. (b) illustrates the method described by Hermans *et al.* (1948) for crystallinity calculation

This technique was widely used for determining the degree of crystallinity of starch and other biopolymers, for example, by Sterling (1960), Nara *et al.* (1978, 1983), Marsh (1986) and many others.

2.3.4.3 Crystallinity from differential intensity measurements

According to this method developed by Wakelin *et al.* (1959), the crystallinity index (*ci*) of a sample is calculated relative to a minimum and a maximum corresponding to an amorphous (*ci* = 0) and a crystalline reference (*ci* = 1) standards respectively. For each angle 2θ in an angular range that includes most of the crystalline peaks of the x-ray diffractogram of the sample, differential intensities are calculated. The crystallinity index is obtained from the slope of the plot of equation 3.31 (Fig 3.18)

$$(I_u - I_a)_{2\theta} = ci\ (I_c - I_u)_{2\theta} + k \qquad (3.31)$$

where I_a, I_c and I_u are the intensities measured at a specific angle 2θ on the amorphous reference, the crystalline reference and the unknown sample respectively. Crystallinity index values obtained should be between 0 and 1, and k is theoretically equal to zero. The value of k is often used to check the calculation for systematic errors which lead to large positive or negative values of k.

The scatter in the results as shown typically in Figure 3.18 increases the error on the calculated relative crystallinity index values. More importantly, this method is not adapted to the study of retrogradation of starch systems where changes other than increase in resolution are often observed in the the x-ray spectrum. For example, the crystalline structure of starch depends on the conditions prevailing during recrystallization such a temperature and sample compostion. Just such an example is reported in chapter 6 (Figures 6.16, 6.17 and 6.29), where changes from the A to the B and the 'pseudo' B polymorphs are clearly demonstrated.

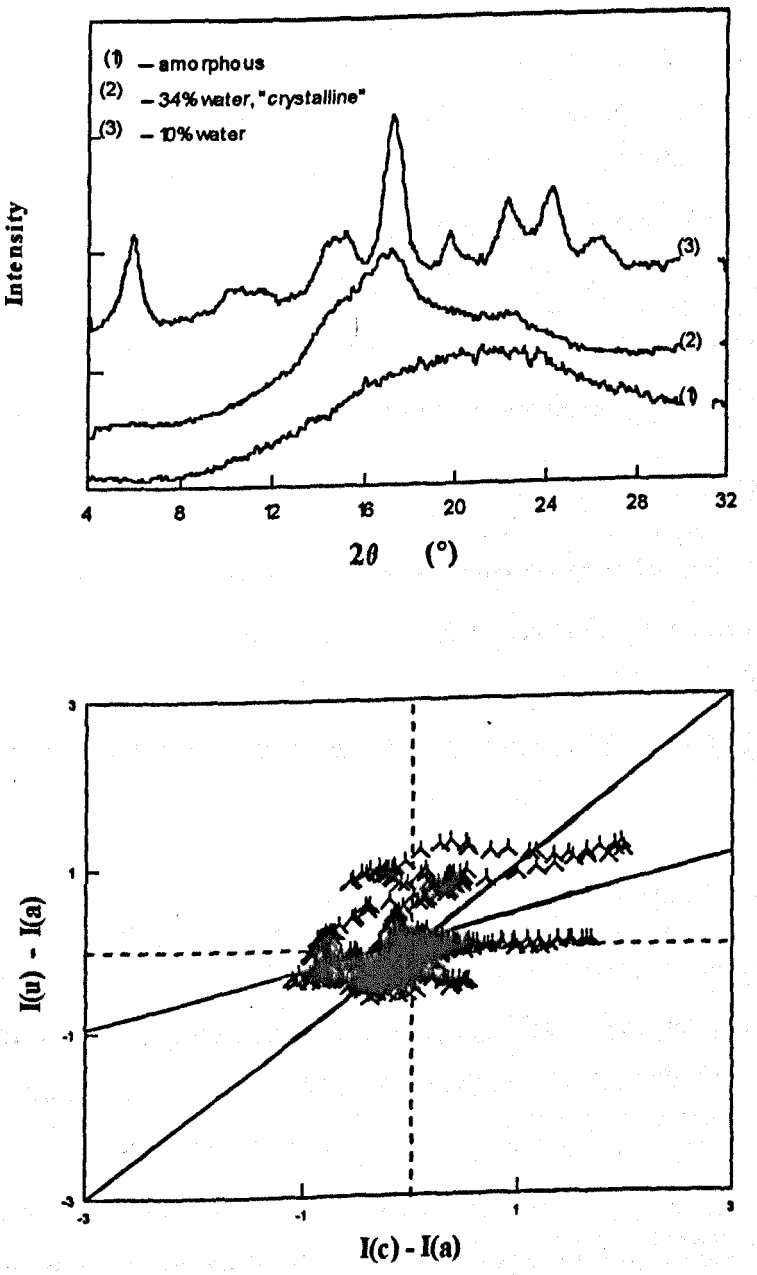

Figure 3.18 The Wakelin *et al.* (1959) method for the calculation of crystallinity indices as applied to a waxy maize starch system containing ~10% water (the crystalline reference used was the spectrum recorded on a 34% water)

2.3.4.4 Empirical methods

A variety of empirical methods have been used to evaluate the relative crystallinity of starch, especially in studies on gelatinization and retrogradation where relative rather than absolute crystallinity indices are needed to investigate the kinetics of the changes in the crystalline order. Ring *et al.* (1987) used the development of the (100) reflection corresponding to a *d*-spacing of 1.6 nm i.e $2\theta \approx 5.6°$ (λ=0.154 nm), whilst Roulet *et al.* (1988) used the intensity of the 16.9° peak. Cairns *et al.* (1991) used both 5.6° and 16.9° peaks. However, the use of the 5.6° peak is limited to starches of the B-type (chapter 6 - Figures 6.16).

Another method for the evaluating the relative change in crystallinity is by monitoring the increase in the spectral resolution by calculating the ratio of the intensities of the maximum to trough for a particular peak, typically the 17° angle (0.516 nm) as it is present in the x-ray spectra of A and B-type starches.

2.3.5 Experimental conditions

A Philips PW 1730 x-ray diffractometer was used. The x-ray generator equipped with a copper tube operating at 40 kV and 50 mA produced Cu K_α radiation of approximately 1.54 Å wavelength. Data were recorded over an angular range between 4° to 38° (2θ) for the study of the retrogradation of amylopectin-sugar-water extrudates and between 4° and 50° for all other investigations. An angular interval of 0.05° was used.

Hydration of biopolymers and biopolymer-sugar systems

Introduction

This chapter describes studies of the hydration properties of two biopolymers: a protein, gelatin and a polysaccharide, xanthan. Gelatin-sugar, amylopectin-sugar systems and maize-sucrose mixtures were also investigated, the latter being an example of a biopolymer-biopolymer-sugar mixture representative of a 'real', simple food system.

The impact of hydration on the molecular order and mobility was investigated using a combination of ^{13}C solid state NMR (75 MHz), ^{1}H relaxation NMR (20 MHz), FTIR and x-ray diffraction. The issue of water partitioning between the various components during the hydration of biopolymer-sugar water mixtures was studied, and its effects on molecular mobility, order and on the glass-rubber behaviour were investigated and are discussed in the final section of the chapter.

1. Hydration of biopolymers

This section reports the results of a study of the hydration of xanthan and gelatin at low to intermediate water contents (0 to 0.75 g of water per g of dry polymer). NMR (^{13}C

and ^{1}H), FTIR and x-ray diffraction were used to assess the effect of increasing water contents upon the physical behaviour of these two biopolymers.

The spin-spin relaxation times (T_2) were measured in order to assess the changes in biopolymer mobility with increased hydration. Molecular mobility and conformational information were described in terms of an increase in the spectral resolution observed by ^{13}C - NMR and FTIR.

While the peak in the ^{13}C - NMR spectrum of xanthan at approximately 97 ppm, emanating from the glycosidic carbons (O-CH-O), was used to probe the conformational changes during the hydration process, the amide region in the FTIR spectrum of gelatin was used for the equivalent purpose in the case of the protein. The role of the glycosidic and amide bonds in the primary and secondary structures of xanthan and gelatin respectively dictated the choice of the optimum technique for the particular investigation.

1.1 Proton relaxation NMR

In general, as the water content increased, the spin-spin relaxation time of the 'solid' component of the NMR FID signal increased (Fig 4.1). This was believed to be the consequence of the enhanced plasticization of the biopolymer by water, yielding an increase in the polymer segmental mobility.

The two hydrocolloids studied showed similar T_2 values for moisture contents below ~20 % (w/w dry solid basis). At higher water contents, gelatin exhibited larger T_2 values, reflecting a higher mobility of the solid component. In the case of gelatin the T_2 increased from ~14 μs at a water content of 5.7% to ~31μs at 46%, but with xanthan the increase was only from ~14 μs at a water content equal to 5.8% to ~20μs at 47%. These differences were not thought to be due to an erroneous numerical treatment of the NMR decay since the relaxation times of the 'liquid' component were comparable for both biopolymers.

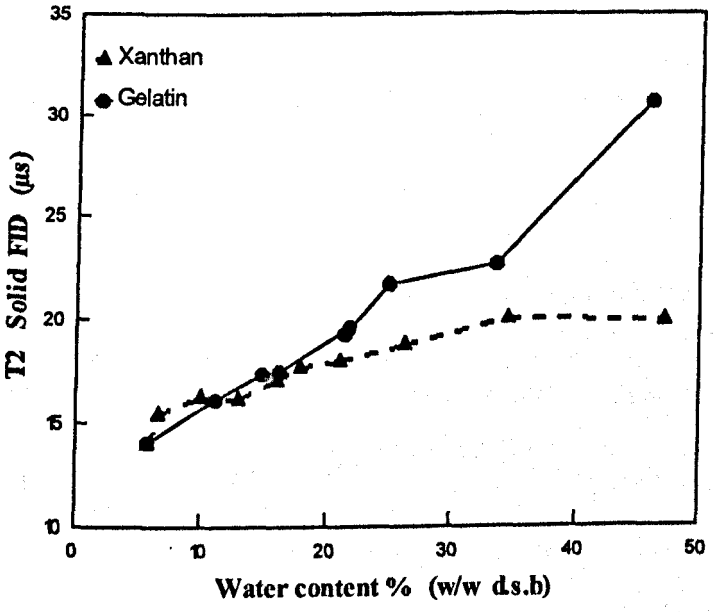

Figure 4.1 Spin-spin relaxation times of the 'solid' FID component as a function of moisture content measured at 20 MHz and 40°C.

The ratio of the amplitudes of the 'liquid' component of the FID relative to the 'solid' component were calculated for xanthan and gelatin at different water contents, and were compared to the values anticipated if the solid component of the NMR signal were attributed to the biopolymer and the 'liquid' signal to water. The expected ratios were calculated taking into account the proton densities of gelatin and xanthan (the proton density is the number of protons per mass unit). The proton density of xanthan was equal to 50/934 = 0.0535 , that of gelatin was calculated from the densities of each constituent peptide taking into account the composition of the protein as reported by Eastoe (1961) (Table 2.3 - chapter 2) and Rodin *et al.* (1994), and was found to be equal to 0.0642 ^1H / g. The details of the calculation of the anticipated liquid/solid ratio are reported in the next section of this chapter in the more general form describing mixed systems. While xanthan followed the calculated line over all the range of water contents under investigation, gelatin showed an increasing deviation from the theoritical line at high water contents (Fig 4.2).

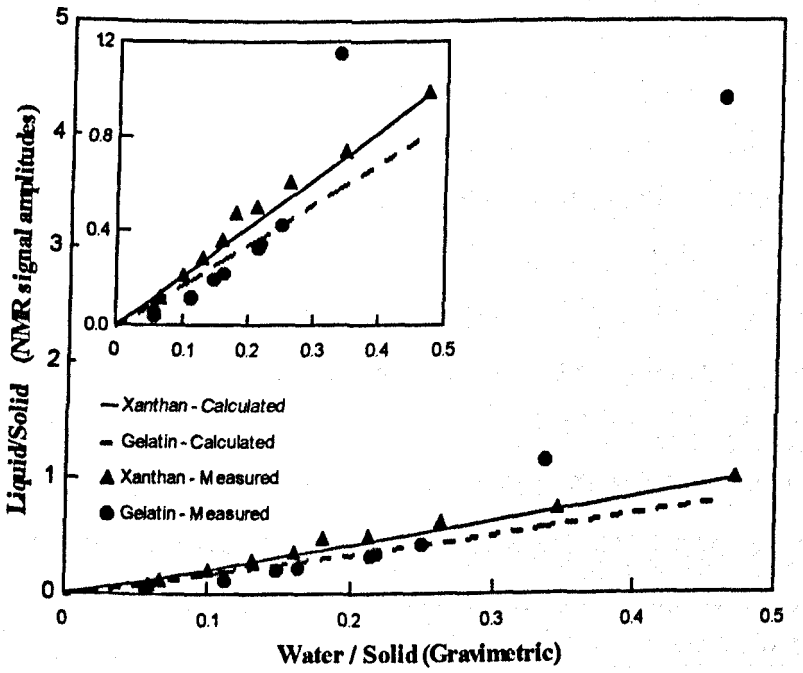

Figure 4.2 Ratio of the amplitudes of the NMR signals resulting from the 'liquid' and the 'solid' components of the FID (the FID was deconvoluted into only 2 components) for gelatin and xanthan.

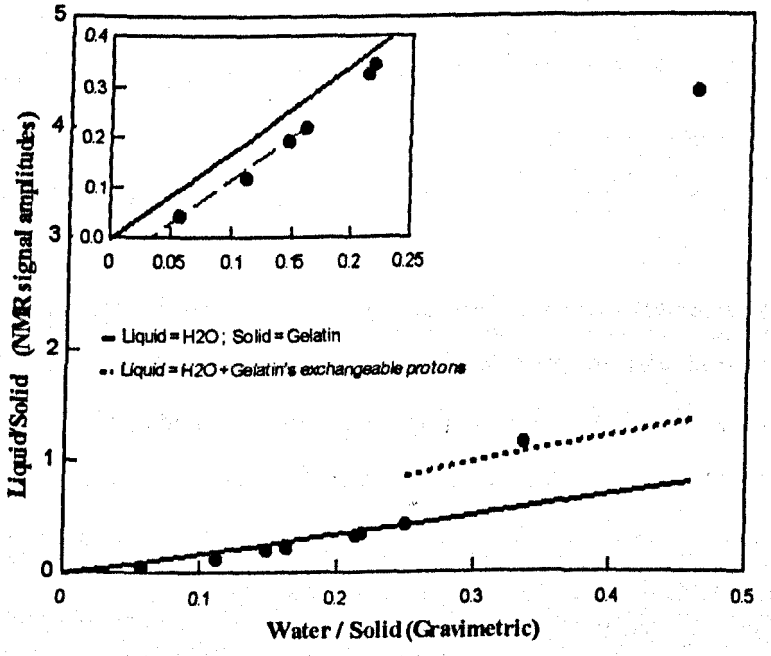

Figure 4.3 Same plot as Figure 4.2, emphasising on the results of gelatin.

For water contents below 0.2 g of water per g of dry solid, the measured liquid/solid ratio was smaller than anticipated on the basis that water yields the 'liquid' component whilst gelatin is responsible for the entire 'solid' component (insert of Figure 4.3). The results followed a straight line with a slope essantially equal to the slope of the calculated line, extrapolating to a value of 0.035 g of water per g of dry solid. This could be due to the fact that the first few water molecules (~3.5%) are tightly bound to the polymer matrix with restricted motion i.e with very short spin-relaxation times and, thereby, contribute to the NMR signal arising from the rigid component. Above 20% water (w/w d.s.b), the measured results deviated increasingly from the calculated line, approaching the line calculated assuming that all the exchangeable ^1H on the protein are in a fast chemical exchange (relatively to the NMR time scale) and thus contribute to the 'liquid' component (Fig 4.3). At water contents above 35% (w/w d.s.b) the chemical exchange could not account for the large deviation from the calculated line which points to the participation of other protons, i.e non-exchangeable ones, to the 'liquid' signal due to a mobilization of either parts of the polymer or low molecular weight components present in the system.

1.2 ^{13}C NMR and FTIR

1.2.1 Xanthan Gum

The FT-MAS spectra showed a broad band on which are superposed fine structures. This broad pattern is due to the rapidly decaying solid component (the line width at half height $\Delta\nu_{1/2} = 1/\pi T_2$) and can be eliminated by using T_2 weighted FT-MAS experiments. As this broad band did not interfere with the desired measurements, conventional FT-MAS experiments were used. This broad peak decreased as the water content was increased. Both CP and FT MAS results exhibited a pronounced enhancement in the spectral resolution as the water content was increased (Fig 4.4). This was accounted for by (i) the greater mobility coupled to an increase in the T_2 which is reflected by a decrease in

the line width, and (ii) by the fewer chemical shift distributions due to ordering of the polymer. The glycosidic peak in the sample containing 75% (w/w d.s.b) water showed three distinct lines corresponding to three different chemical shifts, whereas the sample hydrated to 41% water showed only the first stages of this phenomenon. This spectral line shape suggested that the helical conformation described in xanthan solution (Moorhouse *et al.*, 1977) appears during the early stages of hydration.

Similar patterns were observed in the FT-MAS spectra representing the mobile component of the system. This observation led to the conclusion that both the mobile and the less mobile components in the system were in the same conformation.

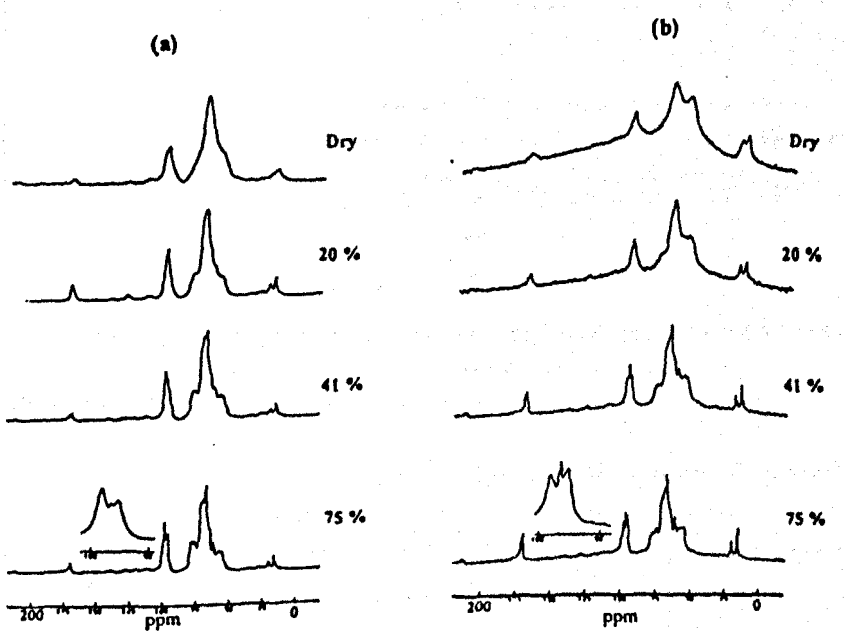

Figure 4.4 CP-MAS (a) and FT-MAS (b) spectra of xanthan (300K - 75MHz) for different degrees of hydration (0, 20, 41 and 75% water w/w d.s.b). The inserts represent the glycosidic (O-CH-O) ~ 97 ppm.

Marked effects of hydration were observed on the infrared bands of the charged and polar groups (COO^-, C=O, O-H, C-O etc..) due to the effect of hydrogen bonding on the charge and the mass distribution in the corresponding bond vibrator. In addition to this,

the deformation region of the mid- infrared spectrum showed an increase in resolution as the water content was increased (Fig 4.5) which was quantified by plotting the peak to trough intensity ratios ($I_{1400\ cm\text{-}1}$ / $I_{1382\ cm\text{-}1}$) against water content (Fig 4.6).

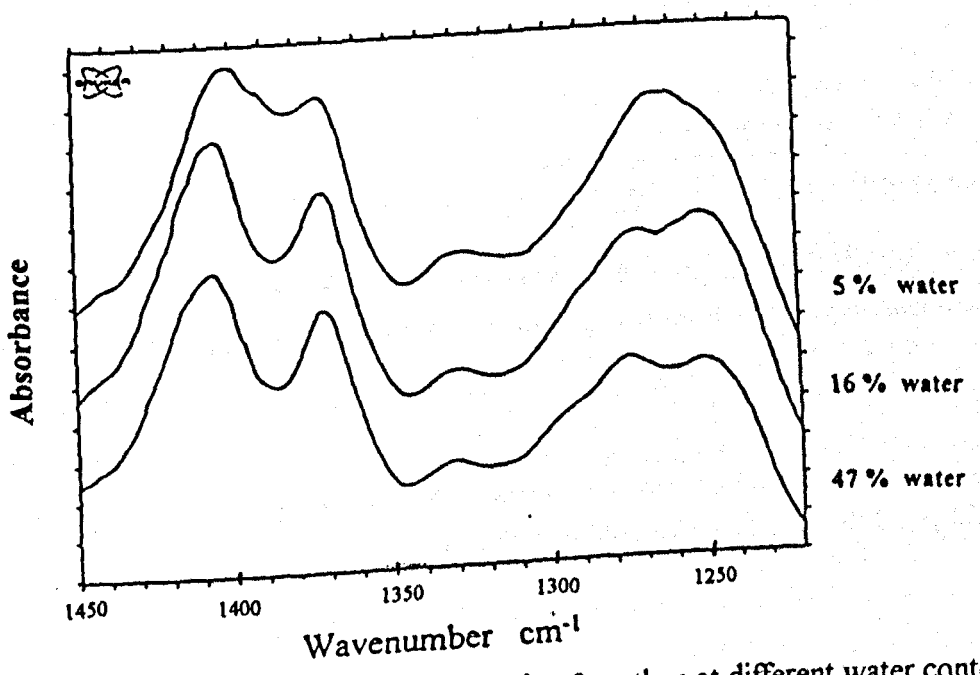

Figure 4.5 FTIR spectra (1450-1220 cm^{-1}) of xanthan at different water contents (5, 16 and 47 % water w/w d.s.b)

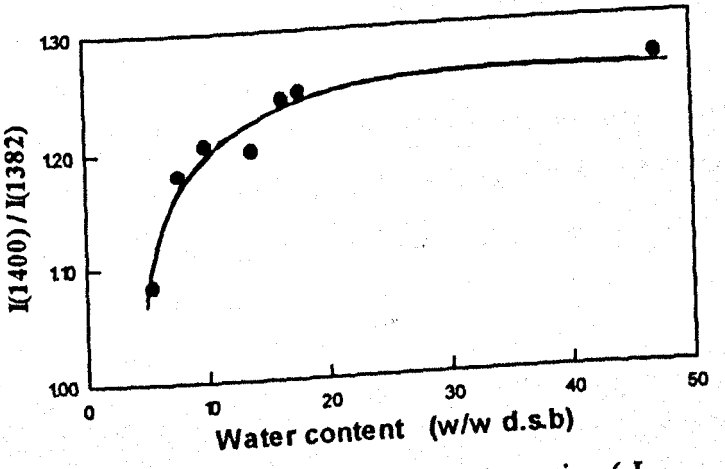

Figure 4.6 FTIR peak to trough intensity ratios ($I_{1400\ cm\text{-}1}$ / $I_{1382\ cm\text{-}1}$) against moisture content for xanthan gum

The FTIR results were consistent with the hypothesis that increased ordering of the biopolymer occurred with enhanced hydration.

1.2.2 Gelatin

A similar increase in resolution was observed in the ^{13}C NMR spectra of both FT and CP MAS experiments throughout the hydration process (Fig 4.7). In the range 0 to 30% water, only slight differences were observed between the spectra obtained by these two techniques. At higher water contents, sharp peaks were observed in the FT-MAS results that were absent from the CP-MAS spectra.

The presence of these sharp peaks was evident in the carbonyl chemical shift region, and a new band was observed at approximately 148 ppm. These sharp bands, present only in the mobile component, were thought to be due to the mobilisation of parts of the biopolymer chains or the solubilization of components of small molecular weight present in the system. This explanation was supported by the proton relaxation results of gelatin described above. Gregory *et al.* (1993) suggested 0.3 g of water / g of protein was needed to fully hydrate lysozyme; which implies the presence of some 'free' water at higher moisture contents which reasonably may mobilize and solubilize side chains and / or low molecular weight components.

The low molecular weight components could be present in the system as a result of the industrial preparation of gelatin and thus the chemical shifts of the sharp peaks should be sensitive to the gelatin source and degree of purification. However, when comparing the FT-MAS at relatively high water contents (>35% w/w d.s.b) of the food grade gelatin produced by Sanofi-Bioindustie with the purified gelatin supplied by Sigma, there was no significant difference between the results. This observation suggests that low molecular weight species are not responsible for the sharp peaks in the FT-MAS spectra, as the amount and composition of low molecular weight components in biopolymers

depend often on the degree of purification, the supplier and sometimes on the particular batch used. However, more experiments are needed to confirm this hypothesis. For example, since low molecular weight components can diffuse more rapidly, an NMR experiment using a pulsed magnetic field gradient should readily check the presence/absence of low molecular weight compounds.

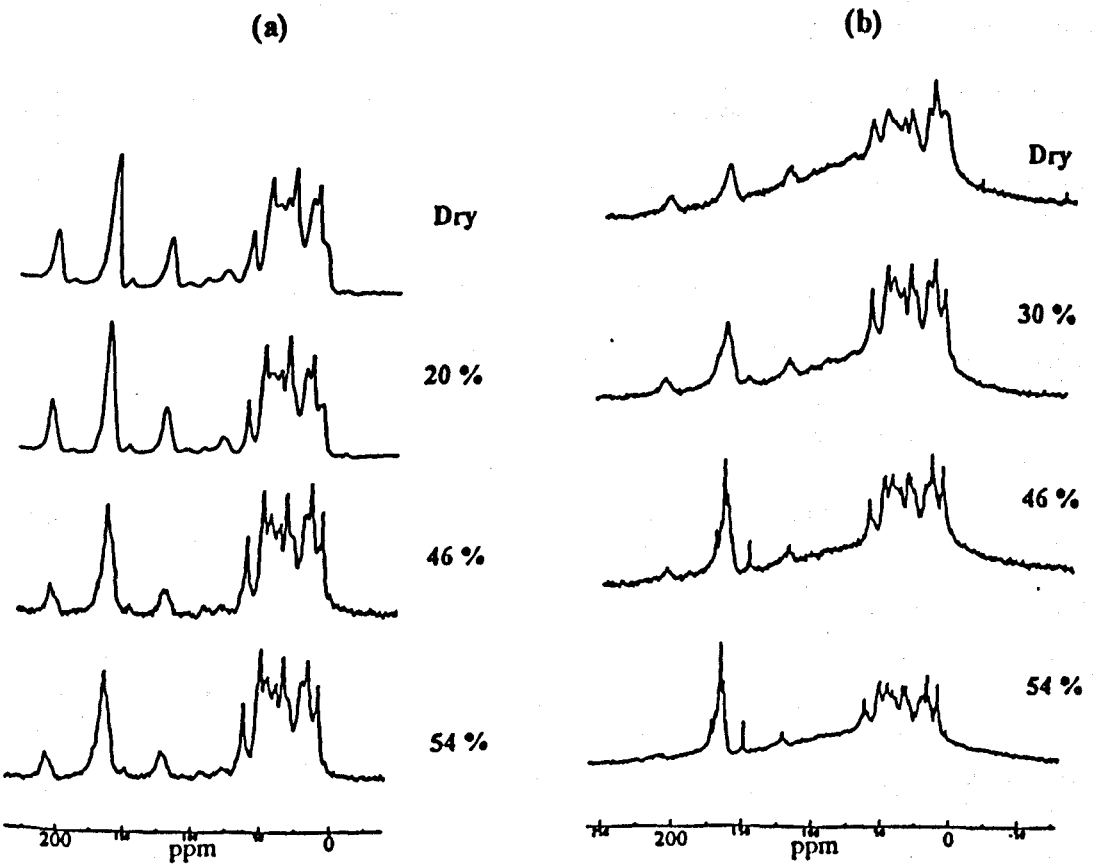

Figure 4.7 CP-MAS (a) and FT-MAS (b) spectra of gelatin (300 K - 75 MHz) for different degrees of hydration (0, 20 or 30, 46 and 54 % water w/w d.s.b). The FT-MAS spectrum of the sample containing 30 % water was shown to emphasize the appearance of the sharp peaks at water contents between 30 % and 46 %.

FTIR spectra showed changes in the bands of the groups affected by hydrogen bonding as described above for xanthan.

Figure 4.8 shows the increase in resolution with increased hydration level. Bending bands such as bands at 1238 and 1205 cm^{-1} were found to be affected by hydration whereas stretching bands such as the C-H stretching bands at 2940 and 2878 cm^{-1} did not exhibit the same behaviour; this being compatible with conformational transitions which would have a more pronounced influence on angle deformation than on bond stretching.

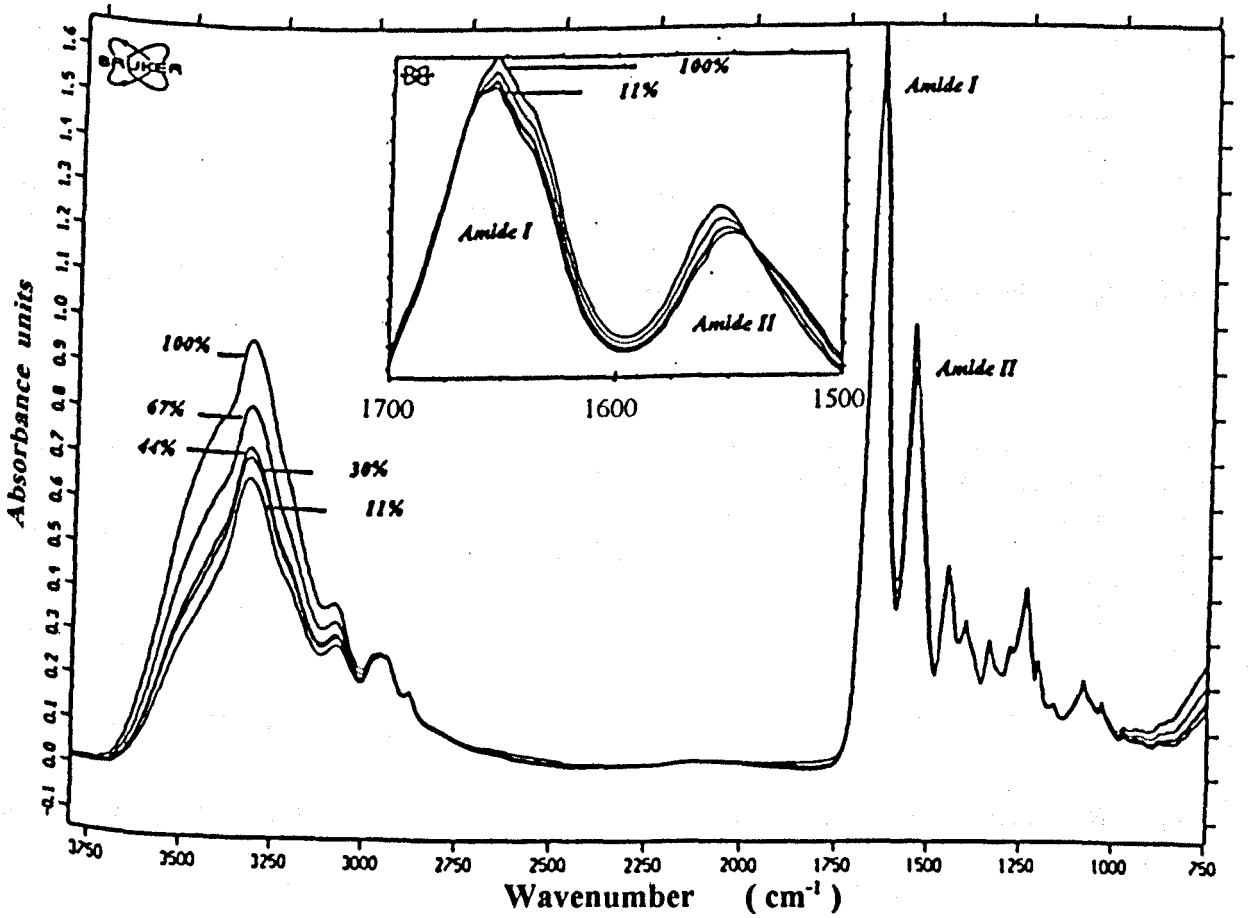

Figure 4.8 Effect of hydration of the mid-infrared spectrum of gelatin films. The the relative humidity of the hydrating air flow is shown for each spectrum. The insert (1700-1500 cm^{-1}) shows the effect of hydration upon the amide 1 and 2 bands.

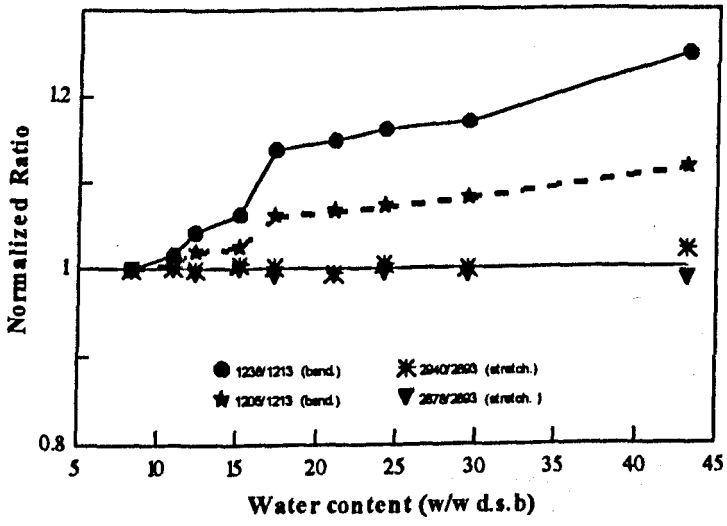

Figure 4.9 FTIR normalized peak to trough intensity ratios against water content for gelatin showing the effect of hydration on (i) the bending vibration modes monitored by the ratios $I_{1238\ cm-1} / I_{1213\ cm-1}$ and $I_{1205\ cm-1} / I_{1213\ cm-1}$ and (ii) the stretching modes illustrated by the ratios $I_{2940\ cm-1} / I_{2893\ cm-1}$ and $I_{2878\ cm-1} / I_{2893\ cm}$

The effect of hydration on the intensity and the frequency of the amide 1 and 2 bands is shown in Figure 4.10. These results were understood in terms of the effects of hydrogen bonding of water on the C=O and N-H groups as discussed more thoroughly in section 2.1.1.3 of chapter 3 (p.p. 58-60).

As anticipated by the approach based on the effect of hydrogen bonding on the dipolar moments of the C=O and N-H bonds, the intensities of both amide 1 and 2 bands increased with hydration. The position of amide 1 band shifted towards low wavenumber values, whilst the frequency of the amide 2 band increased with increased water contents. The effect of hydration on the position of the band is the consequence of several phenomena. The binding of water by hydrogen bonding on a particular group, for instance C=O or N-H, affects the force constant of the corresponding bond and the reduced weight of the C-O and N-H vibrators as they become coupled to the newly formed O-H vibrator. Additionally, the frequency of the amide 1 and 2 bands depend on

the conformation of the peptide (Krimm *et al.*, 1986) and any conformational transition would inevitably lead to a shift in frequency. This latter source of frequency shift is discussed subsequently in this section.

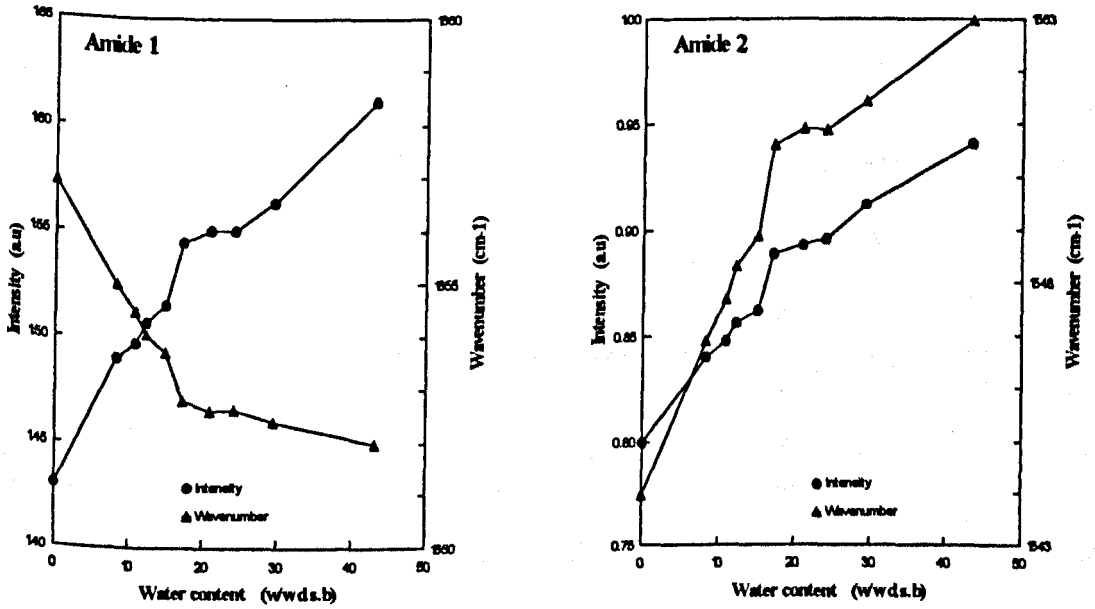

Figure 4.10 Influence of the degree of hydration on the amide 1 and 2

Furthermore, the amide bands are sensitive to conformational changes in proteins as they are constituted from a combination of various stretching and bending vibration modes and, the role of the amide bond in the establishment of the primary and secondary structures of polypeptides makes the amide bands valuable probes to study protein structures. Small changes in dihedral angles (Φ,Ψ) imply changes in the force field and thus in the position of the amide infrared bands (Krimm *et al.*, 1986). The amide I and II bands at approximately 1650 cm^{-1} and 1540 cm^{-1} respectively showed a complex structure that could be deconvoluted into ten different bands (5 for amide 1 and 5 for amide 2) (Fig 4.11). The frequencies of these bands were obtained using the method described by Kumosinski *et al.* (1993) based on the calculation of the second derivative of the infrared spectrum using the Savitzky and Golay method. A Levenberg-Marquardt algorithm was used to adjust the various band parameters (intensity, width, Lorentzian / Gaussian line shape).

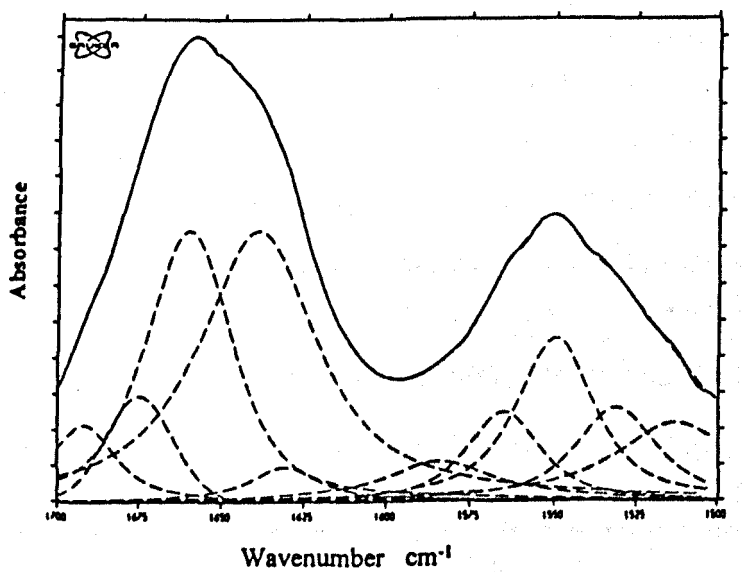

Figure 4.11 The amide I and II region of the FTIR spectrum of a dry gelatin film. The solid line represents the experimental spectrum while the dotted lines represent the calculated individual bands and the resulting calculated spectrum.

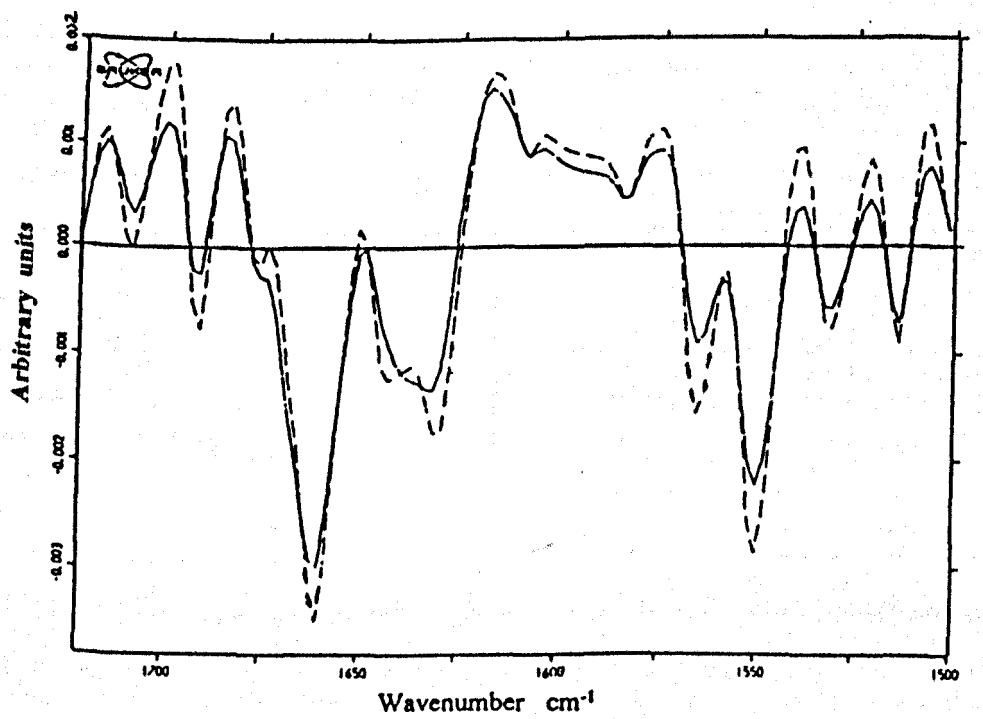

Figure 4.12 Second derivative of the FTIR spectrum shown in Figure 4.11

A satisfactory agreement was obtained between the calculated and the experimental data (Figures 4.11 and 4.12). The individual fitted bands were assigned to different conformations based on the calculations reported by Krimm *et al.* (1986) and their intensities were examined as a function of the water content. The band at 1675 cm^{-1} was attributed to the amide 1 of a turns conformation, 1660 cm^{-1} to the helices, 1640 cm^{-1} to the unordered conformation, while the band at 1630 cm^{-1} was assigned to a combination of a small contribution of the amide 1 extended conformation and a larger one resulting from the water bending band (no substraction of the water spectrum had been performed).

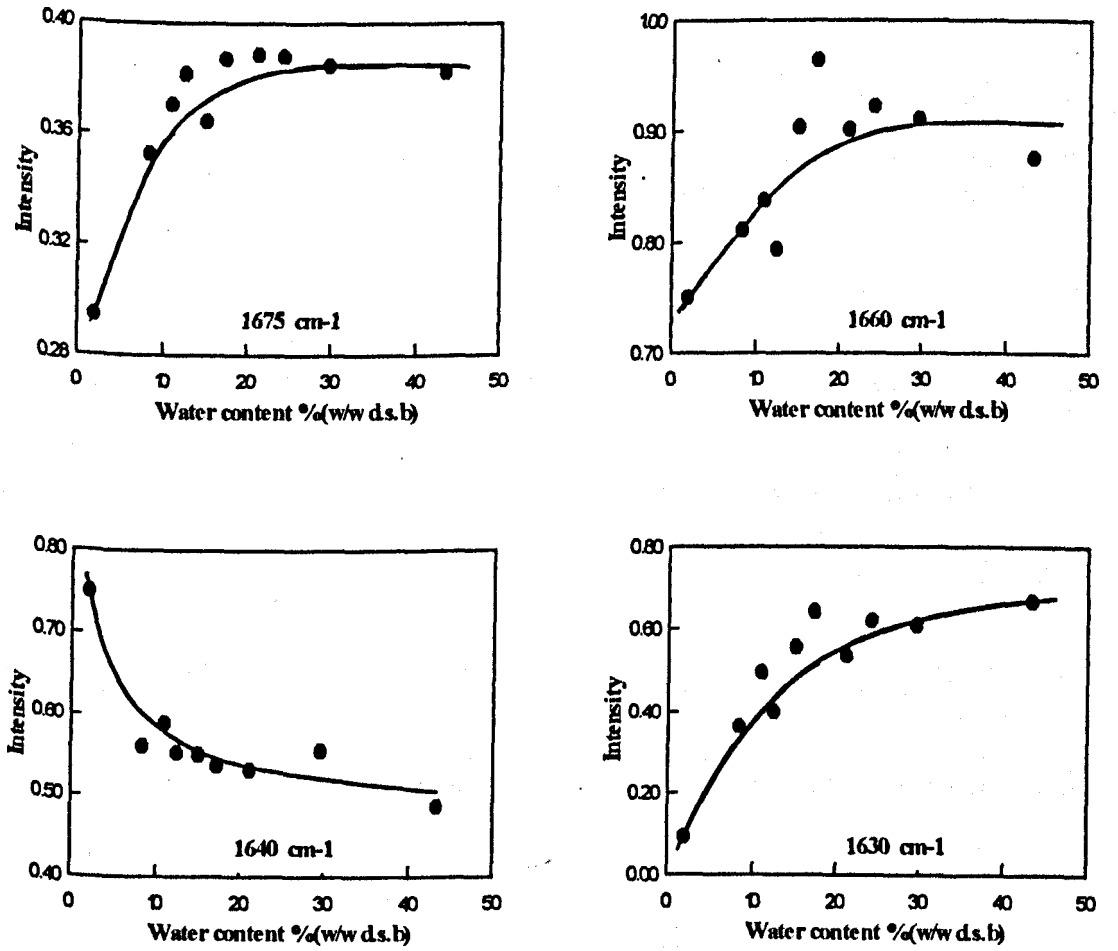

Figure 4.13 Changes in the intensities of the individual components of the 'composite' amide I band of gelatin films as the water content was increased.

Evidences of the presence of an amide 1 contribution at 1630 cm^{-1} were obtained from (i) the presence of this band in the infrared spectrum of dry film and (ii) from isotopic shift experiments carried out using D_2O rather than H_2O in the hydration process.

While the intensities of the amide 1 bands at 1675, 1660 and 1630 cm^{-1}, corresponding to ordered secondary structures, increased with increased water contents, the intensities of the band at 1640 cm^{-1} corresponding to unordered structures decreased (Fig 4.13). The bands at 1660 and 1675 cm^{-1}, corresponding respectively to helices and turns, showed a plateau at approximately 15% water. The 1630 cm^{-1} band assigned to an extended conformation levelled off at a moisture content of 25%. Finally the band at 1640 cm^{-1} attributed to the unordered conformation exhibited its minimum intensity value at a water content of ~15%.

The change in the relative contribution of each conformation to the secondary structure of the protein can be calculated from the change in the intensity of the component at each frequency :

$$\Delta I = I_{fully\ hydrated} - I_{dry} \qquad (4.1)$$

The changes in the intensity between the dry and the 'fully' hydrated films for the individual components of the amide 1 band were found to be as follows :

$\Delta I_{1675\ cm^{-1}} \approx 0.095$

$\Delta I_{1660\ cm^{-1}} \approx 0.19$

$\Delta I_{1640\ cm^{-1}} \approx 0.3$

Therefore the amide 1 contribution at 1630 cm^{-1} can be approximately estimated to :

$\Delta I_{1630\ cm^{-1}} \approx 0.3-(0.095+0.19) = 0.015$ as the components at 1692 cm^{-1} and 1675 cm^{-1} tended to merge into a single band with increased hydration.

This value of $\Delta I_{1630\ cm^{-1}}$ was compatible with the extrapolation to zero water contents of the results at 1630 cm^{-1} in Figure 4.13.

The intensities of each component could be used to estimate the relative contribution of

the different conformations to the secondary structure of the protein (Kumosinski *et al.*, 1993). The results, reported in Table 4.1 showed a general reordering. Furthermore, the hydrated protein seemed to adopt preferentially a helical conformation (fraction ≈ 50%), whilst the extended conformation was negligible (≈2 %). These results suggested the presence of a considerable degree of order in the dry system.

Table 4.1 Changes in the relative fractions of the ordered and unordered secondary structures of gelatin as a result of hydration

Band (cm^{-1})	Intensity dry	Intensity hydrated	Intensity difference	fraction % dry	fraction % hydrated	change during hydration
1640 (Unordered)	0.8	0.5	-0.3	43.4	27.1	-16.1
1630 (Extended)	0.025	0.04	0.015	1.4	2.2	+0.8
1660 (Helical)	0.73	0.92	0.19	39.6	49.9	+10.3
1675 (Turns)	0.29	0.385	0.095	15.7	20.9	+5.2

However, in this calculation, the effect of hydration on the intensity of the amide bands has not been considered. As described in Chapter 2, the binding of water by hydrogen bonding to the amide C=O and N-H groups affects the dipolar momentum of the vibrator, and consequently increases the intensity of the amide bands.

If I_f is the measured intensity of a particular component of the amide 1 band (at a frequency f) in the 'fully' hydrated protein system, and I'_f the intensity at the same frequency if hydration had no effect on the dipolar moment of the bond and therefore on the intensity of its infrared band, then I' depends only on the concentration of the particular component in the system.

$$I_f = I_f' + k\, I_f' \qquad (4.2)$$

where k is a constant and $k\, I_f'$ reflects the intensity increase due to the effect of hydrogen bonding. This increase is understandably proportional to the number of hydrogen bonding sites.

The fraction of a component is given by :

$$fraction = \frac{I_f}{\sum (I_f)} = \frac{(k+1)\, I'_f}{(k+1) \sum (I_f')} = \frac{I_f'}{\sum (I_f')} \qquad (4.3)$$

Consequently, this simplification should not affect the relative fractions calculated above.

1.3 Wide Angle X-ray Scattering

For both polymers, the increase in water content affected the x-ray patterns (Fig 4.14) in two ways :

(i) There was an increase in intensity of the crystalline peaks at 2θ=7° and 31° for gelatin and 5° and 9° for xanthan, corresponding to distances of 1.26 and 0.29 nm for gelatin and distances of 1.77 and 0.98 nm for xanthan. Itoh *et al.* (1994) assigned the peaks at 7° and 31° to long range helical order in gelatin and a similar explanation could be applied to the crystalline peaks observed for xanthan. This was in agreement with the FTIR results where the helical conformation was found to be predominant.

(ii) The broad peak centred at $2\theta \approx 20°$ became broader and shifted to higher 2θ values, a shift of approximately 1.5° for xanthan and 4.5° for gelatin. The observation of a broadening suggests that the disordered region becomes more disordered in terms of long range order as the water was increased. The shift to large angles suggests a closer molecular packing.

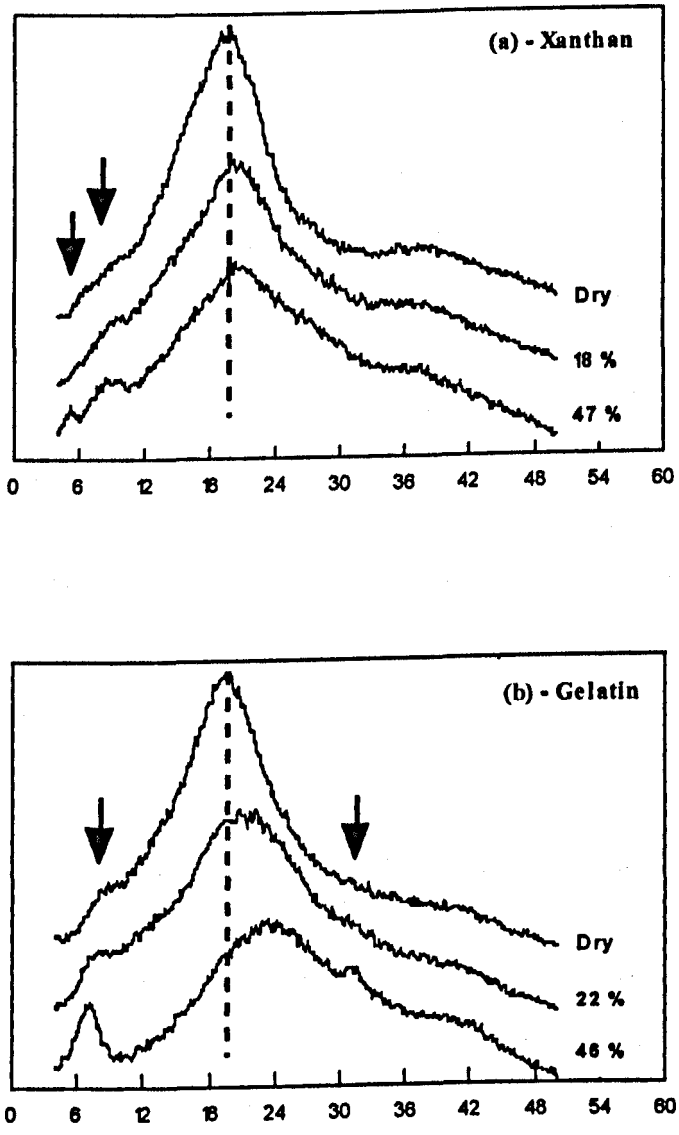

Figure 4.14 WAXS spectra recorded at 3 different water contents (w/w d.s.b):

(a) xanthan gum: 0%, 18% and 47%

(b) gelatin: 0%, 22% and 46%

Conclusion

Xanthan gum and gelatin undergo an ordering process during the first stages of hydration. This increase in the degree of order, although not favourable in terms of the change of the system's entropy, takes place as it involves the relaxation of the polymer. Indeed, the internal energy of the dried biopolymer system is believed to be dominated by the torsion of chemical bonds and the angles between these bonds which involves high amounts of energy.

As a consequence of these conformational transitions during the incorporation of the first water molecules in the biopolymer system, these early stages of the hydration process could prove to be very important in determining the properties and the handling of industrial biopolymers.

2. Hydration of biopolymer-sugar systems

The hydration of mixed system involves various aspects of water partitioning and selective plasticization. These aspects were investigated as a function of the hydration level, by FTIR for gelatin-sugar mixtures and by proton relaxation NMR for starch-sugar systems.

2.1 FTIR study of the hydration of gelatin-sugar mixtures

This section describes the investigation of the hydration of gelatin-sugar systems. FTIR spectroscopy was used to study the differential partitioning of water between the sugar and the protein throughout the hydration process. Furthermore, the hydration properties of these mixed system were assessed in order to obtain information on the specific

molecular interactions between the protein and the various sugars. Samples containing three different sugars and several concentrations were prepared and investigated using direct difference transmission FTIR methodology.

2.1.1 Effect of hydration on the FTIR spectra of gelatin-sugar

The changes in the intensity of the amide bands were used in this study. The direct difference method described by Poole *et al.* (1982 and 1984) was used because it offers several advantages for the study of hydration (chapter 3) such as the use of *non-invasive* hydration of the same film. Furthermore, the fact that a direct difference spectrum (dd-FTIR) displays only the effect of hydration on the FTIR spectrum of the biopolymer investigated is very convenient. Figure 4.15 illustrates a typical example of changes of the dd-FTIR spectra of a protein film measured at different relative humidities. The spectra in Figure 4.15 correspond to the standard FTIR spectra (direct mode) results described earlier (Fig 4.8).

As expected, the effect of hydration was very pronounced on the following bands: 3400-3070 cm^{-1} (N-H and O-H stretching), 1650 cm^{-1} (amide 1), 1540 cm^{-1} (amide 2), 1200-900 cm^{-1} (complex bending bands including the 'sugar bands'). The advantage of subtracting the spectrum of the dry film before performing the FT i.e by adopting the direct difference is illustrated by the quality of the spectra as well as the 'flatness' of the baseline (note that no baseline correction was attempted).

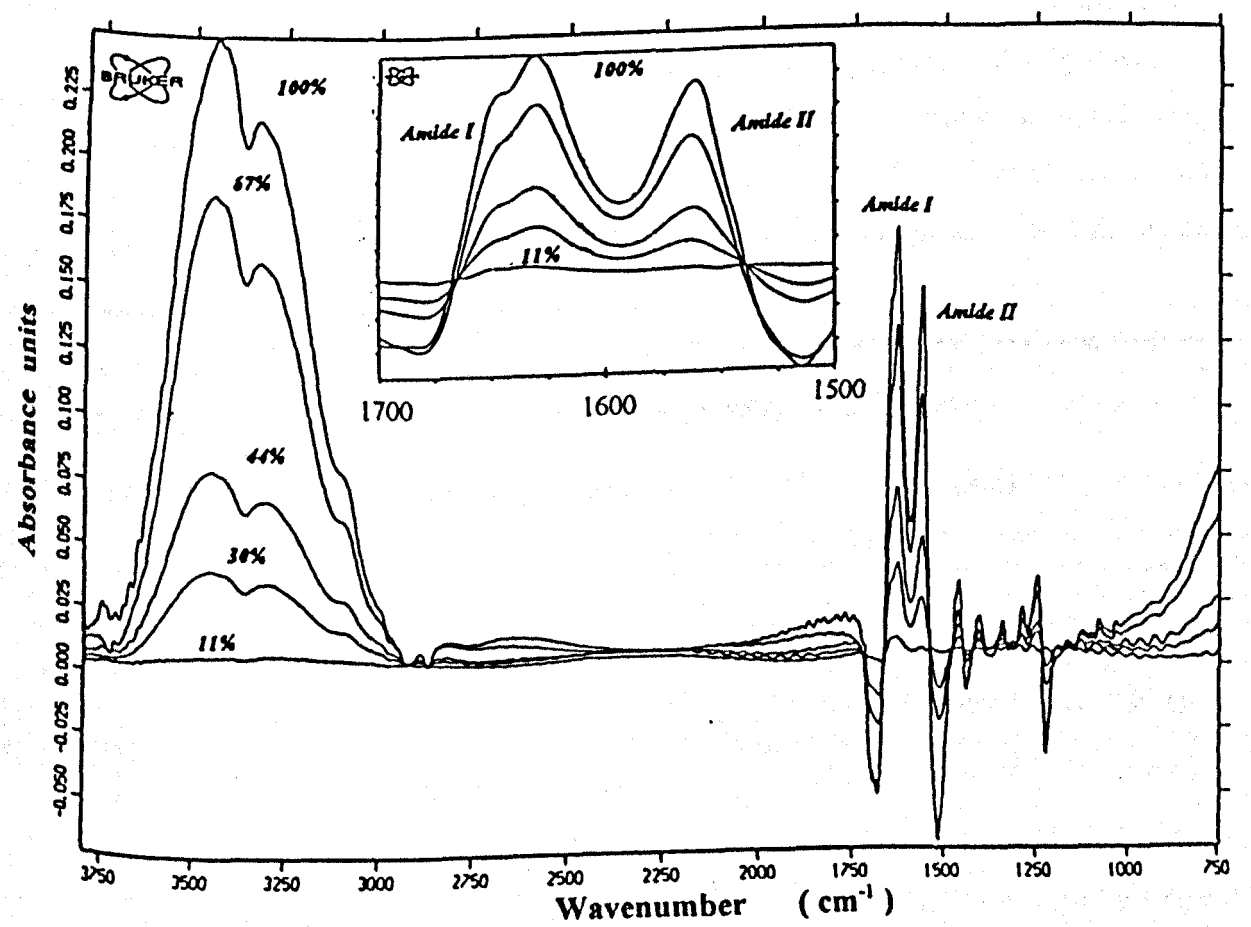

Figure 4.15 Evolution of the direct difference FTIR spectra of gelatin films at successive hydration stages. The insert emphasizes the amide region

2.1.2 *Effect of sugars on the hydration kinetics of gelatin*

2.1.2.1 Direct difference hydration results

While previously the amide 1 band was deconvoluted into its individual components, in this section the intensity (peak maximum) of the composite band was used to study the behaviour of gelatin throughout the process of hydration of gelatin-sugar films using the direct difference technique.

The intensity of the amide 1 band measured from the direct difference spectrum was normalized relative to the intensity of the same band of the dry film recorded by the direct mode (standard) technique ($I_{dd}[RH] / I_{std}[RH=0]$) . This normalization was performed in order to account for the amide 1 concentration. Consequently the results obtained from films of different thicknesses, and likewise, samples with different protein contents can be compared subsequently to this normalization.

The results were modelled using a non-linear fitting routine based on the least squares deviation (χ^2 minimisation) (Fig 4.16). The proposed equation was:

$$I(w) = I_m [1-\exp(-k\, w^n)] \qquad (4.4)$$

Where $I(w)$ is the intensity of the **direct difference** amide band, I_m is the saturation intensity (at high water contents), w is the water content (w/w dry basis), k is a hydration rate constant and n is a constant. This equation is identical to the Avrami model often used to model the crystallization data (chapter 6). The saturation I value (I_m) was understood to represent the saturated state of all the amide groups by water bonding. Likewise, the rate constant (k) describes the kinetics of the water-protein interaction (by hydrogen bonding on the C=O). The significance of the constant n in the equation is not simple. However, it is tempting to relate n to the accessibility of the amide carbonyl group by the water molecules. The broad term 'accessibility' covers several aspects including (i) the affinity of water towards the C=O groups as compared to other binding sites in the protein, such as charged groups, (ii) the steric availability of the carbonyl in the secondary and ternary structure of the protein, but (iii) could also illustrate the steric inhibiting effect of other molecular species which compete to establish hydrogen bonds with the protein C=O. This latter hypothesis is supported by the values of n found by χ^2-minimization fitting. While a value of $n \approx 1.4$ was found for gelatin films, values of 1.5, 1.8 and 2.3 were obtained for the samples containing 20% of glucose, xylose or sucrose respectively. Indeed, increased n values yield an enhancement

of the sigmoidal nature of the hydration curve as predicted by equation 4.4, i.e an increase of the relative significance of the 'lag' taking place prior to the exponential increase of the intensity of the amide band which results from the interaction with the water molecules.

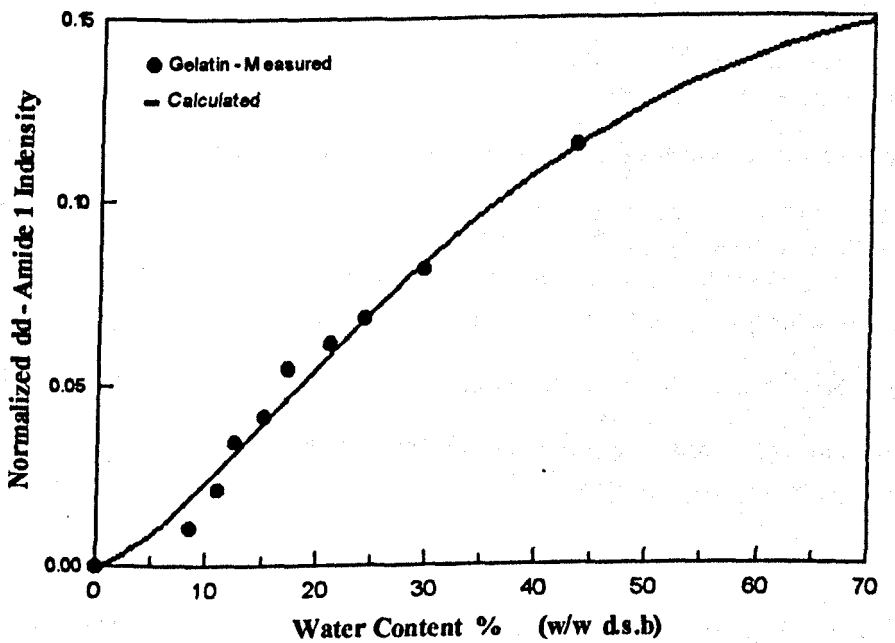

Figure 4.16 The intensity of the amide 1 band measured by the direct difference technique and normalized to the intensity of the amide 1 band in the standard spectrum of the dry film. The line was calculated using equation 4.4 (χ^2=3.10^{-5}).

2.1.2.2 Hydration of protein-sugar systems

In this section, the roles of (i) the interactions between the protein and the sugar molecules and, (ii) the preferential hydration of a particular component (the protein or the sugar) are investigated by examining the dependence of the **normalized** intensity of the **direct difference** amide 1 bands on the water content. These intensities increased from

a value equal to 0 in the dry film (direct difference) and accounted for the variation in protein concentration between different samples (normalized). The changes in gelatin-sugar mixtures were considered relative to the control gelatin system.

a- Protein-sugar interactions and equal partitioning of water

The interaction between sugars and gelatin in the dry film is very likely as homogeneous mixtures were produced by the slow drying of the protein-sugar solution during the film casting (chapter 3). Such interactions could take the form of hydrogen bonding between the O-H groups on the sugars and the amide 1 carbonyl group of gelatin. This would inevitably lead to an increase in the amide band intensity recorded in the standard direct mode (I_0 for the dry gelatin and I_0' for the dry gelatin-sugar film - Fig 4.17-a) spectra.

As the protein-sugar system is hydrated, the intensity of the amide 1 band increases to reach a plateau value. This maximum value should be the same as the value reached if no sugar was present in the system as the results were normalized to the same protein concentration (Fig 4.17-a). The direct difference intensities are similar to the standard mode results where the intensity of the dry film has been subtracted. Consequently, the direct difference amide 1 intensities are shifted by $-I_0$ for the gelatin film and $-I'_0$ for the gelatin-sugar films. Therefore the gelatin-sugar intensity results would be shifted by a constant offset equal to $-(I'_0 - I_0)$ (Fig 4.17-b).
Hence, any shift in the 'plateau' value is expected to be a shift to lower intensity values and is indicative of a specific molecular interaction between the C=0 of the protein and the O-H group of the sugar. In this paragraph, the water was assumed to be equally distributed between the protein and the sugar.

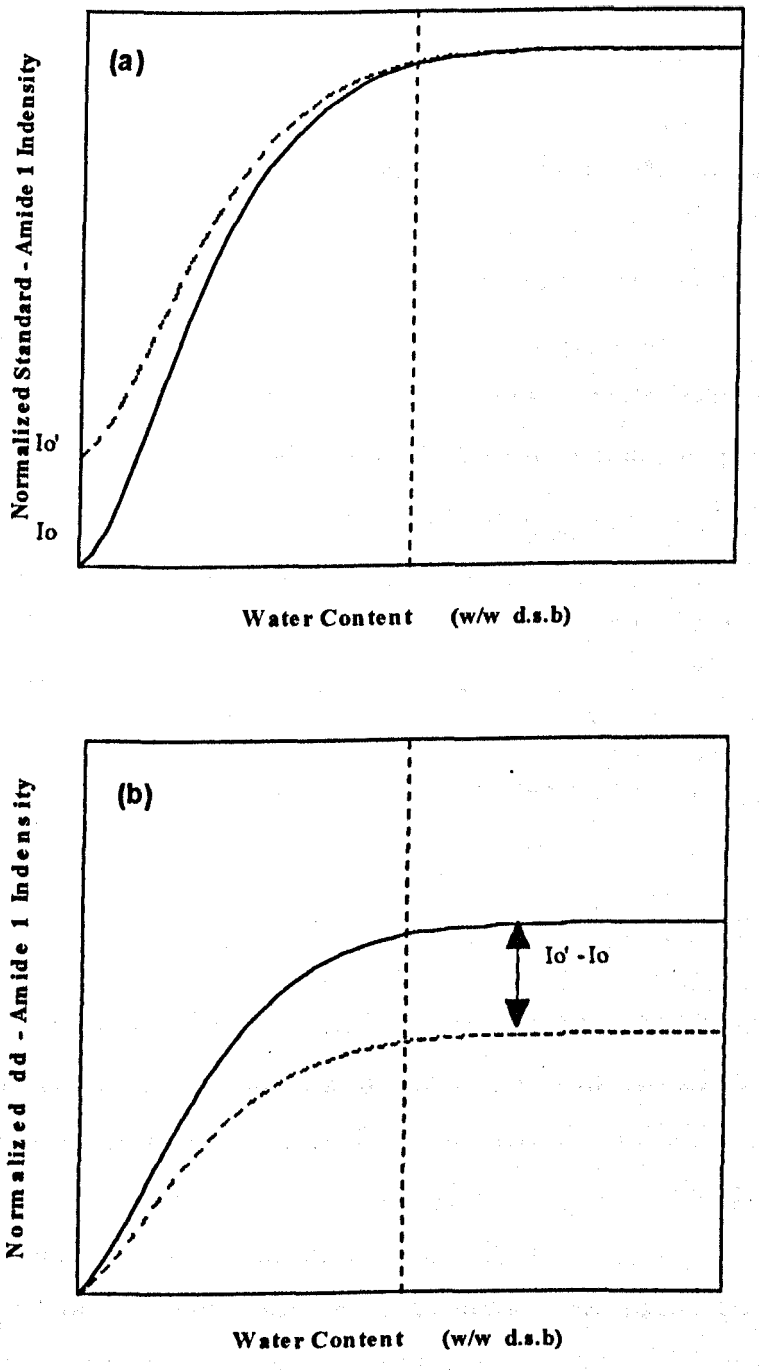

Figure 4.17 The effect of hydrogen bonding of sugar molecules on the C=O group in the dry gelatin-sugar film on the intensity-water content dependence: (a) standard direct mode, and (b) direct difference mode. Equal partitioning of water between the protein and the sugar was assumed. The solid line illustrates the anticipated behaviour of a gelatin film whilst the dotted line describes the situation for gelatin-sugar mixtures.

b- Preferential hydration and no specific protein-sugar interaction

In the more probable case of unequal partitioning of water between the two components present in the mixture, the hydration properties of the protein as defined by the amide 1 intensity would be affected as follows. If the preferential hydration is in favour of the protein and therefore the sugar does not compete for the added water, the rate of gelatin hydration would increase as the probability of an interaction between a water molecule and the C=O is greatly enhanced (Fig 4.18-a). However, in the opposite case, i.e if the sugar competes favourably for the water molecules, the rate of the gelatin hydration as measured by the increase in the amide 1 intensity will be reduced (Fig 4.18-b). Note that in this section, the interaction between gelatin and sugar was not considered and thus there is no shift in the intensity plateau value.

c- Combined effects of protein-sugar interaction and preferential hydration :

However, a better description of real systems could only be obtained if all molecular interactions between all 3 components are considered and therefore a combination of the two previous models should be used. Figure 4.19 illustrates the composite effect of protein-sugar interactions (shift in the intensity) with the role of the preferential hydration of the protein (Fig 4.19-a) or the sugar (Fig 4.19-b).

While the pattern in the case of the preferential hydration of the sugar is easily identifiable, the case for the partitioning of water in favour of the protein is slightly more complex (Fig 4.19-a). However, the water content at which the maximum intensity value is approached (pointing arrow) constitutes a simple check for this latest case.

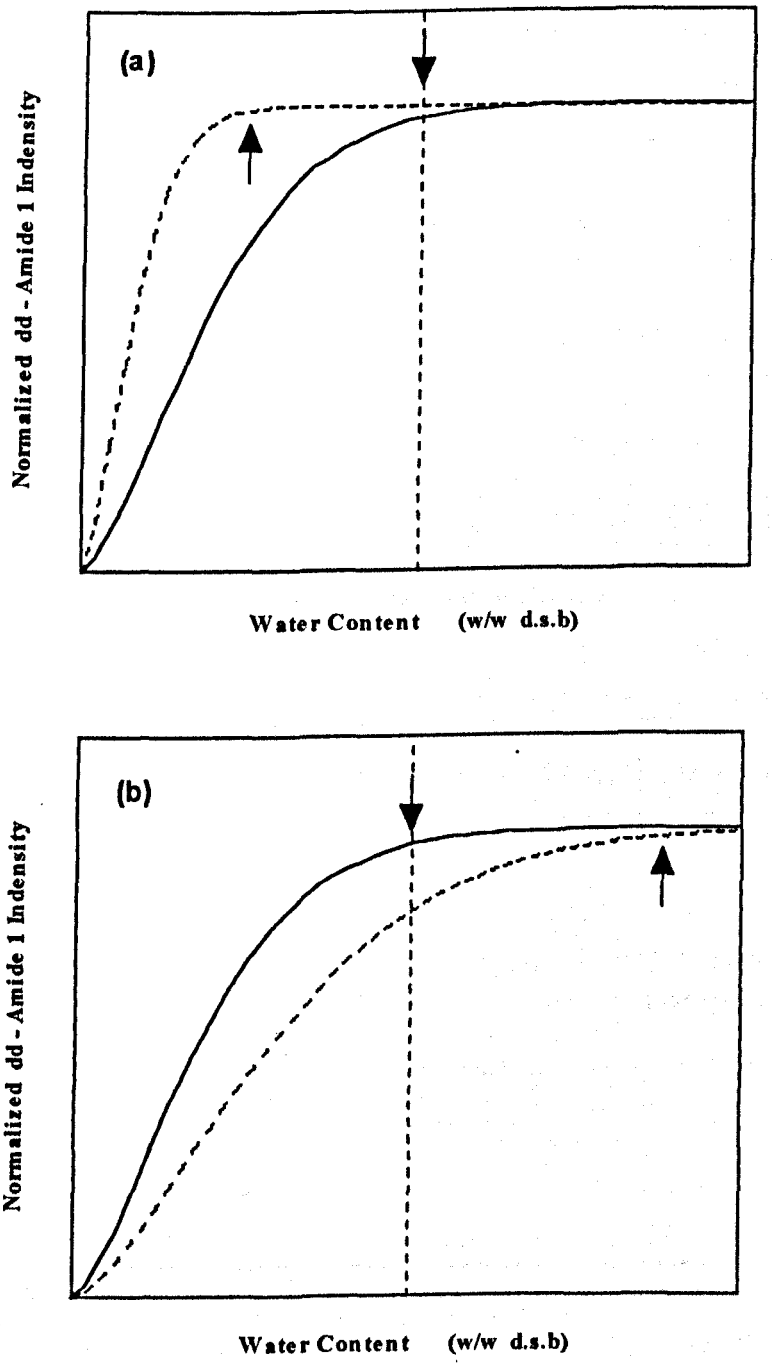

Figure 4.18 Effect of preferential hydration of (a) the gelatin and (b) the sugar. As described for the previous figure, the solid line shows the behaviour of a gelatin film and the dotted line describes the gelatin-sugar system. The arrows point at the approximate water content where the plateau value is reached.

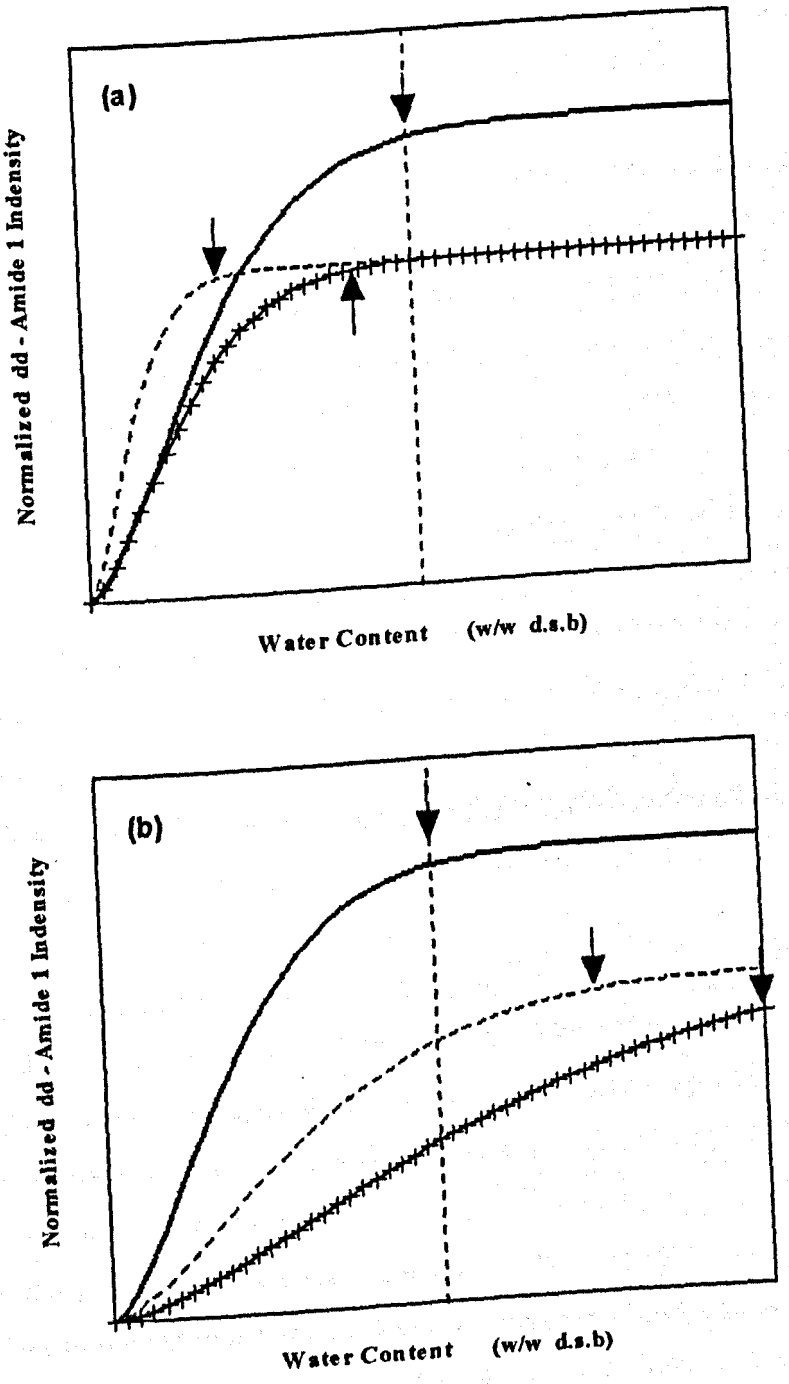

Figure 4.19 The combined effects of protein-sugar interaction with preferential hydration in favour of (a) the gelatin, and (b) the sugar. The solid line illustrates the control (gelatin film) while the dotted line and the crosses describe two examples of gelatin-sugar systems. The arrows point at the approximate water content where the maximum intensity value is approached.

2.1.2.3 Effect of sugars on the hydration kinetics of gelatin

On the basis of the 3 models described above, it was possible to describe the impact of three different sugars (glucose, xylose and sucrose) on the hydration properties of gelatin in gelatin/sugar mixtures containing 80% gelatin and 20% sugar (Fig 4.20). Furthermore, the effect of the amount of sugar was investigated on 3 different gelatin/glucose ratios (100:0, 80:20 and 40:60) (Fig 4.21).

The results in Figure 4.20 approximated closely to model 3. All three sugars showed evidences of a molecular interaction between the sugar and the amide 1 group (C=O). The interaction was found to be comparable for xylose and glucose, but much more significant in the case of sucrose. The origin of this is not fully understood. One possible reason could be a difference in the degree of the phase separation; possibly glucose and xylose phase separated more than sucrose in the protein/sugar mixture (phase separation in amylopectin-xylose systems was observed in some cases as reported in chapter 6 under the same circumstances where sucrose did not phase separate). If phase separation took place in the gelatin-sugar films during drying, the sugar phases of the samples were, nevertheless, in the amorphous state as indicated by a close examination of the 'sugar' bands. Indeed, the line shapes of these bands in the gelatin-sugar films were more similar to those observed in solution rather than in the crystalline state (Mathlouthi *et al.*, 1986). On the other hand, there were clear indications of a preferential hydration of the protein. For all three gelatin-sugar systems, the water content where the intensity reached a plateau value was in the range between 0.2 and 0.4 g of water per g of dry solid, whereas the corresponding value for the control gelatin film was anticipated to be approximately 1.0 to 1.1 g of water per g of dry solid. As expected, both the sugar-protein interaction and the water partitioning aspects were found to depend on the amount of sugar in the system (Fig 4.21).

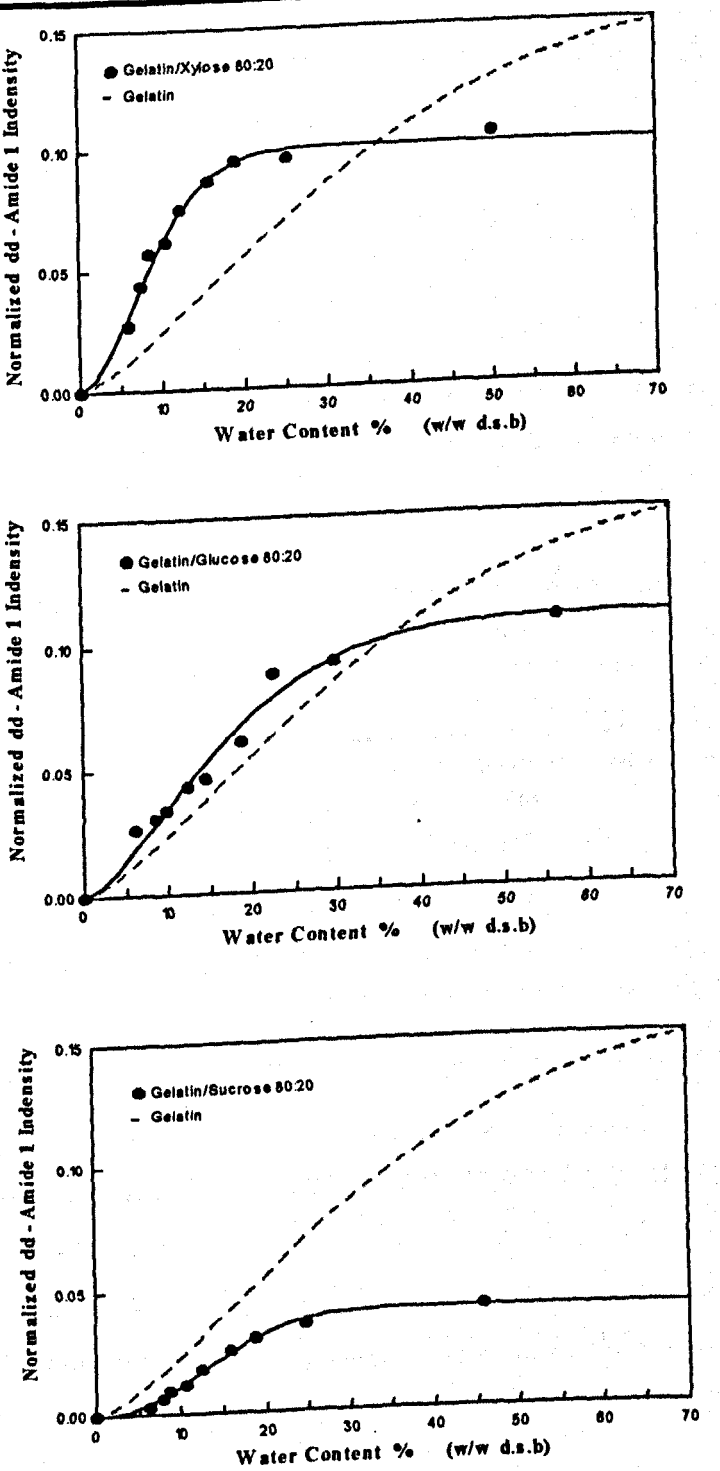

Figure 4.20 Difference in the effects of sugars (a: xylose, b: glucose, c: sucrose) on the hydration properties of 3 different (80:20) gelatin/sugar systems. The dashed line (---) represent the results for the control gelatin film, for reasons of clarity, only the best fit line is shown.

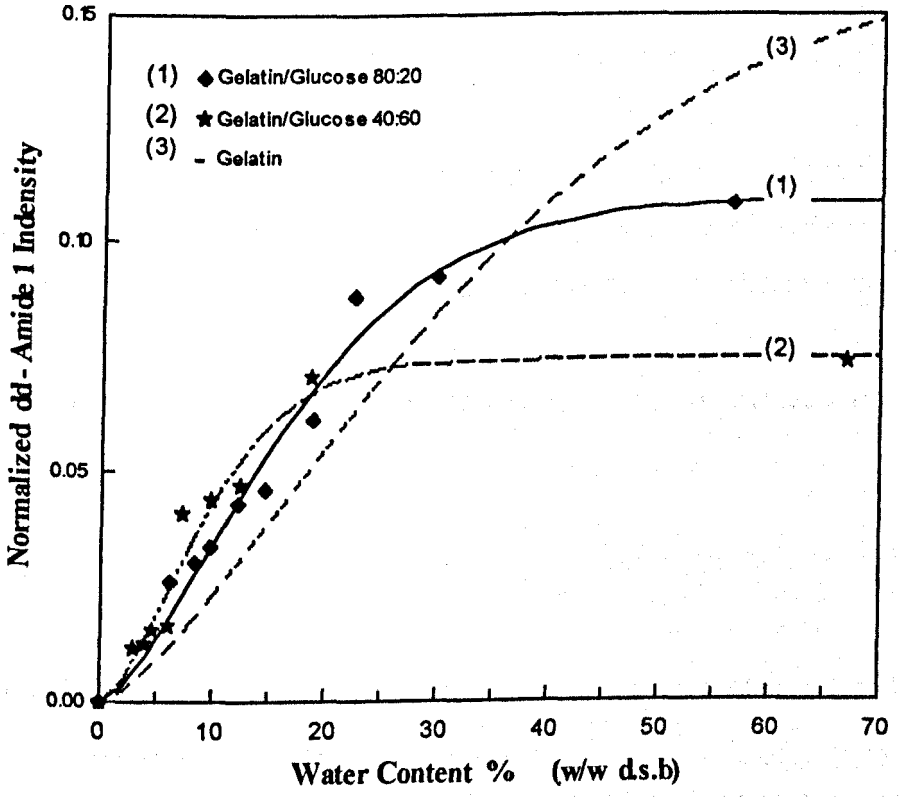

Figure 4.21 Effect of added glucose on the hydration properties of gelatin in gelatin/glucose (80:20 and 40:60) films. The dashed line (---) represent the results for the control gelatin film.

These observations were found to be in good agreement with the water vapour adsorption isotherms of gelatin (measured at 25°C) and amorphous sugars (Iglesias *et al.*, 1982) reported in chapter 2 - Fig 2.14. The water sorption isotherms suggested that gelatin had a higher 'affinity' for water at low RH values. At higher RH values, namely ~70% in the case of sucrose and ~85% in the case of glucose, the hydration of the sugars is favoured.

2.1.3 Discussion and conclusion

The direct difference FTIR methodology was found to be a very useful tool for the study

of the hydration behaviour of protein-sugar mixtures. However, although the technique offered many advantages, the information on the frequency shifts as the hydration process evolved, was lost during the pre-FT subtraction of the spectrum of the dry film.
The role of sugars in the hydration of protein-sugar films was found to be complex. In the dried film, sugar molecules were thought to be closely associated with the protein by means of hydrogen bonds. At relatively low water contents, gelatin was found to hydrate preferentially. This behaviour was as predicted by the water vapour adsorption isotherms.

2.2 Pulsed ^1H NMR study of the hydration of maize-sugar extrudates

Because of their composition (polysaccharides, proteins, sugar and lipids), and processing conditions, maize-sugar expanded extrudates were selected for this study as they constitute a representative model of a wide variety of food products such as breakfast cereals and snacks. In this section the hydration of the maize-sugar system was studied by ^{1}H-NMR in terms of molecular mobility. The effect of extrusion cooking on the properties of maize grits was also established.

2.2.1- Effects of extrusion process on the NMR properties

The spin-spin relaxation properties of the native and extruded maize grit samples recorded as a function of the water content were examined.
Both native and extruded samples displayed a decay time (T_2) for the 'solid' component that increased with increasing moisture content which was consistent with a greater polymer segmental mobility induced by plasticization by water (Fig 4.22). At low water levels, less than 16 %, there was little difference between extruded and non-extruded samples but at higher water levels, the solid T_2 results showed a higher mobility for the various polymers (amylopectin, amylose and proteins) in the extruded material. These

observations are consistent with the following interpretation. Intact starch granules, which are present only in the native samples, can only absorb a certain volume of water, which will serve as a plasticizer. At water contents below this limit, proton mobility is similar in gelatinized and non-gelatinized samples. However, at higher water contents, the extruded gelatinized samples provide the water with a greater access to the starch polymers and permit a more effective plasticization.

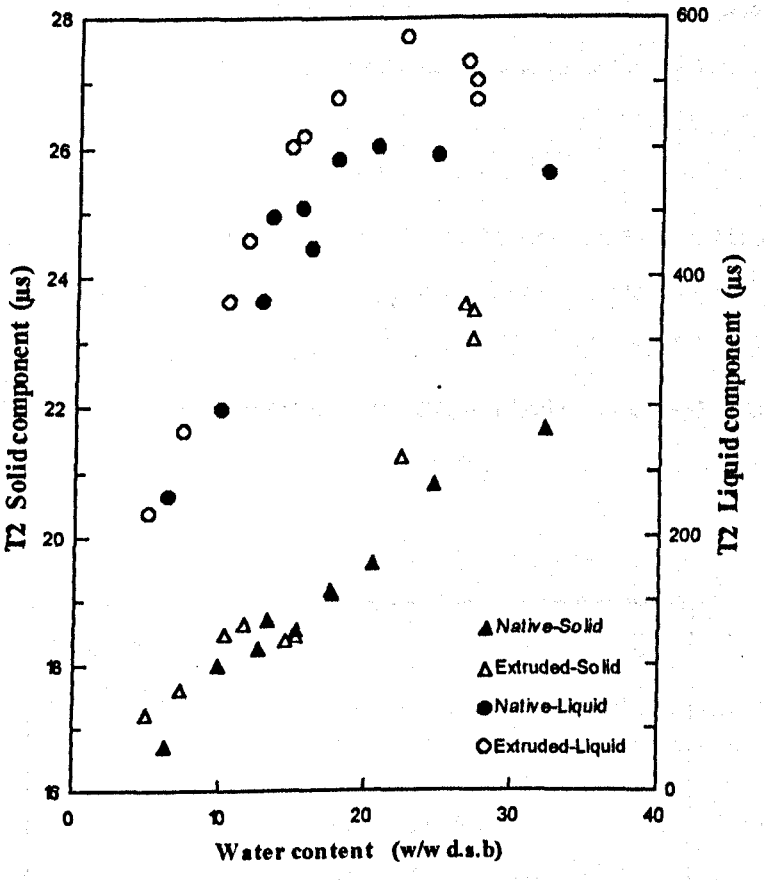

Figure 4.22 The spin-spin relaxation times (T_2) of the solid and the liquid components of the NMR free induction decay. Results obtained on native and extruded maize grits at different degrees of hydration are compared.

This same pattern was observed for the 'liquid' T_2 where the values measured on the extruded samples were greater than those of the native samples. At higher water contents (>20 %) the rate of proton exchange between water and the starch hydroxyl groups

became important on the time scales of the NMR relaxation measurements. The increasingly effective exchange is demonstrated by a decrease in the recorded 'liquid' T_2. Under fast exchange conditions, the observed relaxation rate is the mean of the rate related to free water and to the exchangeable protons, inevitably dominated by the latter. An increase in the observed relaxation rate ($1/T_2$) is evidence of an increasingly effective exchange process.

Although extrusion cooking had an effect on the relaxation times of the rigid and the mobile components of the FID, no significant differences in the relative contribution of the mobile and rigid components to the total NMR signal were found (Fig 4.23). A linear relationship between the NMR liquid/solid ratio and the water content was found. However, the proton densities of the maize and the water contents calculated as described in the next paragraph, predicted the solid line presented on the plot with a zero intercept and a slope of 1.794. Although the slope for the values obtained for water contents below 25% was as predicted by the ratio of the proton densities of water and the maize-sucrose mixture, the intercept was negative leading to a value of approximately 2% water for a liquid/solid ratio of 0.

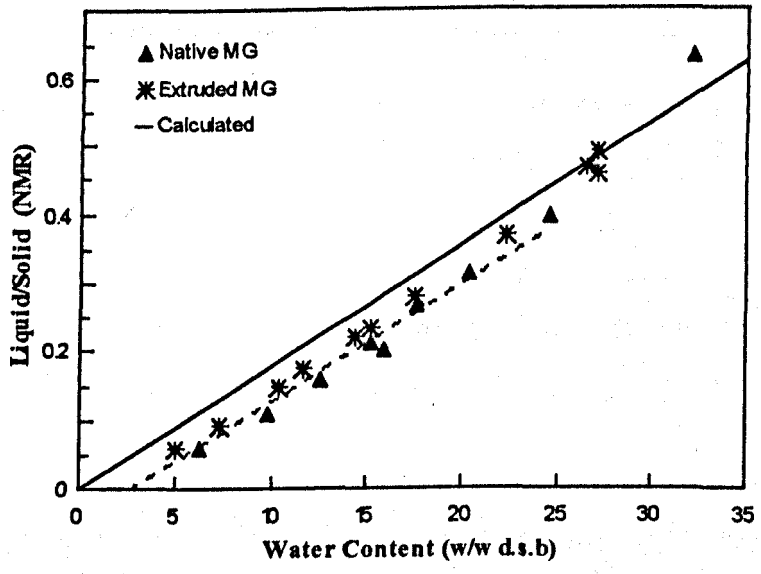

Figure 4.23 The ratio of the NMR signal emanating from the 'liquid' NMR component relative to the 'solid' component as a function of water content defined by oven drying.

These observations indicated that the calculation of the maize proton density described in the next section was a good approximation and that probably the first 2 - 3 % of added water was so tightly trapped in the solid matrix that the water protons contributed to the signal arising from the rigid-lattice. This NMR phenomenon arising from tightly bound water molecules was described in the section concerning the hydration of xanthan and gelatin.

2.2.2 Maize-sucrose systems

The ratio of the liquid relative to the solid component of the FID signal measured on the samples containing sucrose became progressively larger with increasing water content compared to the values determined for the maize sample not containing sucrose (Fig 4.24).

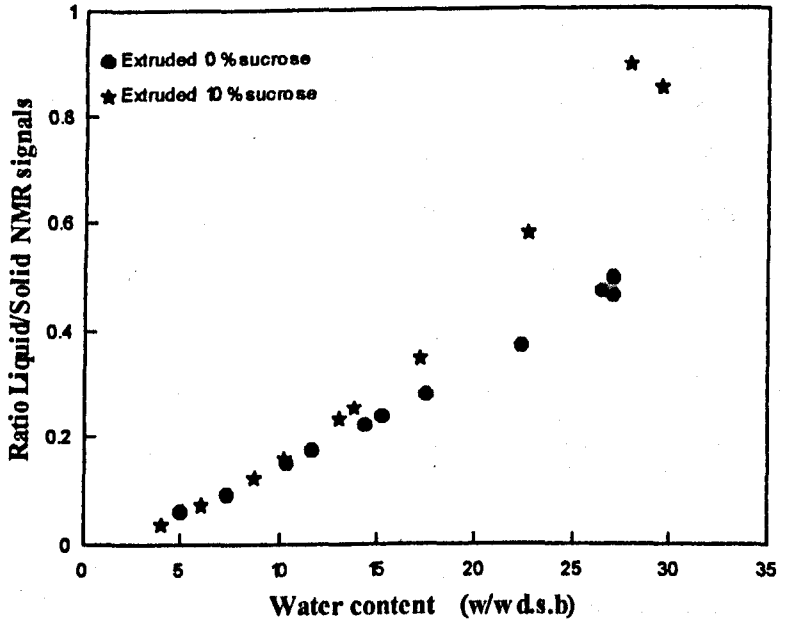

Figure 4.24 The ratio of the liquid to solid NMR signals as a function of the water content for 2 sucrose concentrations (0% and 10%).

The NMR signal amplitudes should, however, be described with respect to the proton densities of the various species in the system. Let S_{MG}, S_W and S_S be the contribution to the total NMR signal, S, resulting from the biopolymers of the maize grits, the water and the sucrose respectively, and w_{MG}, w_W and w_S be the weight fraction of each of these species in the mixture. If d_{MG}, d_W and d_S denote the proton densities of the various components, the proton densities of water and sucrose are $d_W = 2/18$ and $d_S = 22/342$ respectively. Due to the complex composition of the maize grits, d_{MG} was calculated by assuming an approximate composition of 90 % polysaccharides and 10 % proteins. The proton density of the maize grits was calculated as the weighted proton density of these two components. The value used was $d_P = 0.0622$ (the proton density of starch being d_{st}=10/162 ie 0.0617 and the proton density of protein was calculated assuming an equal composition of the 20 most common amino acids d_P= 0.0665). The expected contributions to the total FID signal, S, by the three constituents are:

$S_{MG} = k\ w_{MG}\ d_{MG}$ from maize grits, $S_S = k\ w_S\ d_S$ from sucrose and,

$S_W = k\ w_W\ d_W$ from water, where k is a constant factor.

Analyses of the resulting signal (A_{tot}) led to the isolation of two constituent Gaussian processes, each with an associated amplitude A_{sol} and A_{liq} representing the solid and liquid components respectively, which can be expressed as follows :

The solid component amplitude $A_{sol} = k\,(w_{MG}\,d_{MG} + w_S\,d_S)$ results from maize grits and sucrose, and the liquid component amplitude $A_{liq} = k\,w_W\,d_W$ results from water. The total signal amplitude may then be expressed as $A_{tot} = k\,(w_{MG}\,d_{MG} + w_S\,d_S + w_W\,d_W)$

It is often convenient to normalize all signals to an expected 'solid' signal defined as unity; the solid amplitude fraction of the total can then be described by :

$$A = \frac{A_{sol}}{A_{sol} + A_{liq}} \left(1 + \frac{w_W\,d_W}{w_{MG}\,d_{MG} + w_S\,d_S}\right) \qquad (4.5)$$

After this normalization, the solid amplitude would be constant and equal to 1 when plotted against the water content (Fig 4.25).

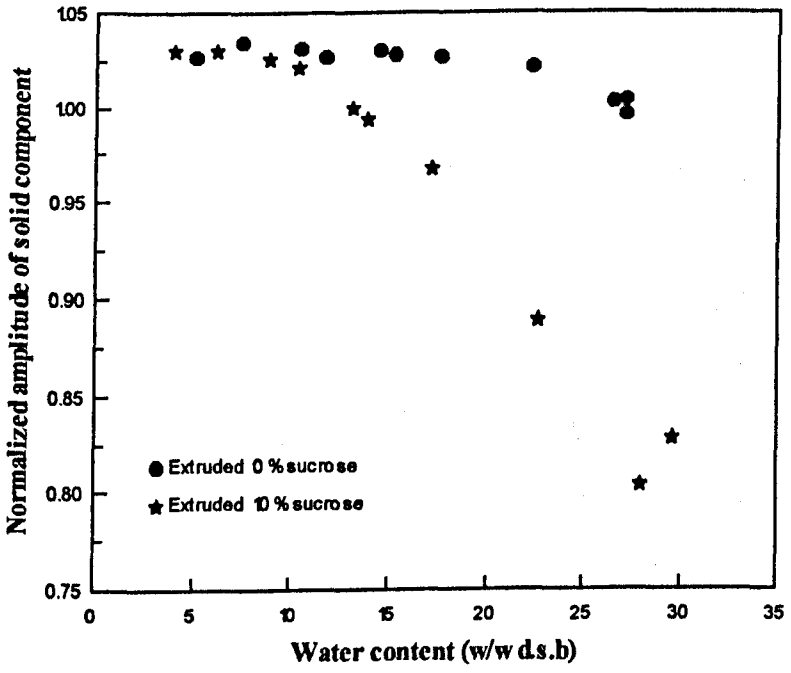

Figure 4.25 The normalised amplitude of the rigid component of the FID plotted versus water content for 0% and 10% sucrose maize grits extrudates.

However, the values for the 0 % sugar sample showed a small offset relative to 1. This is not unusual. In simple starch/water systems a small water fraction is apparently incorporated into the starch matrix and contributes to the solid signal. However, there is a second explanation, namely that the assumption concerning d_{MG} was incorrect as the protein composition was unknown and other biomolecules (lipids) which were not accounted for, were present in the system. However, this second hypothesis was discarded since the results in Figure 4.23 showed that the experimental (1.794) and theoritical (d_W/d_{MG}=1.786) gradients were very similar. The plot of the normalized solid amplitude versus water content clearly displayed the solvation process of sucrose and its subsequent participation in the aqueous phase signal. This suggestion is supported by the shorter T_2 values recorded for the liquid component at water contents above 10 %. T_2 values are thought to be shortened by the increase of the viscosity of the aqueous

phase through the presence of sucrose (Fig 4.26).

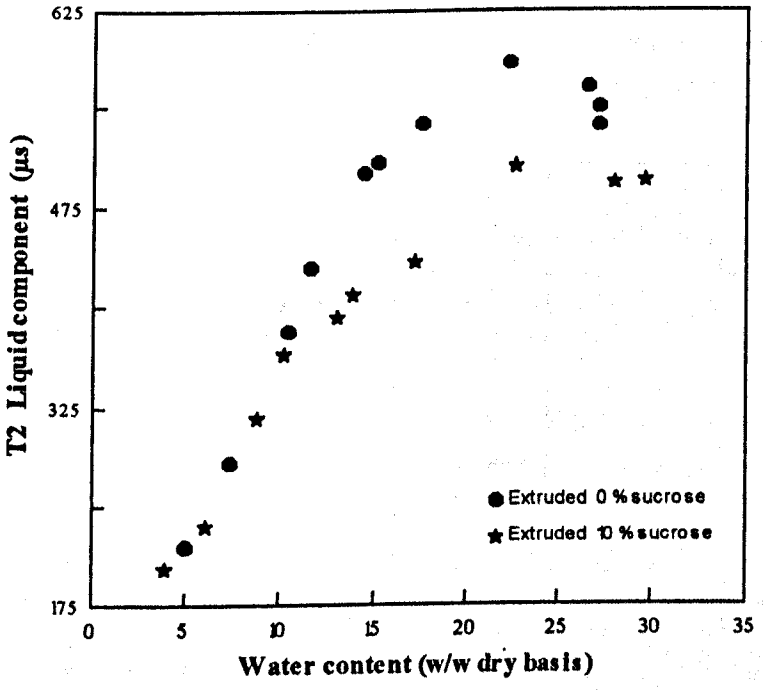

Figure 4.26 The spin-spin relaxation time of the liquid component of the NMR free induction decay of extruded maize grits containing 0% and 10% sucrose as a function of the water content.

The effect of the concentration of sucrose in the system is shown in Figure 4.27. The higher the sucrose content, the larger the changes in the amplitude of the solid component as the samples were hydrated (Fig 4.27-a). At the higher water contents, the solid amplitude was decreased by approximately 5 % for the sample containing 5 % sucrose and 10 % for the sample containing 10 % sucrose relative to the control (0 % sugar). This suggests that the entire sucrose content was dissolved in the aqueous phase at approximately a moisture content of 25 %. Above this water content, the increase in the relative amplitude of the NMR signal is greater than the total amount of sucrose present in the system, which points to a contribution from the maize grit protons to the signal resulting from the liquid component as the rate of proton exchange between the polymer

and the water increases, and the mobility of the biopolymers increases due to the plasticizing effect of water. The decrease in the relaxation times of the liquid component was proportional to the sucrose content (Fig 4.27-c), a consequence of the increase in the viscosity of the liquid phase with increasing sucrose content.

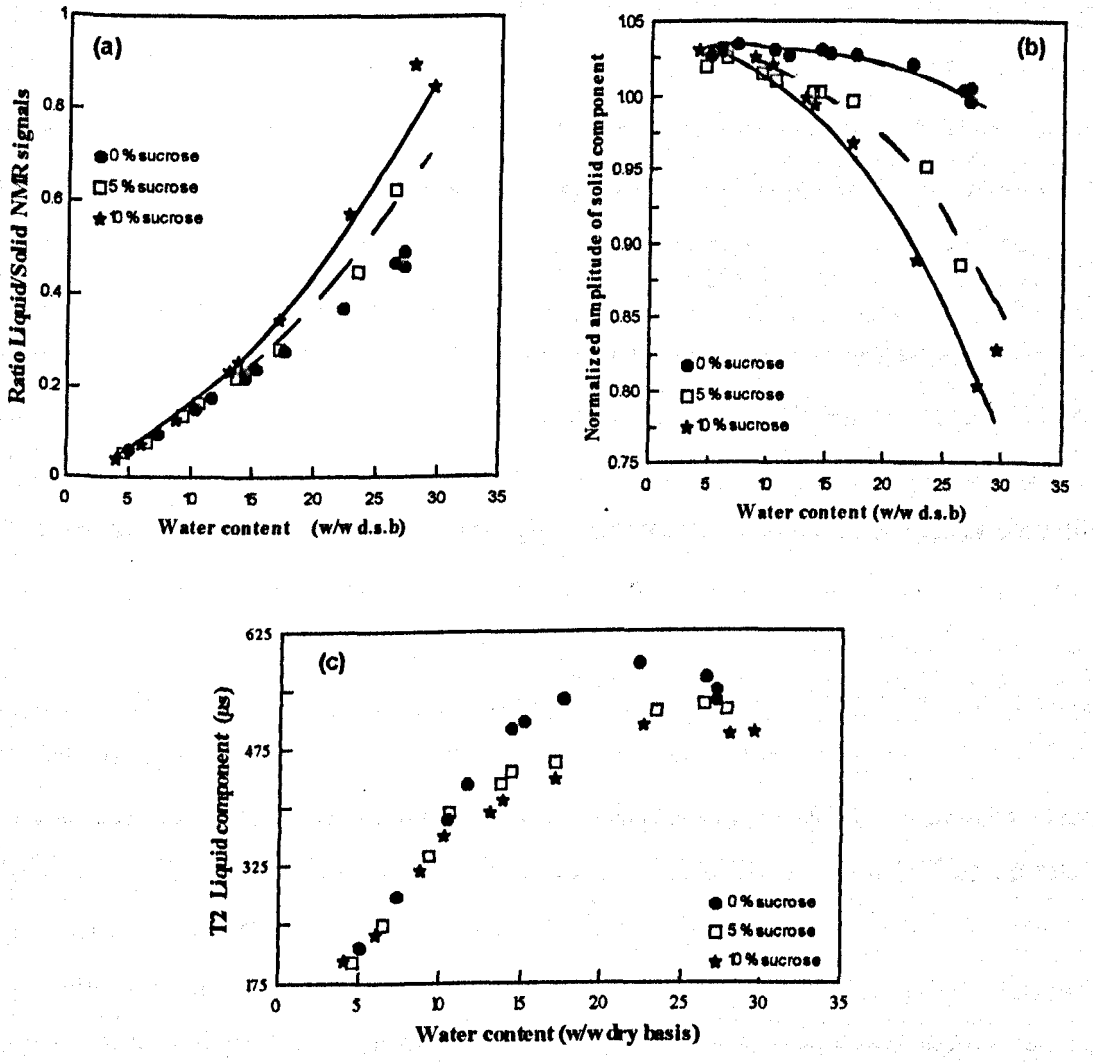

Figure 4.27 Effect of sucrose content (0%, 5% and 10% sucrose) on the hydration properties of maize-sucrose extrudates measured by proton NMR relaxation :

(a) the ratio of the liquid to solid NMR signals

(b) the normalised amplitude of the solid FID. The offset between the 3 lines is of the order of the difference in sucrose content (5 %) between the 3 samples.

(c) the T_2 of the liquid FID component.

These observations suggest that the roles of water and sugar in plasticizing biopolymers may be more complex than is assumed in the derivation of the ten Brinke (ten Brinke *et al.*, 1983) and the Couchman-Karasz (Couchman *et al.* 1978) equations. To determine whether this is so, we can calculate, using these equations, the water content at which a T_g of 40° (the temperature at which the NMR measurements were performed) should be observed and compare these values with those where a contribution of the protons of the 'solid' component to the 'liquid' component of the NMR signal is observed.

Such calculations (equation 2.3 - chapter 2) show that the T_g is equal to 40°C at approximately 22 % (w/w d.s.b) for the system containing no sucrose and 21 and 19 % for the 5 % and 10 % sucrose systems respectively. The contribution of the polymer protons to the liquid NMR signal is observed at water contents above 24 % (w/w d.s.b). The appearance of sucrose in the liquid NMR signal is observed at approximately 17 and 11 % for the samples containing 5 and 10 % sucrose respectively. A clear correlation between these water contents and the glass transition parameters suggests that the generation of a concentrated sucrose solution promotes the plasticization of the polymer component. We suggest, however, that one additional factor should be taken into account when considering ternary systems, namely the differential partitioning of water between the different components.

Despite the reasonably close correlation found by Kalichevsky *et al.* (1993) between the experimental T_g values and those calculated using the ten Brinke *et al.* (1983) equation (equation 2.3 - chapter 2), it is clear that in systems containing sugar, there is a small but systematic departure from the calculated values. The measured values were smaller at low water contents and greater at high water contents. Since the T_g will be greatly influenced by the amount of the plasticizer within the polymer domains, it seems possible that these deviations could be explained by a partitioning of water between the various components such that water is preferentially associated with the polymer at low water contents and with the sugar at higher water contents. This hypothesis of unequal partitioning of water is in agreement with the work of Hartley *et al.*(1995) which described the hydration of other biopolymer mixtures.

The concept of differential water partitioning could imply that the effective T_g values of the systems investigated in this work are lower than the calculated values and therefore the water contents at which the T_g of these samples is equal to 40°C are lower than predicted by the ten Brinke equation. This would consolidate the hypothesis of a direct relationship between the glassy/rubbery state of the polymer and the mobility of the sugar. The water vapour sorption isotherms of amorphous sucrose (25 °C) (Iglesias *et al.*, 1982) and extruded maize measured at 25 °C are shown in Figure 4.28. The figure demonstrates that for relative humidities higher than 45%, the affinity of water for sucrose is greater than that for maize and the value of RH = 45% corresponds to a water content of 10% approximately. This is in good agreement with the water content where the dissolution of sucrose was observed to commence by NMR (15%).

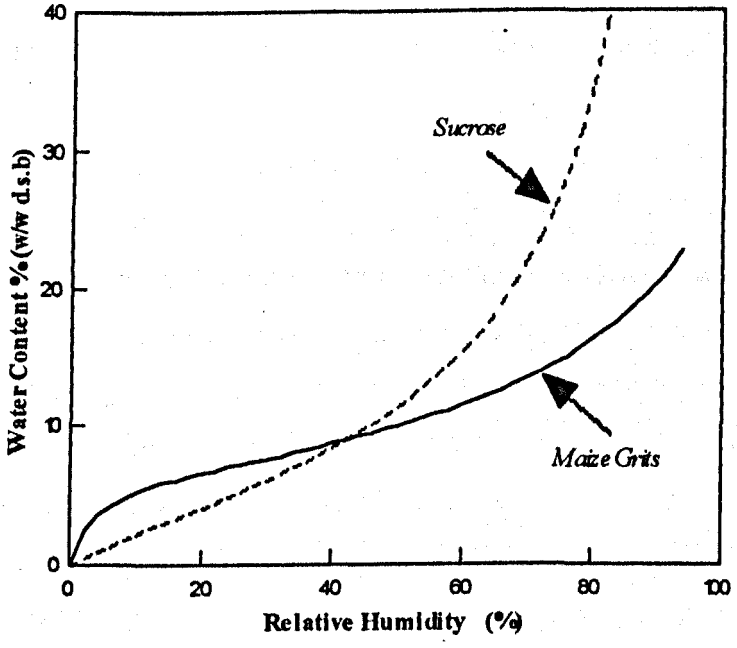

Figure 4.28 Water vapour adsorption isotherms (25°C) of amorphous sucrose (Iglesias *et al.*, 1982) and maize extrudate.

These results are also in agreement with the FT-IR and DSC studies of Pautrat *et al.* (1995) in which they describe the changes they observed in terms of the establishment of hydrogen bonds which they equated with dissolution. Using this definition, it appears that sucrose is incorporated into the solid ie polymer phase at moisture contents below 15 %, but that at higher water contents the dissolution of the sucrose in the aqueous phase occurs. Furthermore, the absence of any evidence of sucrose crystallisation in the x-ray scattering spectra of the samples recorded at different water contents supports the view that the sucrose is fully miscible with the polymer phase at low water contents and in the aqueous phase at high water contents over the whole range of sugar concentrations investigated in this work.

Conclusion

The results suggest an increase in sugar mobility at water contents above 10-15 % when maize-sugar mixtures are progressively hydrated leading to a sugar-water aqueous phase. This solvation process can be probed by time domain NMR since it affects both the signal amplitude and the relaxation rates of the solid and liquid components. The assumption that the maize/sugar/water ratios are constant over the entire moisture content range is therefore not valid as the partitioning of sugar between the solid and liquid phases changes with increasing hydration. This last statement does not exclude the possibility of interactions between the sugar molecules and the biopolymer. Indeed, the absence of a crystalline sucrose phase, especially at low and intermediate water contents, implicates such interactions.

2.3 The hydration of amylopectin-sugar extrudates

Another example of the role of water in mobilising selectively the individual components of a mixed system is reported in this section.
The results were obtained from the same experiments performed to study the retrogradation of amylopectin-sugar systems (chapter 6).

2.3.1 Hydration of amylopectin extrudates

As described in more detail in chapter 6, the spin relaxation properties of starch extrudates depended strongly on their amorphous / crystalline state. Thus the NMR properties change significantly on storage of amylopectin extrudates as the polysaccharide reordered through the process known as retrogradation. The results describing the kinetics of the retrogradation are not reported here as they are outside the scope of this chapter.

In this section, the relaxation NMR properties (spin-spin relaxation times and relative amplitudes) of the freshly gelatinized system were obtained by extrapolation of the results recorded as a function of ageing, to zero storage time (t=0). The NMR properties of the 'fully' retrograded system were obtained from the Avrami non-linear modelling of the retrogradation data (t=∞).
Results of the spin-spin relaxation times of the fast decaying component of the FID describing the rigid polymer component, and the CPMG component describing mainly the water showed the expected direct dependence on the water content. As the water content was increased, the mobility of the polymer in both the 'freshly' gelatinized ($T_{2\ solid}$ at t=0) and after 'full' retrogradation ($T_{2\ solid}$ at t=∞) was enhanced (Fig 4.29). Likewise, increased moisture contents yielded higher $T_{2\ CPMG}$ values i.e enhanced mobility of water. This was understood in terms of the increased fraction of the free water in the system leading to an increase in the weighted T_2 value of the combined bound and free

water populations, which should be represented as a continuum of relaxation times rather than a number of discrete populations.

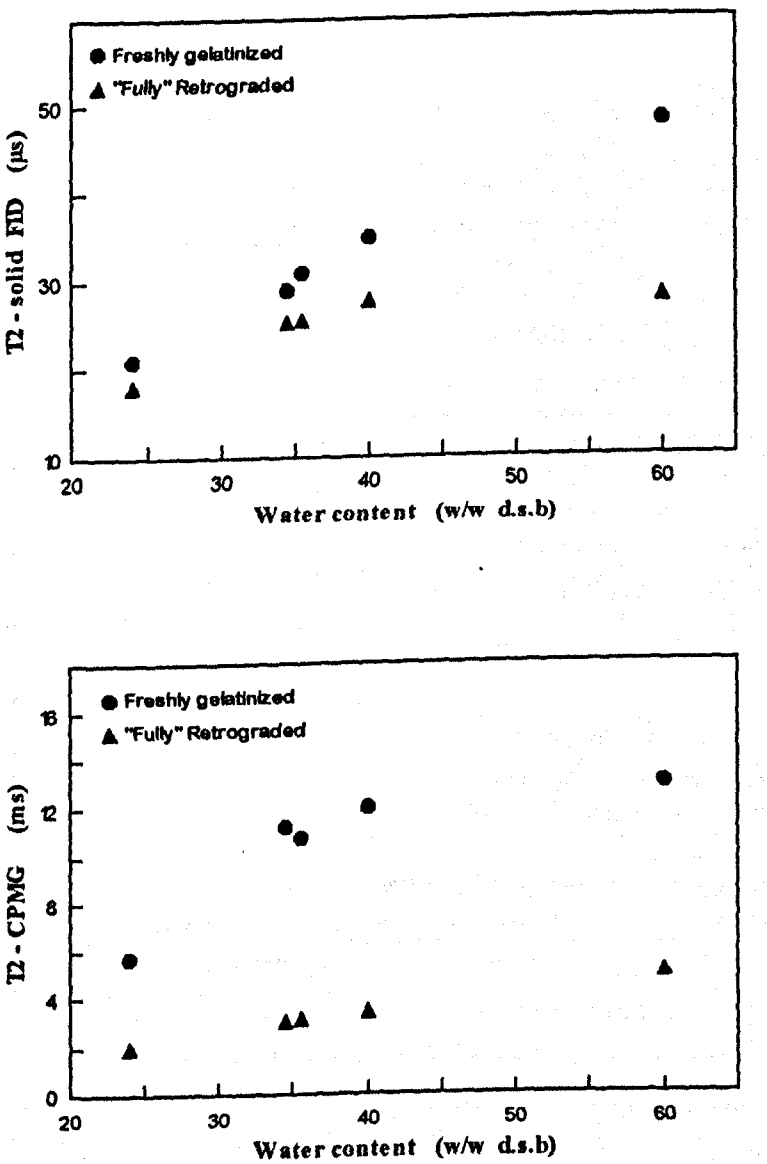

Figure 4.29 The spin-spin relaxation times (T_2) of the 'solid' component of (a) the FID NMR signal and (b) the spin-echo (CPMG) component for 'freshly' gelatinized and 'fully' retrograded amylopectin extrudates

The increase of the moisture content yields an increase in the fraction of water molecules situated at a distance from the relaxation 'sink' (i.e the polymer network) greater than that of the average displacement of a water molecule in the time scale of the experiment, the echo time (2τ= 0.512 ms).

The ratio of the amplitude of the 'liquid' to 'solid' components of the FID increased with increasing water content. The values for the fresh gels were consistently higher than those for the same systems after retrogradation (Fig 4.30). This was anticipated as the mobility of gelatinized amorphous starch components is much greater than the ordered crystalline components.

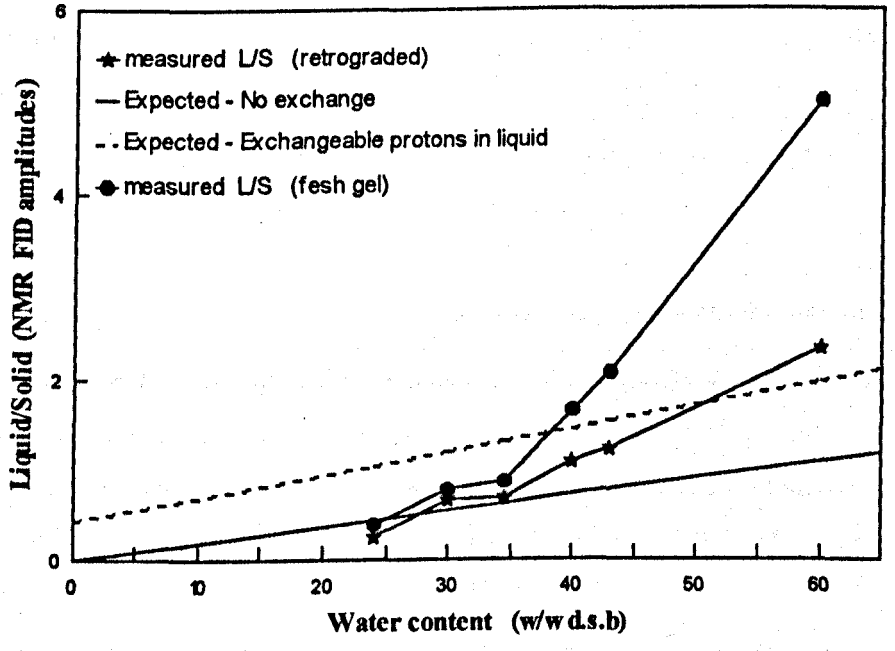

Figure 4.30 The amplitude of the 'liquid' FID component relatively to the 'solid' signal as a function of the water content of amorphous and retrograded amylopectin extrudates

At water contents above ~30% (w/w d.s.b), the measured liquid/solid ratios were increasingly larger than anticipated if the assumption that the liquid signal resulted only

from the water while the starch was responsible for the solid signal. The expected line was recalculated assuming that the exchangeable protons (OH) of the starch were in fast chemical exchange with water and consequently contributed to the 'liquid' component of the free induction decay.

The liquid / solid ratios measured on the retrograded gels were found to lie between the two calculated lines up to 50% water. The values recorded on the fresh gels exceeded the ^{1}H-exchange line at water contents as low as 37%.

This leads to the conclusion that the ^{1}H exchange becomes relevant on the NMR time scale at water contents above 30% (w/w d.s.b) for the range of biopolymers investigated (gelatin and starch polysachharides). At higher water contents, components of the biopolymer are mobilised and consequently have a 'liquid' type behaviour in terms of NMR properties.

2.3.2 Hydration of amylopectin-sugar mixtures

The liquid / solid ratios recorded on the fully retrograded amylopectin and amylopectin-sugar extrudates were compared for fructose, sucrose and xylose (Fig 31-a). The ratios for the sugar containing samples were larger than the control amylopectin-water gels. The samples containing xylose and fructose exhibited similar behaviour in terms of liquid/solid ratios, and the effect was directly proportional to the concentration of sugar in the system (Fig 31-b).

These observations were compatible with the hypothesis developed earlier where it was suggested that when enough water is present in the system, the sugar had a solution type behaviour.

The difference between the two monosaccharides (fructose and xylose) and the disaccharide (sucrose) could be due to differences in the solubility of the particular sugar or to the molecular weight of the sugar which is known to affect the mobility i.e the correlation time.

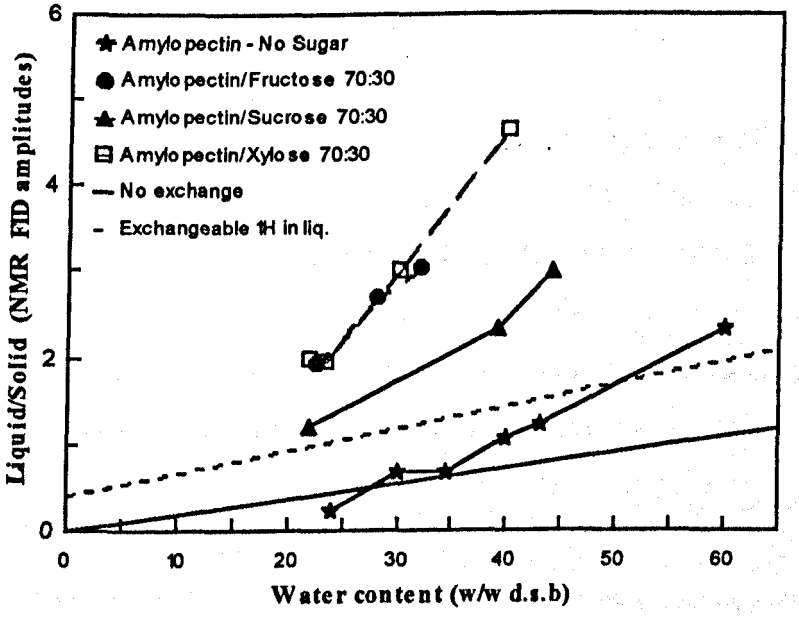

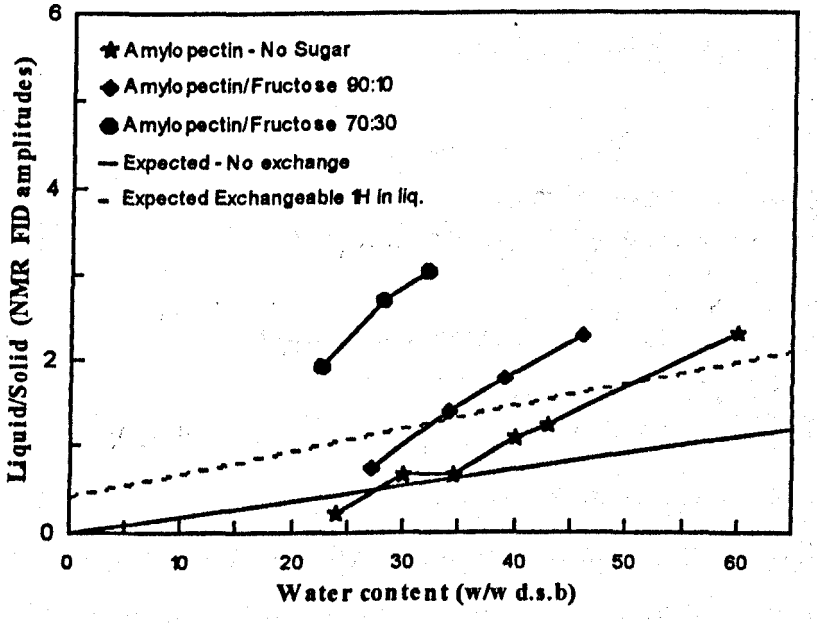

Figure 4.31 The ratio of the amplitudes of the 'liquid' and 'solid' components of the FID as a function of the water content for:

(a) 3 different amylopectin/sugars (70:30) extrudates.

(b) 70:30 and 90:10 amylopectin/fructose extrudates.

2.4 Hydration of multi-component systems

Based on the results described above, a model of the hydration of biopolymer-sugar systems has been suggested (Fig 4.32). The drying of the homogeneous biopolymer-sugar-water mixtures (melt in the extruder barrel or solutions) was achieved by evaporation of the water (when exiting extruder die at high temperatures, by oven or over P_2O_5 drying) (Fig 32-a & b). As the dried mixture is rehydrated (Fig 32-c), the first water molecules (water contents < 10-15%) bind preferentially to the biopolymer. Further hydration (a second stage) is accompanied by the sugar binding the majority of the added water. The implication of this second stage is that a 'solution-type' behaviour is demonstrated by the NMR properties of the sugar molecules which now contribute to the slow decaying mobile component of the FID. The relaxation and the glass-rubber transition of the biopolymers would take place during this hydration process.

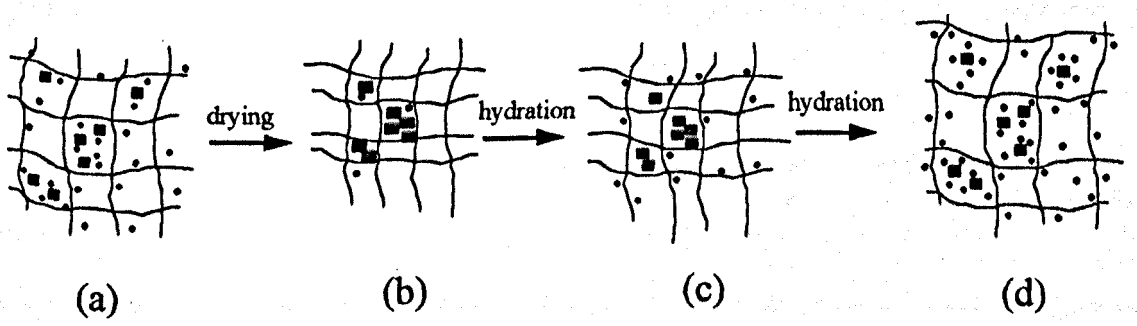

Figure 4.32 Schematic representation of the effect of dehydration/hydration on the different components of a biopolymer-sugar system (the biopolymer network is represented by the lines, the sugar by the squares and the water molecules by the dots:
(a) The biopolymer-sugar-water melt (inside the extruded barrel) or in solution
(b) The same system after the majority of water has been eliminated by evaporation at the exit of the extruder and/or by subsequent oven drying
(c) The first steps of hydration (up to 10-15% w/w d.s.b): the biopolymer is preferentially hydrated
(d) The hydration of the sugar is achieved by the additional water molecules

Conclusion

The synergic combination of various spectroscopic techniques has given a more complete description of the interaction between water on one side, and biopolymers and biopolymer-sugar systems on the other. The hydration of biopolymers is accompanied by the expected increase in the molecular mobility. This plasticization leads to the ordering of the biopolymer and consequently a narrowing of the conformational distribution is observed.

The hydration of biopolymer-sugar mixtures involves differential partitioning of water between the various components. The water vapour adsorption isotherms of the individual components can provide an empirical approach to anticipating the water distribution. The study of the hydration properties of mixed systems provides information on specific interactions between the two components at a molecular level.

Water diffusion in biopolymer gels

Introduction

This chapter describes the results of a study of the self-diffusion coefficient of water in sugar solutions, biopolymer (amylopectin, potato starch and gelatin) gels and biopolymer-sugar-water gels.

The diffusion of water is of major interest in different areas of the food and pharmaceutical industries. It is of primary relevance in hydration/dehydration processes, enzyme activity, drug delivery, etc. Furthermore, there is little doubt that diffusion of water has a direct impact not only on processing and the sensory perception of foods, but also on the shelf life of various products (Karel *et al.*, 1991).
It has been demonstrated that the study of restricted diffusion using pulsed field gradient NMR (Stejskal *et al.*, 1965) techniques, first described by Tanner *et al.* (1968), can be used to probe the structure of hydrocolloid gels (Ohtsuka *et al.*, 1994), the droplet size distribution (Packer *et al.*, 1972; Callaghan *et al.*, 1983; Soderman *et al.*, 1992) in water in oil emulsions and thus serve as a probe of sample morphology.

Although a considerable amount of work on the self-diffusion of water in biopolymer gels can be found in the literature (Jönson B, 1986; Brosio *et al.*, 1994 and Ohtsuka *et al.*, 1994), much less is known about relatively concentrated systems (Kimmich *et al.*, 1993). Moreover, the effect of added sugars and the processing conditions on the diffusion of water have not been investigated. In this chapter, particular attention has been given, firstly, to the diffusion of water in polysaccharide and protein gels over the polymer concentration range between 0 to 3 g of polymer per g of water. Secondly, the translational mobility of water was

investigated in the ternary biopolymer-sugar-water system, which provided the archetypal model for this thesis and for the entire ACTIF II programme. The first section is concerned with sugar solutions i.e a 0:100:w composition of the ternary system (w being the water content). The second section investigates the 100:0:w biopolymer-sugar-water system and the third section illustrates the diffusion of water in the 75:25:w and 50:50:w mixtures.

1. Experimental techniques

1.1 Sample preparation

The gels were prepared directly in the NMR tube by heating a polymer/sugar suspension to 65-70 °C for 5-10 minutes in order to obtain a consistent gel. For the majority of the sample compositions investigated, the gels were found to be consistent at 40°C since the melting point of these systems was, typically, greater than the temperature at which the NMR measurments were performed (40°C) as shown in section 5.2.2 of chapter 6, and for gelatin by Borchard *et al.* (1980) (Fig 5.7).

In order to investigate the effect of the processing conditions, in particular the mechanical energy, upon the diffusion of water in biopolymer systems (Mitchell *et al.*, 1992), samples prepared by extrusion under relatively mild conditions (temperature ≤ 120°C) were compared with the control samples obtained by simple heating.

The samples were sealed and stored at 25±2°C in a temperature controlled room for a minimum of 24 hours to allow for 'full' retrogradation / equilibration of the system. The optimum storage time was estimated from the retrogradation kinetics obtained on similar systems (chapter 6).

Both heat gelatinized and extruded samples were conditioned for 20 minutes in sealed 8 mm NMR tubes at 40±0.1°C in the NMR spectrometer probe head prior to measurement.

1.2 NMR measurements

The pulsed field gradient spin-echo (PFG-SE) and stimulated echo (PFG-StE) methodologies, described in chapter 3, were used to obtain the self-diffusion coefficient of water in systems having water contents ranging from 0.25 to 4 g of water per g of dry solid. The choice between these two techniques depended upon the NMR relaxation properties of the samples. The general trend is for low water content samples to have reduced T_2 values. This leads to a reduction of the time available to complete the diffusion sequence, and the necessity to increase the amplitudes of the field gradient pulses if sufficient signal attenuation is to be obtained to yield an accurate determination of the diffusion coefficient. This technical problem is further intensified by the feature that diffusion itself is reduced in dry samples, leading to a reduced signal attenuation. Some alleviation is produced if the more 'sophisticated' triplet sequence (PFG-StE) is adopted as in general T_1 exceeds T_2.

2. Results and discussion

2.1 Water self-diffusion in sugar solutions and biopolymer gels

2.1.1. Water diffusion in sugar solutions

2.1.1.1 Self-diffusion of water in solutions of different sugars

Diffusion coefficients in sucrose solutions were measured using the PFG-SE pulse sequence with a separation between the 90° and the 180° pulses of τ=5 ms yielding an echo time of 10 ms (2τ). The separation between the 90° and the first gradient pulses was t_i=200 µs while the gradient separation Δ was the same as τ (5 ms). The gradient width δ was increased from 0 ms to 1 ms by steps of 0.1 ms. As the Bruker field gradient equipment gave the gradient amplitude in arbitrary units ranging from 0 to 10, the absolute amplitude was

estimated using the self-diffusion coefficient of water measured at 40°C (~2.38 10^{-9} $m^2.s^{-1}$). The measurements were carried using a gradient amplitude G=7 arbitrary units which corresponded to approximately 1.74 T m^{-1}.

As illustrated by equation 3.24 (chapter 3), the plot of the logarithm of the echo reduction ln(R) recorded at different amplitudes of field gradient (G) or gradient width (δ) as a function of G^2 or $\delta^2(\Delta-\delta/3)$ respectively, should yield a straight line with a slope proportional to the self-diffusion coefficient D.

Plots of -ln(R) versus $\delta^2(\Delta-\delta/3)$ for different sugar solutions gave straight lines. The accuracy of the results and the method was shown by the coefficient of correlation (>0.999) and the zero intercept (-0.012 < intercept < 0.007). The results recorded using this method on sucrose solutions at different concentrations (0, 0.25 and 0.43 g of sucrose per g of water) are shown in Figure 5.1 and reported for all 4 sugars in Table 5.1.

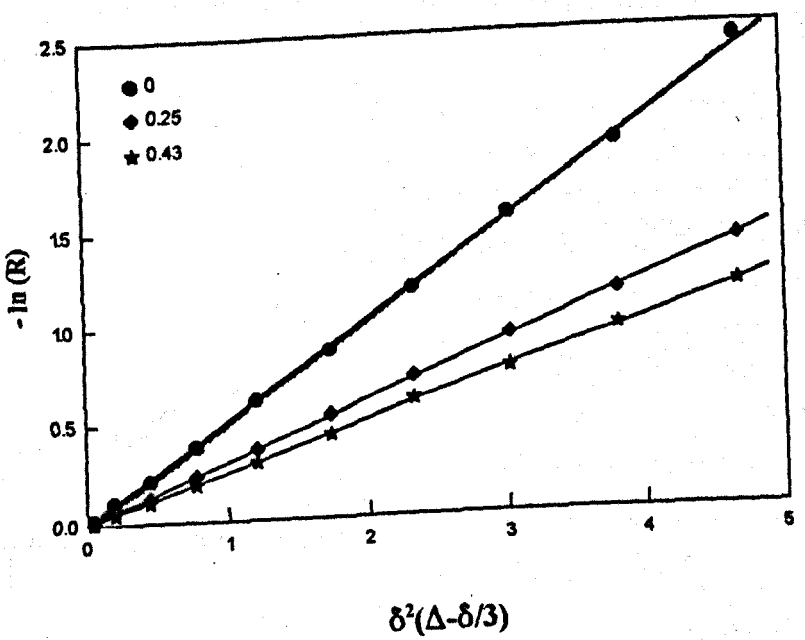

Figure 5.1 Plot of -ln(R) versus $\delta^2(\Delta-\delta/3)$ for distilled water and sucrose solutions containing 0.25 and 0.43 g of sugar per g of water. The slope of each line is proportional to the self-diffusion coefficient.

Table 5.I The results of - ln(R) versus $\delta^2(\Delta-\delta/3)$ plots for 4 different sugars at various concentrations. The standand deviation on the D/D_0 measured was found to be of the order of ±0.04

	Sugar conc. g sug. / g water	Intercept	Slope (ms^{-3})	R	D/D_0
d.d. H_20	0	-0.0120	0.514	0.9994	1
Sucrose	0.25	-0.0005	0.299	0.9992	0.582
	0.43	-0.0026	0.248	0.9999	0.483
Glucose	0.25	0.0059	0.297	0.9999	0.577
	0.43	0.0058	0.226	0.9998	0.440
Fructose	0.25	-0.0039	0.319	0.9999	0.620
	0.43	-0.0041	0.251	0.9998	0.488
Xylose	0.25	-0.0007	0.319	0.9996	0.621
	0.43	0.0065	0.258	0.9997	0.501

The results showed no significant difference between the 4 different sugars studied.

2.1.1.2 Discussion

a. Complexity of the NMR signal

The recorded NMR signal in a sugar solution is a composite of the contribution of the water and the sugar protons. The situation is made even more complicated by the occurrence of chemical exchange between the water ^1H and those on the sugar hydroxyl groups. The recorded diffusion coefficient could therefore be a weighted value of the coefficient of, on one hand the protons of the water and other exchangeable OH and, on the other hand, the

protons of the sugar molecules, the latter being detected by their non-exchangeable ^1H. In principle, it should be possible to record a second attenuation attributable to the diffusion of the dissolved sucrose molecules.

However, in the experimental conditions of limited gradient amplitudes ranges and relatively long τ values, it is believed that the recorded diffusion coefficients were derived principally from the water molecules. The various lines of evidence supporting this hypothesis are reviewed and discussed.

- The spin-spin relaxation times of sugar are expected to be shorter than the T_2 of water, and thus the signal resulting from the sugar non-exchangeable protons is expected, in the inhomogeneous field of the spectrometer (low resolution permanent magnet), to decay much earlier than when the 180° rf pulse is applied (5 ms).

- There was no evidence of non-linearity in the -ln(R) versus G^2 or versus $\delta^2(\Delta-\delta/3)$, with intercept values very close to 0. The measurement of a weighted slope value is thought to lead to relatively large intercept values.

- No significant difference was recorded between the D/D_0 values recorded in sucrose solutions (disaccharide) as compared with the glucose, fructose and xylose (monosaccharides) solutions despite the significant difference in the molecular weight (~ factor of 2).

- The self-diffusion coefficients (D) of these sugars in solution is expected to be approximately 5 times smaller than the self-diffusion of water. In fact, elsewhere in the ACTIF II programme, a value of approximately $0.5\ 10^{-9}\ m^2\ s^{-1}$ was measured in free solution for the N-monofluoroacetyl-D-glucose a ^{19}F labelled sugar analogue having a structure (molecular weight, polarity, hydrogen bonding properties, etc.) comparable to the sugars investigated in this project. This value is in agreement with the diffusion coefficient of glucose in agarose gels of $0.5\ 10^{-9}\ m^2\ s^{-1}$ reported by Andersson *et al.* (1994) and used subsequently by Harrison and Hills (1996).

b. Effect of sucrose concentration

The self-diffusion coefficients were measured for different sucrose contents using the PFG-SE method based on varying the gradient amplitude with the parameters $\Delta=\tau=6$ ms, $t_1=1$ ms and $\delta=0.5$ ms. As the sucrose concentration was increased, the relative self-diffusion coefficient (D/D_0) decreased rapidly to reach a 'negligible' value at a sucrose concentration higher than 1 g of sugar per g of water (Fig 5.2).

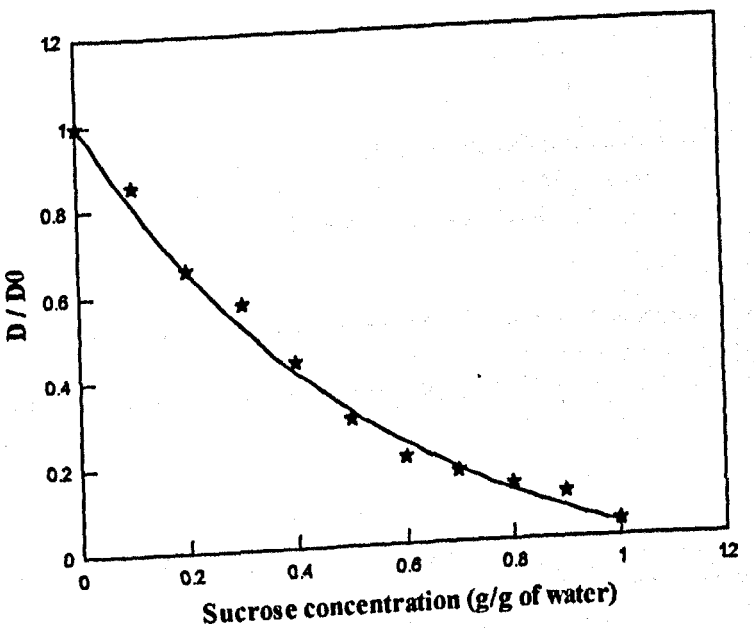

Figure 5.2 The relative self-diffusion coefficient (D/D_0) of water as a function of the sucrose/water ratio

Kimmich *et al.* studied the impact of BSA and gelatin concentration on the self-diffusion coefficient of water. A similar approach was adopted in an attempt to explain the effect of sucrose (the cases of amylopectin and gelatin are treated in the next section) on the translational mobility of water. The plot of the diffusion coefficient on a logarithmic scale, as a function of the sugar concentration calculated on a total wet weight basis showed 3 distinct linear regions (Fig 5.3).

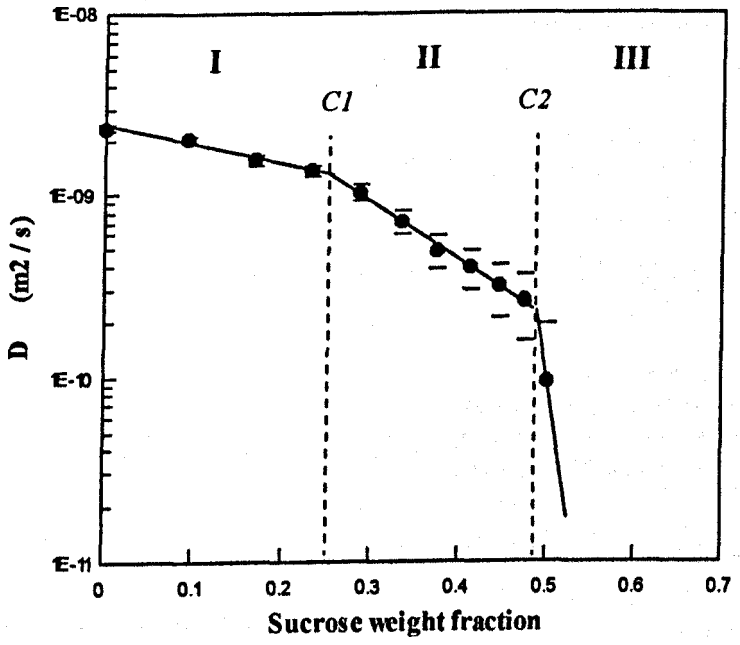

Figure 5.3 The self-diffusion coefficient D of water as a function of the weight fraction of sucrose (the standard deviation of 0.04 is illustrated as minimum/maximum - type plot)

These observations were interpreted as follows :

- For concentrations below C_1 = 0.25 g of sucrose / g of solution, the role of sucrose is believed to be principally due to its obstructive effect on the movement of water. Kimmich *et al.* (1993) characterised this concentration as the 'free-water limit' above which the diffusion coefficient values are dominated by those of the molecules in the 'free' water phase and were described using equation 5.1 :

$$D = D_0 (1 - \beta \Phi) \qquad (5.1)$$

where Φ is the volume fraction of the obstructing species and β a 'shape' factor.

- At intermediate concentrations (between C_1 = 0.25 and C_2 = 0.48), the fraction of the 'bound' hydration water increases. Assuming a fast diffusion process between the hydration layer and the free water molecules, the diffusion coefficient is given by a weighted average of

the diffusion coefficients in the free and the hydration water phases D_f and D_h respectively.

$$D = p_h D_h + p_f D_f \quad \text{and} \quad p_f + p_h = 1 \qquad (5.2)$$

The depression of D with increased sugar concentration (Figure 5.3) is thought to be due to the increasing fraction of the slow diffusing hydration water at the expense of the free water (equation 5.2) as the diffusion of water between these two phases is fast relatively to the time scale of the experiment (Lillford *et al.*, 1980; Belton and Hills, 1987).

- Above $C_2 = 0.48$, the diffusion coefficient of water decreased dramatically, falling to values below the limits measurable by PFG-NMR methods using the available spectrometer. Although only one data point was measured in this concentration range, the pattern was consistent with the results reported by Kimmich *et al.* (1993).

A concentration of sucrose of 48% (g of sucrose per 100 g of solution) corresponds to an average of 20.6 molecules of water per molecule of sucrose. Sucrose has 11 potential hydrogen bonding sites and thus, 20.6 molecules of water approximates to 2 water molecules per site. This is in agreement with the hydration numbers (n_h), i.e the number of water molecules found within a given van der Waals distance from the solute molecule, computed by Grigera (1988). Values of 11.45 and 13.23 were reported for sorbitol and mannitol respectively. These two polyols ($C_6H_{14}O_6$) have 6 hydrogen bonding sites, which supports the hypothesis that there are approximately 2 water molecules per hydrogen bonding site. Hence, a sucrose fraction of 0.48 is consistent with a 'mono-layer' coverage of the sugar molecule. Therefore, it is not surprising that water molecules in these concentrated sugar solutions exhibit low translational mobility (relative to the time scale of the experiment, namely the echo time of 12 ms). Likewise, the concentration value of 25% corresponds to 3 g of water per g of sucrose, i.e to 57 molecules which corresponds to approximately 2 hydration layers. This suggests that the second hydration layer, contains approximately 36 water molecules.

According to these calculations, 'free' water type behaviour is only found in water molecules external to 2 hydration layers. However, diffusional exchange between the various hydration

shells, and also between hydration 'free' water, are the determining factors for the observed overall diffusion coefficient. For water contents below the monolayer hydration coverage, the diffusion of water is thought to be very slow.

2.1.2. Water diffusion in starch and gelatin gels

The self-diffusion coefficients of water were measured in the gels of gelatin and waxy maize (amylopectin) and potato starches.

2.1.2.1 NMR parameters

The PFG-SE technique based on the measurement of the echo reduction for different gradient amplitude values with the parameters $\Delta = \tau = 6$ ms (gradient separation) and $\delta = 0.5$ ms (gradient width) was used for short diffusion times (<10 ms). The stimulated echo (PFG-StE) or triplet sequence where the echo reduction was measured for different field gradient widths was adopted for longer diffusion times (up to 90 ms) with the parameters $\tau_1 = 4$ ms (between the first and the second 90° pulses), $\Delta = \tau_2 = 12$-80 ms (gradient separation) and a variable gradient width $\delta = 0$ to 0.5 or from 0 to 1 ms in 10 steps.

2.1.2.2 D versus diffusion time - probing the gel structure

One of the advantages of using NMR to study diffusion is that the technique readily permits, within the limitations of the relaxation properties, the variation of the time scale over which the diffusion process is being observed (Δ).

While diffusion in pure water showed the expected independence on the diffusion time and an average value of $D/D_0 \approx 1$ (0.998±0.033) over the whole range of Δ values investigated (Fig 5.4), the D/D_0 values in the gels depended strongly on the diffusion time scale. Indeed, the relative self-diffusion coefficient decreased considerably from its anticipated value of 1 at

Δ=0 ms to reach a plateau value $(D/D_0)_{min}$ ≈0.315. This corresponds to a self-diffusion coefficient of 0.75 10^{-9} m^2 s^{-1} calculated relative to the measured value D_0 =2.38 10^{-9} m^2 s^{-1} in distilled water at 40°C.

This led to the conclusion that in the time scale considered by the experiment, the biopolymer acted as a barrier restricting the diffusion process by means of specific molecular interactions (hydrogen bonding, ^1H exchange, etc.) and also by physical, steric obstructions hindering the translational mobility of the diffusing molecule.

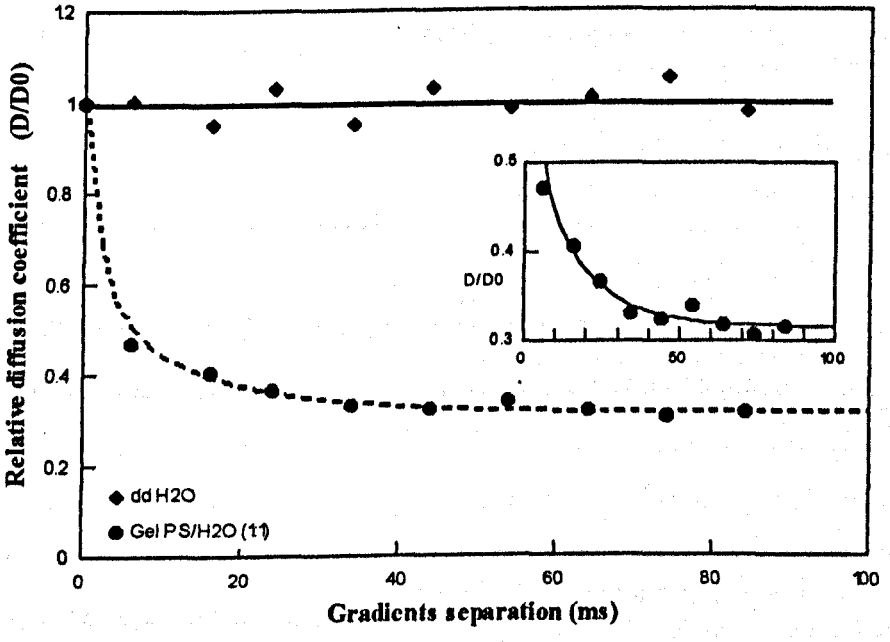

Figure 5.4 The relative self-diffusion coefficient (D/D_0) of water in distilled water and in a 1:1 potato starch gel, measured as a function of the gradient separation (Δ). The insert is an expansion of the gel diffusion curve.

Thus, the self-diffusion coefficient of water can be used to probe the structure of the gel in which the diffusion process is taking place. The average one-dimensional displacement <r> of a water molecule with a self-diffusion coefficient D during the diffusion time t is given by the expression:

$$<r>=\sqrt{2.D.t} \qquad (5.3)$$

For example, for the potato starch gel (1:1) in Figure 5.4, $(D/D_0)_{min}$ was reached after a

diffusion time t≈50ms. This leads to an average displacement <r>≈ 15.4 μm (D=2.38 10^{-9} $m^2.s^{-1}$ measured at 40 °C).

This value of <r>, which indicates the average free displacement of a water molecule, yields an average pore size of 30.8 μm. This value is slightly smaller than the average size of a potato starch granule (12-60 x 15-75 μm). Such a reduction can be attributed to the structure of the gelatinized-retrograded starch system which is thought to be a polymeric network with smaller domains than the colloidal, granular, ungelatinized paste.

The equilibrium value at long diffusion times $(D/D_0)_{min}$ was selected for the study of the effects of the gel composition on the self-diffusion of water.

2.1.2.3 Effect of the gel concentration

The self-diffusion results of water in amylopectin and gelatin gels on a log scale versus the polymer concentration showed comparable features to those found for sucrose in Figure 5.3 (Fig 5.5). However, the second drop of the diffusion coefficient at concentration C_2 was not reached over the range of concentrations investigated. A value of C_2=0.85 was reported by Kimmich *et al.* (1993) for BSA at 20°C. Equation 5.1 was applied to the first linear portion of the results of Figure 5.5 and the results are reported in Table 5.2 .

Table 5.2 Values of the 'free water' limit (C_1) and the 'shape factor' (β) for the diffusion results using equation 5.1

	C_1	β (*)
Sucrose solutions	0.25	2.77
Amylopectin gels	0.55	1.46
Potato starch gels		1.47
Gelatin gels	0.46	2.00

(*) The errors on the 'shape factor' β were less than 0.07. The β values for the biopolymers were calculated on the gels prepared by heating.

The C_1 values for the biopolymers were obtained from the results of the extruded samples

The physical significance of β is not clear but an increase of β reflects the obstructive 'efficiency' of the solute / gel.

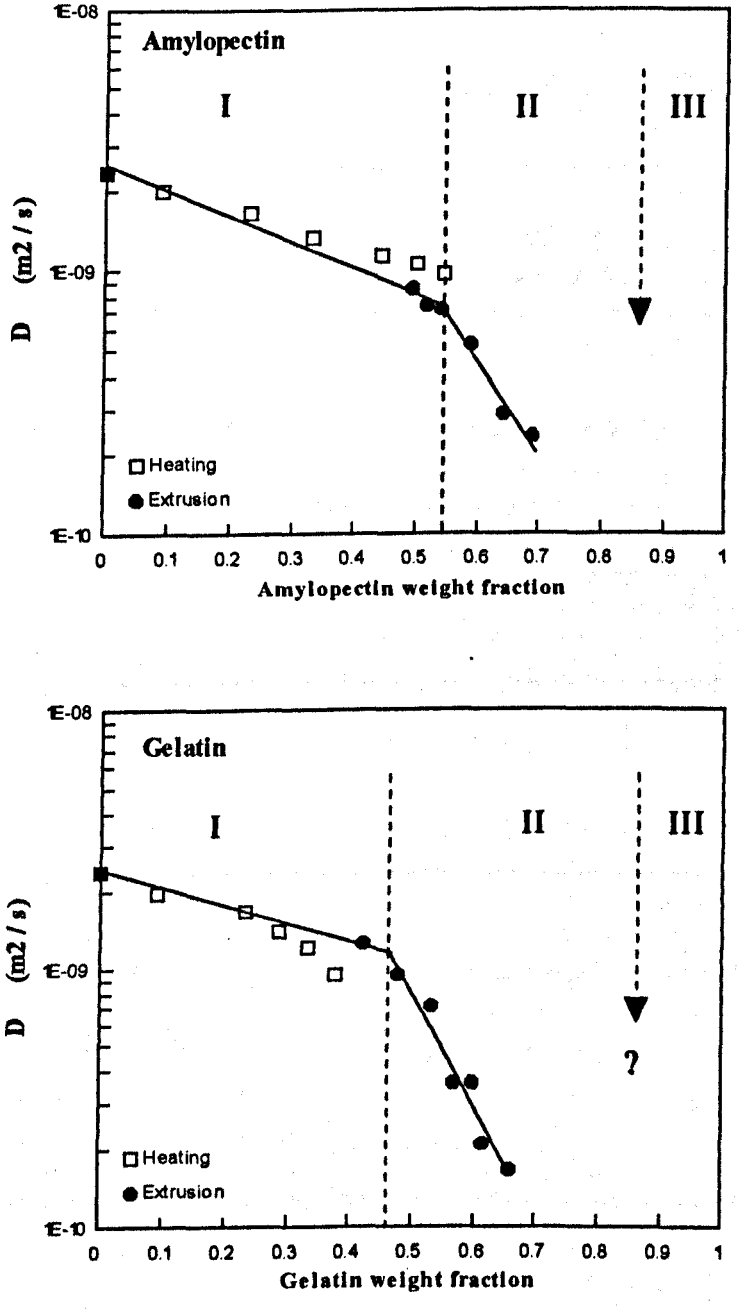

Figure 5.5 Diffusion coefficient of water in (a) amylopectin and (b) gelatin gels as a function of the polymer concentration. Samples prepared by simple heating and by extrusion are shown. The question mark is used to pinpoint the anticipated value for C_2 based on the results reported by Kimmich *et al.* (1993).

2.1.2.4 Restricted diffusion in different gels

Although no significant differences were found between the starch gels from the 2 different botanical sources (Fig 5.6-a), gelatin showed a relatively stronger inhibitory effect on the diffusion of water in the time scale of the experiment (<0.1s) (Fig 5.6-b).

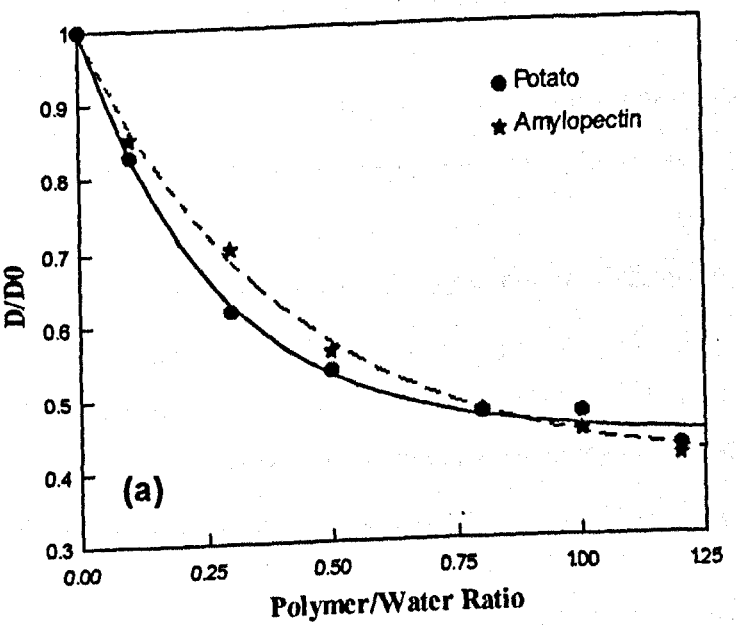

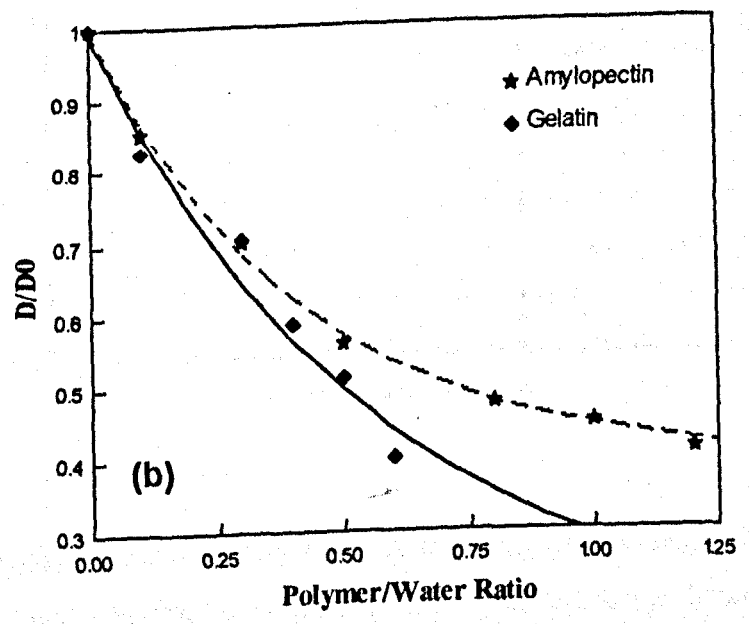

Figure 5.6 Effect of various biopolymers on the self-diffusion coefficient of water measured at 40°C.

This observation has to be considered with caution as results on gelatin gels over a wider polymer concentration are required. The preparation of homogeneous, concentrated gelatin gels was not readily achievable using the method adopted for sample preparation (heating). This was, however, achieved by extrusion as described later in this chapter.

The measured values of the self-diffusion coefficient of water were found to be consistent with the results reported by Ohtsuka *et al.* (1994) for potato starch and by Kimmich *et al.* (1993) for gelatin.

The difference between the effects of gelatin and starch on the diffusion of water could be a consequence of the differences in the molecular interactions between water on one the hand and gelatin or the two starches on the other. Furthermore, the difference in the translational properties of water in these gels could indicate structural differences, between the gels obtained from starch and gelatin. Indeed, a close inspection of the state diagram of gelatin (Borchard *et al.*, 1980) and amylopectin (chapter 6) shows that, in the concentration range of this study (biopolymer fractions between 0 and 0.7), the melting temperatures of amylopectin are, on average, some 60 K higher than those of gelatin systems (Fig 5.7).

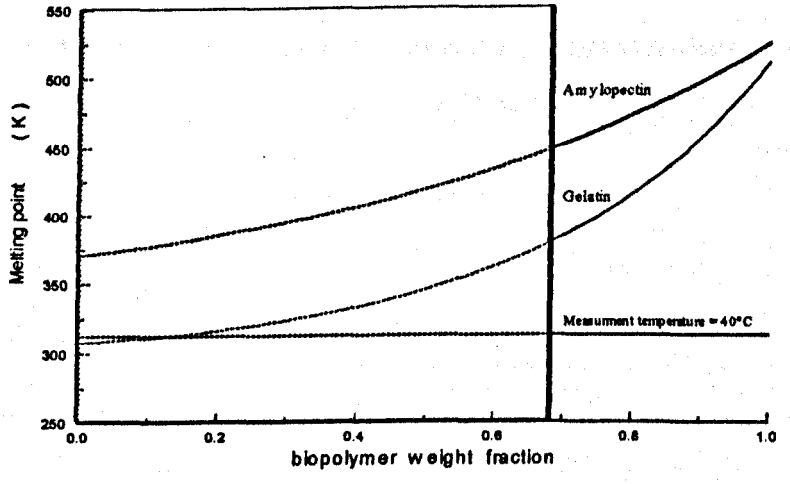

Figure 5.7 The melting temperatures of biopolymer-water systems as a function of the polymer weight fraction for gelatin (adapted from Borchard *et al.*, 1980) and amylopectin (refer to calculation in chapter 6 - section 5.2.2). The dashed line shows the temperature at which the NMR diffusion measurements were performed (313 K) and the 'box' illustrates the range of biopolymer concentrations investigated.

Although the temperature at which the NMR measurements were performed (40°C) was below the melting temperature of all the samples investigated (with the exception of the gelatin/water 1:10 sample), gelatin-water systems were closer to their melting conditions than amylopectin-water gels. Since the network forming the gelatin gel is held by triple helical junction points (as described by Harrington and Rao (1970) and briefly reviewed in chapter 2), the fact that the experimental conditions were adjacent to the melting conditions would lead to a partial melting of the gel, notably at junction points where the triple helices are of relatively short length. The consequence of this would be a partial collapse of the gel structure which, although still appearing consistent on a macroscopic scale, would, on a microscopic scale, be highly heterogeneous with a significant proportion of micro-regions of essentially a melt-type structure. The contribution of the mobility of water in these melt-type micro-domains to the overall diffusion process could explain the limited diffusion of water in gelatin gels as compared to starch gels.

Consequently, an unduly ambitious interpretation of the effects of different biopolymers on the self-diffusion of water described in this section should not be attempted as the structure of the different gels was also affected by the melting process. This latter complication could be avoided by performing the diffusion experiments at temperatures below 300 K (and above 273 K to avoid the freezing of water). Unfortunately, the spectrometer used in this work was not equipped with a temperature controller and therefore the measurments had to be carried out at the preset temperature of 313 K.

2.2 Water self-diffusion in biopolymer-sugar gels

2.2.1 Effect of added sucrose on D/D_0

In order to study the effect of the presence of a third component on the diffusion of water in gels, a proportion of the polymer was replaced by sugar leaving the 'solid' / water ratio in the sample constant.

The relative water diffusion coefficient D/D_0 was decreased by the presence of sucrose. The effect was directly proportional to the amount of sucrose present in the system (Fig 5.8).

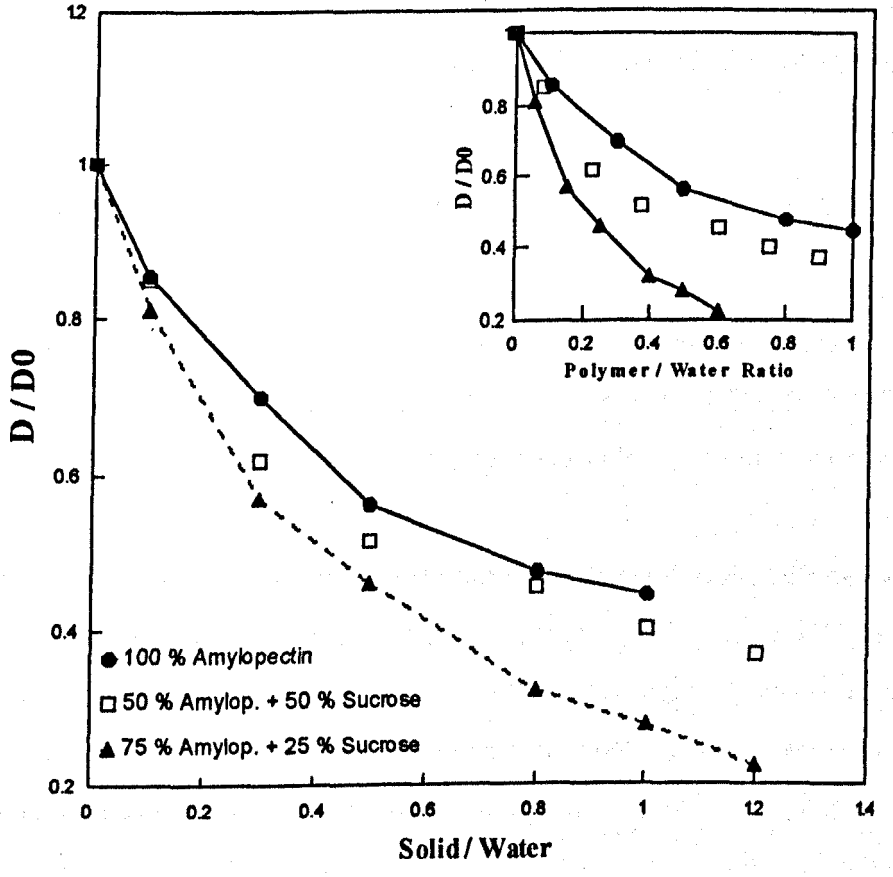

Figure 5.8 Impact of sucrose on the relative self-diffusion coefficient (D/D_0) of water in amylopectin measured as a function of the total solids concentration. The insert shows the same results plotted as a function of the amylopectin/water ratio.

The values of the water diffusion coefficient in the biopolymer gels were compared to those expected on the assumption that the effects of the presence of the biopolymer and the sugar were additive and independant.

Let $(D/D_0)_s$ and $(D/D_0)_p$ the relative self diffusion coefficients of water in a sugar solution and a biopolymer gel of a particular concentration c (sugar / water or polymer / water) respectively.

The concentrations used in Figures 5.8, 5.9 and 5.10 are expressed as follows :

(i) a sucrose solution of a concentration c, contains c g of sucrose per g of water

(ii) a starch gel contains c g of starch per g of water

(iii) a starch-sucrose gel contains c g of sucrose + c g of starch per g of water

If the hypothesis of a simple additivity in the reduction of the self-diffusion coefficients applies, then $(D/D_0)_{mix}$ which is the relative self diffusion coefficient of water in a polymer-sugar (1:1) with a polymer / water ratio = c, is given by :

$$(\frac{D}{D_0})_{mix} = (\frac{D}{D_0})_s \cdot (\frac{D}{D_0})_p \qquad (5.4)$$

The results of this calculation are shown in Figure 5.9 where only the lines representing the best fit for the biopolymer-water and the sugar-water systems are shown. The measured relative self-diffusion results followed closely the calculated line of D/D_0 at low polymer concentration for the two starch gels and over the whole investigated range of concentration for gelatin. However, when the polymer/water ratio exceeded 0.2 in the case of potato and waxy maize starch gels (corresponding to a calculated value of ~0.5 for D/D_0) and > 0.3-0.4 (corresponding to a calculated value of ~0.3-0.2 for D/D_0) for gelatin gels, the measured D/D_0 values became increasingly larger than the values predicted on a simple additivity basis. One reason might be that at low water contents, the preferential interaction between biopolymer and sugar molecules leads to a decrease in the number of binding sites (by hydrogen bonding and proton exchange) on both the sugar and the biopolymer matrix for the water molecules, and thus, the population of the mobile water becomes larger increasing the value of the overall self-diffusion coefficient.
Furthermore, the small size of the water molecule would enable diffusion to take place in the free-volume unoccupied by a concentrated starch-sugar phase (refer to the free-volume theory reviewed in chapter 2).

2.2.2 Effect of the sugar type

As in the case of sugar solutions, the type of sugar had no significant impact on the relative self-diffusion coefficients of water over the entire range of water contents investigated. An example of this is shown in Figure 5.10 where there is no evidence of difference in the water diffusion properties between the 1:1 potato starch / sugar gels prepared with sucrose (disaccharide C12) or with xylose (monosaccharide C5).

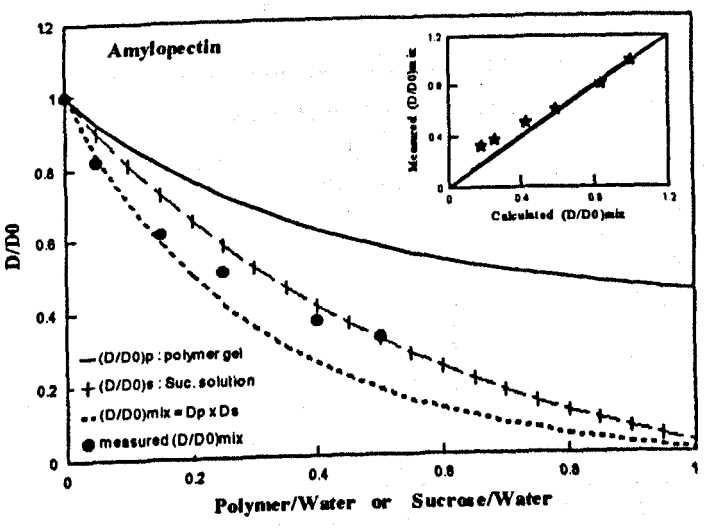

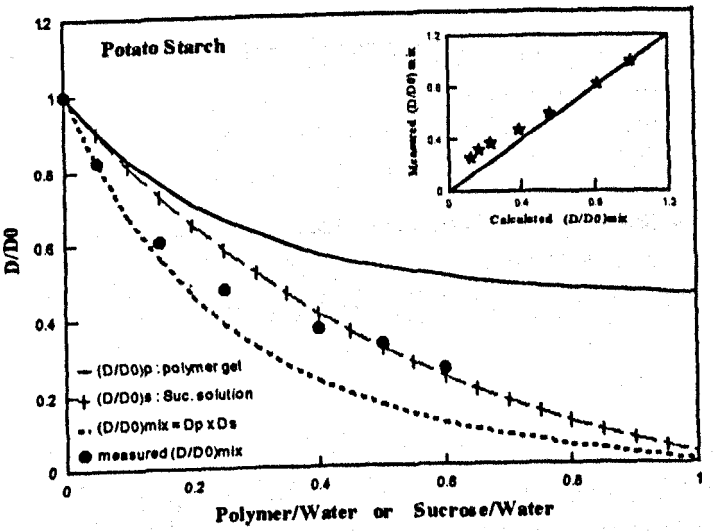

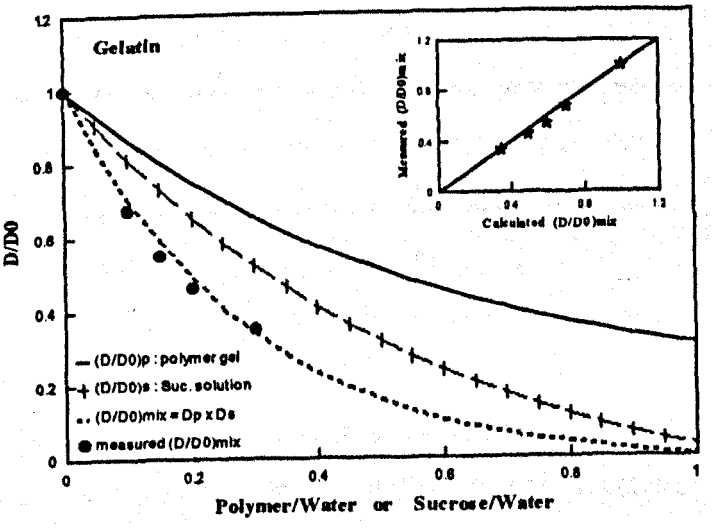

Figure 5.9 D/D_0 as a function of the polymer/water ratio in biopolymer $(D/D_0)_p$ and biopolymer-sucrose gels $(D/D_0)_{mix}$ and as a function of sugar/water in sucrosesolution $(D/D_0)_s$.

Key:

__ best fit of measured $(D/D_0)_p$

++ best fit of measured $(D/D_0)_S$

• measured results of $(D/D_0)_{mix}$

- - - calculated $(D/D_0)_{mix}$ data

$(D/D_0)_{mix} = (D/D_0)_P . (D/D_0)_S$

The inserts show the correlation between the measured and calculated $(D/D_0)_{mix}$ values.

Results for (a) waxy maize starch, (b) potato starch and (c) gelatin are shown.

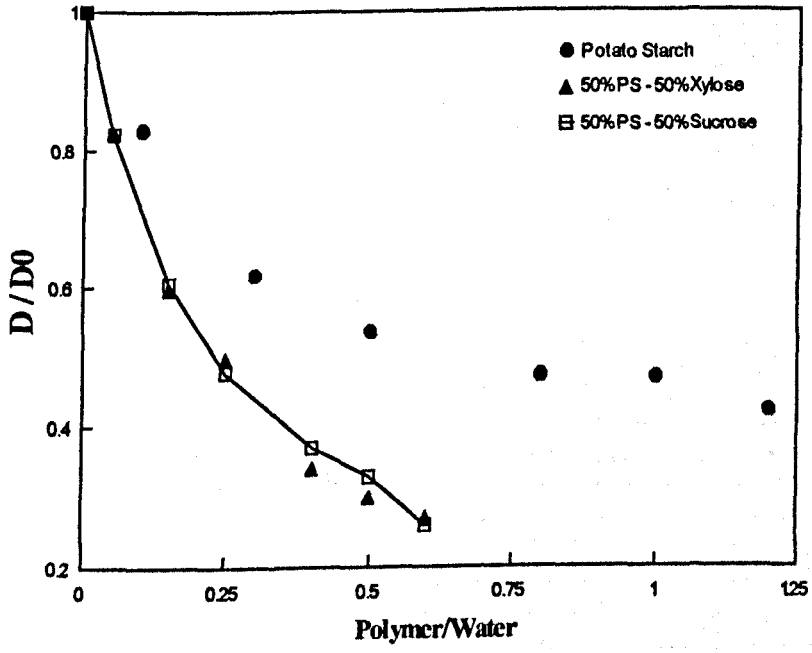

Figure 5.10 Effect of sucrose and xylose on the relative self-diffusion coefficient (D/D_0) of water in potato starch - sugar (1:1) gels.

2.3 Effect of processing on the self-diffusion properties of water

Although it was not possible to produce homogeneous gels over the same concentration range by both processing techniques (simple heating and extrusion), a difference was observed in the diffusion properties of water depending on the processing history of the samples (Fig 5.11). While the curve for the heat-gelatinized amylopectin reached asymptotically a value $(D/D_0)_\infty \approx 0.39$, a much smaller value of $(D/D_0)_\infty$ was observed for extruded samples. A discontinuity was also observed between the diffusion results in the heat treated and the extruded gelatin samples.

Furthermore, Figure 5.5 shows clear differences between the heat-gelatinized and the extruded samples. The most significant one was in the value of the 'free water' limit polymer concentration C_1 .

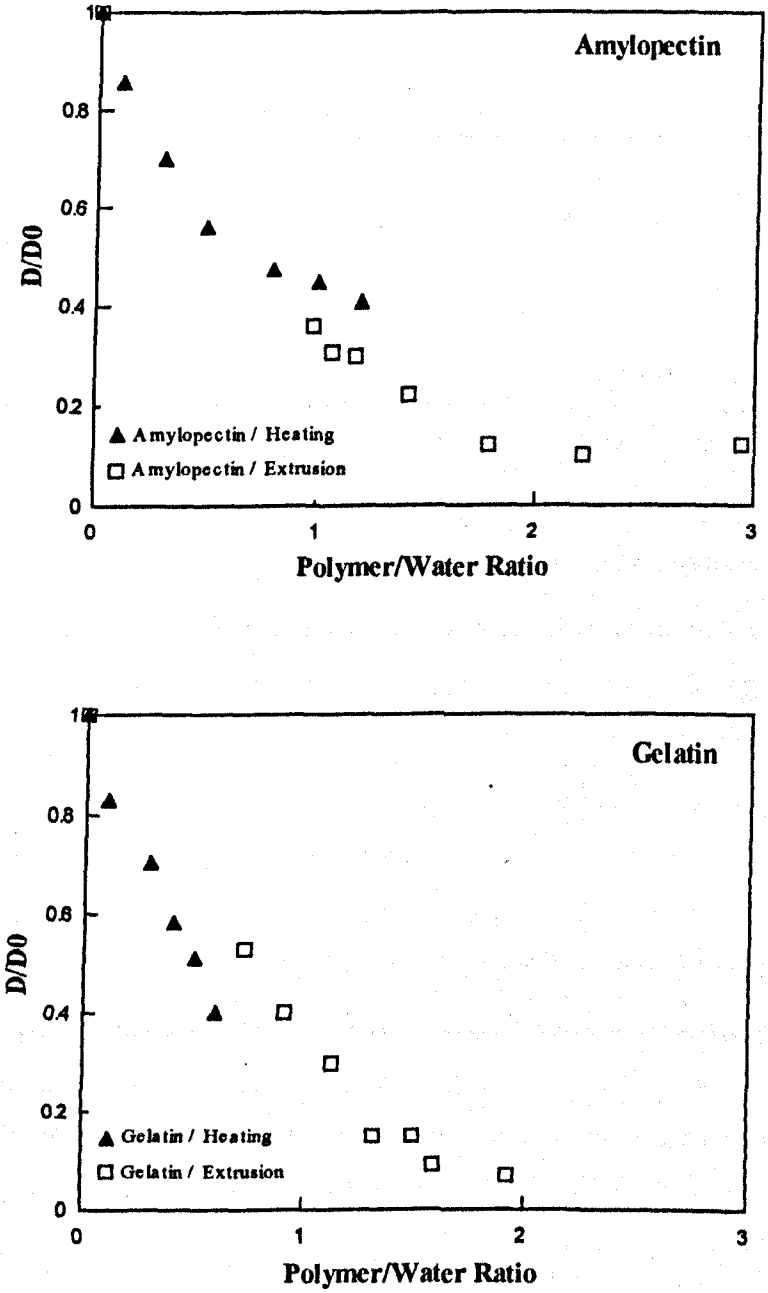

Figure 5.11 Difference between the diffusion behaviour of water in gels prepared by heating and by extrusion of (a) amylopectin and (b) gelatin.

Table 5.3 Effect of processing on the 'free water' limit polymer concentration (C_1)

	Heated-gelatinized	Extruded
Amylopectin	> 0.6	0.55
Gelatin	0.25	0.46

Two features emanate from the results in Table 5.3 :

- The C_1 values for gelatin were significantly smaller than those of amylopectin gels. A smaller C_1 value suggests that a lower hydration level is required before the occurrence of a free-water behaviour. The results also suggest that gelatin is more effective than amylopectin in restricting water mobility or that the hydration shell of gelatin is greater than that of amylopectin.

- The impact of extrusion on the water diffusion properties led to an increase in C_1 for amylopectin. Such behaviour suggests that the process of extrusion of the waxy maize granules has led to the exposure of more water binding sites compared with simple heating of aqueous suspension of starch granules. The opposite behaviour was exhibited by gelatin. The situation in the case of gelatin is not fully understood but one reason could be a conformational transition leading to different hydration properties of the protein.

These differences between heat treated and extruded samples are not surprising (Mitchell *et al.*, 1992) as the extrusion process, in addition to the thermal energy imput it involves a relatively important mechanical energy. The specific mechanical energy involved in the extrusion of the samples used in this study was between 407 and 96 kJ kg^{-1} for amylopectin concentrations between 0.8 and 3 g of polymer per g of water respectively and between 194 and 48 kJ kg^{-1} for gelatin concentrations in the same water content range. These results should, however, be regarded as preliminary and further work is required to check the validity of the difference between extruded and non-extruded materials.

Conclusion

The diffusion of water which is a physical parameter of great importance in the quality of food products was found to be affected by the presence of obstructing molecular species. While the type of the polymer was a determining factor in the diffusion process, the role of the sugar was less specific to the sugar type.

The nature of the effect of sugar and biopolymer molecules on the mobility of water was found to depend on the concentration. While diffusion of water is very slow at lower levels of hydration, this process was greatly enhanced as the degree of hydration increased. Above a certain hydration level, an increase in the water population started to exhibit a 'free-water' type behaviour. At these low concentration levels, the role of the polymer on the diffusion of water was due to obstructive effects.

Within a relatively narrow range of polymer concentrations, the effect of sugars in depressing the diffusion coefficient of water in gel systems can be anticipated using the diffusion results of the binary systems polymer-water and sugar-water.

The preliminary results reported in the last section indicated that the processing conditions could be manipulated in order to produce matrices of different structures where the diffusion of water could be modulated (inhibited or enhanced) according to the technological needs of the final product. This last observation could find applications in the barrier technology domain.

Effects of water and sugars on the retrogradation of extruded amylopectin

Introduction

Despite the considerable amount of work on starch retrogradation published over the last 90 years (Katz, 1928) and briefly reviewed in chapter 3, several areas of great scientific and industrial interest are not yet fully understood. In this chapter, three of these aspects are identified and investigated.

1- Concentrated systems

The majority of the published work on retrogradation deals with dilute and semi-dilute systems. Less attention has been given to the more concentrated systems i.e those containing more than 1g of starch per g of water, although this concentration is comparable to most of the starch based food products where retrogradation is of a technological significance. Some studies of the molecular changes occuring during the retrogradation process in concentrated starch systems have been carried out, among others, by Marsh (1986), Ring *et al.* (1987), l'Anson *et al.* (1990) and Cairns *et al.* (1991), and on bread systems by Wilson *et al.* (1991) and a number of other groups. Recently, Keetels (1996) used dynamic mechanical methods to study the retrogradation of concentrated wheat and potato starch gels. The systems investigated by Keetels

were, however, semi-concentrated rather than 'concentrated' as the starch concentrations investigated ranged between 10% and 30% wt.

Furthermore, although extrusion is widely used in the processing of starch based products, and despite the evidence (Faridi *et al.*, 1984; Inaba *et al.*, 1988) that processing conditions have an effect on the staling kinetics, retrogradation of extruded systems has, surprisingly, received little attention.

Of the various techniques that are available and can provide information on the molecular changes, x-ray diffraction, rheological and thermal methods have been widely used to study the gelation and the subsequent recrystallization of starch systems (Maxwell and Zobel, 1978 and 1981; Ring *et al.*, 1987; Cairns *et al.*, 1991; I'Anson *et al.*, 1990; Marsh *et al.*, 1986 and 1988; Miura *et al.*, 1992 and many others), while Wilson *et al.* (1991) used mid and near infrared spectroscopy to study the staling of bread.

2- Molecular dynamics

Again, surprisingly, despite the extensive investigation of the retrogradation process, very little attention has been given to the molecular dynamics and its influence on the recrystallization of the starch polysaccharides. Only a few workers have dealt with this particular aspect of the retrogradation process. Teo *et al.* (1992) and Le Botlan *et al.* (1995) have used proton relaxation NMR to monitor the retrogradation of starch gels, while Junshi *et al.* (1993) employed magnetization transfer ^{1}H NMR techniques to assess the changes in the mobility of the polymer during the ageing of waxy maize starch gels.

3- Effect of added sugars

Several investigators have studied the effect of added sugars on the kinetics of starch retrogradation exist in the literature; some of these are reviewed in chapter 2 . However, the results are not always consistent. While Marsh (1986) and I'Anson (1990) found that

sugars (with the exception of fructose) delayed the retrogradation of wheat starch, Wang *et al.* (1994) reported the opposite effect as they observed that sugars and maltodextrins enhanced the rate of retrogradation.

The aim of the work described in this chapter was to study the effects of water and sugars on the retrogradation of extruded waxy maize starch (amylopectin) systems. The intention has been to assemble a comprehensive body of information by utilizing a range of complementary techniques.

Pulsed NMR was used to obtain information on the molecular mobility, whilst x-ray diffraction provided information on molecular organization and long range order. ^{13}C solid state CP-MAS and FT-MAS techniques were employed to assess the short range order and the specific molecular interactions between the various components present in the extruded system. Considerable rationalization of the data was attained by exploiting insights on molecular dynamics derived from the glass-rubber transition theory.

The results were correlated with the mechanical properties of the samples measured using stress relaxation techniques.

1. Experimental techniques

1.2 Sample preparation and storage

Amylopectin-sugar extrudates with moisture contents ranging between 20% and 65% (g water per 100 g of dry solid) were prepared as described in chapter 3.

Samples used in the isothermal study of the retrogradation were stored at 40±0.1°C in the NMR spectrometer probehead for the NMR studies, and at 25±2°C in a temperature controlled room for all other measurements.

In order to assess the effect of storage temperature on the retrogradation process, amylopectin extrudates containing different amounts of water were sealed and stored in incubators at different temperatures (4, 10, 25, 30, 50, 65, 80 °C) with a temperature accuracy of ±1°C.

1.3 Physical measurements

1.3.1 ^{1}H relaxation NMR

Proton spin-spin relaxation parameters were obtained from the NMR free induction decay signal (FID) recorded directly after a 90° rf pulse, or from the Carr-Purcell-Meiboom-Gill (CPMG) experiment. The default conditions involved a τ spacing of 262 μs between the 90° and the 180° pulses. The FID decay was recorded using the 'interleaved FID' pulse sequence (described in chapter 3), and was typically deconvoluted into 2 Gaussian components while the spin-echo decay was best described by a single exponential. Spin-lattice relaxation parameters were recorded using the inversion recovery pulse sequence. Twenty different pulse separation values (τ) ranging between 16 and 4096 ms were used and the results were fitted to a single exponential.

1.3.2 ^{13}C solid state NMR

^{13}C cross-polarization and Fourier transform magic angle spinning (CP and FT-MAS) experiments were undertaken at 300 K using a Bruker CXP 300 operating at 75 MHz for ^{13}C as described in chapter 3.

1.3.3 Wide angle x-ray diffraction

X-ray spectra were recorded over the angular range 4° to 38° 2θ. The increase in spectral resolution was used to empirically quantify the increased crystalline order. Crystallinity indices were obtained from the shift corrected intensity of the peak at 17.2° 2θ normalized to the intensity at 16° as follows :

$$ci = \frac{I_{17.2°} - I_{16°}}{I_{16°}} \qquad (6.1)$$

The peak at 2θ=17.2° was chosen as it is present in the x-ray spectra of both A and B-type starches (refer to the discussion of the different methods to calculate the crystallinity index of semi-crystalline materials in section 2.3.4 - chapter 3).

1.3.4 Stress relaxation measurements

These experiments were performed by J.L Melvin. The stress relaxation results are used in this chapter, with the permission of the author (Melvin, 1996), as an example of the textural changes that occur during the retrogradation process. The mechanical properties were evaluated using a TA-HD Texture Analyzer (Stable Microsystems Ltd., Haslemere, UK) in which the sample was stretched at a speed of 1 mm s^{-1} to achieve a 3% deformation. Stress relaxation was followed for a period of 200 seconds. The force was used to determine the tensile modulus E using the equation :

$$E(t) = \frac{F(t)L}{A_0 \Delta L} \qquad (6.2)$$

where F(t) is the force at time t , A_0 is the initial cross-sectional area, L is the initial length of the sample and ΔL is the deformation. The initial tensile modulus E_0 (t=0), the asymptotic value (t=∞) of the modulus or 'relaxed' modulus E_∞ and the relaxation time constant (τ) were studied as a function of the storage time for samples with different water contents.

2. Retrogradation and physical properties

The ageing of gelatinized starch systems yields important changes in their physical properties as a result of the retrogradation process.

2.1 Molecular order

It has been established for more than 90 years (review by Katz, 1928) that retrogradation is the recovery of the starch crystalline order lost during gelatinization. Thus, an ordering of the gelatinized starch was expected to take place during storage.

Figure 6.1 shows the ageing - reordering of extruded waxy maize starch samples. The appearance of sharp peaks was indicative of the increasing fraction of starch in the ordered form. The narrowness of these peaks is an indicator of the size of the ordered domains.

Further evidence of this reordering process was obtained by comparing the ^{13}C solid state CP-MAS spectra recorded on the gelatinized amorphous and the retrograded crystalline systems (Fig 6.2). As in the case of the XRD, sharp peaks were observed in the CP-MAS spectrum of the recrystallized extrudate. This increase in the spectral resolution was thought to be indicative of a decrease in the chemical shift distribution as the system underwent the reordering transition.

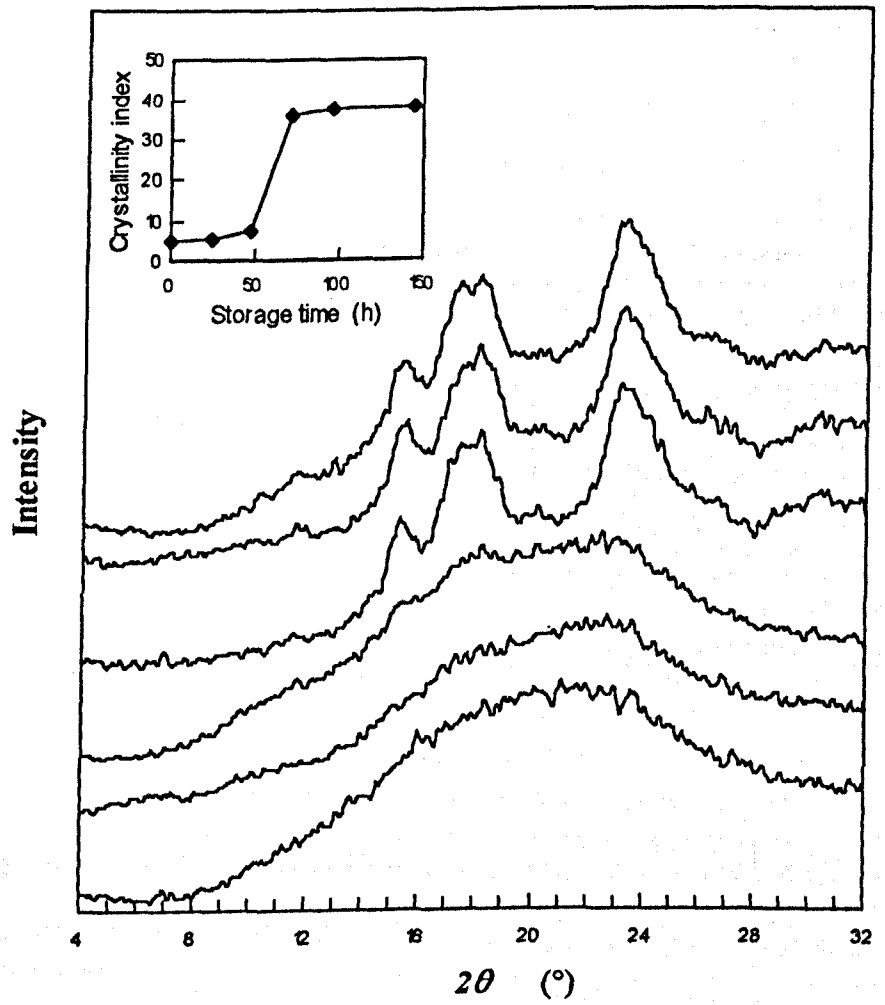

Figure 6.1 The recrystallization nature of starch retrogradation as measured by wide angle x-ray diffraction. The figure shows the XRD spectra recorded 15 min, 1, 2, 3, 4 and 6 days after extrusion of a waxy maize starch sample containing 35% water (w/w d.s.b) stored at 25±2 °C. The insert illustrates the corresponding crystallinity indices calculated using the Hermans and Weidinger (1948) method.

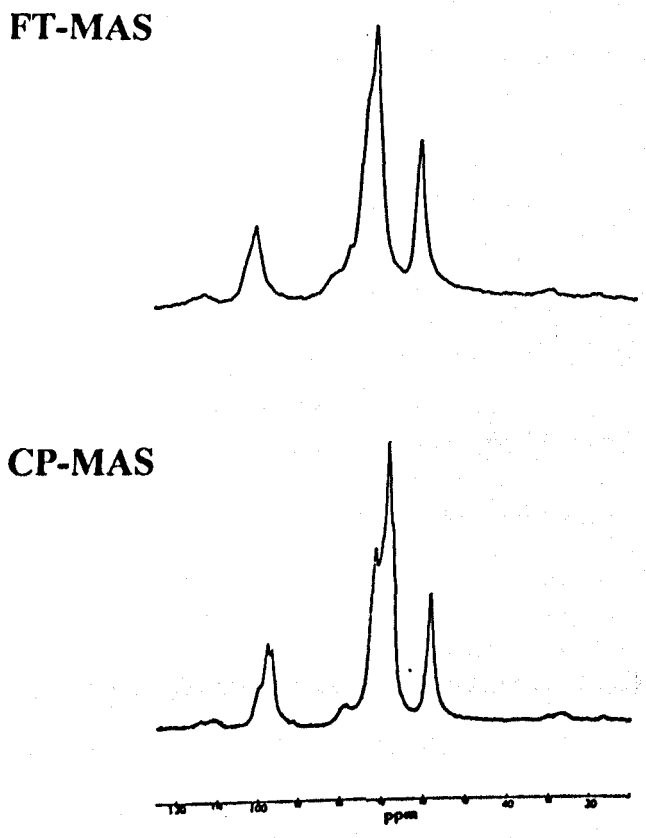

Figure 6.2 ^{13}C solid state NMR (75 MHz): CP-MAS (rigid component) and FT-MAS (mobile component) spectra of a retrograded amylopectin extrudate containing 60% water (d.s.b).

2.2 Molecular mobility

In contrast, the generation of FT-MAS spectra selectively favours mobile species. This provided an understanding of the fact that the CP-MAS spectrum recorded on a retrograded sample exhibited the typical pattern of ordered starch with the charecteristic sharp peaks, whilst the FT-MAS spectrum of the same sample was similar to the pattern recorded on amorphous gelatinized starch systems (Fig 6.2).

recorded on amorphous gelatinized starch systems (Fig 6.2).

These observations suggested that in retrograded starch, the ordered component was rigid and thus recorded only when cross polarization (CP-MAS) techniques were used, while the amorphous component was more mobile and was detected using the less elaborate FT-MAS experiment.

2.2.2 ^1H relaxation results

The effect of the retrogradation on the mobility of the various constituents present in the system was studied by proton NMR relaxation (20 MHz).

2.2.2.1 Spin-spin relaxation (T_2)

The free induction decay (FID) and the spin-echo decay (CPMG) recorded on extruded waxy maize starch samples showed a strong dependence on the duration of storage. The implication is that the NMR properties were affected by the retrogradation process and by the extent of the reordering of the gelatinized amylopectin.

Typical examples of the effect of storage on the FID and CPMG decays are shown in Figure 6.3 for an amylopectin sample having a moisture content of 60 % (w/w dry basis). In Figure 6.3-a, as the retrogradation progressed, the 'solid-like' component of the free induction decay showed enhanced relaxation rates ($1/T_2$) and provided a larger contribution to the total NMR signal. The effect of the retrogradation upon the spin-echo decays recorded using the CPMG pulse sequence was a similar shortening of the relaxation times.

While considerable changes were observed between 0.5 and 4.3 hours of storage (Fig 6.3), no significant difference was noticed on comparing the NMR relaxation results recorded at 24 and 53 h. This suggested that the effect of the retrogradation process on the relaxation parameters of this system reached its equilibrium state during the first 24 hours of storage.

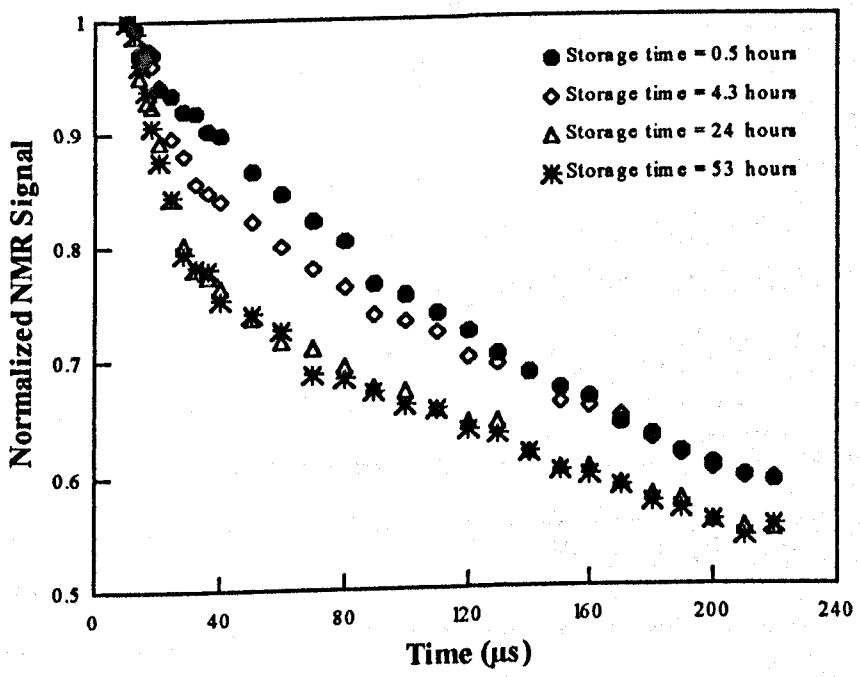

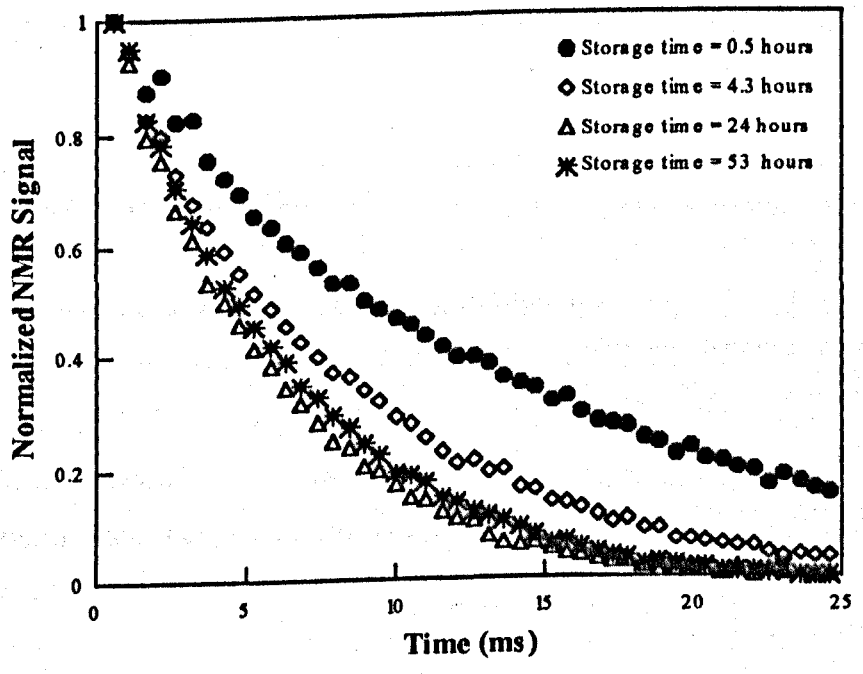

Figure 6.3 Effect of ageing on the ^{1}H - NMR properties of an amylopectin extrudate containing 60% water, stored for 0.5, 4.3, 24 and 53 hours at 40°C : (a) the free induction decays and, (b) the spin-echo decays.

The ^1H relaxation times of the rigid and the mobile components, and the relative contribution of each of these two components to the total NMR signal were obtained by the deconvolution of the FID. The results showed a decrease of the T_2 of the 'solid' component and an increase in the T_2 of the 'liquid' component (Fig 6.4). Furthermore, an increasing fraction of the slowly relaxing protons ('liquid-like' component) became much less mobile as the retrogradation progressed, with decay times between 20 and 40 μs depending on the water content of the sample. This resulted in a greater relative signal amplitude arising from the rigid component.

These results were explained in terms of a decrease in the molecular mobility of the polymer as it underwent the reordering transition. This suggested that the gelatinized starch component was more mobile than the ordered crystalline fraction and confirmed the ^{13}C results reported in the previous section.

The total amplitude of the FID signal was found to be essentially constant during storage, indicating that no significant water loss from the sample had occurred. The total signal amplitude was used to assess any moisture loss from the sealed NMR sample tubes.

2.2.2.2 Spin-lattice relaxation (T_1)

As in the case of the spin-spin relaxation, the spin-lattice relaxation results depended on the ageing of the amylopectin extrudates. The T_1 obtained from the signal component recorded at 11 μs and representing the rigid fraction, and at 71μs for the mobile component increased sharply and then levelled off as shown in Figure 6.5 for a 100:60 amylopectin-water sample. The fraction of the rigid component relative to the total signal followed the same trend.

One important feature of these results was that the T_1 values of both rigid and mobile components were very comparable indicating the effectiveness of the cross relaxation mechanisms between the two components of the system.

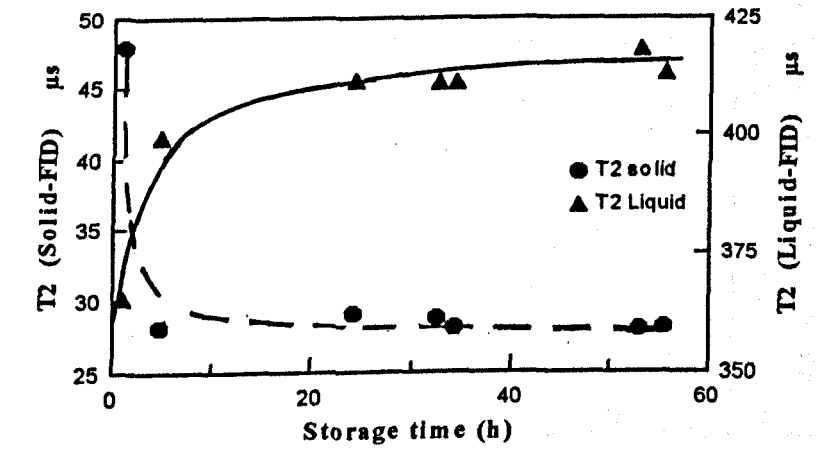

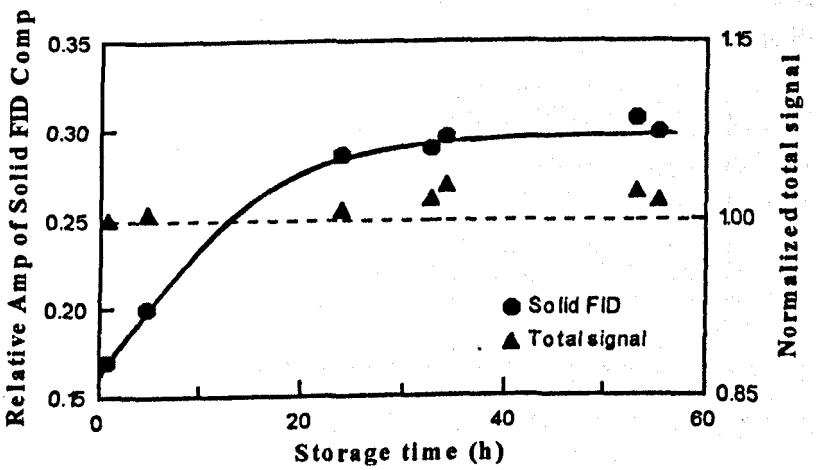

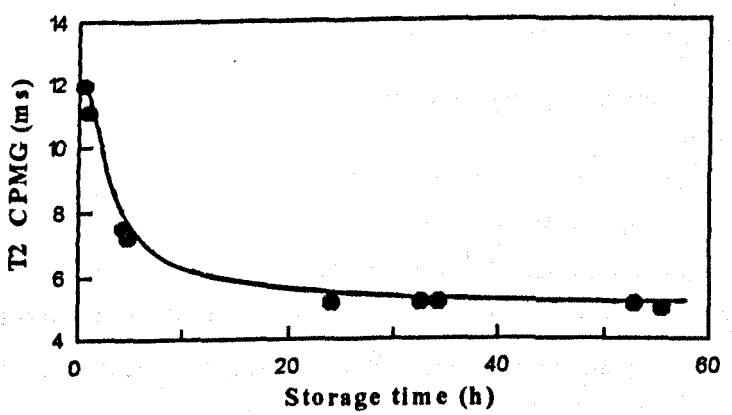

Figure 6.4 Spin-spin relaxation parameters as a function of the storage time for the same sample containing 60% water. The total NMR signal showed no dependence on the storage time proving that, within standard experimental error limits, no noticeable water loss occurred.

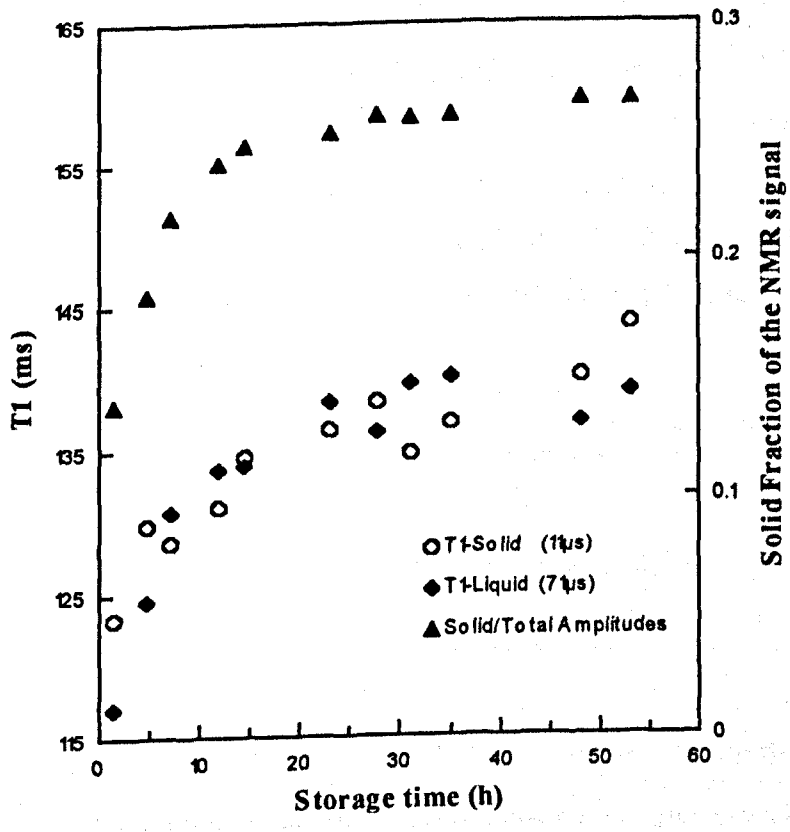

Figure 6.5 Effect of storage on the spin-lattice relaxation parameters for the components recorded at 11 µs (solid) and 71 µs (liquid) for an amylopectin-water (100:60) extrudate.

2.2.2.3 Discussion

The ^{13}C spectra and the ^{1}H relaxation results implied that the rigid crystalline and the amorphous mobile components existed contemporaneously in the system, even when retrogradation reached equilibrium (storage time $\rightarrow \infty$). This was confirmed by the x-ray results where retrograded starch was found to be partially crystalline, i.e crystalline and amorphous phases co-existed in the same system

These results are compatible with the 'fringed micelle' model used widely to describe partially crystalline synthetic polymers (Wunderlich, 1976) and later to describe starch

gels (Levine *et al.*, 1987), where crystallite hydrates are surrounded by amorphous regions containing the plasticizing water. In this model a single long polymer chain can have ordered (helical) segments located within one or more crystallites, and one or more unordered segments in one or more amorphous regions. This is particularly appropriate to the cluster model (French, 1972; Robin *et al.* 1974 and 1975) of the amylopectin structure reviewed in chapter 2.

2.3 Textural Changes

The retrogradation of the extruded ribbons had an important impact on their mechanical properties. The initial modulus E_0, the relaxed modulus E_∞ and the time constant τ were studied as a function of storage and composition of the sample. A typical example of the effect of storage on these rheological parameters is shown in Figure 6.6 (for more details refer toMelvin (1996)). The time dependence of the moduli paralleled the increase in x-ray crystallinity and the decrease in the molecular mobility as measured by NMR.

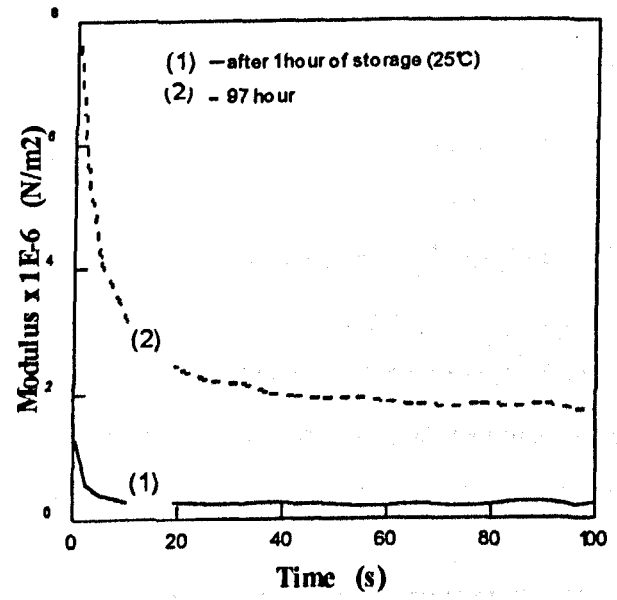

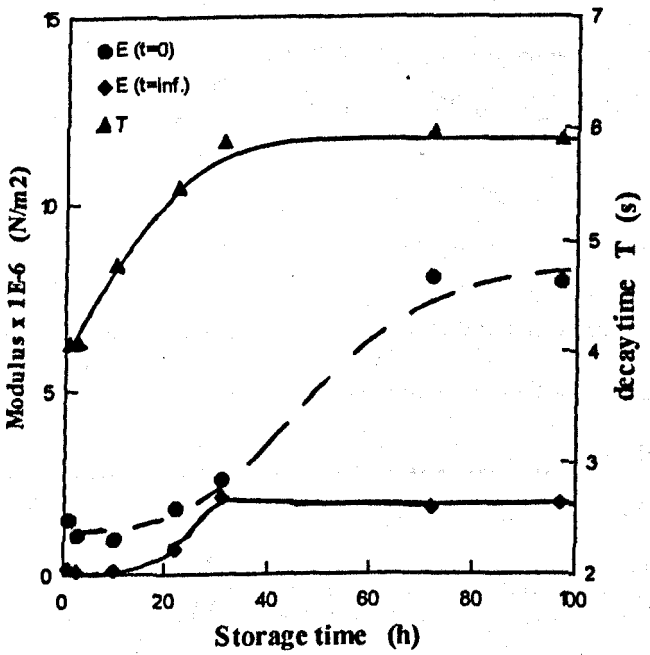

Figure 6.6 Effect of storage on the stress-relaxation behaviour of an amylopectin extrudate containing 41% water (top). The changes in the moduli (initial and relaxed) and the stress-relaxation decay time constant with storage time is also illustrated (bottom).

3. Effect of water contents on the retrogradation of extruded amylopectin

3.1 X-ray crystallinity

The rate of recrystallization of the gelatinized amylopectin was enhanced considerably at increased water contents (Fig 6.7). While a sample containing 35% water did not show any crystalline x-ray pattern before 72 hours of storage at 25±2°C, 6 hours of storage time were sufficient for a higher moisture content sample (60%), stored in the same conditions, to exhibit the typical XRD pattern of a 'fully' retrograded starch system.

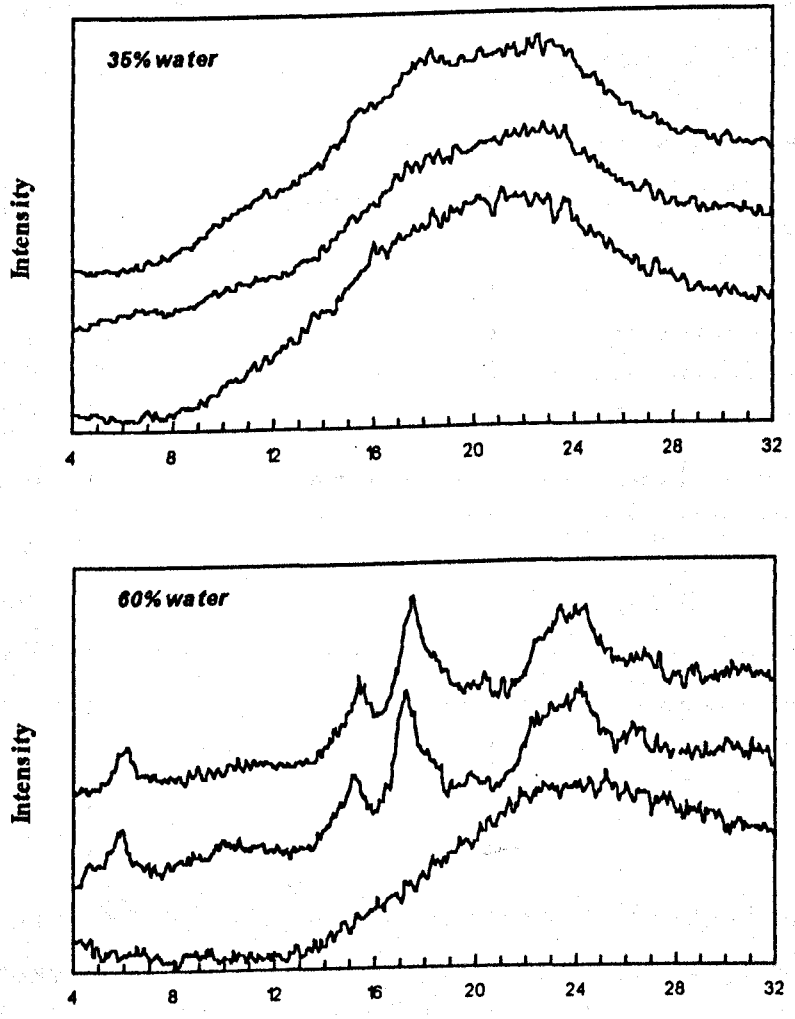

Figure 6.7 XRD spectra recorded during the ageing process of a 35% and a 60% water (w/w d.s.b) samples. Spectra recorded at storage times of, from bottom to top, less than one hour, 24 hours and 48 hours.

The effect of water content on the recrystallization kinetics was quantified through the modelling of the crystallinity index values as reported later in this section.
The line-shape of the spectra of the retrograded samples depended on the water content. This latter result is discussed in more detail in section 3.4 .

3.2 NMR relaxation properties

As described above, the proton NMR relaxation parameters were used to monitor the progress of the retrogradation process. As for the XRD crystallinity index, the changes in the NMR relaxation parameters as a function of storage time, depended strongly on the water content of the sample. This can be clearly seen in Figure 6.8 for the spin-lattice relaxation results and in Figure 6.9 for the spin-spin relaxation data.

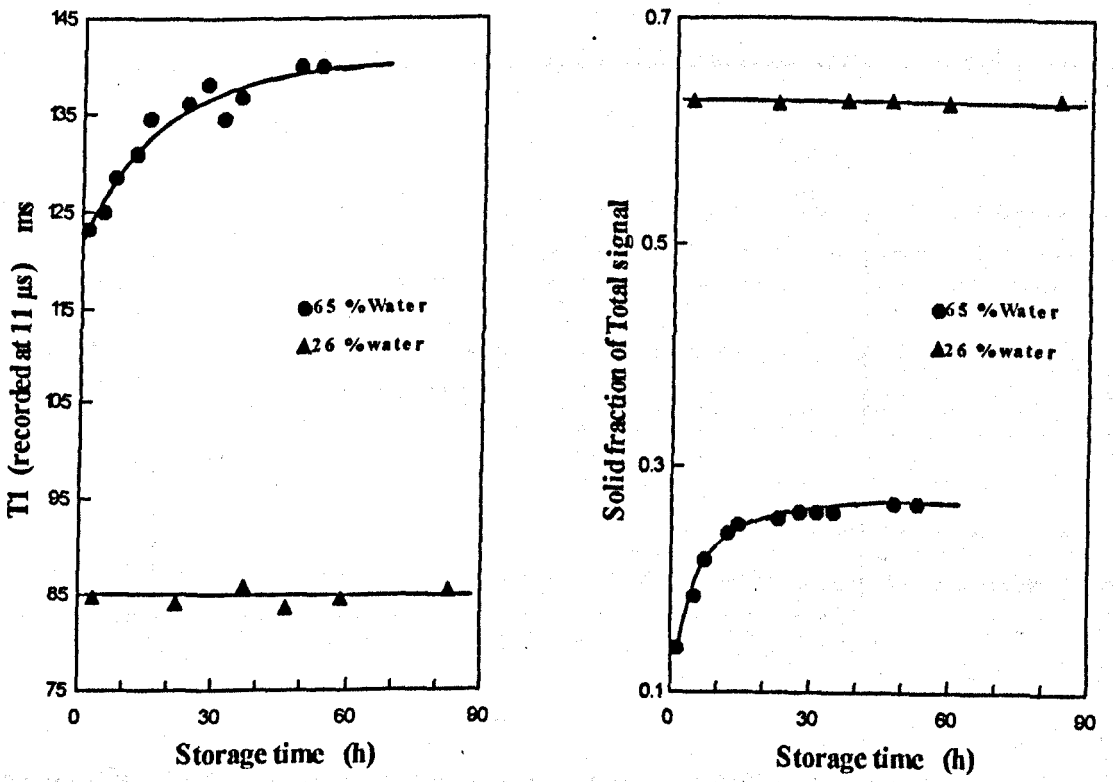

Figure 6.8 Effect of water content on the retrogradation kinetics as measured by spin-lattice relaxation NMR techniques.

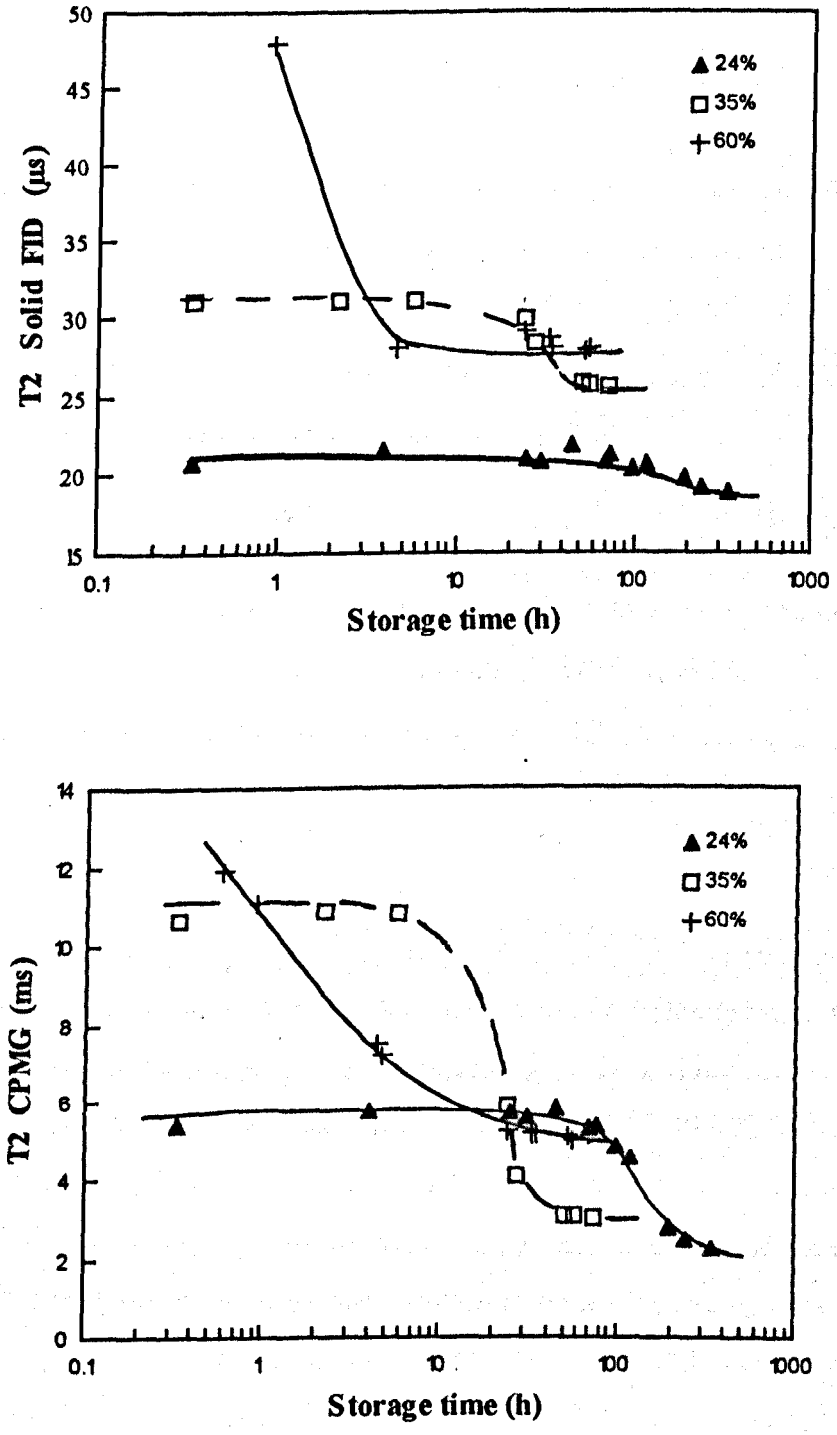

Figure 6.9 Effect of increased moisture contents on the storage time dependence of the spin-spin relaxation times of the 'solid' component of the FID (top) and the CPMG decays (bottom)

3.3 Effect of water content on the retrogradation kinetics

3.3.1 Modelling the retrogradation kinetics - The Avrami model

During the recrystallization of amylopectin, crystals can grow from different nucleation centres. The amount of crystallized material present at a given time is, therefore, a combined function of the crystal growth rate and the density of nucleation reflecting the rate of nucleation. During crystallization, the fraction of unconverted polymer at time t can be described by the Avrami equation :

$$U(t)=\exp(-kt^{n}) \qquad (6.3)$$

where k is a rate constant and n is the Avrami coefficient which, conventionally, is believed to be a function of the type of nucleation (Tiller, 1991).
U(t) was calculated from the experimental data using :

$$U(t)=\frac{Y_{max}-Y(t)}{Y_{max}-Y_0} \qquad (6.4)$$

where Y(t) is any physical property affected, or any parameter related, to the crystallisation of the material. Examples are the x-ray crystallinity index, NMR relaxation properties or mechanical properties measured by rheological methods (stress relaxation, etc.). Y_0 and Y_{max} are, respectively, the initial value (at t=0) and the maximum plateau value of Y(t). Often in the literature, the values of n and k are obtained from equation 6.3 by plotting ln(ln[U(t)]) versus ln(t). Some workers have used the first and the last values of Y(t) measured after gelatinisation to define Y_0 and Y_{max} (Le Botlan *et al.*, 1995). Although relatively satisfactory results were reported, these assumptions would introduce distortions to the calculated kinetic parameters. Therefore, in this study, the results were modelled using a least squares minimisation fitting routine. The equation used was obtained by replacing U(t) by its relationship to Y(t) in the Avrami equation (equation 6.3)

$$Y(t)=Y_{Max} - (Y_{max}-Y_0) \exp[-kt^n] \qquad (6.5)$$

with 4 adjustable parameters Y_0, Y_{max}, k and n. In general, a satisfactory agreement was found between this model and the experimental results ($\chi^2 < 10^{-5}$- 10^{-4}). It is clear that this approach is more accurate as it provides the best calculated approximation of Y_0 and Y_{max} which are of particular interest for the understanding of the sample behaviour and performance upon storage. Figure 6.10 shows a typical example of the results of using equation 6.5 to model the changes of the spin-echo relaxation rate (samples stored and measured at 40±0.1°C) and the x-ray crystallinity index (samples stored and measured at 25±2°C) of a waxy maize starch extrudate containing 35% water during the retrogradation.

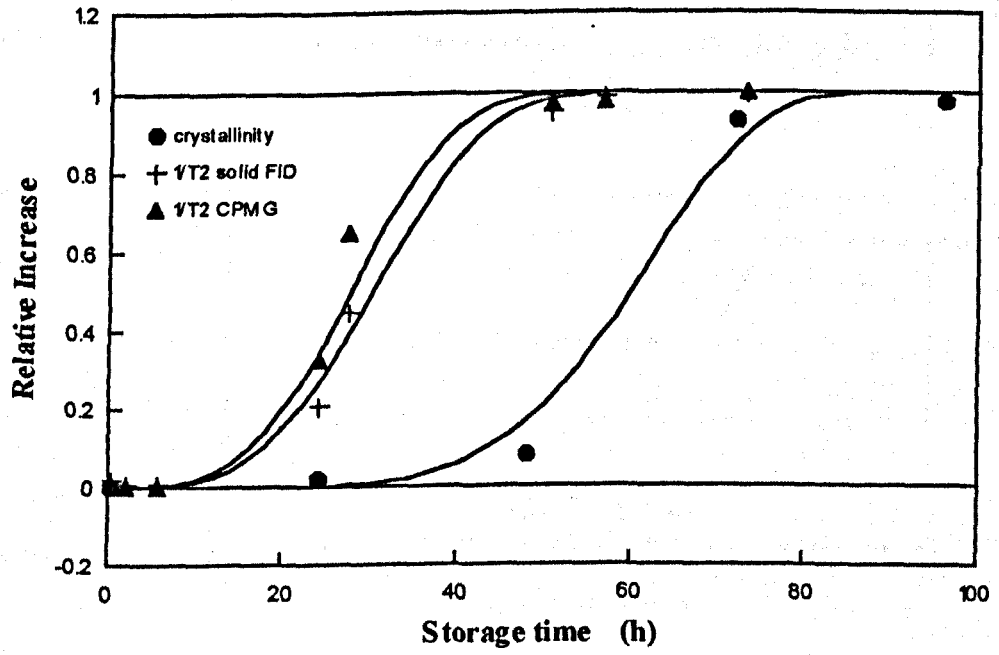

Figure 6.10 Effect of ageing on the spin-spin relaxation rates ($1/T_2$) and the crystallinity index for an amylopectin extrudate containing 35% water. The solid lines illustrates the Avrami fit to the experimental results.

The rate of retrogradation (G) can be obtained by writing equation 6.3 in a slightly different form :

$$U(t)=\exp[-(G\ t)^n] \qquad (6.6)$$

Where G is the rate of retrogradation with an inverse time dimension ($time^{-1}$)

3.3.2 Effects of water content on the kinetic parameters

The rate of retrogradation showed an exponential dependence on the water content (Fig 6.11). The retrogradation rate values calculated from the spin-echo ^1H relaxation rates were found to be greater than those obtained from the x-ray crystallinity results. This difference is discussed later in this section.

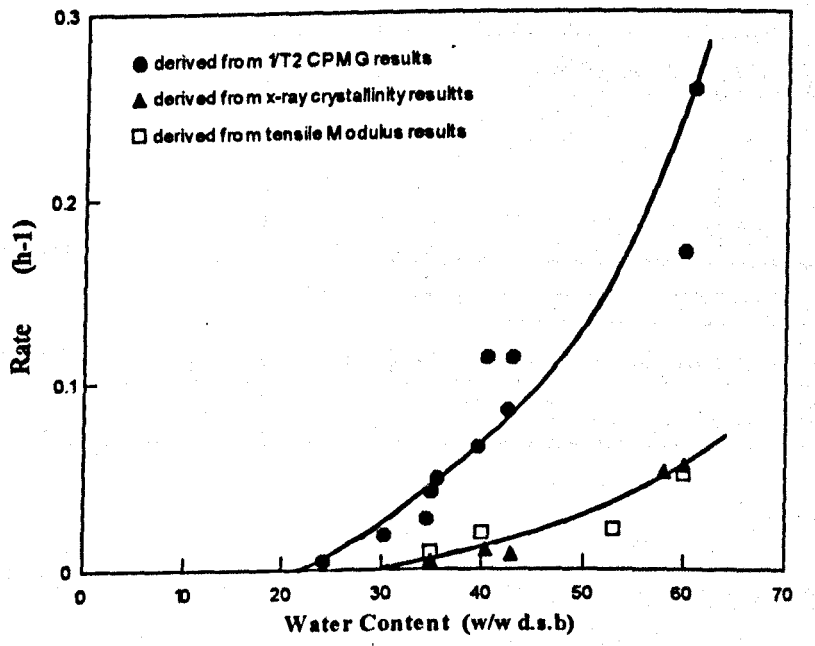

Figure 6.11 Effect of water content on the rate of retrogradation (G) of waxy maize starch extrudates as derived from the spin-spin relaxation rate ($1/T_{2\ CPMG}$) (storage temperature = 40°C), and the crystallinity index (ci) and the original tensile (E_0) modulus (storage temperature = 25°C).

3.3.3 Significance of the glass-rubber transition

3.3.3.1 Calculation of T_g

The glass transition temperatures (T_g) were calculated using equation 2.3 (chapter 2) (ten Brinke *et al.*, 1983).

The values of the glass transition temperatures and the change in specific heat capacities at the glass-rubber transition of the individual components used to calculate T_g of the amylopectin-water systems were those reported by Orford *et al.* (1990) and Kalichevsky *et al.* (1993) (Table 6.1). The data corresponding to the various sugars are used later on in this chapter.

Table 6.1 The T_g and ΔC_p values for amylopectin, water and common sugars.

	T_g (K)	ΔC_p ($J.g^{-1}.K^{-1}$)
Amylopectin	502	0.41
Water	134	1.94
Sucrose	343	0.76
Fructose	280	0.83
Xylose	286	0.95

3.3.3.2. Retrogradation rate and ($T-T_g$)

The water content at which the retrogradation rate approached asymptotically the zero rate value in Figure 6.11 was found to be approximately 22 % for the proton relaxation NMR results and, 30 % for the x-ray crystallinity. These values are in a good agreement

with the W_g values, the water contents where the T_gs are 40°C and 25°C respectively as predicted by the ten-Brinke and Karasz equation. The calculated W_g values were 22 % at 40°C and 26 % at 25°C (w/w dry solid basis).

These observations were as predicted by the glass-rubber transition theory where the molecular mobility is reduced and the viscosity increases dramatically as the system approaches the $T_g = f(W_g)$ boundary (chapter 2 - Fig 2.17). Indeed, Slade *et al.* (1993) introduced an empirical definition where the retrogradation near the glass transition was described to be 'too slow to be observed in the life time of a food product'.

The rate of retrogradation was studied as a function of the temperature offset from the glass-rubber transition temperature $(T-T_g)$ (Fig 6.12), T being the temperature at which the samples were stored (25°C for the x-ray results and 40°C for the ^1H - NMR measurements). T_g was calculated as described in equation 2.3.

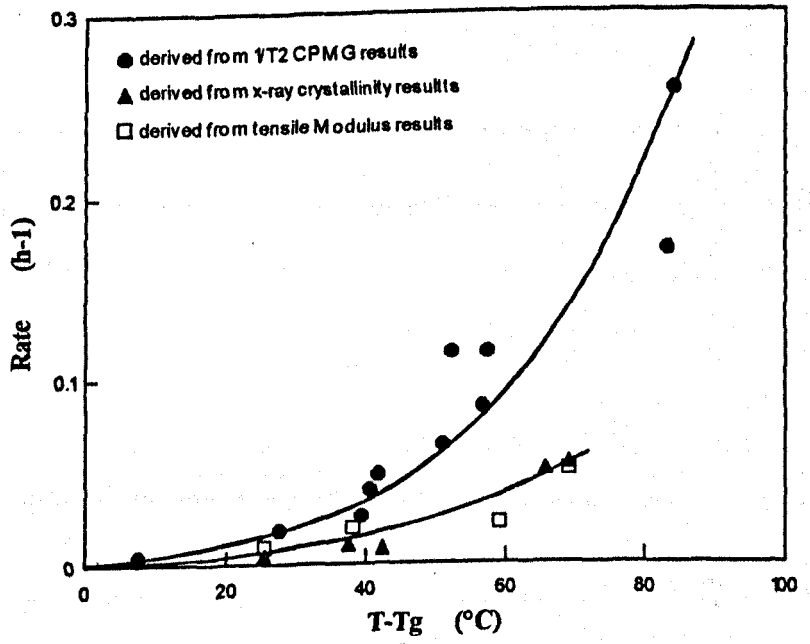

Figure 6.12 The same results as in Figure 6.11 plotted against the corresponding $(T-T_g)$ values.

The rates of retrogradation measured by the different techniques were closer as the ($T-T_g$) values should account for the difference in the storage temperatures used for the samples analyzed by each technique.

However, the rate values obtained by NMR remained greater than those measured by x-ray. This difference is discussed in section 3.3.5 .

A linear relationship was found between ln(G) and ($T-T_g$) with a correlation coefficient of $r > 0.92$ (Fig 6.13).

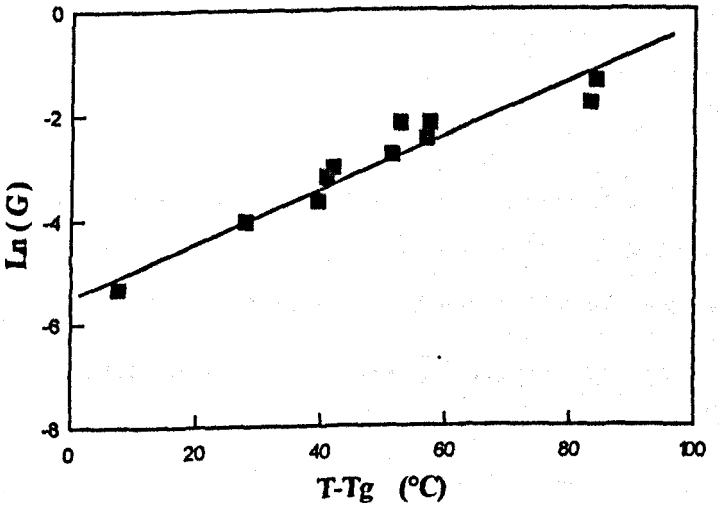

Figure 6.13 The linear relationship between ln(G) as derived from the $1/T_{2\ CPMG}$ results and ($T-T_g$) (R=0.96).

3.3.3.3 Application of the WLF kinetics

The exponential dependence of the retrogradation rate upon ($T-T_g$) and consequently the satisfactory linear relationship between ln(G) and ($T-T_g$) led to the belief that the retrogradation kinetics could be described by WLF kinetics (Williams, Landel and Ferry, 1955).

The WLF equation

The WLF equation was derived from the free-volume theory interpretation of the glass-rubber transition (Williams *et al.*, 1955).

For an arbitrary reference temperature (T_{ref}), the empirical WLF equation is given by:

$$\log_{10} \frac{\eta / (\rho T)}{\eta_{ref} / (\rho_{ref} T_{ref})} = \log_{10}[\frac{\eta}{\eta_{ref}}] \approx -\frac{C_1 (T - T_{ref})}{C_2 + (T - T_{ref})} \qquad (6.7)$$

where η is the viscosity or other diffusion-limited relaxation process and, ρ is the density.

T_{ref} is normally $T_g + 50$ K; in this case C_1 and C_2 are 8.86 and 101.6 for typical amorphous synthetic polymers. If T_g is used as the reference state, then C_1 and C_2 take 'universal' values of 17.44 and 51.6 respectively. The WLF equation was found to describe satisfactorly the behaviour of amorphous polymers for temperatures between T_g and $T_g + 100$ K (Sperling, 1986), while Slade and Levine (1991) showed that it is applicable between T_g and T_m, T_m being the melting point.

Application of the WLF equation to the retrogradation kinetics

All the systems investigated in this chapter are so positioned in the ($T-T_g$) domain that the WLF equation rather than the Arrhenius theory should be applied to describe their kinetic behaviour.

Equation 6.7 can be applied to describe the rate of retrogradation assuming that G is inversely proportional to η :

$$\log_{10} \frac{G_{ref}}{G} = -\frac{C_1 (T - T_{ref})}{C_2 + (T - T_{ref})} \qquad (6.8)$$

However, in the work reported in this chapter, the temperature was kept constant and the T_g was changed by adding various amounts of water (or sugar) as a plasticizer. Equation 6.8 can be rearranged by replacing T by $\Delta T = (T-T_g)$:

$$\log_{10} \frac{G_{ref}}{G} = -\frac{C_1 (\Delta T - \Delta T_{ref})}{C_2 + (\Delta T - \Delta T_{ref})} \qquad (6.9)$$

The fitting of the results to equation 6.9 was satisfactory (correlation coefficient R=0.97) (Fig 6.14) but yielded 'non-standard' values for C_1 (=9.2) and C_2 (=312.7).

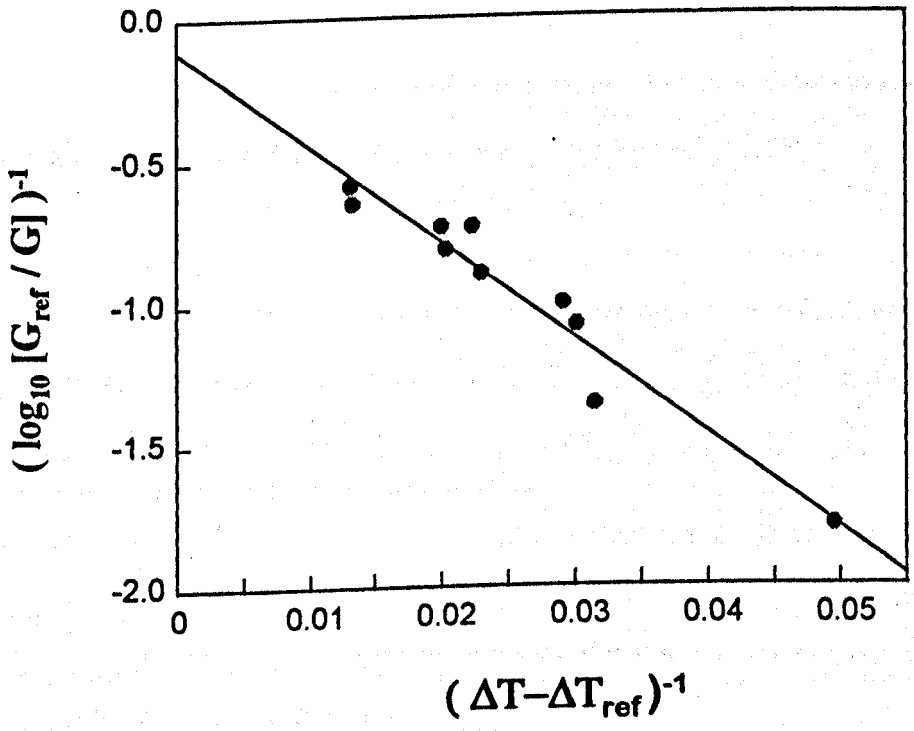

Figure 6.14 The WLF type plot of the retrogradation rate derived from the $1/T_{2\,CPMG}$ ^{1}H-NMR relaxation measurements of amylopectin-water extrudates.

The difference between the calculated C_1 and C_2 values and the 'universal' ones could be due to the non-equivalence of T and ΔT as this latter parameter was changed by shifting T_g through modification of the system composition, and not by changing the storage temperature. The effects of temperature and water content on the rate of molecular mobility are comparable but not, however, entirely equivalent. Furthemore, several workers (Hallbrucker *et al.*, 1988) reported C_1 and C_2 values different from the 'universal' ones, and have shown that these constants were different for different systems and, therefore, are not universal.

3.3.4 Effect of storage temperature on the retrogradation kinetics

The effect of temperature on the rate of crystallisation has been described in detail in the final section of this chapter (section 5). A crystallization rate versus storage temperature profile, typical of semi-crystalline polymers, is shown in Figure 2.6 (chapter 2). Based on the calculation developed in section 5, increased temperature has an enhancing effect on the rate of recrystallization below a particular temperature (T_{max}) which is located approximately halfway between the glass transition temperature T_g and the melting temperature T_m (Slade *et al.*, 1991). Above T_{max} the increase in temperature has a negative effect on the retrogradation kinetics.

The estimated T_{max} values for the different samples were obtained from T_g and T_m as described in section 5 of this chapter. For the majority of the water contents investigated in this section the T_{max} values were greater than the storage temperatures (40°C for the NMR and 25°C for the WAXS measurements) (Table 6.2).

Thus the majority of the measurements carried out were situated on the ascendent part of the rate versus temperature diagram (Fig 2.6).

Table 6.2 Glass-rubber transition, melting and maximum rate of retrogradation temperatures

Water Content % (w/w d.s.b)	T_m (°C)	T_g (°C)	$T_{max}^{(a)}$ (°C)	$T_{max}^{(b)}$ (°C)
20	164.7	50.1	107.4	71
60	130.4	-43.1	43.7	27

(a) : Calculated as described by (Slade et al., 1991)
(b) : Calculated as described in section 5 of this chapter

This interpretation was confirmed by experimental results obtained for samples stored at different temperatures.

An example of the effect of storage temperature on the retrogradation kinetics is shown in Figure 6.15 for a sample containing 30% water. The T_g and T_m of these samples were calculated using equation 2.3 (chapter 2) and equation 6.13 (section 5 of this chapter) respectively. Values of $T_g \approx 13$°C and $T_m \approx 193$ °C were found, yielding a $T_{max}^{(a)}$ of 83°C and $T_{max}^{(b)}$ of 61°C.

While the XRD spectra recorded after 11 days on the samples stored at 10°C, 25°C and 30°C did not show any evidence of crystallinity, retrogradation was evident at 50°C, 65°C and 80°C. These results suggested clearly that the retrogradation conditions for this sample over the entire range of storage temperatures used were situated, as predicted by the calculation in section 5, between T_g and T_{max}, and that the calculation of $T_{max}^{(b)}$ could be an underestimate of T_{max}.

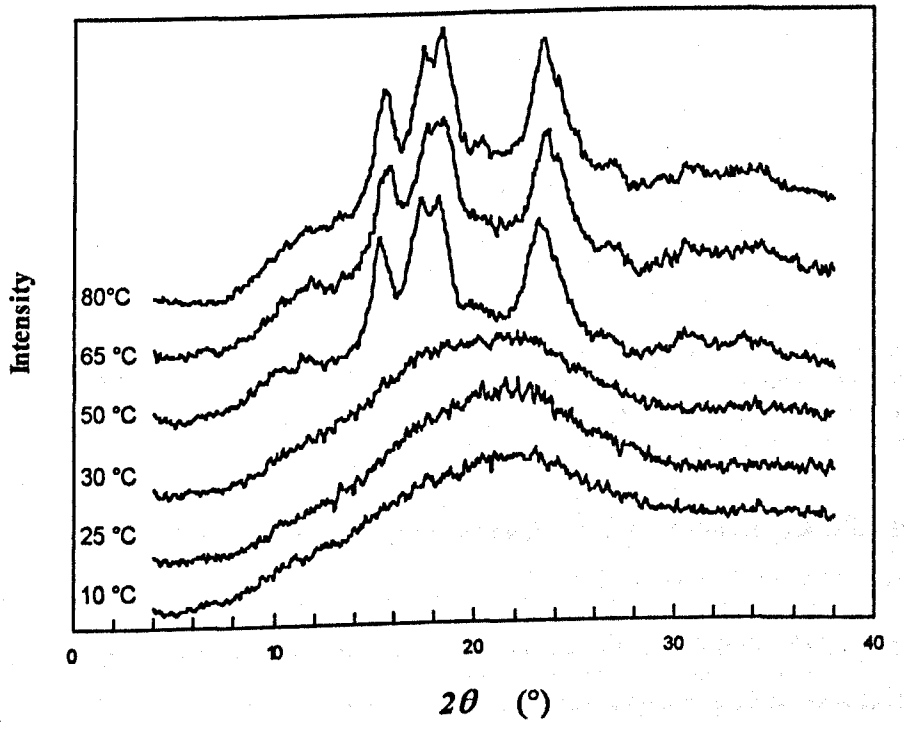

Figure 6.15 XRD spectra recorded after 11 days of storage at different temperatures (from bottom to top: 10, 25, 30, 50, 65 and 80°C) on extruded waxy maize starch samples containing 30% water.

3.3.5 Comparison of the kinetic results derived from the x-ray crystallinity and the NMR measurements

The retrogradation rate values, calculated from the spin-echo ^1H relaxation rates, were found to be greater than those obtained from the x-ray crystallinity and the tensile modulus results. While the NMR experiments were performed at 40°C, the x-ray spectra were recorded at 25°C. As demonstrated in the previous paragraph, the rate measured at 40°C is expected to be greater than at 25°C. Furthermore, NMR relaxation parameters are sensitive to local environment and short range order (Å distance scale) while x-ray describes long range order (nm distance scale). The kinetics at these two distance scales

could, not surprisingly, be different as a short range order is needed for the development of the larger scale organization.

3.4 Effect of water content and storage temperature on the polymorphic form of retrograded amylopectin

The line shape of the x-ray spectra recorded on the fully retrograded samples depended strongly on both the amount of water incorporated into the system during the extrusion gelatinization and, on the storage temperature. The x-ray spectra recorded on samples stored at a particular temperature, progressively exhibited patterns similar to the B-type starch polymorph, with increased water contents. The intensity of the characteristic peak at approximately 5.8° became greater, the peak at 17.2° became sharper, while the line width of the peak at approximately 23° increased. Figure 6.16 shows this progressive transition from the A to the B polymorphs in waxy maize starch extrudates stored at 25°C with increasing water contents. The x-ray spectra of the native waxy maize and the potato starches were used in Figure 6.16 as representatives of the A and B polymorphs respectively.

This shift in the polymorphic form from A to B , for a fixed water content, depended strongly on the storage temperature. A sample containing 42% water gave rise to an A-type crystalline form when the retrogradation process took place at temperatures of 25°C and above, while a B-type pattern was observed at lower temperatures (Fig 6.17).

These results are in agreement with the A/B temperature-water content polymorph diagram described by Marsh (1986). Indeed, Marsh obtained, by recrystallization of wheat starch gels, A type crystals at high temperatures and/or low water contents, while the B polymorph was observed at lower temperatures and higher water contents.

The dependence of the crystal type on the water content of the system is compatible with the structure of the cell unit of the starch polymorphs as described by Imberty *et al.* (1988) and reviewed in chapter 2 . The cell unit of the A-type starch polymorph contains 4 molecules of water while the B-type cell holds 36 molecules of water.

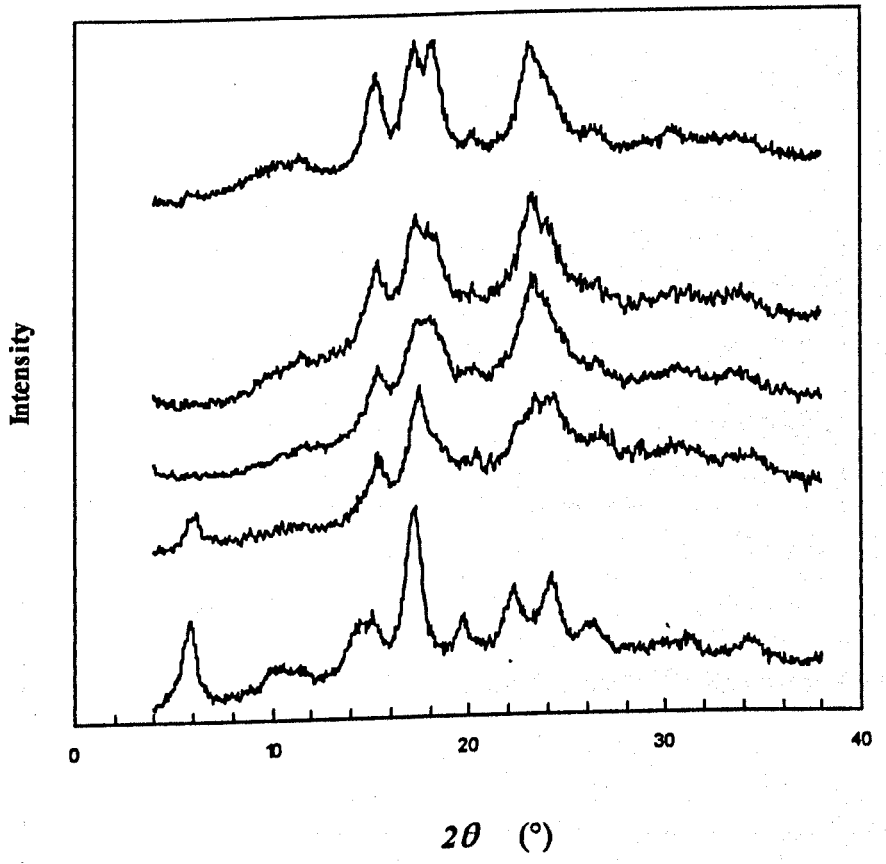

Figure 6.16 Changes in the type of the amylopectin polymorphs induced by the amount of added water. From top to bottom : native waxy maize starch (34% water), 'fully' retrograded waxy maize starch extrudates containing 35%, 40% and 60% water, and finally native potato starch containing 34% water.
The spectra of the native waxy maize and the potato starches are shown for comparison, respectively the A and B polymorphic forms.

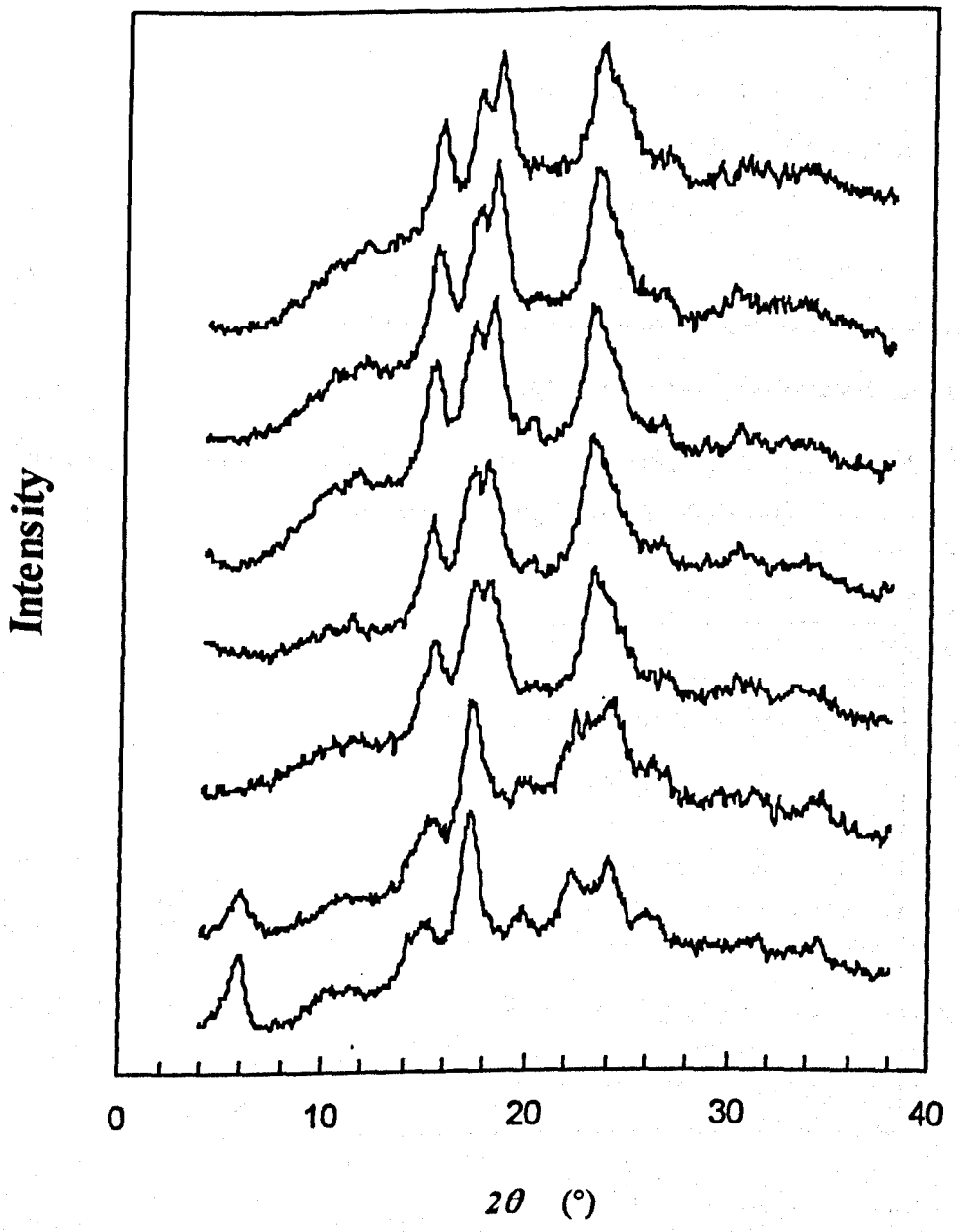

Figure 6.17 Changes in the polymorphic form of an amylopectin extrudate containing 42% water as a function of the storage temperature. Samples stored for 11 days at, from bottom to top: 4, 10, 25, 30, 50, 65 and 80 °C.

The Avrami exponent

The Avrami exponent n was adjusted during the non-linear modelling of the retrogradation kinetic results. The values obtained for n decreased with increasing water contents (Fig 6.18). These values approached asymptotically a value of 1 for $(T-T_g)$ greater than 60°C corresponding to a moisture content of 45% at 40°C (NMR results) and 54% at 25°C (x-ray and texture results). This is in agreement with the widely reported (Miura *et al.*, 1992) value of n=1 which reflects the fact that most of the published work is carried out on more dilute starch gels. However, the use of n=1 in more concentrated gels by some workers (Wilson *et al.*, 1991) is arbitrary and could constitute a source of errors in modelling retrogradation kinetics.

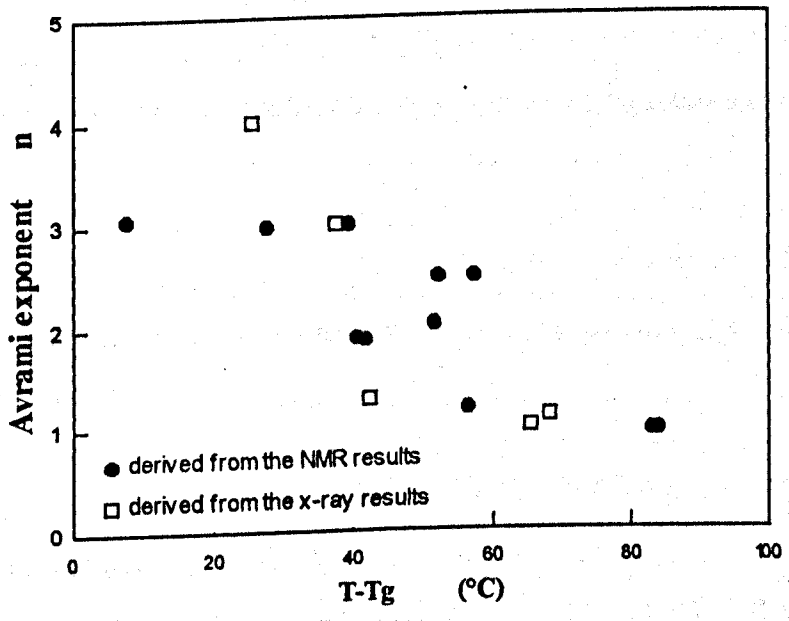

Figure 6.18 The Avrami exponent n results derived from the spin-spin relaxation rates (40°C) and the x-ray crystallinity indices (25°C) as a function of $(T-T_g)$ for amylopectin extrudates.

4. Effect of sugars on the process of amylopectin retrogradation

4.1 Wide angle x-ray diffraction

The effect of added sucrose, fructose or xylose at concentrations of 10% and 30% (w/w total dry solid) on the recrystallisation of waxy maize starch was studied using the same approach, methodologies and interpretations developed to describe the effect of water in the previous section.

The starch granules were found to be fully gelatinised in the extruder despite the presence of the sugar plasticizers. Indeed, the x-ray spectra recorded shortly after extrusion showed one single broad peak centred around 20° characteristic of amorphous starch. No evidence of sugar crystallization in the systems was observed from the x-ray diffraction results, with the exception of the samples containing 30% xylose and less than 24% water which showed several intense sharp peaks (line width less than 1°). These samples were not considered in this work as quantification of the starch crystallinity was extremely difficult, and these systems were highly phase separated and should be considered as such.

As described earlier, the x-ray spectra recorded at different storage times indicated an increase in the degree of crystallinity of the starch as the retrogradation progressed. The impact of fructose on enhancing the retrogradation of amylopectin extrudate is shown in Figure 6.19, where, although only 10% of the amylopectin was replaced by fructose, a considerable increase in the retrogradation rate was observed.

The crystallinity indices were calculated, and the kinetics results were modelled using the Avrami equation (equation 6.5).

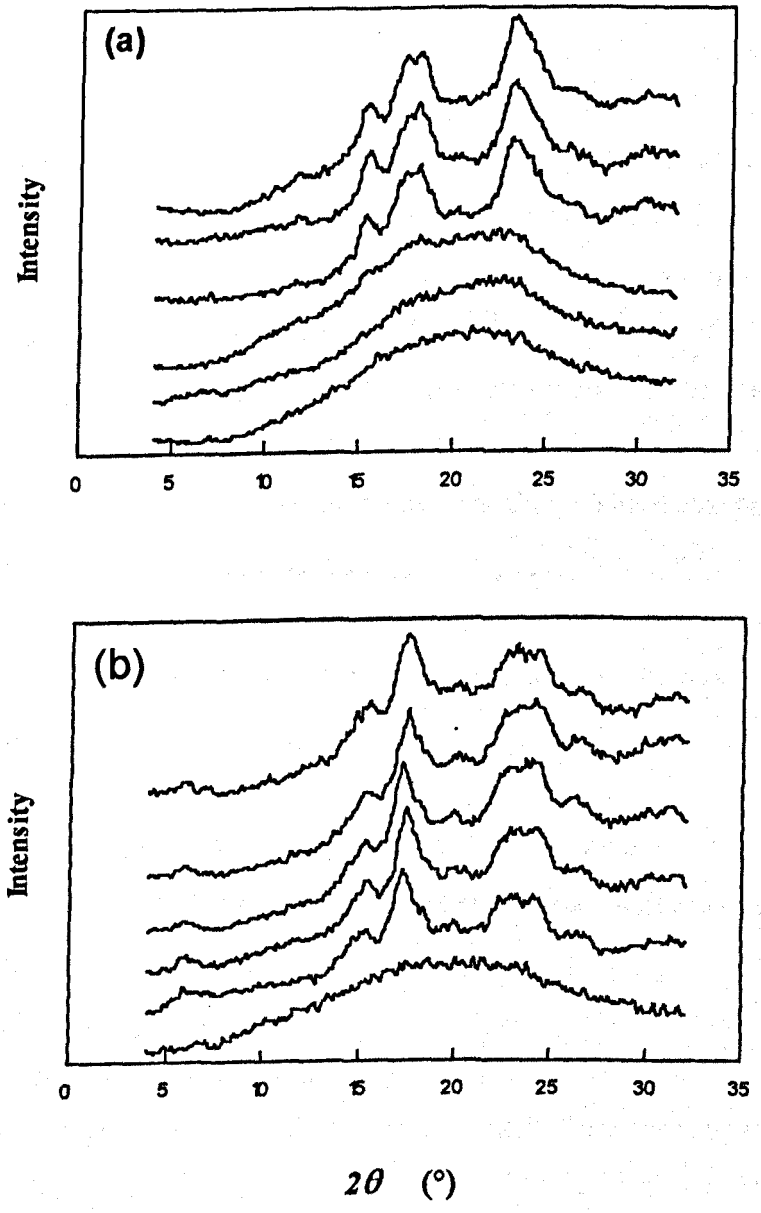

Figure 6.19 XRD spectra recorded at different storage times on (a) amylopectin and (b) 10% fructose - 90 % amylopectin extrudates both containing 35 ± 1% water (w/w d.s.b) samples. On each figure the spectra were recorded , from bottom to top, shortly after extrusion, and after 1, 2, 3, 4 and 6 days of storage at 25°C.

4.2 ^1H relaxation NMR

Whereas the ^{13}C solid state NMR performed at a resonance frequency of 75 MHz permits differentiation between starch and sugar on the basis of their chemical shifts, the proton relaxation NMR experiments carried out using a lower resolution spectrometer (20 MHz) suffered from the extremely low chemical shift resolution. Consequently, the only discriminating criterion between the various molecular species was their relative molecular mobilities and their effects on the various NMR relaxation parameters.
As described previously for the amylopectin - water systems, the free induction decay (FID) and the spin-echo decay (CPMG) recorded on the starch - sugar - water extrudates showed considerable dependence on the storage time. These changes were similar to those described for the systems containing no sugar, involving a general increase in the rigidity of the system recorded in terms of shortening of the spin-spin relaxation times and an increase in the amount of the 'rigid-like' component as a fraction of the total proton NMR signal.

The presence of sugars was found to affect the behaviour of the various NMR parameters. These effects could be divided into two different categories which are directly or indirectly related: (i) the sugars affect the kinetics of the starch retrogradation and thus affect the rate at which the rigid ordered component of the starch is being formed; (ii) the replacement of a fraction of the biopolymer by sugar would increase the molecular mobility of the polymer by means of plasticization, and of the water by introducing a new population of 'relaxation sink' partners having a mobility higher than that of the polymer and constitute, therefore, a less efficient 'relaxation sink' for the water molecules (Belton *et al.*, 1987).
The effect of the sugar depended strongly on its type and concentration in the system. Figure 6.20 illustrates the effects of the incorporation of 30% fructose, sucrose, xylose (w/w total dry solid basis) on the spin-spin relaxation rate versus storage time diagram at a water content of 35±1%. The solid lines represented the non-linear fit using the Avrami equation 6.5 .

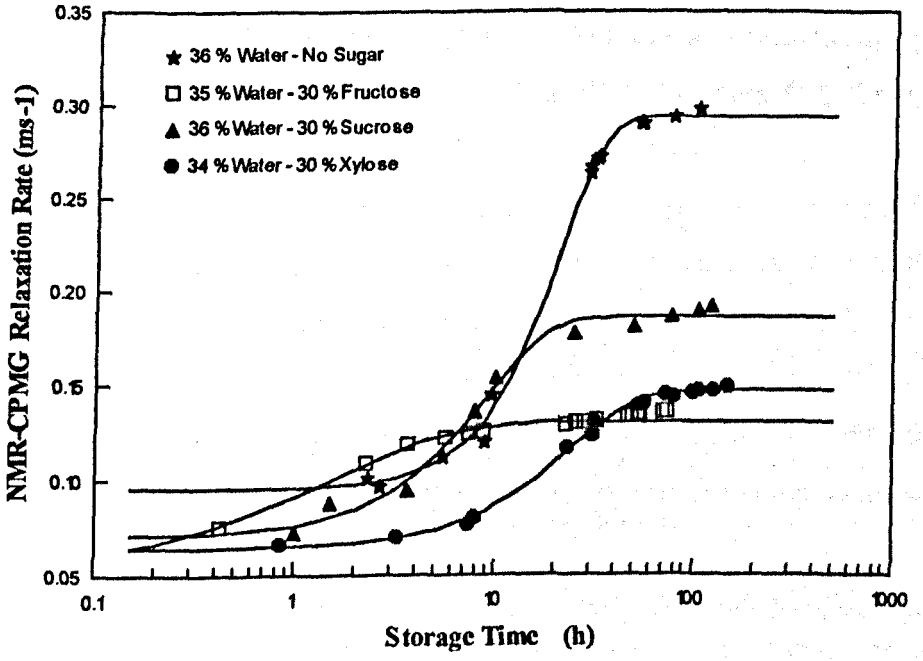

Figure 6.20 Effect of the presence of sugars on the retrogradation kinetics of amylopectin-sugar-water (70:30:35) systems measured by the spin-spin relaxation rate $1/T_{2\ CPMG}$ at 40°C.

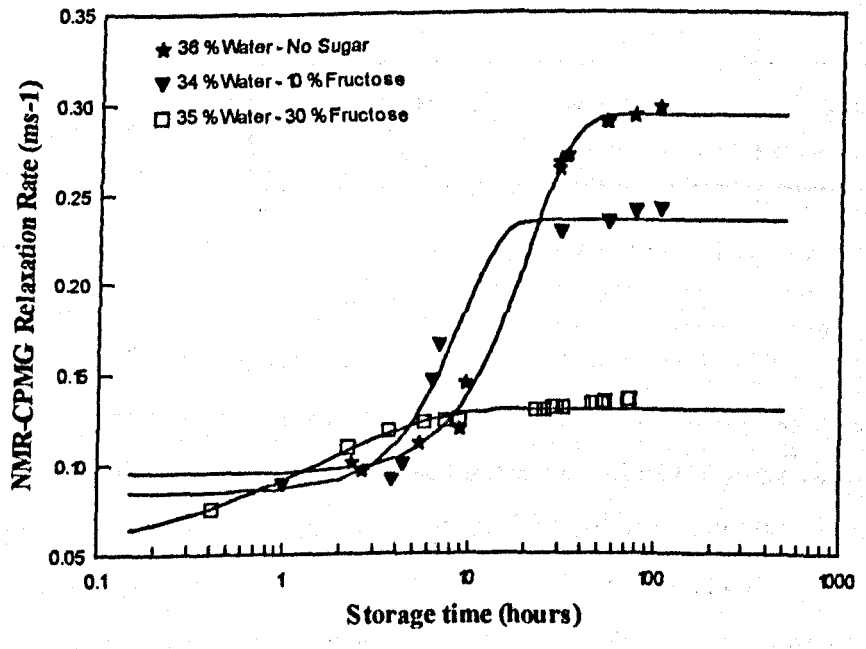

Figure 6.21 Effect of the concentration (10% and 30% w/w total dry solid) of the added fructose on the retrogradation kinetics of amylopectin-fructose-water systems measured by the spin-spin relaxation rate $1/T_{2\ CPMG}$.

For the sample containing no sugar, the increase in $1/T_2$ started after a 'delay' time t_1 of approximately 4 hours and levelled off just after 50 hours (t_2), these times were significantly shorter for the samples containing sucrose or fructose. Xylose was found to delay the changes and increase t_1 and t_2. For a particular water content, the effect of sugar was found to be proportional to the amount of sugar in the sample (Fig 6.21). The results obtained from Figures 6.20 and 6.21 are summarized in Table 6.3 .

Table 6.3 Effects of sugars on the retrogradation rate of waxy maize starch samples containing 35±1% water (w/w d.s.b) as calculated from the NMR spin-spin relaxation rates

Sugar	Concentration (w/w total dry solid)	t_1 (h)	t_2 (h)
No sugar	0	4	50
Fructose	10	2	20
Fructose	30	0.2	7
Sucrose	30	1	25
Xylose	30	5	70

The presence of sugar decreased considerably the values of the initial (at zero storage time t=0) and the equilibrium (at long storage time $t = \infty$) relaxation rates.
This observation was somehow 'contra-intuitive' as part of the sugar was thought to be in solution in the aqueous phase (Farhat *et al.*, 1996b), increasing the viscosity and thus decreasing the relaxation time (T_2) of the component of the NMR signal which mainly describes mainly the water component. However, since the concentration of the sugar in the system was calculated as a fraction of the total dry solid, this representation results in the replacement of a fraction of the polymer by an equivalent amount (weight) of a

monomer (fructose and xylose) or a dimer (sucrose). This was thought to have several implications:

(i) A reduction in the restriction of the mobility of water as the sugar molecules would have a significant mobility compared with amylopectin.

(ii) The T_2 of water is affected by the mobility of the biopolymer and / or the sugar through various surface relaxation processes such as , for example, proton exchange (Belton *et al.*, 1987b). The partial replacement of polymer by the less efficient 'relaxation sink' i.e the sugar, would, therefore, lead to an increase in the T_2 values of the spin-echo component.

(iii) The decrease in the average molecular weight of the mixture leads to a reduction of the glass transition temperature of the system, and consequently to an increase in the molecular mobility of the biopolymer decreasing its effeciency as a relaxation surface for the water molecules.

This interpretation was supported by the fact that the effect of sugar on the initial and equilibrium $1/T_2$ values was approximately proportional to the molecular weight of the sugar (with the exception of xylose).

4.3 Impact of the added sugars on the retrogradation kinetics

Information on the rates of retrogradation of systems containing no sugars provided a control allowing the assessment, by a process of comparison, of the effect of each sugar on the retrogradation of the waxy maize starch.

4.3.1 The retrogradation rate

As shown for the starch-water system, the rate of retrogradation was found to increase exponentially with the water content. The presence of fructose also considerably

increased the retrogradation rate value for a particular water content. As for the samples containing no sugar, the rate results calculated from the NMR relaxation rate measurements (40°C) were greater than the values obtained from the crystallinity index (25°C) measured by x-ray diffraction.

However, when the same results were plotted against the calculated deviation from the glass transition temperature ($T-T_g$), where T=40°C for the NMR results and 25°C for the x-ray results, the plots overlapped for the samples containing sugar. This was the case for all sugars at all concentrations investigated. An example is displayed in Figure 6.22 for the systems containing 30% fructose and those containing 10% xylose. This was thought to be a result of the role of sugars in (i) decreasing the T_g as anticipated by the Couchman-Karasz and the ten-Brinke equations, and (ii) increasing the melting temperature (Blanshard, 1986). Therefore, the presence of sugars in the system would lead to an increase in the width of the rate-temperature diagram (Fig 2.6 - chapter 2) and consequently to a decrease in the difference between the retrogradation rates predicted at 25°C and 40°C.

While fructose increased considerably the rate of retrogradation, and its effect was directly proportional to the amount of sugar in the system at a particular water content, the roles of sucrose and xylose were much more complex (Fig 6.23).

10% sucrose slightly increased the retrogradation rate. The role of sucrose at a concentration of 30% depended on ($T-T_g$) and thus on the moisture content.

For values of ($T-T_g$) below approximately 53 °C corresponding to a water content of 36% (w/w d.s.b) in the starch-sucrose (70:30) extrudate, the sugar was found to enhance the retrogradation under these conditions but it seemed to retard the retrogradation process at higher values of ($T-T_g$). However, in order to support this hypothesis, more results are necessary in the high water content range. The preparation of extrudates containing sugar and a large amount of water presented the risk of incomplete gelatinization of the starch in the relatively mild extrusion conditions of relatively high water contents and relatively low temperature. Indeed Fan *et al.* (1996) showed clearly that the degree of starch conversion depended on the glass transition temperature and thus

the viscosity of the melt, and that this conversion was considerably reduced by the presence of sugars. Xylose had no effect on the rate of waxy maize starch retrogradation at concentrations of 10% and slowed the retrogradation when the xylose concentration attained 30%. All the rate retrogradation versus ($T-T_g$) profiles extrapolated satisfactorily to a zero rate for ($T-T_g$)=0.

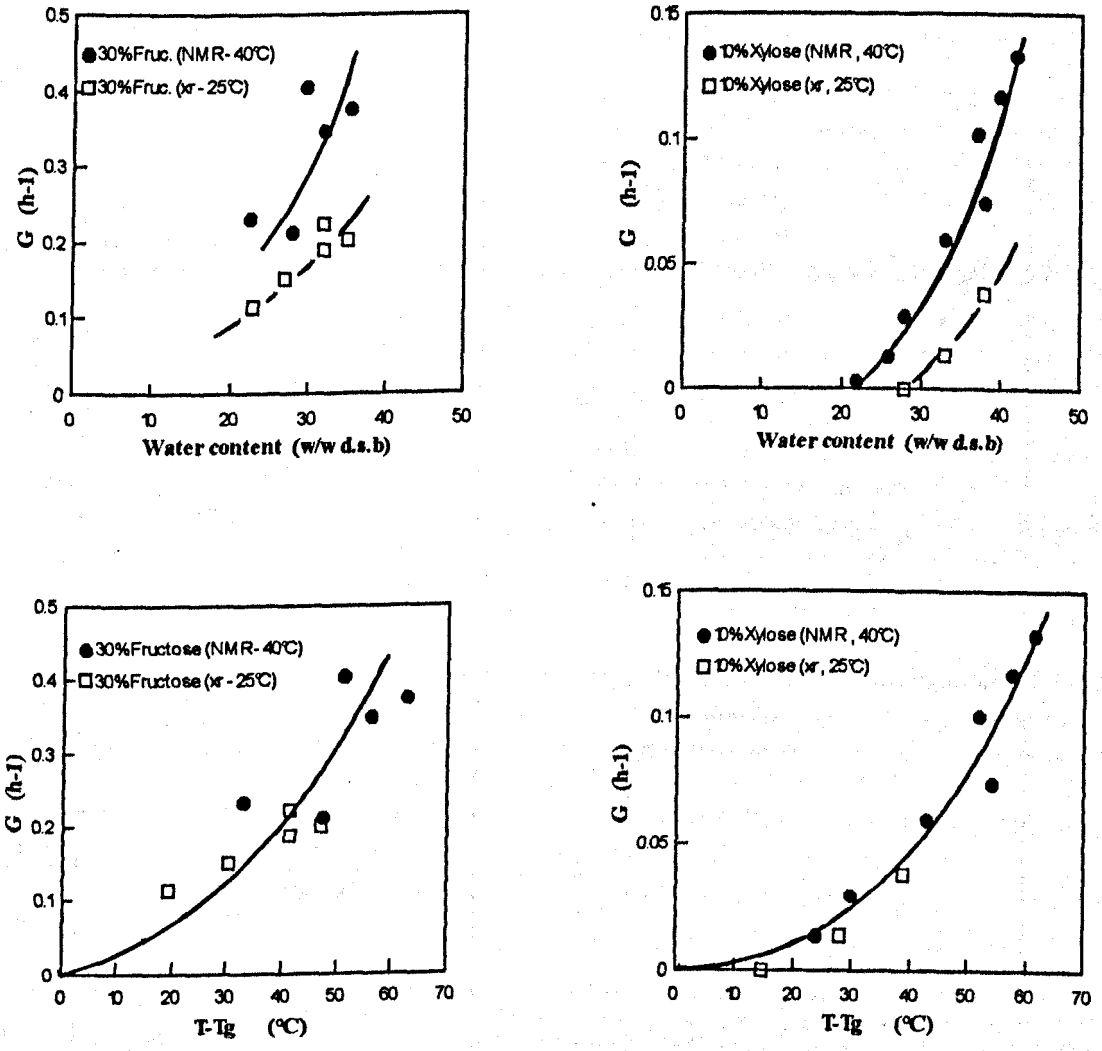

Figure 6.22 Retrogradation rate (G) as a function of water content (top) and the corresponding $T-T_g$ (bottom) for samples containing 30% fructose (left) and 10% xylose (right) (w/w total dry solid). The results derived from the Avrami modelling of the NMR spin-spin relaxation rates $1/T_{2\,CPMG}$ (40°C) are shown in solid symbols while the x-ray crystallinity results (25°C) are plotted in open symbols.

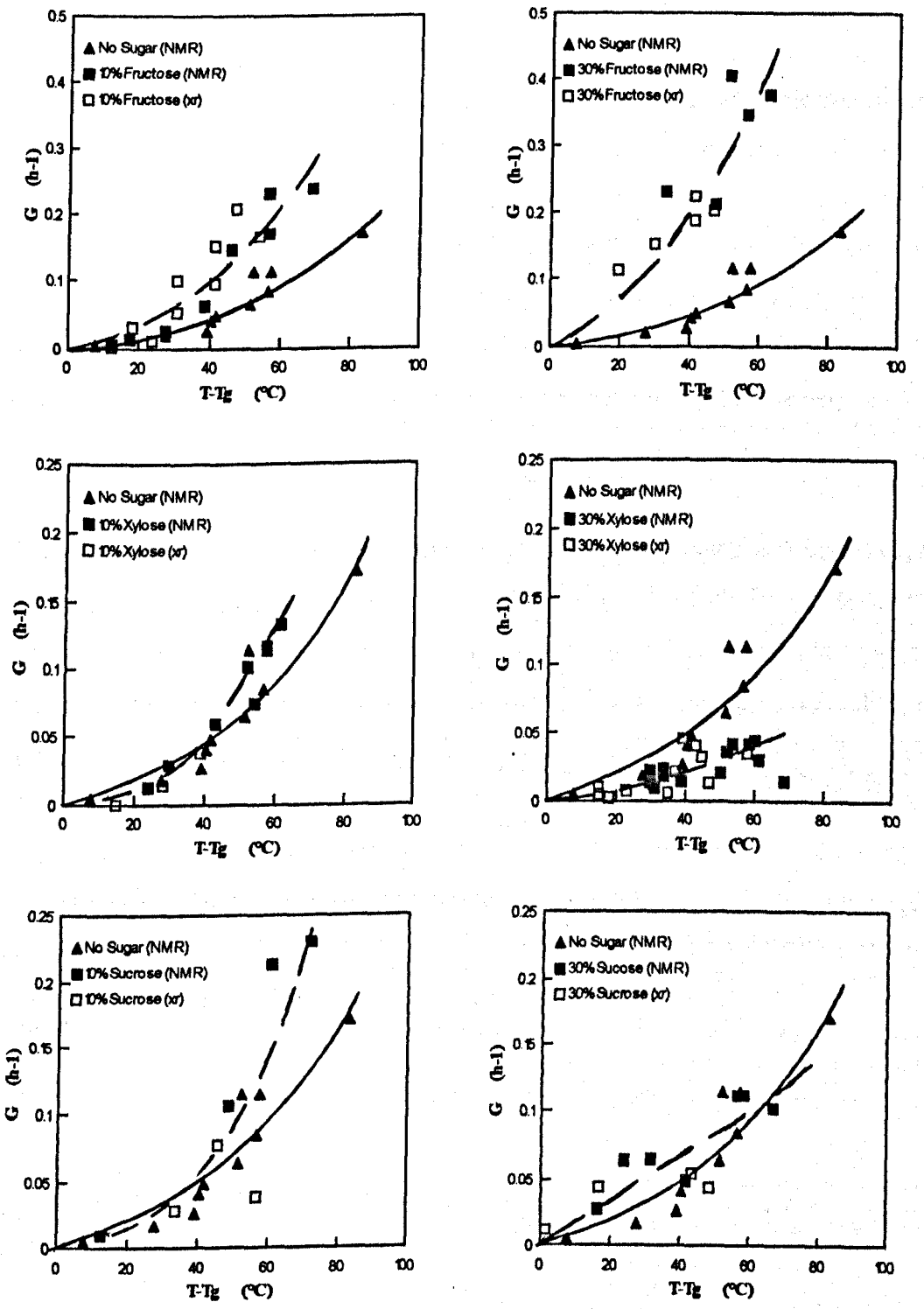

Figure 6.23 Retrogradation rate (G) results derived from the NMR spin-spin relaxation rates $1/T_{2\,CPMG}$ (40°C) and the x-ray crystallinity results (25°C) plotted against ($T-T_g$) for systems containing fructose, xylose and sucrose at concentrations of 10% and 30% (w/w total dry solid).

Furthermore, the values of water contents at which the rate versus moisture content curves extrapolated to zero ($W_{G=0}$) showed a satisfactory correlation with the water content values at which the T_g was 40°C for the rate results calculated from the NMR, and 25°C for those obtained from the x-ray (W_g), regardless of the type and concentration of sugar. The plot of $W_{G=0}$ as a function of $W_{40°C}$ (NMR), shown in Figure 6.24 yielded a slope very close to 1 (0.997), an intercept of 0 and a coefficient of correlation of 0.95, regardless of the sample composition (type and concentration of the sugar).

This was anticipated from the glass transition theory which predicts a dramatic reduction in the molecular mobility as the viscosity increases (10^{11} -10^{13} Pa s) as the system approaches the glass-rubber transition line of the phase diagram (Slade *et al.*,1991). Indeed, Slade and Levine (1991 and 1993) predicted that the rate of crystallization would be negligible near the glass transition. A linear relationship was found between ln(G) and ($T-T_g$) confirming the exponential character of the rate versus ($T-T_g$) diagrams (Fig 6.25). The results presented as a natural logarithm of the retrogradation showed the impact of fructose in accelerating the retrogradation of waxy maize starch, the water content dependence of the effect of 30% sucrose and the inhibitory role of xylose on the recrystallization of gelatinized starch in starch-sugar (70:30) systems.

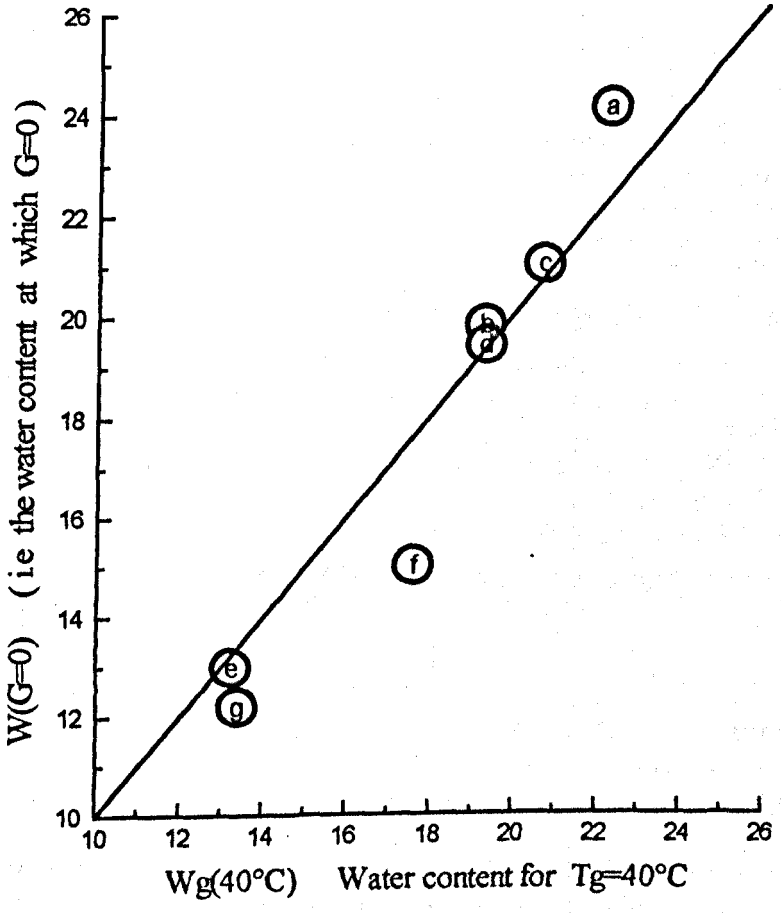

Figure 6.24 A correlation between the water contents at which the rate (derived from the $1/T_{2\,CPMG}$ at 40°C results) extrapolated to zero ($W_{G=0}$) and the water content at which the T_g is 40°C W_g, for the systems containing: (a) no sugar, (b) 10% fructose, (c) 10% sucrose, (d) 10% xylose, (e) 30% fructose, (f) 30% sucrose and (g) 30% xylose.

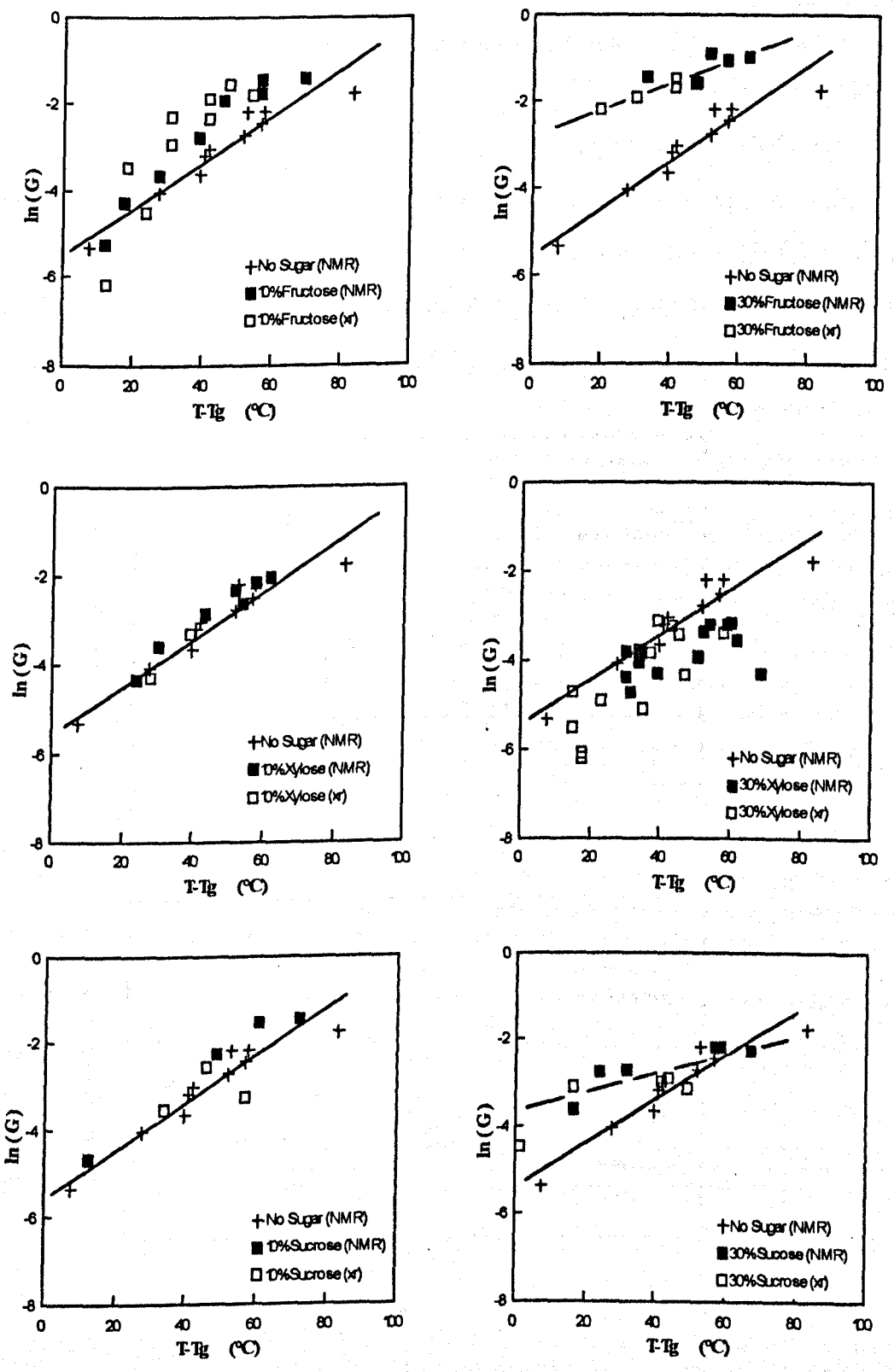

Figure 6.25 Plots of ln(G), the rate of retrogradation as a function of $(T-T_g)$ showing the effects of added sugars at concentrations of 10% and 30% (w/w total dry solid).

4.3.2 Effects of water and sugar on the Avrami exponent

Values of n between 1 and 4 were obtained, and the results depended on the sample composition (water content, sugar type and concentration). The n values obtained from NMR and x-ray results were comparable when samples with similar $(T-T_g)$ value were considered (Fig 6.26). As described earlier for the binary systems, the values of n decreased exponentially with increasing $(T-T_g)$ to reach a value of n=1 for high $(T-T_g)$ values.

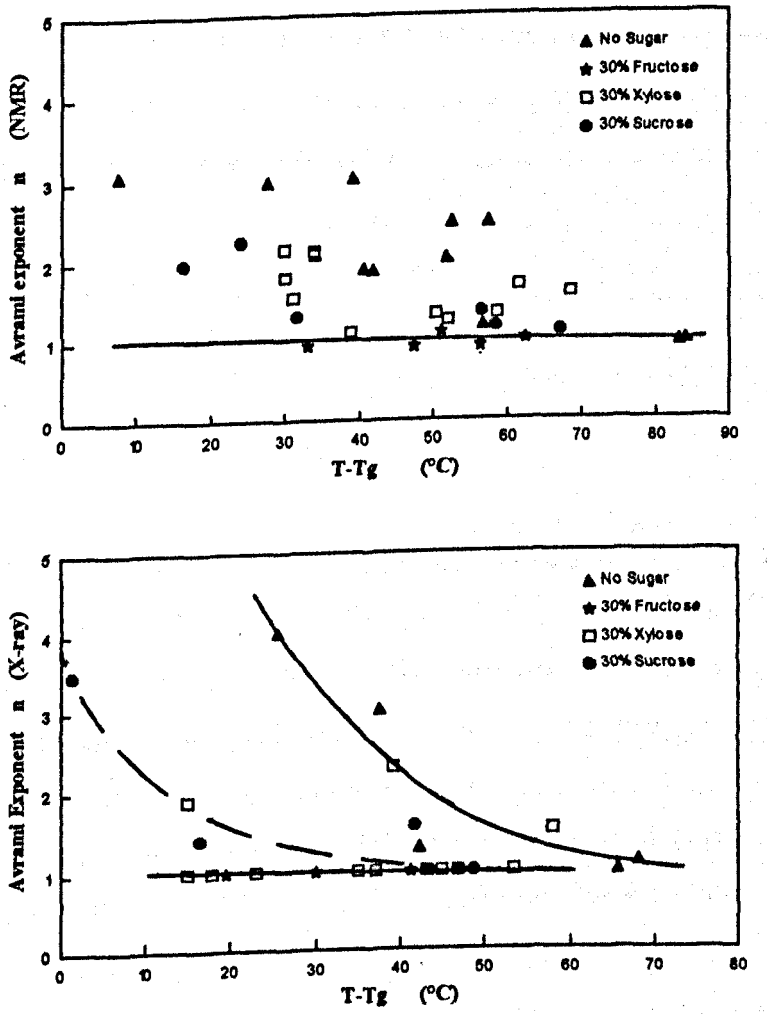

Figure 6.26 Effect of added sugars on the value of the Avrami exponent n derived from the NMR CPMG relaxation rates (top) and the x-ray crystallinity indices (bottom) as a function of $(T-T_g)$.

The rate at which these curves decreased was accelerated by the presence of sucrose. For fructose, the value of n=1 was found over the whole range of water contents examined. It is possible that, for fructose, only the final part of the more general decay of n has been obtained. The situation seemed more complex in the case of xylose as the scatter was considerable.

The value of n has commonly been related to the nature of the nucleation stage of the crystallization process (Tiller, 1991). The nucleation phase is affected by the temperature i.e $(T-T_g)$ and consequently by the moisture content. Furthermore, this dependence of n on the water content and $(T-T_g)$ was intuitively expected as results showed that the particular polymorph formed depended on the water content and the presence of sugar. However, we have not been able so far to establish a systematic relationship between n and the polymorphic form of the starch crystal. Only the significance of the Avrami exponent in the kinetics of recrystallization was considered.

4.4 The mobility of the sugar in the system

The ^{13}C solid state NMR spectra recorded using the CP-MAS and the FT-MAS techniques showed distinct lines for amylopectin and the sugars. The chemical shifts characteristic of the sugars were present only partially in the CP-MAS spectra of the amylopectin-sugar-water mixtures, but contributed largely to the FT-MAS spectra.

As CP-MAS records the rigid component whilst FT-MAS measures the more mobile component, the dominant presence of the sugar signal in the FT-MAS spectra is indicative of its high rotational mobility, implying a solution-type behaviour of the sugar in these extruded mixed systems. This was confirmed by the results reported in chapter 4 on the hydration properties of amylopectin-sugar extrudates where the majority of the sugar present in the system was found to have a high mobility as it contributed to the 'liquid' component of the FID.

4.5 Role of the sugars

The role of the sugar in the system can be described in terms of (i) non-specific effects of the sugar such as the plasticization of the biopolymer, and (ii) more specific molecular interactions between the sugar the biopolymer.

4.5.1 Plasticizing effect

The depression of the glass transition temperature of polymers by the presence of small and intermediate sized molecules, known as plasticization, is a phenomenon well established in the science of synthetic polymers. Equation 2.3, which was discussed in detail in chapter 2, can be extended to three-component systems and used to calculate the effect of composition on the T_g value of mixed amylopectin-sugar-water systems using the parameters listed in Table 6.1. Figure 6.27 illustrates the effect of replacing 30% of the biopolymer by sucrose or xylose on the temperature of the glass-rubber transition as predicted by equation 2.3 .

The consequence of the plasticization of the amylopectin by the combined presence of water and sugar is an increase in the molecular mobility of the polymer. This should be manifested by an increase in the relaxation time of the rapidly decaying component of the FID ($T_{2\,sol}$) which derives from the ^1H of the rigid polymer matrix. In the present experimental conditions of water content and temperature, the sugar protons are thought to have relatively long decay times and thus contribute to the more mobile 'liquid' FID component as demonstrated in chapter 4.

However, somewhat surprisingly, the presence of the sugars had no significant impact on the $T_{2\,sol}$ values recorded on the freshly gelatinized (storage time $t \to 0$) and on the 'fully' retrograded ($t \to \infty$) amylopectin-sugar-water extrudates (Fig 6.28).

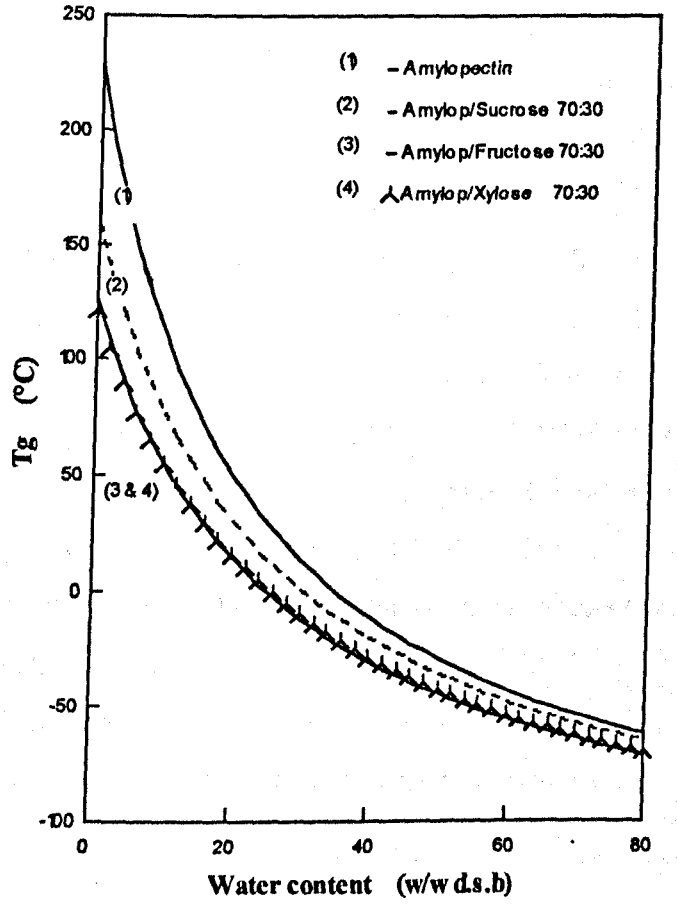

Figure 6.27 A plot of T_g versus water content, also illustrating the plasticization of amylopectin by sugars.

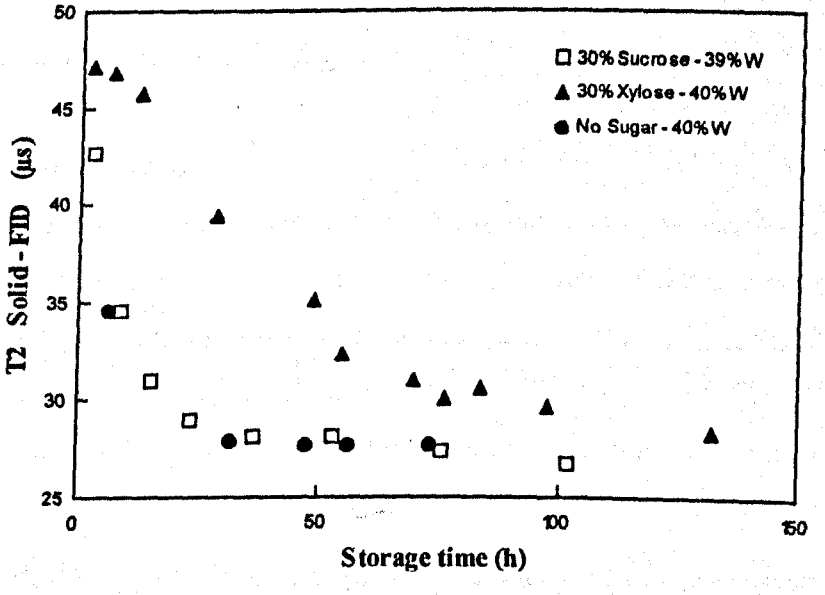

Figure 6.28 Effect of added sugars on the spin-spin relaxation times of the 'solid' component ($T_{2\,solid}$) of the free induction decay.

4.5.2 Effect of sugar on the ordering properties of amylopectin

The presence of sugar in the system was found to enhance the formation of the 'pseudo-B' polymorph in fully retrograded samples. This polymorph shows all the characteristic features of the B type x-ray pattern described in the previous section : the sharp peak at 17.2° (this peak is doubled by a second peak at ~18.2° in the A-type) and the presence of two peaks at approximately 22.3° and 24.2° (these two peaks merge to one single peak at ~23.2° in the A-type), but the peak at 5.6-5.8° which is very pronounced in B-type polymorphs was much smaller (Marsh, 1986). The effect of fructose, sucrose and xylose on the polymorphic form of amylopectin crystal generated during the retrogradation of extruded waxy maize starch, initially of the A-type, is illustrated clearly in Figure 6.29 . It has also been established that the formation of the B polymorph is enhanced by high water content and/or low temperature conditions (Imberty *et al.* 1988; Marsh, 1986).

There are two possible explanations for these effects:

(i) A first hypothesis attempts to explain the effect of the sugar on the type of polymorph grown during the isothermal retrogradation of starch-sugar gels in terms of the effect of the sugar on the distribution of water between the various components in the system. More water could have been made available for the starch by a less competition from the sugar, leading to the association of a greater amount of water with the biopolymer than predicted by an equatl partitioning of the total amount of water present in the system. This hypothesis was discarded on the basis of the sorption isotherms of starch and sugar (Iglesias *et al.*, 1982) which predicted that the sugar had a greater affinity for water in the range of moisture contents of interest in this work (Fig 2.14 - chapter 2) (Farhat *et al.*, 1996b).

(ii) The second hypothesis is derived from the 3-dimensional structure of the cell unit of the starch crystalline structure devised by Imberty *et al.* (1988). It was suggested that

a 'cavity' existed inside this cell unit of the B-type polymorph (Fig 6.30-a). The accessible domain in this cavity has a diameter of approximately 0.7 nm, which could accommodate a sugar molecule (a monomer or, a dimer in an optimum conformation). Thus the cell unit could have grown around sugar molecules, which might have triggered the nucleation step of the crystallisation process (Fig 6.30-c). The role of impurity in enhancing nucleation is a well known phenomenon in synthetic polymer and mineral crystallisation. The x-ray spectra recorded on the starch-sugar fully retrograded extrudates showed some differences compared to the normal B-type pattern, the most pronounced being the reduction or absence the peak at around 5.8°. This was thought to be due to the imperfections of the cell unit due to the presence of the sugar in the centre of the arrangement of the 6 double helices (Fig 6.30-c). The size of the sugar is of a primary importance in the formation of the 'pseudo-B' polymorph. In the absence of any sugar, this cavity in the centre of the arrangement of the 6 double helices is occupied by 36 molecules of water (Fig 6.34-c(i)). The detailed explanation for the modification of the 5.8° feature is as follows: the presence of a sugar molecule of an optimum size would lead to a displacement of the water molecules from this 'inter-helical' space. This would lead to the disappearance of the peak at ~5.8° resulting from the water existing in the original B-type structure. The system containing fructose exhibited such situation (Fig 6.29).

However, a somewhat smaller sugar (less than the critical size of a 0.7 nm diameter) could be accommodated in the cavity but leave space for some water molecules (Fig 6.30-c (ii)). This would lead to the presence of a reduced peak at 5.8°, as observed in the case of xylose (Fig 6.29).

Finally, a larger sugar such as sucrose would only fit in the cavity if it adopted a particular 3-dimensional conformation minimizing its steric volume and thus a mixture of B (where no sugar is incorporated in the cell unit) and 'pseudo-B' polymorphs would coexist leading to the reduced peak at 5.8°C observed in x-ray pattern of the sucrose containing sample in Figure 6.29.

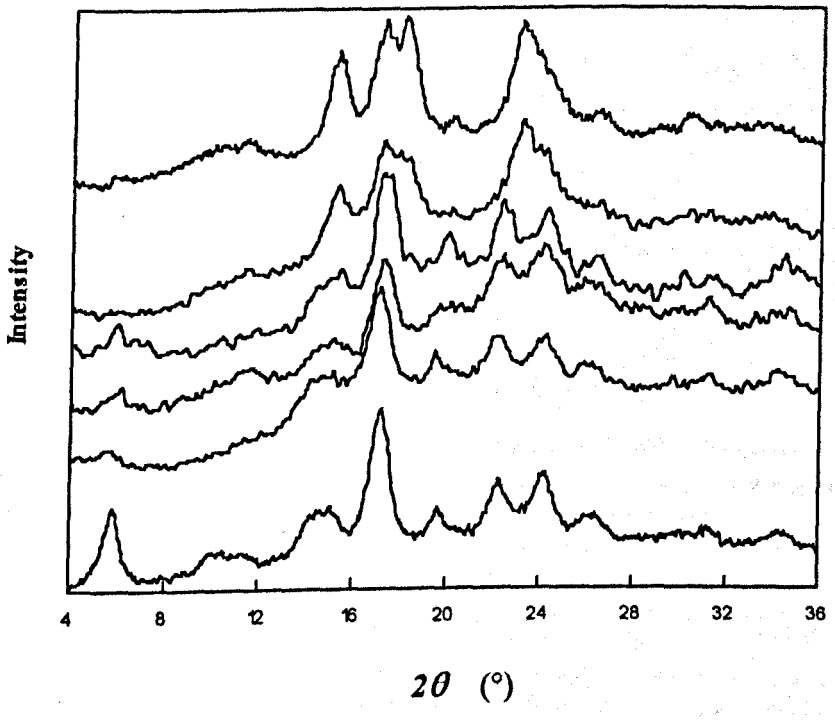

Figure 6.29 XRD spectra of 'fully' retrograded (25°C) waxy maize starch systems containing 35±1% water. From top to bottom: native waxy maize starch, extruded with no sugar, extruded with 30% xylose, extruded with 30% sucrose, extruded with 30% fructose and finally native potato starch.

The spectra of the native waxy maize and the potato starches at the same water content of (35±1%) are represented for being typical of the A and B polymorphic forms respectively.

The existence of molecular interactions between starch and the sugars was supported by the occurence of sugar chemical shifts in the CP-MAS ^{13}C solid state NMR spectra. This result suggested the occurrence of a fraction of the sugar with limited mobility, and could, therefore, be indicative of a molecular interaction between amylopectin and some of the sugar molecules.

The reminder of the sucrose was more mobile and had a solution-type behaviour in terms of molecular mobility, and hence, was recorded using the FT-MAS technique (Fig 6.31).

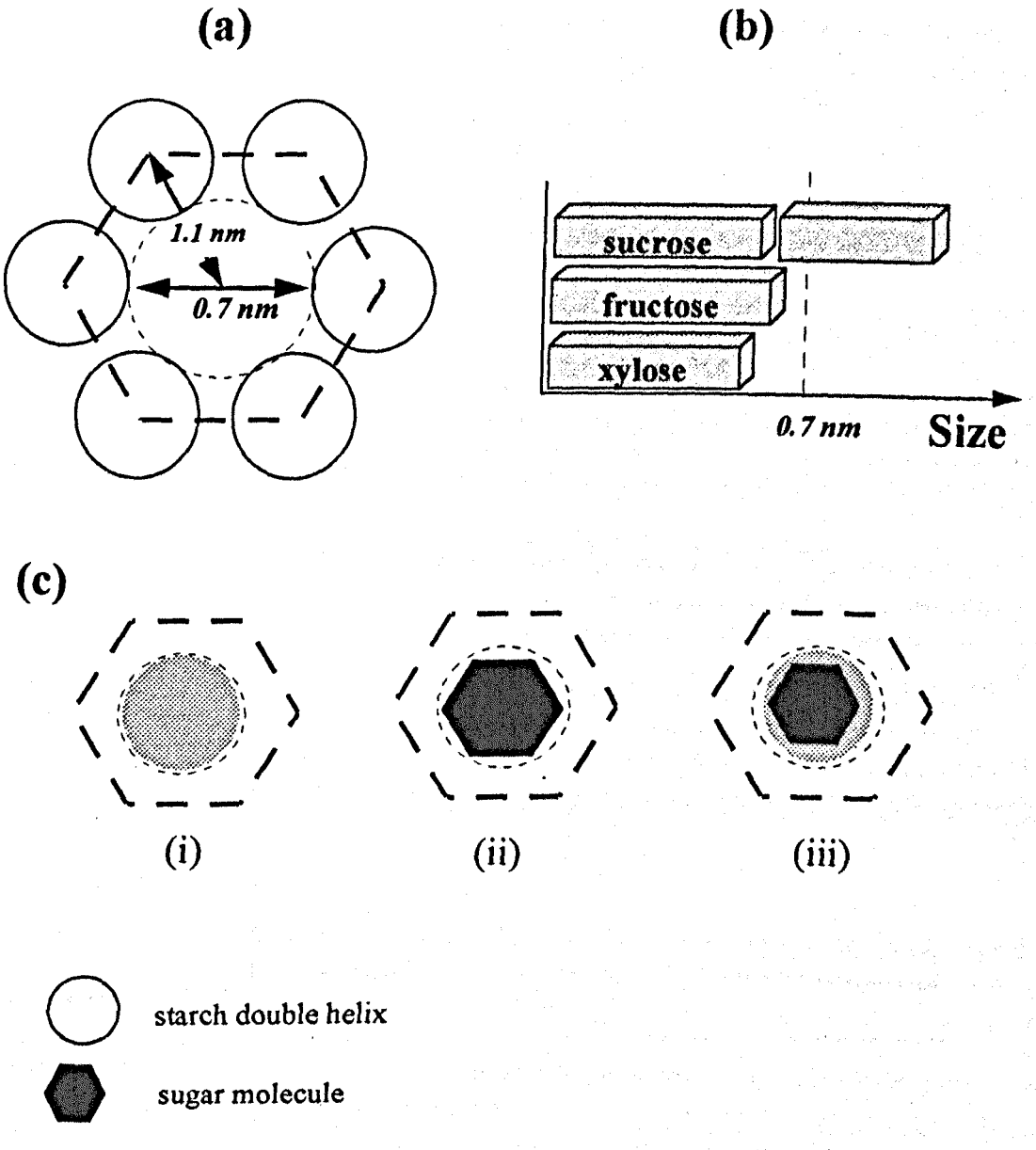

Figure 6.30 Schematic representation of :

(a) the B-type cell unit with the corresponding dimensions (adapted from the results reported by Imberty *et al.* (1988) and reviewed in chapter 3)

(b) the typical dimensions of sucrose, fructose and xylose molecules

(c) the proposed model describing the involvement of the sugar molecule in the formation of the cell unit of the 'pseudo-B' starch polymorph according to the size of the sugar

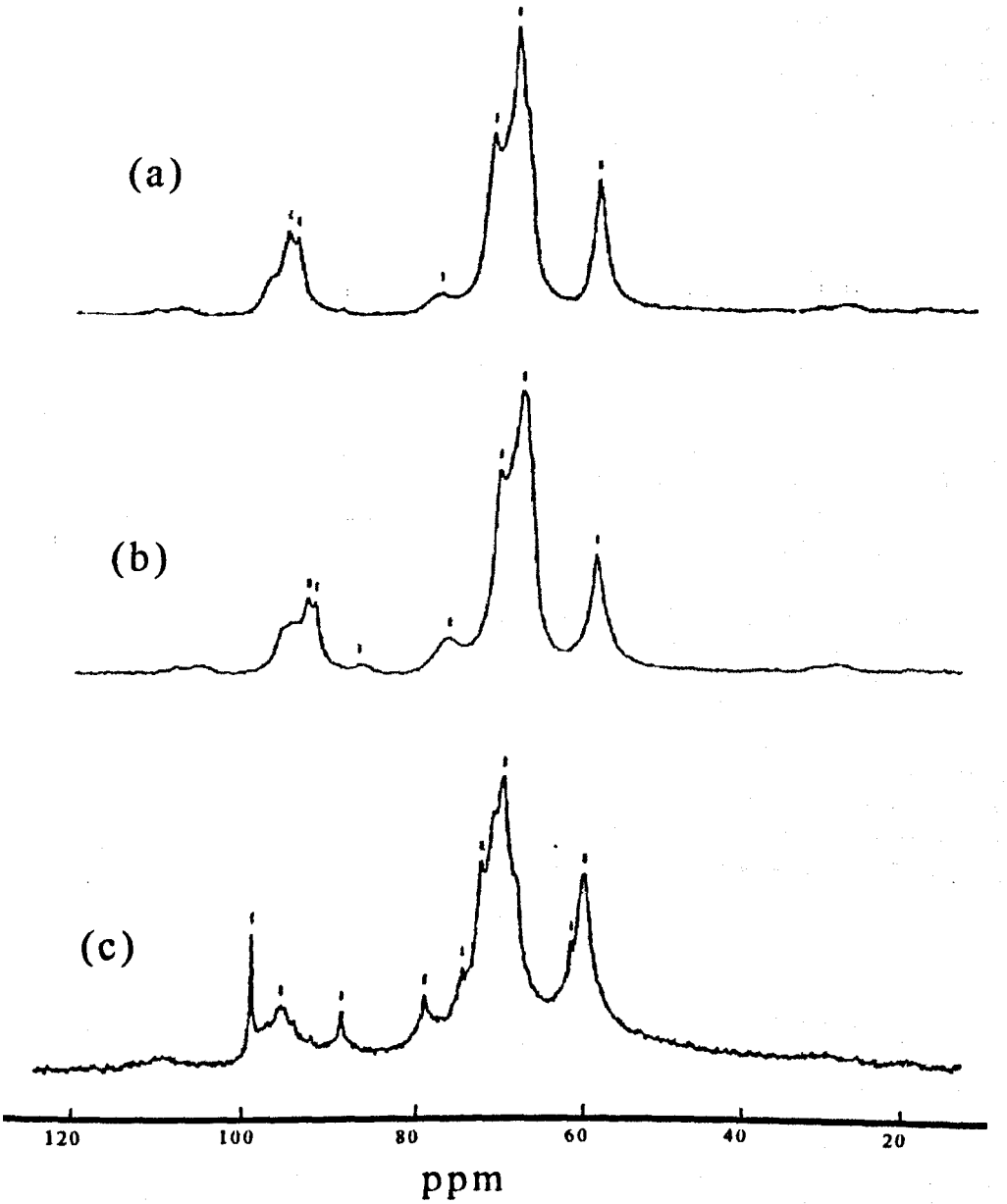

Figure 6.31 ^{13}C NMR spectra (75 MHz) recorded on 'fully' retrograded extrudates

a- CP-MAS spectrum of an amylopectin-water (100:60)

b- CP-MAS spectrum of an amylopectin-sucrose-water (70:30:44)

c- FT-MAS spectrum of an amylopectin-sucrose-water (70:30:44)

The sharp lines in (a) show the solution type behaviour of a large proportion of the sucrose present in the system, the sharp lines particularly at 80.6, 91.4 and 102.9 ppm in (b) show the contribution of a fraction of sucrose to the signal of the rigid component; (a) is shown for comparison purposes

5. A simulation of the combined effects of water content and storage temperature

5.1 Crystallization rate versus temperature diagram

The dependence of the crystallization rate on the storage temperature can be described using the Lauritzen-Hoffman (Lauritzen *et al.*, 1973) theory of the growth of chain-folded polymer crystals. The growth rate (G) of bulk polymers is given by the expression:

$$G(T) = G_0 \exp[-\frac{U^*}{R\,(T-T_\infty)}] \exp[-\frac{K_g}{T\,\Delta T\,f}] \qquad (6.10)$$

where :

T the crystallization temperature (K)

U^* the activation energy for the steady state reptation of the polymer chain ($J.mol^{-1}$)

R the gas constant ($R=8.314\ J.K^{-1}.mol^{-1}$),

ΔT the undercooling $\Delta T=T_m-T$; T_m being the melting temperature

f factor accounting for the change in the heat of fusion with temperature

K_g constant

While Lauritzen and Hoffman assumed $f = 1$ in their calculations of G of various synthetic polymers, Marsh and Blanshard (1988) obtained f from equation 6.11:

$$f = \frac{2\,T}{T_m + T} \qquad (6.11)$$

T_∞ is a hypothetical temperature at which viscous flow is supposed to cease.

T_∞ is related to the glass transition temperature T_g .

$$T_\infty = T_g + \delta T \qquad (6.12)$$

Both Lauritzen *et al.* (1973) and Marsh *et al.* (1988) reported a value of $\delta T \approx 30$ K for synthetic polymers and wheat starch respectively.

5.2 Calculation of T_g and T_m

5.2.1 The glass transition temperature T_g

The glass transition temperatures (T_g) were calculated using the ten Brinke and Karasz (1983) equation (equation 2.3 - chapter 2).

5.2.2 The melting temperature T_m

According to the Flory equation (Flory, 1953) the following relation holds between the melting point of a polymer and the diluent concentration:

$$\frac{1}{T_m} - \frac{1}{T_m^0} = \frac{R}{\Delta H_u} \frac{V_u}{V_1} (\upsilon_1 - \chi_1 \upsilon_1^2) \qquad (6.13)$$

where ΔH_u is the change in enthalpy of fusion per repeating unit (glucose), V_u/V_1 is the ratio of the molar volumes of the repeating unit in the chain to that of water, R is the gas constant, T_m(K) is the melting point of the polymer-diluent system, T_m^0 is the true melting point of the undiluted polymer, υ_1 is the volume fraction of the diluent and χ_1 is an interaction parameter. A plot of $1/T_m$ against υ_1 gives a straight line.

For a plot of $10^3/T_m$ versus υ_1, a slope of approximately 0.8 was reported for a wide variety of starches (Donovan 1979 and Biliaderis *et al.*, 1980) while the intercept values depended on the type of starch, values between 2 and 2.3 corresponding to T_m^0 values between 500 and 435 K. An intercept of 1.9 corresponding to an approximate $T_m^0 =$ 525 K was used as amylopectin is a large molecular weight polysaccharide. Indeed,

Takeda *et al.* (1987a) reported a DP=570 for wheat starch corresponding to approximatly a molecular weight of 98 000, while Zobel (1988) reported a molecular weight between 3.10^5 and 3.10^6 for amylopectin. Consequently, waxy maize starch is expected to have high T_m^0 compared to other starches having various amounts of amylose.
The density of starch was assumed to be 1.5 $g.cm^{-3}$.

The calculated T_g and T_m values of the amylopectin-water samples studied in the previous sections are shown in Figure 6.32.

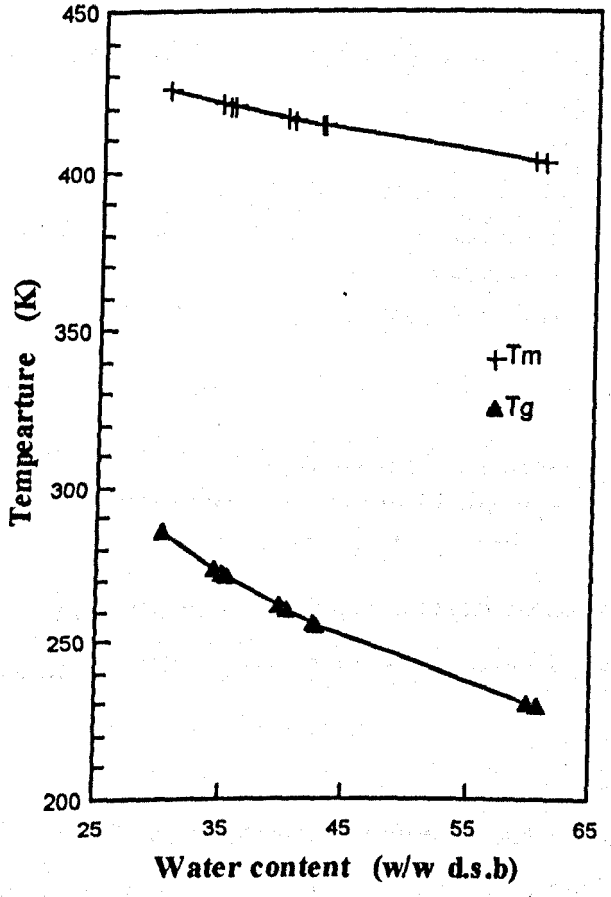

Figure 6.32 The calculated values of glass transition (T_g) and melting (T_m) temperatures of amylopectin samples as a function of the water content

5.3 Calculation of U^*, δT, K_g and G_0

The various parameters in equation 6.10 are not accessible directly but can be obtained graphically. Equation 6.10 can be written as follows :

$$\ln(G) = \ln(G_0) - \frac{U^*}{R\,(T-T_g+\delta T)} - \frac{K_g}{T\,(T_m-T)\,f} \qquad (6.14)$$

which can be rearranged to give :

$$\ln(G) + \frac{U^*}{R\,(T-T_g+\delta T)} = \ln(G_0) - K_g \frac{1}{T\,(T_m-T)\,f} \qquad (6.15)$$

As reported earlier in this chapter, the rate of recrystallization of amylopectin was measured for samples with different moisture contents, i.e with different T_g and T_m values. These results were obtained by NMR at a temperature of T=313 K (40°C).

A plot of the term on the left hand side of equation 6.15 versus $[\,T\,(T_m-T)f\,]^{-1}$ should yield a straight line with an intercept equal to $\ln(G_0)$ and $-K_g$ as slope (Marsh *et al.*, 1988).

The values of U^* and δT were optimized to give the best correlation coefficient for a straight line fit to equation 6.15 . The optimization was carried out with the values reported by Marsh as initial guess (U^*= 15000 J.mol^{-1} and δT= 30 K).
The detailed results of the calculation are listed in Table 6.4. The best correlation was acheived for U^*= 15000 J.mol^{-1} and δT= 65 K (Fig 6.33 and 6.34).

Table 6.4 Optimization of the U^* and δT using equation 6.15

Input			Output	
δT (K)	U^* (J.mol^{-1})	ln(G_0) (s^{-1})	K_g x10^5 (K)	Correlation coefficient
30	5000	7.7	3.03	0.913
30	7500	22.7	6.13	0.938
30	10000	37.7	9.23	0.942
30	12500	52.8	12.23	0.943
30	15000	67.8	15.4	***0.944***
30	17500	82.8	18.5	0.944
30	20000	97.8	21.6	0.943
35	15000	58.9	13.4	0.949
40	15000	51.4	11.6	0.954
45	15000	44.9	10.1	0.957
50	15000	39.4	8.89	0.961
55	15000	34.6	7.8	0.963
60	15000	30.4	6.86	0.965
65	15000	26.7	6.04	**0.967**
70	15000	23.4	5.31	0.967
75	15000	20.4	4.67	0.967
80	15000	17.8	4.1	0.966

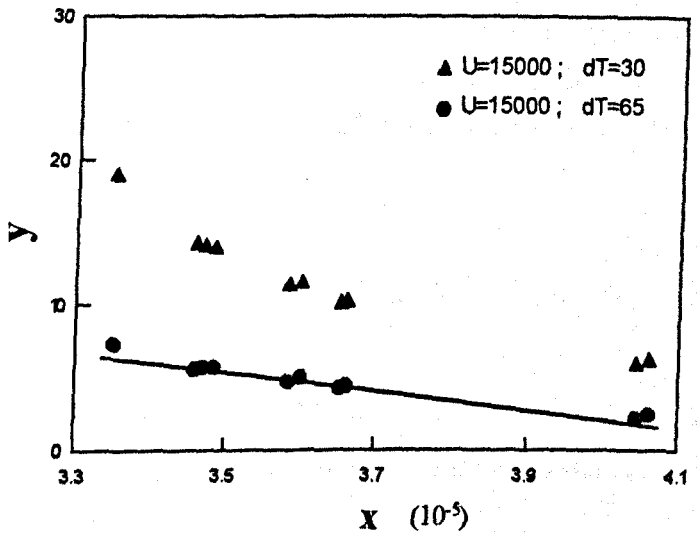

Figure 6.33 Linear plot of equation 6.15 where :

$$X = \frac{1}{T(T_m - T)f} \qquad Y = \ln(G) + \frac{U^*}{R(T - T_g + \delta T)}$$

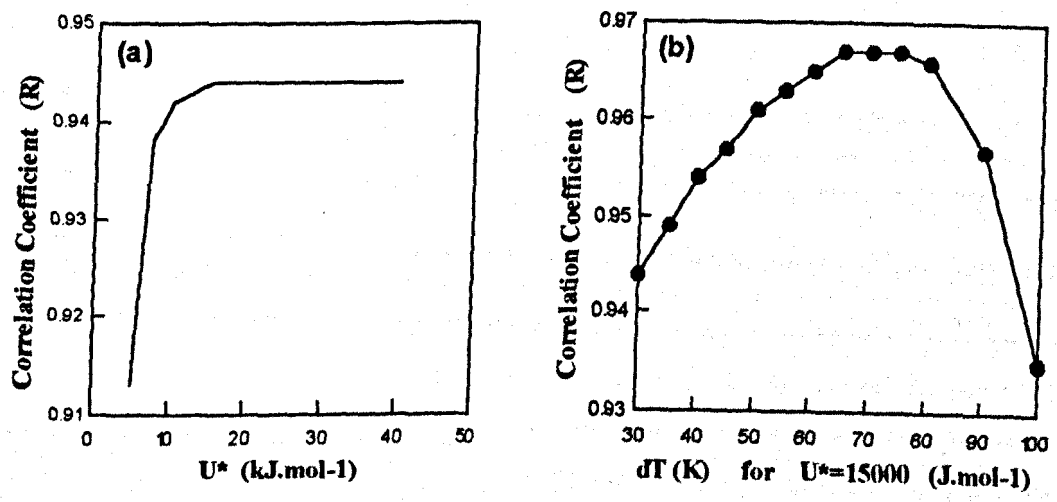

Figure 6.34 A plot of the coefficient of correlation obtained by applying a linear regression treatment to equation 6.15 as a function of (a) U^* and (b) δT. The plot summarizes the results reported in Table 6.4 and shows that the best linearity for equation 6.15 was obtained for U^*=15 kJ mol^{-1} and δT=65 K.

5.4 Effect of water content on the isothermal rate value

The effect of moisture content on the rate versus temperature diagrams, according to the previous calculations is, therefore, given by Figure 6.35. Despite the shift of the temperature at which the G(T) reaches its maximum (T_{max}) to lower temperatures with increasing water contents (Fig 6.35), the shape of the diagram was independent of the moisture content.

Indeed, the parameter α describing the symmetry of the G(T) curves caculated using the following equation :

$$\alpha = \frac{T_{max} - T_{\infty}}{T_m - T_{\infty}} \qquad (6.16)$$

A value $\alpha = 0.56 \pm 0.06$ was found, showing no dependence on the water content (Fig 6.36).

Athough all the steps of the calculation were based on the retrogradation results derived from NMR measurements at a single temperature (313 K), the Lauritzen-Hoffman theory used with the parameters optimized in this section is anticipated to constitute a satisfactory model of results of the retrogradation of waxy maize starch extrudates. An example of this correlation is shown in Figure 6.37 where rate results obtained at 298 K and 313 K by NMR seemed to follow closely the predicted diagram. A more complete study of the rate - temperature dependence has recently been undertaken but the results are not available yet.

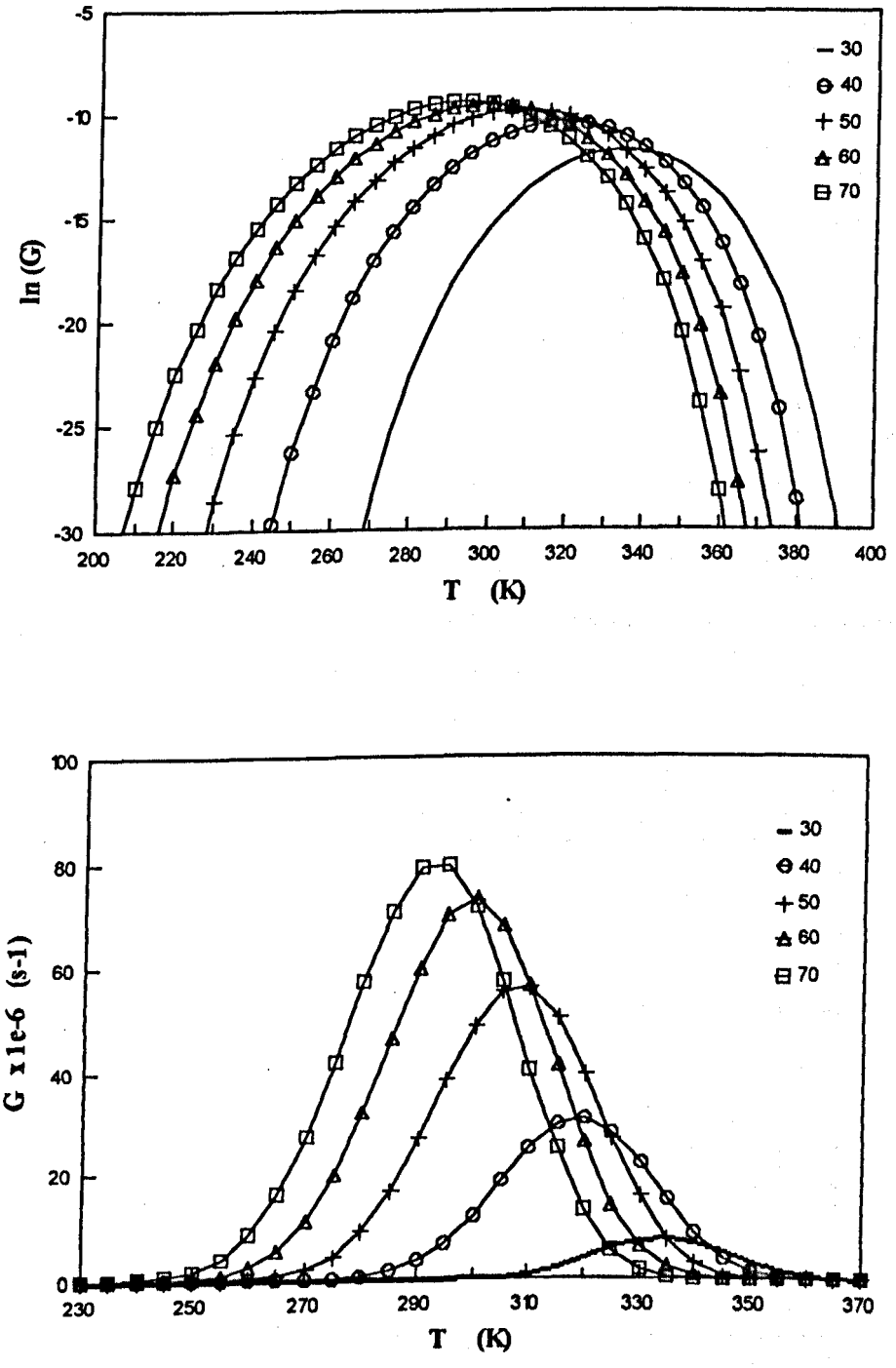

Figure 6.35 The combined effects of water and storage temperature on the retrogradation kinetics of waxy maize starch - water extrudates : effect of water content on the (a) ln [G(T)] and the (b) G(T) as predicted using the calculated of T_g and T_m (Fig 6.37), U^*=15 kJ mol^{-1} and δT=65 K.

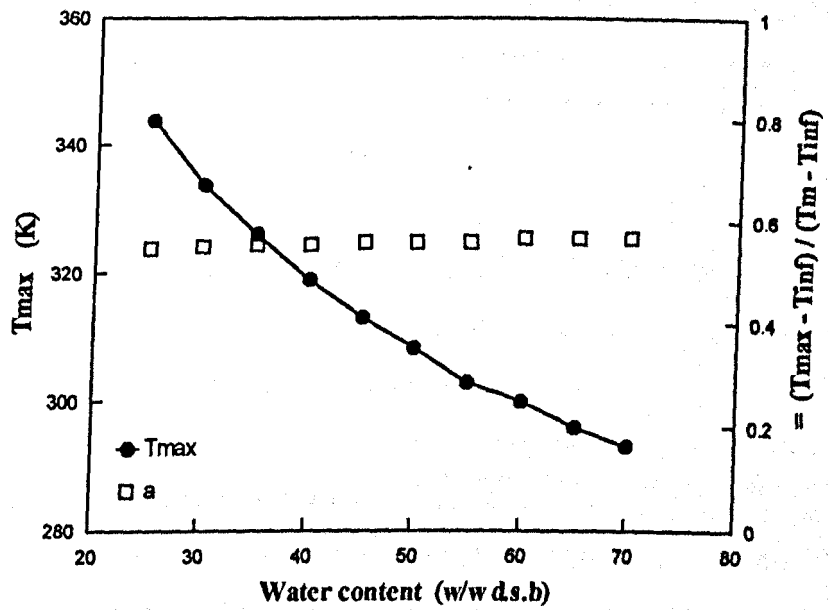

Figure 6.36 The effect of water content on the temperature for which G is maximum (T_{max}) and on the symmetry of the G(T) diagram (Estimated by the value of α)

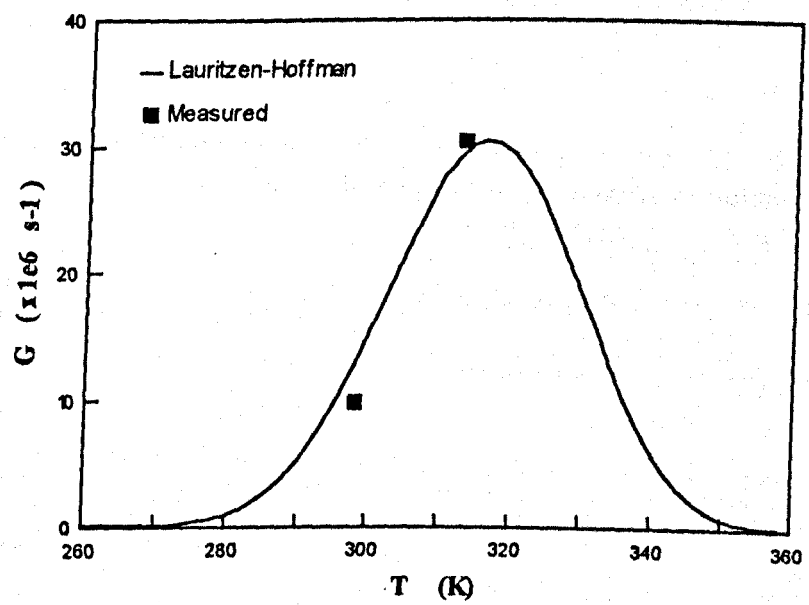

Figure 6.37 Correlation between the retrogradation rate derived from the NMR results measured at 298K and 313 K for a sample containing 42% water (w/w d.s.b) and the calculated G(T) diagram predicted by the Lauritzen-Hoffman theory for the same water content using the optimized parameters.

5.5 Discussion

This approach could be extended to the amylopectin-sugar-water systems using the approach developed by Lelièvre (1976) and Blanshard (1986) to obtain the melting temperatures for different sample compositions.

This simulation of the combined effects of water content and storage temperature, could provide a valuable tool for the prediction of storage properties of starch based systems (Fig 6.35). It shows clearly that the effect of temperature can be predicted from the T_g and the T_m of the system, and how the water content affects the various parameters defining the rate of retrogradation.

However, the calculation relies on two parameters T_g^0 and T_m^0 the glass-transition temperature and the melting point of the pure amylopectin, which are still matters of some scientific uncertainty as they are generally obtained by extrapolation of experimental results to zero water content.
Furthermore, the low rates of retrogradation obtained at 40°C for samples having less than 30% water induced slight distortions in the simulation. These could be avoided by using isothermal rates obtained at higher storage temperatures.

6. General discussion

A number of interesting points have emerged from the results reported in this chapter.

1. Firstly it is clear that the particular polymorph which results from the recrystallization of the starch is a function of the water content and temperature. The temperature of

maximum rate of recrystallization is also a function of water content.

2. From an experimental point of view, it is not surprising that a number of NMR parameters are sensitive to the development of increased retrogradation. These include the T_2 of the solid and the T_2 of the liquid components of the FID, the relative amplitude of the solid component of the NMR signal, and the T_2 derived from the CPMG measurements. The fact that a sample can be left in the spectrometer probehead during retrogradation thereby providing an uninterrupted recording of the process with a satisfactory control over the storage temperature (±0.1 °C) and the water content is particularly useful.

3. A detailed study of a whole range of results shows quite clearly that although the water content, particularly in ternary systems, is a poor indicator of the presence of conditions conducive to retrogradation, replotting the results with $(T- T_g)$ as the abscissa shows that the rate does indeed approach zero at $(T-T_g)=0$.

4. An examination of a whole range of results of the effects of different sugars on the rate of retrogradation shows that the rate is a function of both the water content and the particular sugar. Figures 6.23 and 6.25 summarise the effects of 10% and 30% sugars on the retrogradation rate values derived by NMR and x-ray diffraction. The results are notably different and indicate that whereas xylose slightly reduces the rate of retrogradation, sucrose enhances the retrogradation when $(T-T_g) < 60$ °C. At higher $(T-T_g)$ values, i.e > 60°C, sucrose would appear to depress the rate. Fructose, under the conditions of the experiment, uniformly enhances retrogradation but, like sucrose, might well reduce retrogradation rates at high $(T-T_g)$ (>135°C). Such conditions could be obtained, either by increasing T , the storage temperature, or reducing T_g by increasing the water content.

Conclusion

A number of significant observations have emerged from these studies which require further investigation. For example, the apparently progressive decrease in the mobility of water molecules with retrogradation has important implications for the perceived dry texture of staled products.

Conversely, the effect of sugars upon the x-ray spectrum as illustrated by the reduction or even elimination of the 5.8° 2θ peak suggests that water is being displaced from the helical structure and may then be more available as a textural plasticizer.

The exact role of sugars in relation to the recrystallization of the starch is not fully understood yet. It is also interesting that sugars which apparently enhance the rate of crystallization at temperatures just above T_g (sucrose and fructose) display a behaviour which demonstrates (sucrose) or suggests (fructose) that at high values of $(T-T_g)$, they will exert an inhibitory effect upon the reorganization process.

Chapter 7

General Discussion and Conclusions

Each of the preceeding chapters containing experimental results has been followed by a detailed discussion an conclusion sections. However, in this final chapter, the impact of molecular mobility on the organization and the properties of biopolymer-sugar-water systems is discussed in general terms, in an attempt to develop a 'universal' understanding of the role of the individual components in the behaviour and industrial performance of the mixed system.

"Ternary systems such as a biopolymer-sugar-water system, are rather like an early impressionist painting. From a distance the image is clear and the subject is distinct, but closer inspection yields confusion, lines blur and subtle shadings become evident and the precise definition of each object becomes more difficult" (*). In the same way, mixed systems in the broad view appear as essentially homogeneous mixtures with predictable physical properties (glass-rubber and melting transitions, kinetics of molecular mobilisation and ordering, etc.). However, a more detailed examination reveals the complexity of such mixtures, that is due to various phenomena such as phase separation and unequal partitioning of water between the various components, which consequently, influence the microscopic and macroscopic physical properties of biomolecular mixtures.

(*) quote adapted from Veis (1964) in 'The Macromolecular Chemistry of Gelatin', p.127

The complexity of the situation arises partly from the fact that one has to consider the interactions between the individual components, i.e biopolymer-water, biopolymer-sugar and sugar-water, but also between the corresponding binary system where, for example, the properties of the water in plasticizing a particular component (the sugar or the biopolymer) depends on the role of water in the binary system it forms with the other biomolecule (the biopolymer or the sugar respectively) present in the system.

The hydration of biopolymers led, as expected, to enhanced polymer mobility through plasticization processes, which enabled the biopolymer to undergo the conformational transitions necessary to reach its minimum energy state of short and long range order. Although, the resulting degree of molecular order and mobility depended on the macromolecule under investigation, a general pattern emerged in which the degree of order in the secondary structure of biopolymers increased when the level of hydration increased in the range between 0 to 0.75 g of water / g of dry biopolymer. The ordering transitions occurring at these relatively low water contents would affect the hydration/solubility properties of biopolymers. This could prove to be important in determining their industrial performance, particularly when used in dried food systems or in formulation of pharmaceutical tablets.

Another important example of biopolymer reordering as a consequence of increased molecular mobility is the effects of plasticizers such as water and sugars on the kinetics of the retrogradation of extruded waxy maize starch systems. Once more, molecular mobility and order were found to be strongly dependent. A certain degree of mobility was found to be necessary to allow the diffusion of the biopolymer molecules or intra-molecular chains required for the nucleation and the subsequent growth of ordered crystallites. Therefore, one can postulate that 'enhanced mobility leads to enhanced order'. However, as shown from the NMR studies of the retrogradation (both ^{1}H relaxation and ^{13}C solid state results), the crystallized fraction of amylopectin had a

reduced mobility relative to the amorphous one. This, consequently, suggested that 'increased order leads to reduced mobility'and as far as recrystallization is concerned, the process is self limitting.

Although the presence of sugars decreased the translational mobility of water, the role of sugars as a plasticizing agent was illustrated in their ability to enhance the rate of amylopectin retrogradation. In addition, the presence of sugars was found to affect the polymorphic form of the recrystallized amylopectin possibly as a consequence of specific interactions between the biopolymer and the sugar. The sugar could be at the centre of the 'pseudo-B' arrangement of the 6 amylopectin double helices forming the unit cell of the crystal. Such interactions are believed to affect the water distribution in the system further enhancing the rate of retrogradation and the crystal type.
The effect of the sugars on the retrogradation kinetics depended on the water content. The results obtained on extruded amylopectin/sugar (70:30) systems suggested that while sugars enhanced the rate of retrogradation at low water contents, the opposite effect was observed (sucrose) or anticipated (fructose) at higher moisture contents. While the effects of sucrose and fructose followed this pattern, xylose reduced the rate of retrogradation over the entire water content range investigated. A hypothesis based on the role of the size of the sugar molecule offered a possible interpretation for the effect of sugar in favouring the 'pseudo-B' amylopectin polymorph and explained the difference between the behaviour of the 3 sugars in this regard.

Despite the significant differences in the behaviour of the various sugars, in terms of their effect on the kinetics of recrystallization of amylopectin and on the water partitioning in mixed systems, there was no evidence of any difference in their effects on the diffusion of water in sugar solutions nor in starch gels.

In recrystallized starch systems, the crystalline fraction was found to be rigid, whilst the amorphous fraction had a higher mobility. In xanthan, however, ordered helical forms were found in both the rigid and the mobile components of the system as illustrated by the

results of studies using solid state ^{13}C CP- and FT-MAS NMR.

The investigation of the hydration properties of gelatin-sugar films by FTIR revealed evidences of (i) molecular interactions between the biopolymer and the sugar and, (ii) unequal partitioning of water between the 2 components of the mixed system. The specific interactions between the individual components (gelatin-water, sugar-water and gelatin-sugar) depended on the water content of the system.

The differential partitioning water, an aspect very often overlooked, is an important parameter to consider when formulating mixed systems. In general, the competition for water was found to be in favour of the biopolymers investigated at low water contents (up to 20% w/w d.s.b depending on the sugar concentration). At higher water contents, the preferential hydration of the sugar was favoured. The water vapour sorption isotherms of the individual components of a mixed system were found to provide an empirical tool to describe qualitatively the amount of water associated with each component. The principle of unequal partitioning of water in mixed systems could lead to interesting industrial application. Indeed, the 'water management' approach could prove of particular value in determining the macroscopic properties of the final product in terms of texture, stability on storage, etc. providing a better control over food product deterioration processes such as staling of starch based products, sugar crystallization, flavour release, etc.

This thesis is based on the following publications :

Published / In press

Farhat I.A, Mitchell J.R, Blanshard J.M.V and Derbyshire W (1996), 'A pulsed ^1H NMR study of the hydration properties of extruded maize-sucrose mixtures', *Carbohydrate Polymers*, **28**, in press.

Farhat I.A, Moreau P, Mitchell J.R, Derbyshire W and Blanshard J.M.V (1996), 'Spectroscopic studies of hydrocolloid water interactions', in *Gums and Stabilizers for the Food Industry.* IRL-Oxford University Press, **8**, 27

Farhat I.A, Blanshard J.M.V, Melvin J.L and Mitchell J.R (1996), 'The effects of water and sugars upon the retrogradation of amylopectin in the region ($T-T_g$) between 0 and 85°C', Paper presented at *Starch: Structure and Function international conference*. Cambridge-UK, 1996, in press

Melvin J.L, Farhat I.A, Mitchell J.R and Blanshard J.M.V (1995), 'Effects of sugars on the retrogradation of extruded amylopectin', poster presented at *The 9th World Congress of Food Science and Technology*, 1995, Budapest, HUNGARY

In preparation

Farhat I.A, Melvin J.L, Blanshard J.M.V, Mitchell J.R AND Derbyshire W, 'The retrogradation of extruded waxy maize starch: a molecular dynamics approach'

Farhat I.A , Moreau P, Orset S and Blanshard J.M.V, 'A FTIR study of the hydration phenomena in protein - sugar systems'

Bibliography

Ablett S, Darke A.H, Izzard M.J and Lillford P.J (1993), in *The Glassy State in Foods*, Eds. Blanshard, J.M.V and Lillford, P.J, Nottingham University Press, 189

Alexander L.E (1969), *X-ray Diffraction Methods in Polymer Science*, John Wiley & Sons Inc. USA

Allen G (1993), in *The Glassy State in Foods*, Eds. Blanshard, J.M.V and Lillford, P.J, Nottingham University Press, 1

Ames W.M (1952), *Journ. Sci. Food. Agr.*, **3**, 579

Ames W.M (1944), *Journ. Soc. Chem. Ind. (London)*, **63**, 200, 234, 277, 303

Andersson A.P and Öste R.E (1994), *Journal of Food Engineering*, **23**, 631

Astbury W.T (1940), *Journ. Inter. Soc. Leather Trades' Chemists*, **24**, 69

Avrami M, 1941, *J. Chem. Phys.*, **9**, 177

Balian G and Bowes J.H (1977), in *The Science and Technology of Gelatin*, Eds Hoecker B, Kaplan O.K and Scheraga H.A, Academic Press Inc.(London) Ltd, UK, 1

Banks W and Greenwood C.T (1967), *Starch/Stärke*, **19**, 394

Bear R.S and French D (1941), *J. Am. Chem. Soc.*, **63**, 2298

Belton P.S (1994), *Progress in Biophysics and Molecular Biology*, **61**, No.1, 61

Belton P.S and Hills B.P (1987a), *Molecular Physics*, **61**, No.4, 999

Biliaderis C.G, Maurice T.J and Vose J.R (1980), *Journal of Food Science*, **45**, 1669

Belton P.S, Hills B.P and Raimbaud E.R (1987b), *Molecular Physics*, **63**, No.5, 825

Blanshard J.M.V (1995), in *Physico-chemical Aspects of Food Processing*, Ed. Beckett S.T, Blackie Academic & Professional, UK, 17

Blanshard J.M.V and Lillford P.J (1993), *The Glassy State in Foods*, Nottingham University Press

Blanshard J.M.V (1987), in *Starch: Properties and Potential*, Ed Galliard T, Critical Reports in Applied Chemistry, Society of Chemical Industry, London, 16

Blanshard J.M.V (1986), in *Chemistry and Physics of Baking*, Eds. Blanshard J.M.V, Frazier P.J and Galliard T, The Royal Society of Chemistry, 1

Blanshard J.M.V, Bates D.R, Muhr A.H, Worcester D.L and Higgins J.S (1984), *Carbohydrate Polymers*, **4**, 427

Bloch F, Hansen W.W and Packard M.E (1946), *Phys. Rev.*, **69**, 127

Borch J, Sarko A and Marchessault R.H (1972), *J. of Colloid and Interface Sci.*, **41**, No.3, 574

Borchard W, Bremer W and Keese A (1980), *Colloid & Polymer Sci.*, **258**, 516

Bornstein P and Traub W (1979), in *The Proteins*, Eds Neurath H, Hill R.L and Boeder C.L, Academic Press, London, **4**, third edition, 412

Boussingault J.B (1852), *Ann. Chimie Physique*, **36**, 490

Bower D.I and Maddams W.F (1989), in *The vibrational spectroscopy of polymers*, Cambridge University Press, UK, 1

Bragg W.L (1913), *Proc. Cambridge Phil. Soc.*, **17**, 43

Brosio E, Dubalo A, Verzegnassi B (1994), *Cellular and Molecular Biology*, **40**, 4 567

Brunauer S, Emmett P.H and Teller E (1938), *J. Am. Chem. Soc.*, **60**, 309

Bryan W.P (1987), *Biopolymers*, **26**, 1705.

Bueche F (1962), *Physical Properties of Polymers*, Wiley and Sons Inc., New York

Buttrose M.S (1960), *J. Ulta. Res.*, **4**, 231

Cael J, Koening J.L and Blackwell J (1973), *Carbohydrate Research*, **32**, 79

Cairns P, I'Anson K.J and Morris V.J (1991), *Food Hydrocolloids*, **5**, 1, 151

Callaghan P.T, Jolley K.W and Humphrey R.S (1983), *J. Colloid Interface Sci.*, **93**, 521

Callet F, Milas M and Tinland B (1987), in *Gums and Stabilisers for the Food Industry*, Eds. Philips G.O, Wedlock D.J and Williams P.A, IRL-Oxford University Press, **4**, 203

Cameron R.E and Donald A.M (1993a), *Carbohydrate Research*, **244**, No.2, 225

Cameron R.E and Donald A.M (1993b), *J. Polymer Sci.*, **31**, No.31, 1197

Cameron R.E and Donald A.M (1992), *Polymer*, **33**, No.12, 2628

Cerofolini G.F and Cerofolini M.J (1980), *Colloid Interface Sci.*, **78**, 65

Chinachoti P and Steinberg M.P (1984), *Journal of Food Science*, **49**, No.6, 1604

Chinachoti P and Schmidt J.S (1991), in *Water Relationships in Foods*, Eds Levine H and Slade L, Plenum Press, New York, 561

Choy C.L and Young K (1978), *Polymer*, **19**, 1001

Colonna P, Buleon A, and Mercier C (1987), *Starch: Properties and Potential*, Ed. Galliard T, John Wiley and Sons, New York, 79

Colonna P, Tayeb J and Mercier C (1989), in *Extrusion Cooking*, Eds. Mercier C, Linko P and Harper J.M, American Association of Cereal Chemists, USA, 247

Colthup N.B and Daly L.H (1990), *Introduction to Infrared and Raman Spectroscopy*, Academic Press, Inc. USA, 1

Cornforth S.J, Axford D.W.E and Elton G.A.H (1964), *Cereal Chemistry*, **41**, 216

Couchman P.R and Karasz F.E (1978), *Macromolecules*, **11**, 117

Courts A. And Stainsby G (1958), in *Recent Advances in Gelatin and Glue Research*, ed. Stainsby G, Pergamon Press, London, 204

D'Arcy R.L and Watt I.C (1970), *Trans. Faraday Soc.*, **66**, 1236

Derbyshire W (1982), in *Water : A Comprehensive Treatise*, Edited by Franks F., Plenum Press, New York, 7, 339

Doi K and Doi A (1969), *J. Jap. Soc. Starch Science*, **17**, 89

Donald A.M, Warburton S.C and Smith, A.C (1993), *The Glassy State in Foods*, Eds by Blanshard, J M V and Lillford, P J, Nottingham University Press, 375

Donovan J.W (1979), *Biopolymers*, **18**, 263

Eastoe J.E (1961), *Biochem. Journ.*, **79**, 652

Eastoe J.E and Leach A.A (1977), in *The Science and Technology of Gelatin*, Eds. Hoecker B, Kaplan O.K and Scheraga H.A, Academic Press Inc .(London) Ltd, UK, 73

Ehrlich D And Silescu H (1990), *Macromolecules*, **23**, 1600

Eisenberg A (1984), in *Physical Properties of Polymers*, Eds. Mark J.E, Eisenberg A, Graessley W.W, Mandelkern L and Koenig J.L, American Chemical Society, Washington, 55

Fan J (1994a), *Bubble growth and starch conversion in extruded and baked systems*, PhD Thesis, University of Nottingham - UK

Fan J, Mitchell J.R and Blanshard J.M.V (1994b), *J. Food Engineering*, **24**, 337

Fan J, Mitchell J.R and Blanshard J.M.V (1996a), *Int. J. Food Technology*, **31**, 55

Fan J, Mitchell J.R and Blanshard J.M.V (1996b), *Int. J. Food Technology*, **31**, 67

Farhat I.A, Moreau P, Mitchell J.R, Derbyshire W and Blanshard J.M.V (1996a), in *Gums and Stabilizers for the Food Industry*, Eds. Philips G.O, Wedlock D.J and Williams P.A, IRL-Oxford University Press, **8**, 27

Farhat I.A, Mitchell J.R, Blanshard J.M.V and Derbyshire W (1996b), *Carbohydrate Polymers*, **30**, 219

Farhat I.A, Blanshard J.M.V, Melvin J.L and Mitchell J.R (1996c), Paper presented at the *Starch: Structure and Function international conference*. Cambridge-UK, 1996, in press

Faridi H and Rubenthaler G.L (1984), *Cereal Chemistry*, **61**, No.2, 151

Flory P.J (1953), *Principles of Polymer Chemistry*, Cornell University Press, Ithaca, New York

Flory P.J and Weaver E.S (1960), *J. Am. Chem. Soc.*, **82**, 4518

French D (1984), in *Starch: Chemistry and Technology*, Eds. Whistler R.L, BeMiller J and Paschall E.F, Academic Press Inc., London, 183

French D (1972), *J. Jap. Soc. Starch Sci.*, **19**, No.1, 8

Fukushima E and Roeder S.B.W (1981), *Experimental Pulse NMR - A Nuts and Bolts Approach*, Addison-Wesley Publishing Vompany Inc. USA, 279

Gernat C, Radosta S, Anger H and Damaschun G (1993), *Starch/Stärke*, **45**, No.9, 309

Gibbs J.H and DiMarzio E.A (1958), *J. of Chem. Phys.*, **28**, 373

Gibbs J.H (1956), *J. of Chem. Phys.*, **25**, 185

Greenwood C.T (1979), in *Polysaccharides in Food*, Eds. Blanshard J.M.V and Mitchell J.R, Butterworth & Co. Ltd, London, 100

Gregory R.B (1995), in *Protein-Solvent Interactions*, Ed Gregory R.B, Marcel Dekker Inc., USA, 191

Gregory R.B, Gangoda M, Gilpin R.K and Su W (1993), *Biopolymers*, **33**, 513

Grigera J.R (1988), *J. Chem. Soc. Faraday Trans. I*, **84**, 2603

Guilbot A and Mercier C (1985), in *The Polysaccharides*, Ed. Aspinall G.O, Academic Press, Vol 3

Hallbrucker A, Mayer E and Johari G.P (1988), *Phyl. Magazine B*, **60**, 179

Hansen L.M, Setser C.S, Paukstelis J.V (1989), *Cereal Chemistry*, **66**, No.5, 411

Harrington W.F and von Hippel P.H (1961), *Arch. Biochem. Biophys.*, **92**, 100

Harrington W.F and Rao N.V (1970), *Biochemistry*, **2**, 3714

Harris P.I. and Chapman D. (1995) *Biopolymers (Peptide Science)*, **37**, 251

Harris R.K (1983), *Nuclear Magnetic Resonance Spectroscopy*, Pitman Books Ltd

Harrison M and Hills B.P (1996), *Int. Journal of Food Science and Technology*, **31**, 167

Harper J.M (1981), in *Extrusion of Foods*, CRC Press Inc., **Vol. 1**

Hartley L, Chevance F, Hill S.E, Mitchell J.R and Blanshard J.M.V (1995), *Carbohydrate Polymers*, **28**, No.2, 83

Hartley L.P (1996), *Hydration of biopolymers to low water content*, PhD Thesis, University of Nottingham - UK

Hartmann S.R and Hahn E.L (1962), *Phys. Rev.*, **128**, 2042

Hermans P.H and Weidinger A (1948), *J. App.Physics*, **19**, 491

Hills B.P, Takacs S.F and Belton P.S (1990), *Food Chemistry*, **37**, 95

Hills B.P (1990), *Molecular Physics*, **76**, No.3, 489

Hills B.P and Paradoe K (1995), *Journal of Molecular Liquids*, **63**, No.3, 229

Hizukuri S (1986), *Carbohydrate Research*, **147**, 342

Hizukuri S (1960), *Agr. Biol. Chem.*, **25**, 45

Hollinger G and Marschessault R.H (1975), **14**, 265

Hyde P.D, Evert T.E, Cicerone M.T and Ediger M.D (1991), *Non-crystalline Solids*, **131**, 42

Iglesias H A, Chirife J, (1982), *Handbook of food isotherms*, Academic Press

Imberty A and Pérez S (1988a), *Biopolymers*, **27**, 1205

Imberty A, Chanzy H, Pérez S, Buléon A and Tran V (1988b), *J. Mol. Biol.*, **20**, 2634

Imberty A, Buléon A, Tran V and Pérez S (1991), *Starch/Stärke*, **43**, No.10, 375

Inaba H, Hatanaka Y, Imura H, Matsumura Y and Mori T (1988), *J. Jap. Soc. of Food Sci.and Tech.*, **35**, No.1, 15

Itoh M, Okawa H, Kobayashi H, Ohno T, Okamoto Y and Katoch T (1994) *The Journal of Photographic Science*, **42**, 14

Jane J, Kasemsuwan T, Leas S, Zobel H. And Robyt J.F (1994), *Starch/Stärke*, **46**, No.4, 121

Jenkins P.J (1994), *X-ray and neutron scattering studies of starch granule structure*, PhD Thesis, University of Cambridge, UK

Jenkins P.J, Cameron R.E and Donald (1993), *Starch/Stärke*, **45**, No.12, 417

Jenkins P.J, Cameron R.E, Donald A.M, Bras W, Derbyshire G.E, Mant G.R and Ryan A.J (1994), *J. Polymer Science*, Part B: Polymer Physics, **32**, 1579

Jönson B (1986), *Colloid and Polymer Science*, **264**, 77

Junshi Y.W and Thomas M.E (1993), *Carbohydrate Polymers*, **20**, 51

Kalichevsky M.T, Jaroszkiewicz E.M, Blanshard J.M.V (1993a), *Polymer*, **34**, No.2, 346

Kalichevsky M.T, Blanshard J.M.V (1993b), *Carbohydrate Polymers*, **20**, 107

Kalichevsky M.T (1993c), *Factors influencing the glass transition and mechanical properties of food biopolymers*, PhD Thesis, University of Nottingham - UK

Kalichevsky M.T, Jaroszkiewicz E.M, Ablett S, Blanshard J.M.V and Lillford P.J (1992a), *Carbohydrate Polymers*, **18**, 77

Kalichevsky M.T, Jaroszkiewicz E.M, Blanshard J.M.V (1992b), *Int. J. Biol. Macromol.*, **14**, No.5, 257

Kalichevsky M.T and Blanshard J.M.V, (1992c), *Carbohydrate Polymers*, **19**, 271

Kaminski W and Al-Bezweni M. (1994), *Int. J. of Food Sci. and Techn.*, **29**, 129

Karel M and Langer R (1988), in *Flavor Encapsulation*, Eds. Risch S.J and Reineccius G.A, American Chemical Society Symposium Series 370, Washington D.C, 177

Karel M and Saguy I (1991), in *Water Relationships in Foods*, Eds. Levine H and Slade L, Plenum Press, New York, 157

Kassenbeck P. (1978), *Starch/Stärke*, **30**, No.2, 40

Kassenbeck P. (1975), *Starch/Stärke*, **27**, No.7, 217

Katz J.R (1928), in *A Comprehensive Survey of Starch Chemistry*, Ed. Walton R.P, The Chemical Catalog Company Inc., New York, **1**, 100

Katz J.R and Van Italie T (1930), *Z. Physik. Chem*, **A150**, 90

Katz J.R and Derksen J.C (1930), *Z. Physik. Chem*, **A150**, 100

Keetels C.J.A.M (1996), *Retrogradation of concentrated starch systems*, PhD thesis, University of Wageningen, The Netherlands

Kennedy S.D and Bryant R.G (1990) *Biopolymers*, **29**, 1801

Kimmich R, Klammler F, Skirda V.D, Serebrennikova I.A, Maklakov A.I and Fatkullin N (1993), *Appl. Magn. Resonance*, **4**, 425

Kitamura S, Kuge T and Stokke B.T (1989), in *Gums and Stabilisers for the Food Industry*, Eds. Philips G.O, Wedlock D.J and Williams P.A, IRL-Oxford University Press, **5**, 329

Krimm S and Bandekar J (1986), *Adv. Protein Chem.*, **38**, 181

Kumosinski T.F and Farell H.M,Jr (1993), *Trends in Food Science and Technology*, **4**, 169

Kumosinski T.F and Farell H.M,Jr (1991), *Protein Chem.*, **10**, 3

Kuntz I.D and Kauzmann W (1974), *Adv. Prot. Chem.*, **28**, 239

I'Anson K.J, Miles M.J, Morris V.J, Besford L.S, Jarvis D.A and Marsh R.A (1990), *J. Cereal Sci.*, **11**, 243-248

Labaki L.C, Torriani I.L and Grigera J.R (1991), *Brazilian Journal of Medical and Biological Research*, **24**, No.1, 15

Labuza T.P (1970), in *Procedings of the 3rd International Conference on Food Science and Technology*, Institute of Food Technologists, Washington DC, 618

Lang K.W and Steinberg M.P (1983, *Journal of Food Science*, **48**, 517

Lauritzen J.I and Hoffman J.D (1973), *Journal of Applied Physics*, **44**, No 10, 4340

Le Botlan D and Desbois P, (1995), *Cereal Chemistry*, **72**, No 2, 191

Le Meste M., Voilley A. And Colas B. (1991), in *Water Relationships in Foods*, Eds.Levine H. And Slade L, Plenum Press, USA, 123-138

Lecourtier J, Chauveteau G and Muller G (1986), *International Journal of Biological Macromolecules*, **8**, No.5, 306

Ledward D.A (1968), *Physicochemical study of some chemically modified gelatins*, PhD Thesis, University of Leeds, UK

Ledward D.A (1986), in *Functional Properties of Food Macromolecules*, Eds. Mitchell J.R and Ledward D.A, Elsevier Applied Science Publishers ltd., England, 121

Leiras M.C and Iglesias H.A (1991), *Int. J. of Food Sci. and Technology*, **26**, 91

Lelievre J. (1976), *Polymer*, **7**, 854

Lelievre J. (1974), *Starch/Stärke*, **26**, 85

Lelièvre J. (1973), *J. of Applied Polymer Science*, **18**, 293

Lesikar A.V (1977), *J. Soln. Chem.*, **6**, 81

Lesikar A.V (1975), *J. Chem. Phys.*, **63**, 2297

Levine H and Slade L (1987), in *Water Science Reviews*, edited by Frank F, Cambridge University Press, **3**.

Levine H and Slade L (1986), *Carbohydrate Polymers*, **6**, 213

Levine H and Slade L (1988), in *Water Science Reviews*, Ed. Franks F, Cambridge University Press, **3**, 79

Lewis D.F (1981), *Scanning Electron Microscopy*, Chicago SEM Inc. **III**, 391

Lillford P.J, Clark A.H and Jones D.V (1980), in *A.C.S Symp. Series*, **127**, 177

Linnecar K.E.M (1995), *Nature of starch granule resistance to digestion*, PhD Thesis, University of Nottingham, UK

Mansfield M.L (1993), in *The Glassy State in Foods*, Eds. Blanshard, J.M.V and Lillford, P.J, Nottingham University Press, 103

Marsh R.D.L (1986), *A study of the retrogradation of wheat starch systems using x-ray diffraction*, PhD Thesis, University of Nottingham, UK

Marsh R.D.L and Blanshard J.M.V (1988), *Carbohydrate Polymers*, **9**, 301

Mathlouthi M, Cholli A L, Koenig J L, (1986), *Carbohydrate Research* **147**, 1

Maxwell J.L and Zobel J.F (1978), *Cereal Foods World*, **23**, 124

McBrierty V.J. and Douglass D.C. (1981) *Journal of Polymer Science - Macromolecular reviews*, **16**, 295

McBrierty V.J and Packer K.J (1993), *Nuclear magnetic resonance in solid polymers*, Cambridge University Press, 16

Melvin J.L (1996), *Development of structure and destruction of spores in extruded starch*, PhD thesis, University of Nottingham, UK

Mercier C, Charbonnière R, Grebaut J and De La Guerivière J.F (1980), *Cereal Chemistry*, **57**, 4

Mercier C, Charbonnière R, Gallant D and Guilbot A (1979), *Polysaccharides in Foods*, edited by Blanshard J.M.V and Mitchell J.R, Butterworths, London, **10**, 153

Millane R.P, Narasaiah T.V and Wang B (1989), in *Gums and Stabilisers for the Food Industry*, Eds. Philips G.O, Wedlock D.J and Williams P.A, IRL-Oxford University Press, **5**, 365

Mitchell J.R and Areas J.A.G (1992), in *Food Extrusion Science and Technology*, Eds. Kokini J.L, Ho C.T and Karwe M.V, Marcel Dekker Inc., New York, 345

Mitchell J.R and Hartley L (1996), in *Gums and Stabilizers for the Food Industry*, Eds. Philips G.O, Wedlock D.J and Williams P.A, IRL-Oxford University Press, **8**, 3

Miura M., Nishimura A. and Katsuta K. (1992), *Food Structure*, **11**, 225

Moorhouse R, Walfinshaw M.D and Arnott S (1977), in *Extracellurar microbial polysachharides*, Eds. Sandford P.A and Laskin A, ACS Symposium Series **45**, ASC Washington, USA, 90

Morris E.R, Rees D.A, Young G, Walkinshaw M.D and Darke A (1977), *Journal of Molecular Biology*, **110**, 1

Morrison W.R, Milligan T.P and Azudin M.N (1984), *J. Cereal Science*, **2**, 257

Muller G, Lecourtier J, Chauveteau G and Allain C (1984), *Makromolekulare chemie-rapid communications*, **5**, No.4, 203

Muller G, Lecourtier J (1988), *Carbohydrate Polymers*, **9**, No.3, 213

Mussulmann W.C and Wagoner J.A (1968), *Cereal Chemistry*, **45**, 162

Mustapha W.A (1997), *Influence of the matrix on the Maillard reaction*, PhD Thesis, University of Nottingham - UK

Mustapha W.A, Hill S and Mitchell J.R (1996), *unpublished results*

Nara S, Mori A. and Komiya T. (1978), *Starch/Stärke*, **30**, 111

Nara S and Komiya T. (1983), *Starch/Stärke*, **35**, 407

Naryshkina E.P, Volkov V.Y, Dolinnyi A.I and Izmailova V.N (1982), *Kolloid Zh.*, **44**, 322

Noel T.R, Ring S.G and Whittam M.A (1990), *Trends in Food Science and Technology*, **1**, 62

Nordin P, Moser H, Rao G, Giri N and Liang T (1970), *Starch/Stärke*, **22**, No 8, 256

Nyquist H (1983), *Int. J. Pharm. Tech. & Proc.*, **4**(2), 47

Ohtsuka A, Watanabe T, Suzuki T (1994), *Carbohydrate Polymers*, **25**, 95

Oksanen C.A and Zografi G (1993), *Pharmaceutical Research*, **10**, No.6, 791

Oostergel G.T and Van Bruggen E.F.J (1989), *Starch/Stärke*, **41**, 331

Orford P.D, Parker R and Ring S.G (1990), *Carbohydrate Research*, **196**, 11

Orford P.D, Parker R and Ring S.G (1989), *Int. J. Biol. Macromolecules*, **11**, 91

Packer K.J (1996), in *Encyclopaedia of NMR*, Wiley Press, *in press*

Packer K.J and Rees C (1972), *J. Colloid Interface Sci.*, **49**, 206

Parry D.A.D and Creamer L.K (1979), in *Fibrous proteins : scientific, industrial and medical aspects*, Academic Press, London, **1**

Pautrat C, Bressan C and Mathlouthi M (1995), in press

Peschier L.J.C, Bouwstra J.A, Debleyser J, Junginger H.E and Leyte J.C (1993), *Biomaterials*, **14**, No.12, 945

Piez K.A (1967), in *Treatise on Collagen*, Ed. Ramachandran G.N, Academic Press, London, **1**, 207

Pines A, Gibby M.G and Waugh J.S (1973), *Journ. Chem. Phys*, **59**, 569

Poole P.L (1994) *Journal of Food Engineering*, **22**, 349

Poole P L, Finney J L, (1982), *Journal of Physics E*, **15**, 1073

Poole P L, Finney J L, (1984), *Biopolymers*, **23**, 1647

Prestrelski S.J, Tedeschi N., Arakawa T and Carpenter J (1993), *Biophys. J.*, **65**, 661

Purcell E.M, Torrey H.C and Pound R.V (1946), *Phys. Rev.*, **69**, 37

Ramachandran G.N (1967), in *Treatise on Collagen*,Ed. Ramachandran G.N , **1**, 103

Ramachandran G.N (1958), in *Recent Advances in Gelatin and Glue Research*, Ed. Stainsby G, Pergamon Press, New York, 32

Ring S.G, Colonna P, L'Anson K.J, Kalichevsky M.T, Miles M.J, Morris V.J and Orford P.D (1987), *Carbohydrate Research*, **162**, 277

Robin J.P, Mercier C, Charbonnière R and Guilbot A (1974), *Cereal Chemistry*, **51**, 389

Robin J.P, Mercier C, Duprat F, Charbonnière R and Guilbot A (1975), *Starch/Stärke*, **27**, No.2, 36

Rodin V.V and Izmailova N. (1994), *Colloid Journal*, **56**, 66

Roos Y and Karel M. (1990), *Biotech. Prog.*, **6**, 159

Roos Y and Karel M. (1991a), *Journal of Food Science*, **56**, 38

Roos Y and Karel M. (1991b), *Journal of Food Science*, **56**, 1676

Roos Y and Karel M. (1992), *Journal of Food Science*, **57**, 775

Roos Y and Karel M. (1993), in *The Glassy State in Foods*, Eds. Blanshard, J.M.V and Lillford, P.J, Nottingham University Press, 207

Roozen M.J.G.W, Hemminga M.A and Walstra P (1991), *Carbohydrate Research*, **215**, 229

Roozen M.J.G.W and Hemminga M.A (1990), *Journal of Phys. Chem.*, **94**, 7326

Roozen M.J.G.W and Hemminga M.A (1991), *Special Publication of the Royal Society of Chemistry*, **82**, 531

Roulet Ph, MacInnes W.M, Würsh P, Sanchez R.M and Raemy A, (1988), *Food Hydrocolloids*, **2**, No.5, 381

Rupley J.A and Carreri G (1991), *Adv. Prot. Chem.*, **41**, 37

Sandreczki T.C and Brown I.M (1988), *Macromolecules*, **21**, 504

Schmitt F.O, Gross J and Highberger J.H (1955), *Symp. Soc. Exp. Biol.*, **9**, 148

Slade L and Levine H (1991), in *CRC Critical Reviews in Food Science and Nutrition*, **30**, 115

Slade L and Levine H, (1993), in *The Glassy State in Foods*, Eds. Blanshard J.M.V and Lillford P.J, Nottingham University Press, 35

Soderman O, Lonnqvist I and Balinov B (1992), in *Emulsions - A Fundamental and Practical Approach*, Ed. Sjöblom, Kluwer, Dordrecht, 239

Sperling L.H (1986), in *Introduction to Physical Polymer Science*, J. Wiley and Sons Inc., New York

Stejskal E O, Tanner J E (1965), *Journal of Chemical Physics*, **42**,1, 288

Sterling C (1962), *J. Polymer Science*, **56**, S10

Sterling C (1960), *Starch/Stärke*, **12**, 182

Sutherland I.W (1990), *Biotechnology of microbial exopolysaccharides*, Cambridge University Press; 73

Takeda Y, Hizukuri S, Takeda C, Suzuki A (1987a), *Carbohydrate Research*, **165**, No.1, 139

Takeda Y, Hizukuri S, Juliano B.O (1987b), *Carbohydrate Research*, **168**, No.1, 79

Tanfani F, Kochan Z, Swierczynski J, Zydowo M.M and Bertoli E (1995), *Biopolymers*, **36**, 569

Tanner J E, Stejskal E O, (1968), *Journal of Chemical Physics* **49**,4, 1768

ten Brinke G, Karasz F.E and Ellis T.S (1983), *Macromolecules*, **16**, 244

Teo C.H, and Seow C.C (1992), *Starch/Stärke*, **44**, 288

Tiller W.A, (1991), *The Science of Crystallisation : Microscopic interfacial phenomena*, Cambridge University Press, 376

Tohyama K and Miller W.G (1981), *Nature*, **289**, 813

van den Berg C (1985), in *Properties of water in food*, Eds. Simatos D and Multon J.L, 119

van den Berg C (1981), *PhD Thesis*, University of Wageningen - The Netherlands

Veis A (1964), in *The Macromolecular Chemistry of Gelatin*, Academic Press Inc. (London) Ltd, UK

Wakelin J.H, Virgin H.S and Crystal E (1959), *J. App. Physics*, **30**, 1654

Wang Y.J and Jane J (1994), *Cereal Chemisrty*, **71**, No 6, 527

Ward A.G and Courts A (1977), in *The Science and Technology of Gelatin*, Eds Hoecker B, Kaplan O.K and Scheraga H.A, Academic Press Inc.(London) Ltd, UK

White G.W and Cakebread S.H (1966), *J. of Food Technology*, **1**, 73

Williams M.L, Landel R.F and Ferry J.D (1955), *J. American Chemical Society*, **77**, 3701

Wilson R.H, Goodfellow B.J, Belton P.S, Osborne B.G, Oliver G and Russel P.L (1991), *J. Sci. Food & Agric.*, **54**, 471

Wu H.C.H and Sarko A. (1978a), *Carbohydrate Research*, **61**, 7

Wu H.C.H and Sarko A. (1978b), *Carbohydrate Research*, **61**, 27

Wunderlich B (1976a), *Macromolecular Physics*, Academic Press NY, **1**.

Wunderlich B (1976b), *Macromolecular Physics*, Academic Press NY, **2**.

Xie W.B and Lecourtier J (1992), *Polymer Degradation and Stability*, **38**, No.2, 155

Yamaguchi M, Kainuma K and French D (1979), *J. Ultrastruct. Res.*, **69**, 249

Zobel H,F (1988), *Starch/Stärke*, **40**, No 2, 44